Development of Microneedle Systems for Transdermal Sensing: New Routes to Assessing Cardiovascular Health

Catherine Hegarty

BSc

Faculty of Computing, Engineering, and the Built Environment of

Ulster University

Thesis submitted for the degree of

Doctor of Philosophy

October 2020

I confirm that the word count of this thesis is less than 100,000 words

Contents

List of Figures

List of Tables

Acknowledgements

Firstly, I would like to express my sincerest thanks and gratitude to Professor James Davis, who has provided unwavering support, enthusiasm, and guidance for the entirety of my PhD journey. You truly are extraordinary, with your wacky ideas, contagious humour, and unique quirks. I quite literally could not have asked for a better supervisor as evidenced by the Best Supervisor Award 2020. 'From This Moment On', you have provided me with new aspirations in life, even beyond career development, for that I thank you (Twain, S. 1997).

My appreciation and thanks extend to all the academic and NIBEC staff who have provided advice and assistance throughout my PhD including: Mrs. Ann Blair, Miss Ruth Holman, Mr. Andrew Toye, Mr. Damian McDonald, and Mr. Brian McGrath.

Ruairi, Aaron, Jordan, Anna, Ashleigh and Sean, it was a pleasure to work with you all, I cherish all the laughs we shared and thank you for the support and knowledge you've offered me. Michael, Robert, Amy, Sarah, and Teri, you've all been a great source of encouragement and more importantly, entertainment, thank you - the lab family legacy lives on.

Dr. Aaron McConville, this thesis wouldn't have been possible without you and your home grown tomatoes. It is a privilege to have known you, you're greatly missed.

Dr. Charnete Casimero, here's to forever changing the response to our rendition of 'Say ma name, say ma name'. Words don't comprehend the pillar of emotional, motivational and informative support you have been, always going above and beyond to help anyone in need. I count myself incredibly lucky to have an 'angry wee pleb' friend like you to navigate this PhD journey with. I want to thank you for all the laughing fits, gossip sessions, emotional outbursts and sassy speeches that have made this a genuinely enjoyable experience.

Finally, I would like to thank my family and friends who have been a cloud of reassurance over the years. To Barry, Carla, Dearbhala, Fiona, Fionnuala, Shannon, and Shawnee, thank you for consistently being there for me and always providing comical relief during stressful times. Roseanne and Matthew, thank you for being so understanding, tolerating me, and always helping in any way you can, I'm forever grateful to you both. To my parents, Michael, you've always been my inspiration, thank you for always pushing me to be better. Marion, you are the living example of resilience, thank you for your endless compassion and always believing in me (my own personal cheerleader).

No thanks to Covid-19, this thesis is finally done and as Shania Twain would say, 'Life's About To Get Good' (Twain, S. 2017).

Copyright / Credit Notices

Within this thesis, material (like text, figures, or tables) from the author's publications is reprinted. The copyright / credit notices are listed at this place in common for all the related chapters, paragraphs or sections. The material might have been modified slightly, however these copyright / credit notices still apply.

Acknowledgement is given for the original source of publication for:

Hegarty, C., McConville, A., McGlynn, R. J., Mariotti, D., & Davis, J. (2019). Design of composite microneedle sensor systems for the measurement of transdermal pH. *Materials Chemistry and Physics*, 227(August 2018), 340–346.

The final publication is available at Science Direct via 10.1016/j.matchemphys.2019.01.052

Acknowledgement is given for the original source of publication for:

Hegarty, C., Mckillop, S., Dooher, T., Dixon, D., & Davis, J. (2019). Composite Microneedle Arrays Modified with Palladium Nanoclusters for Electrocatalytic Detection of Peroxide. *IEEE Sensors Letters*, 3(9), 1–4.

The final publication is available at IEEE via 10.1109/LSENS.2019.2935831

Acknowledgement is given for the original source of publication for:

Anderson, A., **Hegarty, C.**, Casimero, C. & Dvais, J. (2019). Electrochemically Controlled Dissolution of Nanocarbon-Cellulose Acetate Phthalate Microneedle Arrays. *ACS Applied Materials and Interfaces*, pp. 35540–35547.

The final publication is available at ACS via 10.1021/acsami.9b09674

Abstract

Healthcare systems are under increasing pressure to decentralise blood analysis procedures, especially with the burden of an ageing population and the lengthy processing times associated with laboratory analysis. Of late, there has been a significant push towards developing point of care diagnostics that would overcome many of the issues surrounding conventional methods of blood withdrawal and subsequent examination. It has been recognised that a smart sensor, capable of monitoring a variety of biomarkers in situ would radically transform disease management, providing earlier diagnosis and therefore, more timely intervention.

In light of this, the core strategy of the project research outlined herein was largely focused on the formation of a minimally invasive transdermal method of assessing cardiovascular health. The design and development of a composite microneedle biosensor has been described, with the vision of potential for future integration within a smart wearable system. Multiple formulations for low-cost rapid production of conductive carbon-based microneedle arrays were investigated. The facile means of microfabrication, and inclusion of carbon nanoparticulate, afforded further exploration by application of a variety of electrochemical modification techniques. The composite microneedle arrays were assessed by numerous characterisation techniques, validating the efficacy of their capability to penetrate the stratum corneum of skin, whilst maintaining sensing functionality.

The electroanalytical performance of the microneedle arrays was demonstrated by the detection of clinically relevant biomarkers within biologically complex media. An attractive feature of the composite system, being the interchangeability of material composition, lends itself to not only biosensing, but also, transdermal drug delivery. As such, the electroanalytical capacity of the microneedle design was beyond initially anticipated. This facilitated proof of concept exploration of a composite microneedle system capable of harmonious biosensing and consequential release of a therapeutic drug. Numerous applications which would benefit from the composite microneedle approach have been investigated and its commercial feasibility critically appraised.

Abbreviations

Ag	Silver
AgCl	Silver Chloride
BBP	Blood Borne Pathogen
BE	Binding Energy
BEHP	Bis(2-ethylhexyl) phthalate
BFC	Biofuel Cell
BGA	Blood Gas Analyser
BLA	Biochemical Lab Analyser
BR	Britton-Robinson
CAP	Cellulose Acetate Phthalate
C-CAP	Carbon-Cellulose Acetate Phthalate
CDC	Centers for Disease Control
CE	Counter Electrode
CFM	Carbon Fibre Mesh
CNC	Computer Numerical Control
C-Ps	Carbon-Polystyrene
CSW	Cerebral Salt Wasting
CT	Computed Tomography
CV	Cyclic Voltammetry
DCM	Dichloromethane
ECF	Extracellular Fluid
EDX	Energy Dispersive X-Ray Spectroscope
ELISA	Enzyme-linked Immunosorbent Assay Immunoassay
emf	Electromotive Force
GP	General practitioner
H_2O_2	Hydrogen Peroxide
HB	Horse Blood
HBV	Hepatitis B Virus
HCW	Healthcare Workers
HeNe	Helium-neon
HER	Hydrogen Evolution Reaction

HIV	Human Immunodeficiency Virus
ICU	Intensive Care Unit
ICURe	Innovation to Commercialisation of University Research
ISE	Ion-selective Electrode
ISF	Interstitial Fluid
IVD	In Vitro Diagnostic
K-TCPB	Potassium tetrakis (4-chlorophenyl) borate
LoD	Limit of Detection
MEMS	Micro-machining or Micro-electromechanical systems
mHealth	Mobile Health
MN	Microneedle
MW	Molecular Weight
NASICON	Sodium Super Ionic Conductor
NHS	National Health service
NSI	Needle-stick Injury
OSHA	Occupational Safety and Health Administration
PBS	Phosphate Buffered Saline
PDMS	Polydimethylsiloxane
PEO	Polyethylene Oxide
PET	Photo-induced Electron Transfer
POC	Point of Care
PVC	Polyvinyl Chloride
RE	Reference Electrode
SAM	Self-assembling Monolayer
SC	Stratum Corneum
SED	Safety Engineered Devices
SEI	Secondary Electron Imaging
SEM	Scanning Electron Microscopy
SIADH	Inappropriate Secretion of Sntidiuretic Hormone
SPE	Screen Printed Electrode
SWV	Square Wave Voltammetry
TAT	Turnaround Time
TBO	Toluidine Blue
ToA	Take-off Angle

UA	Uric Acid
WE	Working Electrode
WESS	Wide Energy Survey Scans
XPS	X-Ray Photoelectron Spectroscopy

Notes on Access to Contents

“I hereby declare that with effect from the date on which the thesis is deposited in Research Student Administration of Ulster University, I permit

1. the Librarian of the University to allow the thesis to be copied in whole or in part without reference to me on the understanding that such authority applies to the provision of single copies made for study purposes or for inclusion within the stock of another library.
2. the thesis to be made available through the Ulster Institutional Repository and/or EThOS under the terms of the Ulster eThesis Deposit Agreement which I have signed.

CHAPTER 1

Introduction and Project Aims

Abstract

Alleviating the healthcare system from conventional laborious blood analysis methods with a point of care diagnostic sensor capable of monitoring a surplus of cardiovascular related biomarkers is at the forefront of this research. A minimally invasive, transdermal approach is proffered as being particularly advantageous within this sector, eliminating many of the disadvantages that exist with current methodologies. The research outlined here seeks to develop a low-cost production technology, which has the potential to be used as a smart sensing device within community care. This chapter summarises the research to be undertaken and outlines the project aim and corresponding objectives.

1.1 Introduction

Expansive research has been committed to the efforts of improving point of care (POC) biosensing capabilities. Electrochemical sensors in particular, have new and continually emerging sensing capacities. This is due to the increased availability of manufacturing techniques, but also, ever evolving modification strategies. Whilst this has created opportunities for various applications within the research community, their use for diagnostic biosensing is often limited by the processing steps for blood analysis. As such, many of these new designs never reach commercialisation for biosensing purposes since their constraints are no different to current methodologies. This is glaringly obvious among communities which require routine blood sampling, with no significant step away from painful discrete sampling. Hence, patient compliance has become a prominent issue, frequently associated with painful sampling procedures.

Another factor associated with blood withdrawal and analysis which has become increasingly concerning, is the prevalence of needle-stick injuries (NSIs). Over 80% of percutaneous injuries recorded within healthcare settings are attributed to NSIs (Panlilio *et al.*, 2004; CDC, 2008; Grimmond and Good, 2017). Additionally, an increased pressure to decentralise healthcare has seen an increase in routine sampling and medical procedures taking place at home. This may be by trained professionals or self-administered. Therefore, these NSIs are not limited to healthcare settings (and professionals) but are also accounted for in community care. Besides the unfortunate pain and potential trauma associated with a sharps injury, there is also an elevated risk of contracting blood borne pathogens (BBPs). Moreover, the reuse and improper disposal of sharps among self-administering patients is a distressing factor to consider, where recycling of needles and lack of effective waste management will only contribute to BBP transmission statistics. This becomes an alarming consequential risk in less developed countries where scavenging is prominent.

As a result, there has been a significant push in research supporting minimally invasive approaches for transdermal drug delivery and more recently, blood analysis. One particular method which has captured a lot of interest involves microneedle (MN) technology. With the maturation and increasing availability of microfabrication technology comes the

miniaturisation of devices. This has proven to be particularly beneficial for transdermal drug delivery methods by means of microneedles. The minimally invasive nature of MN technology also offers a much preferred painless method of application. Thus, providing a suitable alternative for patients who present with needle phobia, therefore, improving patient compliance but should also theoretically avoid potential NSIs. Whilst transdermal drug delivery MNs are recognised as having significant medical potential, fabrication of microneedles for biosensing purposes has traditionally been restricted by expensive fabrication methods and affiliated biocompatibility issues. However, recent advances in microfabrication techniques have provided the research community greater access to explore microneedle technology for biosensing applications.

Point of care biosensing has been recognised as a key solution for the burden of lengthy processing times for blood analysis, especially for highlighting signs and symptoms of cardiovascular related issues. Most recently, a new wave of smart wearables has dominated the market, focusing primarily on vital signs monitoring. Initially these smart devices were aimed at the health and physical fitness market but have recently attained medical grade standards. Thus, the concept of introducing biosensors within smart wearables, which can be monitored within community care, holds the promise of reducing the economic toll on healthcare systems by prompting earlier diagnostic and therapeutic interventions. Smart wearables which possess the ability to continuously monitor a variety of biomarkers could provide a comprehensive biochemical assessment of the wearer's health. This idealisation of connected health would be particularly advantageous navigating the strains placed on healthcare systems with an ageing population. Ultimately, biosensing devices such as these would contribute significantly in advancing personalised healthcare and therefore, better patient outcomes.

1.2 Project Aim and Objectives

The aim of the project detailed in this thesis was to investigate the design and validity of a transdermal approach to electrochemical POC biosensing which could be capable of independent monitoring with collaborative remote capabilities. The focus was to optimise the technology for detecting relevant metabolites for the analytical assessment and

therefore, diagnosis of cardiovascular related conditions. Ideally the project research would significantly contribute to the cardiovascular diagnostic sector for researchers and clinicians alike, but also, work towards a device that is qualified to distinguish a variety of markers via label free detection. This project lays the foundations for a multiparametric test which could be applied to the cardiac field and expand into other areas such as glucose sensing, nutrition and other detectable biomarkers. Through further development, the diagnostic biosensor should then be capable of transferring electrochemical sample composition data wirelessly, to operate as a remotely accessible POC sensor. Ultimately, its envisaged that the proposed technology could be integrated within a smart wearable, which eventually could be adapted to operate as a fully autonomous / closed loop system with the simultaneous delivery of therapeutic agents.

The objectives associated with this project were:

- Research and consider preceding published articles related to the fabrication and modification of screen printed electrodes and microneedles.
- Transfer the electrochemical sensing capabilities of carbon based screen printed electrodes to microneedle technology.
- Design and develop a conductive composite microneedle system capable of transdermal sensing application.
- Characterise the surface chemistries and structural composition of the microneedle electrodes and optimise their electroanalytical performance.
- Optimise the surface and formulation modifications of the microneedle electrodes as appropriate for detection of various biomarkers.
- Assess and validate the capacity of the composite microneedle arrays for transdermal application whilst maintaining sensing functionality.
- Demonstrate versatility of the composite systems and potential for new modalities of drug delivery and biosensing.
- Explore prospect of smart microneedle sensing commercialisation.

1.3 Summary of Chapters

This thesis is comprised of 9 chapters and a summary of each is given:

Chapter 2 details a concise summary of the relevant background literature regarding current and emerging research relating to point of care blood analysis. Particular focus is paid to screen printing and microneedle technology for biosensing applications, with the advantages and limitations discussed for each in preparation for the challenges within this project. This chapter serves as a fundamental understanding for the research conducted in this project and lays the foundation for the proceeding chapters.

Chapter 3 describes the experimental procedures and methodologies used throughout the project. Routine parameters are defined within this chapter, however, variations outside the standard approaches for independent experimentation are detailed in the appropriate sections within subsequent chapters.

Chapter 4 highlights the electroanalytical capacity of a carbon based screen printed electrode system and the implementation of simple modification strategies which facilitate detection of pH. It is through this chapter that the screen printed electrode technology is translated to microneedles, recognising the advantages and limitations of planar carbon substrates. Through this chapter, carbon is identified as an invaluable, versatile material, which could be incorporated into the composite microneedle system.

Chapter 5 details the design and development of the composite microneedle approach. Within this chapter, the necessary performance requirements of the microneedles are outlined. Material selection for the composite formulation is explored and refined to produce microneedles which maintain their structural integrity through the micromoulding process. The transfer of technology from the screen printed electrodes is shown to be successful, as the conductive microneedles show that they can be easily modified by the same strategies. Characterisation of the microneedles demonstrate their capability for transdermal application and potential for electrochemical biosensing applications.

Chapter 6 further investigates the electroanalytical capabilities of the composite microneedle sensor. Through facile surface modification techniques, the microneedles are showcased as a voltammetric sensor. The microneedles are examined within complex biological media and demonstrate their ability to maintain functionality after transdermal application. This chapter highlighted that the electroanalytical capabilities of the sensor were beyond the expectation of the investigation.

Chapter 7 examines the composite nature of the microneedles and demonstrates the versatility offered through this rapid prototyping method. The microneedle formulation is adapted for exploitation as an electrochemically controlled drug delivery method. Surface modifications are again applied with ease and are characterised. This chapter demonstrates the potential for future applications which may combine the biosensing unit as an actuator for electrochemically initiated drug release.

Chapter 8 displays the multifaceted nature of the microneedle method, lending itself to potentiometric sensing of sodium ions. The adaptability of the fabrication method was exploited to include ion selective formulations to perform as a transdermal diagnostic sensor for hyponatraemia. It was noted through this chapter that there are many clinically relevant, point of care applications which may benefit from microneedle sensing technology.

Chapter 9 discusses the concluding remarks from each study carried out within this research. This chapter also touches on the commercial feasibility of microneedle sensors as initially determined from participation in an Innovate UK/ ICURe three month secondment and explores the future prospects for the technology.

CHAPTER 2

Summary of Literature: Medical Diagnostics, Challenges, and Opportunities

Abstract

Emerging research has seen a prevalent increase in interest surrounding point of care medical diagnostics over the years. Smart devices in particular have accumulated remarkable success among the health and physical fitness market, but more recently, has transcended into medical grade smart sensing, making wearable diagnostics within the community more readily available than ever. An overview of the current and emerging electrochemical diagnostic methods for blood analysis and their critical evaluation is described here, along with the potential opportunities for further expansion of research into micro-sensing devices. Thus, the focus was to provide a detailed literature review which would serve as the background from which research in this project would be derived.

Work contained within the chapter has been published in:

McConville, A., **Hegarty, C.** and Davis, J. (2018) 'Mini-Review: Assessing the Potential Impact of Microneedle Technologies on Home Healthcare Applications'. Medicines, 5(2), p. 50.

2.1 Introduction

Current approaches towards medical diagnostics rely heavily on centralised laboratories performing diagnostics by large automated analysers, putting additive strain on healthcare systems with increased waiting times and costs. Not only this, but the issue with patient compliance and lack of self-health management only adds to the burden. It has been long recognised that disease progression and optimisation of therapeutics can be well managed with the aid of rapid diagnostics. Particularly with cardiovascular related diseases, there has been a shift in focus towards continuous monitoring of biomarkers for earlier intervention and prevention of cardiovascular events. Thus, there is a looming necessity to miniaturise and mobilise these devices to be utilised within the community or at the patient's bedside. In recent years, considerable advancements have been made in wearable sensor technology in terms of vital signs monitoring, however, there are still a host of other markers, especially those within the blood, to be monitored that contribute to a persons' health and well-being. Inevitably, the idealisation of intertwining smart diagnostics with smart therapeutics according to a patient profile is the ultimate goal for personalised healthcare.

2.1.1 Conventional Methods of Blood Withdrawal

The analysis of blood provides key information on the presence or concentration of biological analytes which can inform clinical decision making. Therefore, when a patient presents as feeling unwell, as well as the standard observational tests, it is common for the clinician to request a variety of blood screening tests. Conventional methods of blood analysis requires blood withdrawal from the vein of an arm by a hollow-bore needle and transporting the sample to a central laboratory where the analysis is typically conducted using a biochemical lab analyser (BLA). This process for central laboratory sample analysis is highlighted in **Figure 2.1.1.A**. This practice is well established and is typically regarded as highly accurate and reproducible. However, the overall turnaround time (TAT), which is defined by the point of request for blood screening to the time of therapeutic intervention, can be time consuming (Osredkar, 2017). The therapeutic TAT can be broken down into several steps as shown in **Figure 2.1.1.B**, all of which add to the lengthy processing times associated with central lab testing and further contribute to disease progression, worsening the patient's health before

treatment has been initiated. It has also been highlighted that the time taken to transport a sample to the central lab for analysis often results in sample degradation before analysis has even taken place, which may skew data analysis. Once a blood sample has been extracted, it is effectively out of date, meaning a longer TAT can be ascribed to mistreatment of a disease.

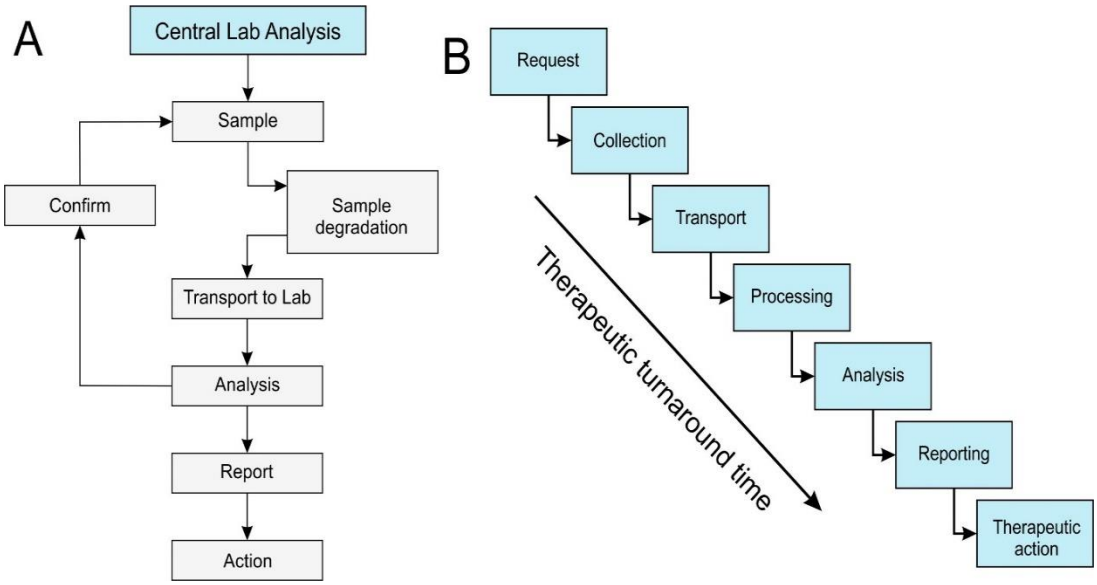

Figure 2.1.1 (**A**) Typical processes involved for central laboratory sample analysis and (**B**) the processing steps contributing to increasing therapeutic turnaround times.

Furthermore, centralised testing incurs significant capital and staffing costs for healthcare systems, especially when they are mis-used or over-used. It has been reported that up to 40% of laboratory tests are considered unnecessary (Gopal Rao, 2003). It's estimated that improving the efficiency of laboratory in vitro diagnostic (IVD) tests and eliminating inappropriate testing could save the UK National Health Service (NHS) up to £1 billion per annum (Bogavac-Stanojevic and Jelic-Ivanovic, 2017). Parallel to this, is the necessity for trained professionals required to carry out the lab testing, as well as the extraction of blood sampling in the first place. Since the traditional method of venipuncture involves a sharp hypodermic needle to penetrate the skin beyond the dermal nerve network demonstrated in **Figure 2.1.2**, this inevitably creates the sensation of pain and may be quite distressing for some patients, especially for those who suffer from needle phobia. The association of pain with venipuncture often escalates the issue of patient compliance with self-health

management (Ialongo and Bernardini, 2016). Patient compliance becomes particularly relevant when it comes to disease treatment that relies on routine blood testing and, where a patient's ownership of managing their own disease can be crucial. A patient's view of how beneficial the therapeutic intervention will be, has been demonstrated as a factor of therapeutic compliance and, in contrast to oral medications, injectable methods present with additional difficulties in patient adherence due to the association of factors such as pain tolerance, complications in regimen and the stress of societal issues (Lau *et al.*, 2008; Peyrot *et al.*, 2012; Spain *et al.*, 2016). Some patients may also be reluctant to attend their GP practice knowing that they will require blood extraction or medical injection, only worsening their condition and prolonging therapeutic intervention, again, adding strain on the healthcare system.

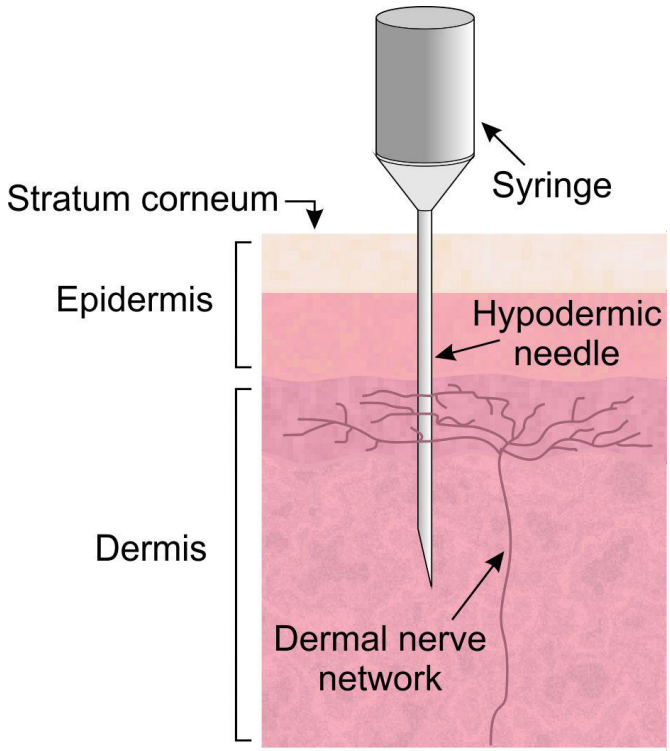

Figure 2.1.2 The typical depth of puncture from a hypodermic needle coming into contact with the dermal nerve network during blood extraction.

Phlebotomy can also become quite challenging in relation to paediatric, neonatal and geriatrics patients. The small total of blood volume present in infants requires careful consideration when extracting blood, but also the distress caused during the procedure. For

this reason, capillary blood sampling is often used for paediatric patients, where small volumes of blood are required for testing in an attempt to avoid the risk of anaemia (Lenicek Krleza *et al.*, 2015). Children specifically tend to be needle phobic by nature, with the presence of a needle being injected into their skin causing disruptive behaviour and so, secondary assistance is always required when drawing blood from neonates to stabilise the venous site (World Health Organization, 2010). With relation to elderly patients, venous access becomes increasingly difficult with age, as skin loses its tone and elasticity making it hard to locate veins for puncture. Additionally, an elderly patient's susceptibility to dehydration and low blood pressure will only contribute to the complexity of venous access. The loss of subcutaneous tissue also decreases vein stability, meaning they are prone to roll under the skin or collapse, which may result in the formation of haematomas (Menegolo *et al.*, 2018). Furthermore, geriatrics patients are more likely to present with comorbidities which can even further complicate blood extraction methods. It is estimated that up to 70% of elderly patients suffer from 5 or more chronic health conditions (Lomonte *et al.*, 2016). Elderly patients who suffer from arthritis, stroke or other injuries will have significantly less range of movement, thus, the simple hyperextension of an arm for venous access can prove difficult (Klosinski, 1997). The deterioration of muscle mass may result in their inability to clench a fist, again, only adding to the difficulty of blood extraction. Moreover, ageing patients may suffer from cognitive impairment or delirium and may therefore be unable to cooperate for blood sampling. These complications of fragile or inaccessible veins and needle phobia make it exceptionally challenging for patients who require regular blood testing.

Another concern that comes with phlebotomy procedures is the risk of a sharps injury. These sharps injuries include needle-stick injuries (NSIs), percutaneous injuries and mucocutaneous injuries. The potential for a NSI is a long-standing issue within the healthcare setting associated with the use and disposal of hazardous sharps. It's estimated that 80% of percutaneous injuries within care settings are attributed to NSIs, with over 300,000 needle-stick injuries reported annually in the US (Panlilio *et al.*, 2004; CDC, 2008; Grimmond and Good, 2017). It should be noted that this does not include the NSIs which go unreported, meaning the true value is conceivably more. Along with sharps incidents comes the risk of exposure and transmission of bloodborne pathogens (BBP). Accidental infection by exposure to blood or bodily fluids is greatly increased with the handling of sharps, since a needle that is used to penetrate the skin could potentially have been subject to tissue or blood containing

an infectious disease. With over 60 known BBPs, hepatitis B virus (HBV), hepatitis C virus and human immunodeficiency virus (HIV) account for the majority of occupation-related infections (Tarantola, Abiteboul and Rachline, 2006). Among healthcare professionals, the possibility of a NSI and furthermore, contracting an infectious disease by means of a sharps injury has detrimental effects to mental health, with 60% dealing with enhanced needle phobia and 42% associated with having post-traumatic stress disorder or depression post NSI (Elseviers *et al.*, 2014).

Needle-stick injuries are not confined to clinical settings but rather, are inclusive of community and home healthcare environments. An increase in home healthcare due to an ageing population, but also the devolution of centralised healthcare to community care, has resulted in many medical procedures that are routinely performed in the hospital now taking place at home, either by home healthcare workers (HCWs) or by self-administration (Quinn *et al.*, 2009). This puts care providers and self-administrating patients at risk of BBP infections by means of percutaneous sharps injuries, either during use or disposal of the waste. For this reason, many legislative requirements surrounding the topic of NSIs have been put in place to promote a safe working environment. The Occupational Safety and Health Administration (OSHA) Bloodborne Pathogen (BBP) Standard and the Needlestick Safety and Prevention Act of 2000, reported the most effective outcome in reducing sharps incidents by 34% after implementation (Jagger *et al.*, 2008). These legislations improved controls of keeping sharps injury records, better waste management and introducing safety engineered devices (SED) amongst other measures put in place to reduce transmission of BBPs by sharps injuries, however, despite these efforts, NSIs still occur (Tatelbaum, 2001). The incidence of these NSIs can typically be broken down into three categories: post procedure but prior to disposal (15%), during the procedure (40%) and during disposal (40%). These events can be further broken down as evidenced by the Centres for Disease Control and Prevention which is highlighted in **Figure 2.1.3**.

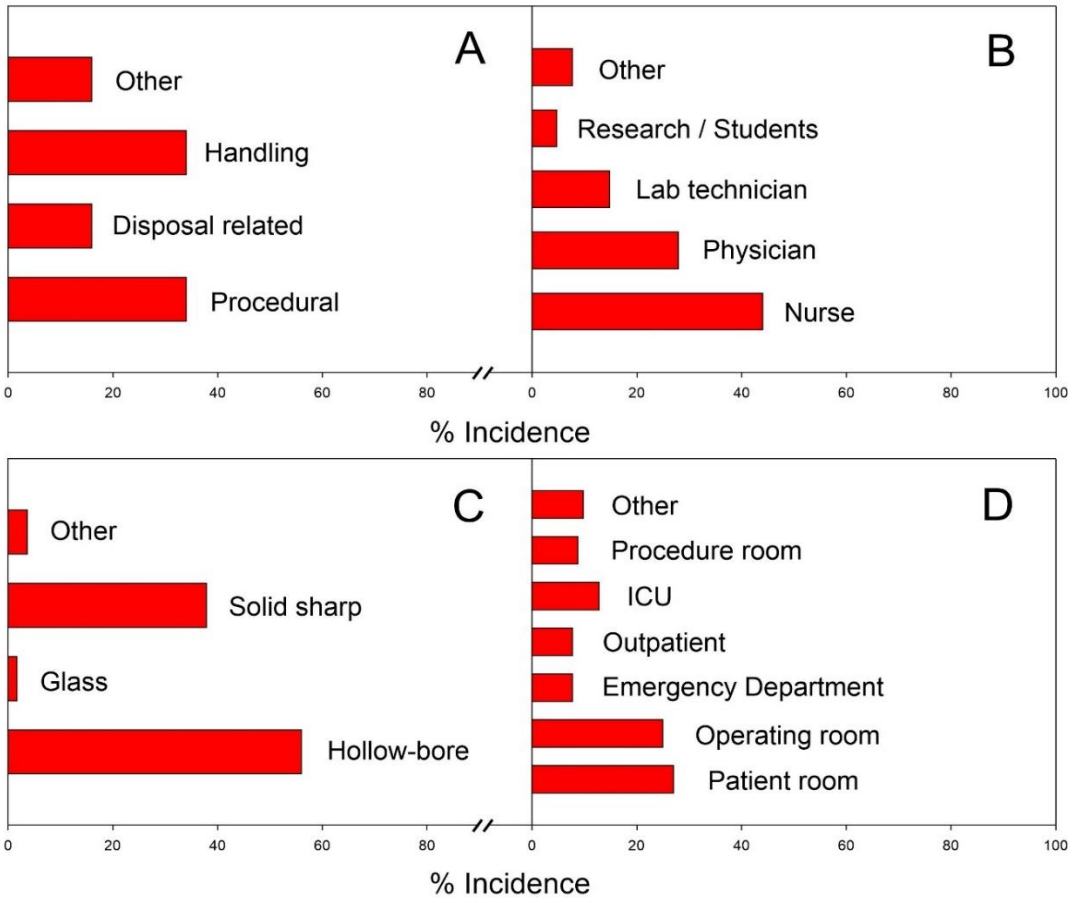

Figure 2.1.3 Incidence of needle-stick injury broken down by (**A**) process, (**B**) person, (**C**) device type and (**D**) location.

Another cause for concern, especially among self-administrating patients is the reuse of needles. This has become a worrying trend principally among the diabetic community. Disregarding the advice against the reuse of needles or lancets since it increases the susceptibility to infection, many diabetic patients reuse their sharps due to convenience at the time of measurement. Not only this, but the mechanical integrity of needles deteriorate with each use, creating the possibility of metallic fragments being left behind in the skin as well as advancing tissue scarring (Becton Dickinson, 2006). The issue of reusing and recycling needles is also common in less developed countries, again increasing the risk of transmission of BBPs. Additionally, in these less developed countries where scavenging is not uncommon, the combined lack of effective waste management procedures substantially increases the risk of NSIs and therefore, transmission of infectious diseases (Coker *et al.*, 2009). The consequences of improper disposal of sharps waste is a perennial safety issue that still exists within well-regulated environments, with the majority of disposal related sharps incidents

resulting from hypodermic syringes not being appropriately segregated from soft wastes and placed in plastic refuse bags (Blenkharn and Odd, 2008). The major contributing factor here lies in carelessness during disposal, which isn't surprising since it has been reported that 86% of diabetic patients do not follow the pertinent guidelines (Costello and Parikh, 2013). In light of this, a needle-free method of transdermal delivery for injections would be highly desirable in reducing the risk of NSIs.

2.2 Point of Care Diagnostics

Advancements in centralised laboratory testing has resulted in these systems becoming progressively more automated and efficient (Abel, 2015). Hospitals rely heavily on these large-scale automated systems for diagnostics however, they are unsuitable for bedside or emergency medicine where time is of the essence. Hence, there has been a shift in adopting point of care diagnostics which can process clinical samples in a range of environments such as, laboratories, ambulances, emergency rooms, general practitioner offices and within a patient's home. A point of care system is known as an integrated device that can be used near or in close proximity to a patient. The portability of a POC device encourages quicker turnaround times and medical decisions. Ultimately the short TAT of POC diagnostics is a faster route to treatment of the patient and, overall, improves patient outcomes (Vashist, 2017). Recent advancements in technology such as, micromachining, microfluidics, nanotechnology and 'lab on a chip' systems has further propelled the evolution of POC diagnostics and enabled the miniaturisation of diagnostic tools (Abel, 2015).

The evolution of biosensors in recent years has become the most auspicious movement towards a highly sensitive, cost-effective and rapid means of analysis within medical diagnostics (Mascini and Tombelli, 2008). The biosensor is recognised as the most critical component of POC devices since it is accountable for the bioanalytical performance of the diagnostic device (Vashist, 2017). The term biosensor has been defined multiple times, however, the core meaning associates an analytical device with a bioreceptor unit and a physiochemical transducer, an example of which is shown in **Figure 2.2.1**. The transducer element of the biosensor is generally categorised as an electrochemical, optical, piezoelectric, thermal or magnetic system and is used to compute the measurand from the

bioreceptor to an electrical or optical signal (Koyun, Ahlatcolu and Koca, 2012). Although there have been many developments from the first reported biosensor by Clark and Lyons in 1962, describing an electrochemical glucose oxidase (GOD) biosensor, blood glucose monitoring devices for use within a decentralised setting have since dominated this diagnostic POC biosensor market (Nambiar and Yeow, 2011; Makarona *et al.*, 2016).

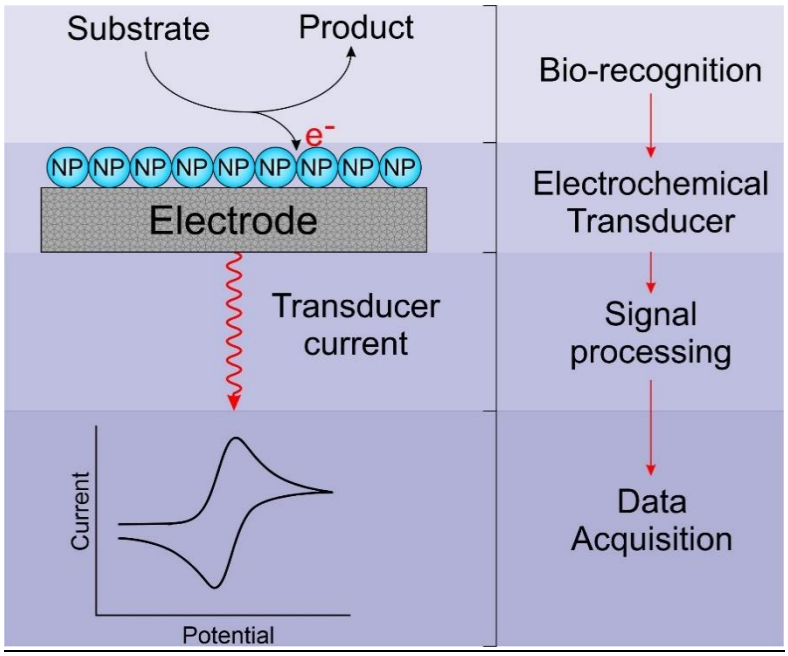

Figure 2.2.1 Depiction of the core elements within an electrochemical biosensor.

The expansion of POC diagnostics has transformed the way patients with diseases that require continuous monitoring or routine monitoring can manage their health. The increasing availability of biosensors that avoid the use of time-consuming conventional enzyme-linked immunosorbent assay immunoassay (ELISA) methods, or large non-mobile machines for vital signs monitoring has revolutionised the timely intervention of treatment for patients within clinical settings (Mascini and Tombelli, 2008). Not only this, but it has provided the opportunity for patients to manage their own health from the comfort of their own homes, especially for those who suffer from chronic illnesses such as diabetes, where routine discrete glucose sampling is required (Gouvea, 2011). The assimilation of wireless connectivity along with POC apparatus has found these devices transcending into a world of eHealth diagnostics. Previously many POC tools were only available to healthcare professionals (blood pressure meters, glucometers), but in recent years, these technological

advancements have instigated their availability and use among patients, thus, popularising the idea of mHealth (mobile health) applications and encouraging patients to engage with managing their own health (Nayak *et al.*, 2017; Christodouleas, Kaur and Chorti, 2018).

In recent years, the evolution of wearable sensors has seen a significant peak of interest encompassing wearable diagnostics for monitoring health status as shown in **Figure 2.2.2**. Again, supporting the prevention of disease for earlier intervention, thereby decreasing healthcare expenditures. Cardiovascular biomarkers in particular have garnered interest from MedTech companies for the idealisation of producing a wearable diagnostic with the capability of assessing these markers with the same level of reliability as current approaches of blood sampling. Biomarkers refer to a subcategory of medicine which can be accurately and reproducibly measured to provide characteristic information on the medical status of a patient (Strimbu and Tavel, 2010). The most commonly known biomarkers associated with cardiovascular health include: Cardiac Troponin, Creatinine Kinase, Myoglobin, C-reactive Protein and B-type Natriuretic Peptide. This is not an exhaustive list of cardiac markers, since novel markers are constantly being evaluated to determine the efficacy of their use for diagnostics purposes, some of which are explored within the investigative chapters of this thesis (Dutt *et al.*, 2005; Strimbu and Tavel, 2010).

In addition to this, galvanic skin response has also received substantial attention over the years with continuous research ongoing to fully understanding the systemic effects for variation in electrical properties of the skin. This form of electrodermal activity has previously been used for the development of ECG diagnostics and has been proven to be a direct marker for emotional or psychological strain (Crifaci et al., 2013; Posada-Quintero and Chon, 2020). It has also been recognised that the ability of sweat markers to reflect the metabolic state of a patient via electrolyte monitoring, holds the promise for next generation diagnostics (Brasier and Eckstein, 2019). However, this type of sensing is susceptible to the limitations of non-invasive smart wearable diagnostics. Inconsistencies with metabolite concentration along with the variation of sweat volume poses a huge issue for calibration. Sweat composition tends to vary depending on gender, ethnicity, age, physical fitness and a range of other environmental factors and, since sweat glands are not evenly distributed along the body's skin surface, in combination with sweat evaporation, this makes it incredibly difficult to design an accurate and reproducible diagnostic device for sweat analysis (Brasier

and Eckstein, 2019). Despite sweat markers remaining a topical point of discussion for numerous diseases such as tuberculosis, schizophrenia and Parkinson disease, blood sampling remains the reliable option for biomarker analysis (Brasier and Eckstein, 2019).

There has been considerable commercial success from tech companies like Fitbit® and Apple Watch® in the wearable sensors market. These applications have allowed tracking of vital signs such as heart rate, blood pressure and SpO2, granting this information to be monitored by the wearer and furthermore, can be invaluable data for a clinician in the event of a medical emergency. The endorsement of these types of wearable sensing technologies has also proven enticing to insurance companies, whom in the future may use this data to their benefit for health insurance policies and to encourage wearers to lead a healthier lifestyle (Spender *et al.*, 2019). Parallel to this, the concept of mHealth applications has directed a move away from traditional diagnostic methods for diseases which require regular sampling. An example of an early attempt at this includes the FreeStyle Libre® glucose monitoring system by Abbott. The FreeStyle Libre® demonstrates a smart wearable patch for discrete sampling of blood glucose, rather than the traditional sequence of glucose monitoring which requires a pin prick of blood to be dropped onto an external biosensing device. This initiative decreases the numerous times a diabetic patient would have to perform blood extraction for glucose sampling, which carries an association of fear and pain for many patients. The smart glucose patch is a highly desirable alternative for many users, however, it still requires a painful application method of the patch that needs to be replaced every 14 days and requires high costs for manufacture (Sharma *et al.*, 2017). The benefits of smart biosensing have captivated the medical diagnostic community and has driven this field of research over the last decade. It has been noted that the integration of a biosensor into a smart wearable which is capable of sensing a range of analytes within the blood could be integral to the next generation of decentralised health monitoring (Miller, Narayan and Polsky, 2016). Going a step further than this, a futuristic approach of a closed loop system or an autonomous smart wearable could be envisaged, where a sensor detecting an abnormality would feed back information to the wearer or carer, and allow the transmission of signal to a complementary actuator component that could administer appropriate drug concentrations to the patient – ideally integrated within the same wearable.

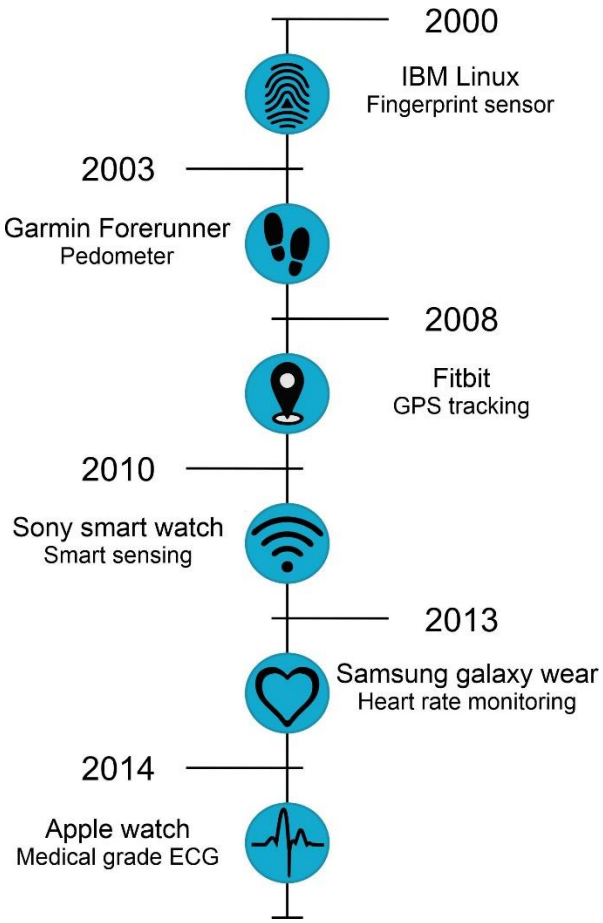

Figure 2.2.2 Timeline demonstrating the major technological advancements in wrist wearable sensors.

The vast volume of research put into POC diagnostics has seen an exponential growth in the market, which was once estimated being worth more than $23 billion in 2016 and is now expected to increase to $37 billion in 2021 (Vashist, 2017; Dhawan, 2018). Contrastingly, it should be noted that the difficulty in bringing an innovative diagnostic device from concept to market has also increased. The predicted cost of bringing a new biodevice (i.e. 510(k) product) from initial concept, through various development phases and into commercial reality is approximately $30 million. The majority of this cost is driven by regulatory dependant and/or related activities required to gain regulatory approval such as obtaining investigational device exemption, where inefficiency or unforeseen delays have a direct impact on accumulation of cost (Makower, Meer and Denend, 2010; Christodouleas, Kaur and Chorti, 2018). The success of a new clinical product is defined by the device design characteristics, where careful consideration should be applied when deciding if it is solving a 'real world' problem or need (Kumar *et al.*, 2015). Other attributes which play a vital role in device design include

selectivity, sensitivity and robustness, all of which contribute to the overall performance of a biodevice but may also garner commercial advantage if competing against an already existing product. Another factor which has developed in correlation with emerging mHealth technologies, involves the level of interactivity between the POC device with the user, as well as the ease of use. Again, this relates to the necessity of trained professionals being required to use high end laboratory equipment, whereas a POC device should eliminate certain complexities and avail of non-trained users being able to navigate the technology with ease. It can be anticipated that this would most certainly have an impact on user compliance, where the user may become reluctant to use the technology if it is time consuming, complex and/or requires a substantial amount of user input (Mascini and Tombelli, 2008; Bhalla *et al.*, 2016). This further highlights the progression towards personalised medicine with autonomous smart systems capable of minimal user input (Miller, Narayan and Polsky, 2016).

2.3 Screen Printed Electrodes

When designing a biosensor, there are many crucial features to consider such as: the limit of detection (LoD), resolution, multi-parameter analysis capability, dynamic change, cost/time effectiveness and degree of user-friendliness. In terms of biosensing, electrochemical sensing methods are seen as advantageous given their relatively simplistic fabrication and adaptability for miniaturisation. Additionally, electrochemical analysis is rapid considering the transducers used are highly specific and sensitive bio-recognition sites, thus, their exploitation for biomedical diagnostics is ever increasing (Vestergaard *et al.*, 2015). Disposable screen printed electrodes (SPEs) are an example of an ideal electrode for electrochemical sensing which has become the standard electrode component used and integrated within POC blood glucose sensors (Mascini and Tombelli, 2008). Diabetic patients are common users of enzyme functionalised SPEs to evaluate their blood glucose levels. This is typically done by obtaining a capillary blood sample (i.e. finger prick) which, when applied to the SPE connected to the portable meter can provide a diagnostic reading in less than one minute. Since coming into effect, blood glucometers have dominated the biosensing market, capturing 90% of the global sector (Cinti, Moscone and Arduini, 2017). Although there have been several advancements in blood glucose detection technology, there has been a lack of development in the painful blood extraction method for glucose readings. This has of course

led to reluctance of some patients to comply with managing their disease due to needle phobia and is still an issue that the medical sector is trying to overcome.

The attractiveness of using SPEs rests on the ease of low-cost mass production and the reduced volume of sample required for diagnosis. Fabrication of the electrodes involves depositions of successive ink layers onto a hard heat-resistive substrate, typically a plastic or ceramic material. The ink layers are generally printed through a patterned screen or mesh into a three-electrode format demonstrated in **Figure 2.3.1** (working, reference and counter electrode), thereby defining the geometric area. The final product is then subjected to a thermal curing process, annealing the ink layers with the substrate and increasing the stability of the electrode (Yamanaka, Vestergaard and Tamiya, 2016). This relatively cheap fabrication method also lends itself to the 'single shot measurement' characteristic of blood glucometers, as currently these systems rely on discrete sampling, affording the SPEs to be disposed of after one use. On the contrary, it has been highlighted that the disposable nature of the electrodes may contribute to issues with safe disposal, since the used SPEs effectively become hazardous waste after use (Vranić *et al.*, 2020). Or, it could be argued that the single use of SPEs avoids common problems with conventional solid electrodes, such as tedious cleaning processes (Taleat, Khoshroo and Mazloum-Ardakani, 2014). Despite this, the expendable attribute of SPEs and their affordability has made them increasingly available within healthcare settings but also within the community. This has been a critical step in advancing towards self-management of diseases through the use of POC biosensors.

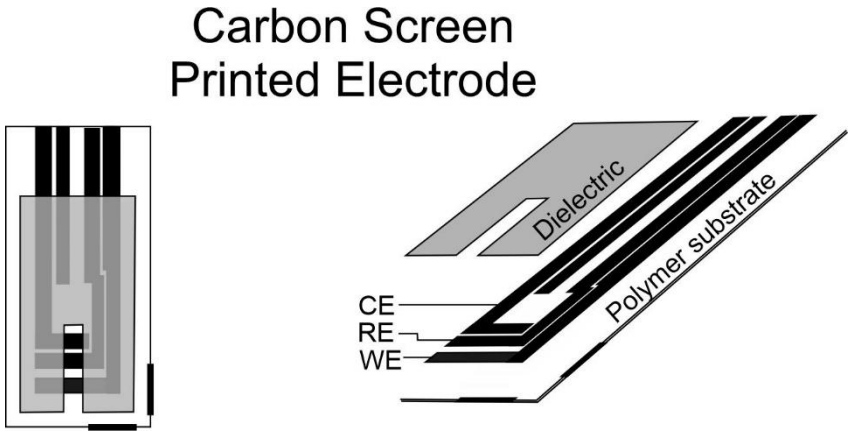

Figure 2.3.1 Schematic of typical carbon-based screen printed electrode employed by the KEYA Smart® glucose meter (courtesy of Inside Biometrics Ltd).

Recent innovations in technology have streamlined manufacturing processes for ease and low-cost, mass production of screen-printed electrodes. Although this kind of thick film technology has been around for thousands of years since the early beginning of printing, it's only in the past few decades that the technology has been utilised for POC diagnostics (Vestergaard *et al.*, 2015). The fundamental development in blood glucometers was the downsizing or miniaturisation of testing created by the use of SPEs and their portable analyser counterpart. In doing so, it has reduced the volume of blood required per sample to mere microlitres for electrochemical analysis, further helping to minimise the size of the overall device (Taleat, Khoshroo and Mazloum-Ardakani, 2014). Again, this has contributed to the move away from laboratory testing and onwards to POC diagnostics. With ever-developing nanofabrication techniques, the dispersion of these inks onto flexible substrates has consequently resulted in the production of highly reproducible, robust and stable electrodes. This innate design of easily modifiable inks onto a plethora of substrates has provided SPEs with an unprecedented advantage in versatility and accuracy, which has largely contributed to their unrivalled success with respect to POC glucose sensing (Vestergaard *et al.*, 2015; Yamanaka, Vestergaard and Tamiya, 2016).

Another advantage of using SPEs is the variety of inks that can be used to print, which can allow the fine tuning of the base substrate's sensitivity and selectivity towards particular target analytes. Commercially available carbon and silver inks are most commonly used for printing the working and reference electrodes respectively as they are relatively inexpensive. The formulation of carbon inks are of particular interest within electrochemical sensing applications due to their broad potential window and low background currents. The carbon inks are typically composed of graphite particles in a polymeric binder which can be supplemented by the addition of other compounds (metals, enzymes, complexing agents etc.) to aid the dispersion and adhesion between the ink and substrate (Wang *et al.*, 1996; Economou, 2018). Although, selection of the particular type of carbon ink will depend on the technique and end application. This was highlighted by Wang et al (1998) when they investigated the use of four different commercial carbon inks and compared their relative electroanalytical performances (Wang *et al.*, 1998). Slight variations in curing conditions,

size and carbon loading can alter the electron transfer and ultimately the analytical performance of the resultant carbon sensor. Conversely, the versatility of these inks offer an extensive range of surface modifications, making them suitable for a diverse field of applications such as, electrochemical immunosensors, aptasensors and enzyme based biosensors (Taleat, Khoshroo and Mazloum-Ardakani, 2014; Yamanaka, Vestergaard and Tamiya, 2016).

Aside from the commonly used conductive components of SPEs, insulating polymers are routinely used for electrical shielding, creating a dielectric pathway to define the geometric area of the deposited inks, but also to increase the shelf life of the electrode (Vestergaard *et al.*, 2015). Although inert carbon ink remains the ideal choice of conductive material due to its cheap availability, other metal inks have been demonstrated to provide their own advantages, such as gold. The application of gold paste employed in SPEs has become increasingly researched among the electrochemical biosensor community, since the strong affinity between gold and thiol moieties can be easily modified to form self-assembled monolayers. This has broadened the exploitation of SPEs to be used as enzymatic, immuno- and genosensors (Taleat, Khoshroo and Mazloum-Ardakani, 2014). Other processes like pretreatment of the SPEs have also been used to improve electrode performance. Electrochemical methods such as potential cycling and pre-anodisation have been established as appropriate methods to enhance sensing abilities of SPEs (Metters, Kadara and Banks, 2012). Moreover, methods of removing contaminants in the ink to reduce electron transfer resistance include using printed pastes rather than inks, since insulating polymer may be found integrated within the ink. Noble metals have also been composed within the pastes acting as electrocatalysts, further enhancing electron transfer kinetics, although, as noble metals are known to be expensive, manganese oxide and bismuth oxide have been utilised as suitable alternatives (Wang and Tian, 1993; O. Domínguez and Arcos Martínez, 2007). The trend to be noted here is that little promise is held in detecting analytes of interest from standard carbon ink SPEs, but rather by modification of the electrode (Taleat, Khoshroo and Mazloum-Ardakani, 2014).

With particular focus on the application of SPEs as medical biosensors, modification techniques remain popular. As previously mentioned, the most common modification employs enzymatic approaches for glucose analysis in order to confer a high degree of

selectivity towards the key analyte B-D-glucose (Wang and Chen, 1994; Taleat, Khoshroo and Mazloum-Ardakani, 2014). The facile means of modification strategies for SPEs makes them ideal for glucose POC diagnostics, however, it also drives their potential to be utilised in other ways. There are a vast number of analytes, more specifically cardiovascular related analytes, that still depend on ELISA techniques or other oversized automated equipment for analysis (Mascini and Tombelli, 2008). Thus, there is scope to mimic or rather adapt the base system for use with other enzyme catalysts for the application of multi-analyte sensing. Unmodified personal glucose meters for use other than sensing glucose was first reported by Xiang and Lu (2011). In their observation, they proposed the use of the enzyme invertase which catalyses the hydrolysis of sucrose into fructose and furthermore, glucose, deriving a direct relationship between invertase and glucose. From this, they developed detection methods for non-glucose targets including, cocaine, adenosine, interferon-gamma of tuberculosis and uranium, with many more instances of blood glucose meters being used to detect non-glucose targets reported since (Lan, Zhang and Lu, 2016). This displays the unrivalled adaptability of SPEs to be tailored for a diverse range of analytes through simple modification techniques. Thus, the field of SPE application continues to grow as evolving research emerges.

The versatile nature and increasing adaptability of SPEs has propelled their research into diverse categories providing many diagnostic advantages to clinical, agricultural, food and environmental industries (Cinti, Moscone and Arduini, 2017). Nonetheless, the overriding disadvantages to using this type of technology still exist, including the painful finger prick required for blood sampling and the restriction of screen printing being limited to flat substrates. Further repercussions from these disadvantages have resulted in compliance issues with patients and problems with safe disposal of hazardous waste. In light of this, initiatives such as the FreeStyle Libre® glucose monitoring patch is an example of the progressive step towards smarter sensing modalities. The system offers the wearer discrete wireless sampling and has been shown to increase the frequency of self-testing among wearers, thereby improving compliance. Although the patch reduces the persistent number of painful blood sampling extractions, it is highly dependent on the specific placement of the patch and may cause irritation during daily activities with movement of the arm or the patch itself (Al Hayek, Robert and Al Dawish, 2020). Thus, there is capacity for further improvements to migrate towards a non-painful, smart sensing application (Sharma *et al.*, 2017).

2.4 Microneedles

In relation to microsensors, the past decade has seen significant interest around the use of microneedles (MNs) as a drug delivery method and for in vivo sensing (Khanna *et al.*, 2008; Arya and Prausnitz, 2016). In light of this, the research project described here is primarily focused on the development of microneedle sensors. A microneedle can be described as a multiplicity of micron-sized protrusions, in varying lengths, assembled on the face of a supporting base plate. Microneedles can confer numerous advantages over the conventional use of hypodermic needles for the withdrawal of blood or injection methods. Microfabrication methods of MNs makes them suitable for piercing through the stratum corneum of the skin to contact the blood supply, but the projections on the base plate are not long enough to disrupt the dermal nerve network and so, no pain is felt, as shown in **Figure 2.4.1** (Miller, Narayan and Polsky, 2016). Their minimally invasive nature makes it virtually painless for the patient, thus overcoming barriers such as needle-stick injuries (NSI) and emotional trauma associated with traditional methods of blood sampling. Avoiding the distress of needle injections can be particularly important when applied to the paediatric population thus, microneedles provide a much more appealing option and may also increase patient compliance (Jeong *et al.*, 2017; Quinn, Hughes and Donnelly, 2018). Not only this, but the ability of the MNs to penetrate the stratum corneum and deliver a drug, escapes the need for gastrointestinal metabolism of medications. It also makes them a suitable alternative to transdermal drug patches, where drug administration can be severely limited by permeability of macromolecules across the skin (Duarah, Sharma and Wen, 2019).

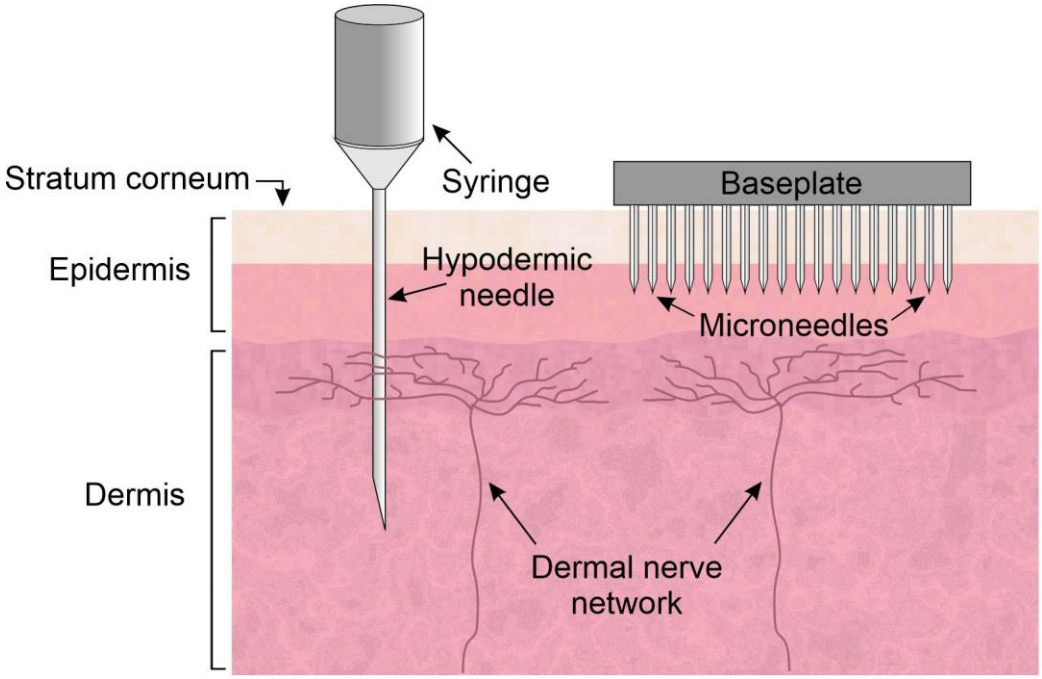

Figure 2.4.1 Penetration depth of microneedle against conventional hypodermic needle.

The concept of MNs was first disclosed in 1976, which described a percutaneous administering drug delivery device comprising of an array of projections, extending from a drug containing reservoir (Gerstel and Place, 1976). However, the theory of MNs wasn't experimentally studied until the 1990s when Henry et al. (1998) examined the application of MNs for transdermal drug delivery (Prausnitz, 2004). Advances in microfabrication technology were the main driving force that enabled this theoretical application of microneedles to be tested practically. Their investigation observed the effects of using solid microneedles, fabricated by a reactive ion etching technique, for transdermal drug delivery of calcein across human epidermis as opposed to traditional chemical enhancement techniques. A 'poke and patch' approach of inserting the MNs for varying lengths of time was employed, thereby creating micro-channels in the skin, followed by the topical application of calcein drug upon removal of the MNs. It was also noted that the holes generated would reseal, however, the kinetics of resealing was not yet known at that point. Their study indicated an increase in percutaneous transport by more than 4 orders of magnitude and was the first demonstration of how microneedles can be applied to permeabilise human skin in a nonpainful, safe manner (Henry *et al.*, 1998).

Subsequent research in the microneedle community has predominately focused on novel microfabrication techniques. The variety of innovative fabrication technologies and geometric designs has seen MNs applied to a diverse range of applications from microneedle mediated immunisation in 2002, to the first reported use of microneedle based diagnostic sampling in 2005 (Mikszta *et al.*, 2002; Wang, Cornwell and Prausnitz, 2005). Currently, MN fabrication can be classified into five categories: solid, hollow, coated, swellable and dissolvable (Chege, McConville and Davis, 2017). The basic mode of operation for each is summarised in **Figure 2.4.2**. Microneedles have previously been developed from a variety of materials such as metals, ceramics, biodegradable and non-biodegradable polymers. More recently, there has been particular interest surrounding metallic and polymeric materials for MN construction among the scientific community. This can be placed on the advancements from traditional micro-machining or micro-electromechanical systems (MEMS) and lithographic methods, to micromoulding technology for microfabrication of biosensors (Duarah, Sharma and Wen, 2019). It should be noted that the type of microneedle, material composition and fabrication technique to be employed depends on the microneedle functionality required. A summary of the diverse range of methods and materials for microneedle manufacture can be observed in **Table 2.4.1** (Yun Yang *et al.*, 2013; Chege, McConville and Davis, 2017; Duarah, Sharma and Wen, 2019; J. Yang *et al.*, 2019).

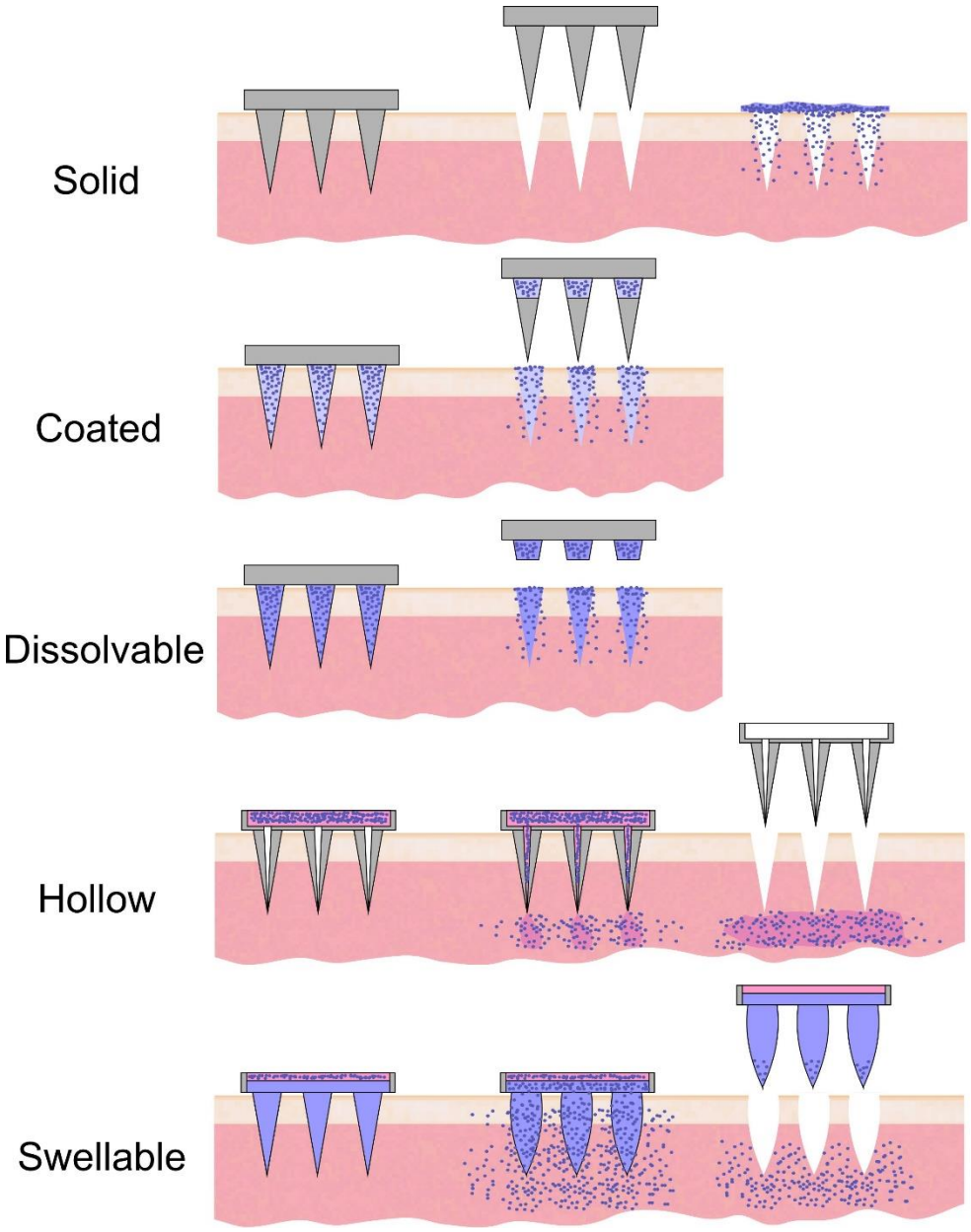

Figure 2.4.2 Representation of microneedle categories and their respective method of application.

Table 2.4.1 Common methods of microneedle fabrication and materials used.

Type	Fabrication method	Materials
Solid	Dry-etching, wet-etching, reactive ion etching, acid etching, photo lithography, magnetorheological lithography, laser ablation, micromoulding, electroplating, 3D-printing, micromachining	Non-biodegradable (silicon), biodegradable polymers (PMVE/MA, polycarbonate, PMMA, maltose), metals (stainless steel, titanium, and nickel), ceramics and biopolymer films.
Coated	Coating methods include dip coating, Layer by layer, piezoelectric inkjet printing	MN coatings of drug-containing dispersion particularly those of high molecular weight (DNA, proteins, peptides, vaccines).
Dissolvable	Micromoulding, ultrasonic welding, 3D-printing, micromachining, ion etching, centrifugal lithography	Polysaccharides, polymers (PLA, PGA, PLGA, PVP, PVPMAA, PMVE-MA), biopolymers (sodium hyaluronate, chondroitin sulphate) and carbohydrates (sugars, carboxymethyl cellulose, maltose)
Swellable	Solvent casting, micromoulding, micromachining, ion etching, centrifugal lithography	Polymeric compositions, thermosensitive copolymers (maltose, PS-PAA).
Hollow	Lithographic moulding, micromachining, photolithography, 3D-printing, ion etching, wet chemical etching, milling, resin polymerisation, two-photon polymerisation, metal electroplating, drawing lithography,	Silicon, metals, glass, polymers, ceramics and carbohydrates.

(Poly methyl vinyl ether-maleic anhydride (PMVE/MA), polymethylmethacrylate (PMMA), polylactic acid (PLA), polyglycolic acid (PGA), polylactic-co-glycolic acid (PLGA), polyvinylpyrrolidone (PVP), poly vinylpyrrolidone-co-methacrylic acid (PVPMAA), polystyrene-block-Poly acrylic Acid (PS-PAA))

2.4.1 Microneedle Sensing

2.4.1.1 Microneedle Assisted Fluid Extraction

With such a vast number of fabrication techniques available, the microneedle geometry can be tailored to suit the depth of needle penetration required. The projections of MNs have been produced in a number of shapes (pyramidal, conical etc.) and sizes (25 – 2000 μm in length), making them ideal candidates to penetrate the skin and come into contact with blood. The ability to adapt needle geometry according to MN purpose has seen a huge focus on drug delivery methods by means of microneedles, but more recently, their use for biosensing is becoming apparent (Miller, Narayan and Polsky, 2016). Prausnitz et al. (2005) were the first to report the utilisation of microneedles as a transducer for glucose monitoring. Their methods involved hollow glass MNs for extraction of interstitial fluid (ISF) by reverse iontophoresis, followed by analysis ex vivo. This established the opportunity to use these microscale needles as a biosensing unit. The majority of research on microneedle-based sensors has since focused on glucose monitoring, with limited publications based on targeting analytes other than glucose. Societal demand for an alternative solution to the finger prick method for blood glucose sampling has been the main reason for such focus on MN based glucose sensing, although, this has resulted in a neglect of other analytes present in the underutilised ISF (Miller *et al.*, 2018).

2.4.1.2 Microneedle-Based In Vivo Sensing

The composition of interstitial fluid has previously been described as information rich, containing invaluable biomarkers such as nitrogen oxides (typically NO as well as NO_2^-/NO_3^-) , glucose, potassium and sodium ions (Takeuchi and Kim, 2018). As a result, the first instances of MN biosensing has revolved around MN assisted biological fluid extraction for analysis. A number of issues have been identified with this method, namely that it presents with the issue of delay in analysing the sample, much like the POC blood glucose sensors, where, once the fluid is extracted, the measurement is effectively outdated. Swellable and

hollow microneedle designs have both been shown to be successful in facilitating the extraction of biological fluids for ex vivo analysis (Caffarel-Salvador *et al.*, 2015; Takeuchi and Kim, 2018). However, solid, coated-solid and hollow microneedles have previously been demonstrated as appropriate, minimally invasive continuous monitoring systems for the direct measurement of glucose, lactate and antibiotic drug dosage from extracellular fluid (ECF) (Rawson *et al.*, 2019). The ability of these MNs providing real-time analysis of biological fluid in vivo has many advantages over the latter option of fluid extraction for external analysis, especially the possibility to incorporate a closed-loop system in the future.

The application of hollow microneedles for biosensing has been well established using fluid extraction methods, either by capillarisation of the ISF or by integrated sensor designs (Takeuchi and Kim, 2018). However, research produced by Windmiller et al. (2011) demonstrated the importance of transdermal sensing at the MN interface and initiated the use of hollow MNs as an electrode transducer. In their 2011 study, they presented 3D printed hollow MNs packed with carbon paste, effectively creating a solid microneedle. The carbon paste, which is known as a desirable material for electroanalysis due to its low background currents and surface modification properties, was chosen as the conductive element of the electrode (Windmiller *et al.*, 2011). They expanded on this work by incorporating an on-body biofuel cell (BFC) to act as a self-powered biosensor (Valdés-Ramírez *et al.*, 2014). These hollow MNs were exhibited to be functioning biosensors, yet it should be noted the 3D printing approach remains difficult to obtain the resolution required at the micro level, is not always an accessible feature in the typical laboratory setting and may not lend itself easily to upscaling for mass production of disposable hollow MN electrodes.

For the purposes of biosensing, where a microneedle patch would most likely be single use, much like the screen-printed electrodes used for glucose sensing, it would make sense for the fabrication method to involve a facile means of low-cost rapid prototyping. Since techniques like micromachining and ion etching are known to be costly or complex, it is of no surprise that of the limited literature available for sensing microneedles, a converging interest around micromoulding technologies within a laboratory setting has become apparent (Rezaei Nejad *et al.*, 2018). Micromoulding offers the opportunity to quickly cast MNs repeatedly from different material compositions, optimising the desired parameters

and eventually up-scale the fabrication process for mass production (Krieger *et al.*, 2019). Micromoulding methods for fabrication of solid MNs typically involve a MN mould of the desired geometry and casting the chosen material into the mould, either in molten form and allowed to cool (hot embossing and injection moulding) or dissolved in a solvent and allowed to evaporate off (solvent casting), as demonstrated in **Figure 2.4.3**.

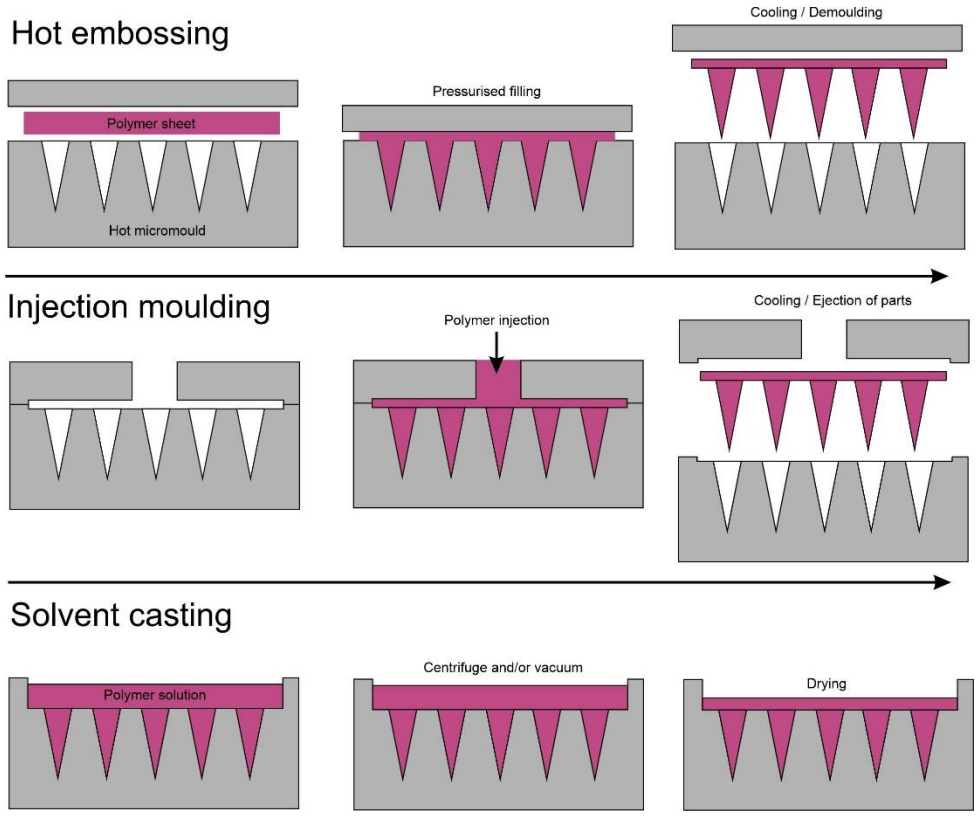

Figure 2.4.3 Fabrication processes for micromoulding methods of solid microneedles.

Another factor to consider when micromoulding is the material composition of the needles, which would also be required to transmit some form of signal, hence, a conductive type of material (metallic or otherwise) is typically incorporated to facilitate the MN array acting as an electrochemical transducer. Material selection is vital with relation to biosensing performance, as selectivity, functionalisation, protein adhesion, electrical and electrochemical properties all rely on the physical composition of the electrode. Thus, micromoulded MN biosensors are generally constructed by a polymer or a composite material containing a polymeric substitute that has been sputtered with a conductive coating. Sharma et al. (2017) recently described the cost-effective production of

functionalised micromoulded MN arrays for use as molecular sensors. Polycarbonate MN arrays were manufactured by injection moulding and subsequently sputtered with a chromium/platinum coating to facilitate functionalisation towards a specific analyte by electropolymerisation of the retrospective polyphenol. This work demonstrated a forward-thinking approach for the application of low cost MNs to be incorporated within smart wearables as minimally invasive diagnostic sensors.

An appealing feature of utilising micromoulding as the chosen method for MN fabrication is the extensive variety of materials that can be incorporated, especially when integrating a material that gives rise to different functionalities. This can be done either in the form of a composite material or the application of a coating to the moulded part. In the work reported by McConville et al. (2016), they characterised a palladium|polymer composite microneedle array as a transdermal sensor. Their methods included solvent casting of the composite material into silicone microneedle templates. The incorporation of palladium nanoparticles into the composite MN enabled electrical conduction for electrochemical analysis, but also facilitated surface modification by means of thiol monolayers upon immersion in cysteine solutions. Cysteine is known to be a biocompatible amino acid modifier, thus, adsorbing these thiol functional groups to the metallic Pd MN interface was shown to improve electron transfer kinetics and overall electrochemical performance (McConville and Davis, 2016). This approach highlights the advantages of micromoulding techniques for MN fabrication, where the facile means of rapid prototyping within a laboratory setting, can be easily customised towards sensing a range of transdermal analytes by the substitution of the metallic component with another viable nano particulate.

Many of the studies that focus on sensing microneedles, requiring an electrochemical interface between the biological fluid and MN surface, have employed a coating of conductive layers onto the electrode surface. This method of coating is typically done by electroplating or vapor deposition to overcome the cost and complexity of MEMS techniques (Takeuchi and Kim, 2018). Although, as mentioned previously, the availability of micromoulding offers the opportunity to incorporate these conductive materials directly into composite MN arrays for sensing functionality (McConville and Davis, 2016). Carbon-based materials have recently gathered considerable interest among electrochemists. Their high conductivity facilitates fast electron transfer and, in some cases, remarkable chemical

reversibility has been observed (Ji, Zhang and Zhang, 2015). Additionally, the slow kinetics of carbon oxidation provides a wide potential range for electrolysis. A carbon-based material will also possess a rich surface chemistry, of which the carbon backbone may also be functionalised towards other atoms, which provides promise that the material can be tailored for a variety of other applications (Ambrosi *et al.*, 2016). Much like with screen printed electrodes, the versatility of conductive materials that may be introduced into micromoulded MNs creates endless possibilities to sense a multitude of analytes. However, it must also be noted that during the micromoulding process, a balance of material ratio (polymeric binder : conductive element) is required to maintain electroconductivity and mechanical structure of composite MN arrays (McConville and Davis, 2016).

Material selection is critical and depends on the structural integrity and biocompatibility of the needles. Although the fabrication of conventional hypodermic needles and lancets is now well established as a biocompatible method of blood extraction, these sharps are considered biohazardous waste after use and may contribute to an increase in cross contamination or risk of infection if used on more than one person (Vranić *et al.*, 2020). The disposal of these hazardous needles has been recognised as a serious health and safety issue, considering 80% of percutaneous injuries within healthcare settings is attributed to needle-stick injuries (NSI) (McConville, Hegarty and Davis, 2018). Microneedles on the other hand, overcomes many of the obstacles affiliated with hypodermic needles. With the projections from MNs being a matter of hundreds of microns in length, it takes minimal force to penetrate the skin, approximately the same force (<10 N) as to push an elevator button (Henry *et al.*, 1998; McConville, Hegarty and Davis, 2018). As before mentioned, particularly with the 'poke and patch' approach, which leaves microchannels in the skin, the passive resealing of skin after MN puncture is not yet understood. Another factor that becomes relevant when utilising a MN patch over a period of time is the process of desquamation, where humans shed their entire outer layer of skin occurs every 2 to 4 weeks (Weschler *et al.*, 2011). Henry et al. (1998) recorded in their study of transdermal drug delivery, the event of needle tips breaking upon insertion. It was noted that only the top 5 to 10 µm of the needles were damaged and could be easily removed from the skin. In light of this, a lot of research into needle integrity after skin penetration has been studied across a variety of material compositions. Thus, it is important to avoid initiating an immune response from the chosen material, but also that the mechanical properties are strong enough to withstand

needle tips breaking and being left behind in the skin which could evolve into a biocompatibility issue.

The idealisation of exploiting microneedles for painless methods of biosensing, expands their application beyond drug delivery methods and promotes an abundance of possibilities, particularly their integration with smart sensors. The wearable sensor market is expected to grow to over 1.1 billion users in the year 2022 (Statista, 2019). Integrating MNs within smart wearable systems could become the next wave of body wearing technology. It could well become the next generation of decentralised testing and home health monitoring. Not only would this minimise the relationship between needle phobia and conventional POC methods, but it delves into the prospect of continuous monitoring of analytes within the blood, rather than the standard discrete sampling approach. Wireless telemetry of this data could also be vital for clinicians or statisticians to enable earlier interventions and improve clinical outcomes thereby, relieving the healthcare system of laboratory testing duties (Miller, Narayan and Polsky, 2016). Furthermore, the ability to harmonise a MN electrode within a smart wearable system gives rise to the possibility of engineering a fully autonomous, closed loop system, where a therapeutic drug could be directly released through MN projections and into the blood. However, much work needs to be done before MN sensors could be fully translated into medically recognised wearable systems (Goud *et al.*, 2019).

2.5 Conclusions

Considering the literature based here, it is evident that there is a need for an alternative to conventional blood analysis methods. Of the current diagnostics and smart wearable sensors available on the market, the limitations of slow turnaround times, painful sampling procedures and resultant injuries from exposure to sharps still exist. There is scope to miniaturise these blood sampling techniques and provide point of care measurement in the form of a micro-sensing system. Thus, a microneedle array capable of sensing parameters within the blood would provide a suitable platform for minimally invasive continuous monitoring in vivo and, potential for a wireless smart system for use in community care. Until now, many microneedle arrays capable of biosensing are manufactured by expensive

micromachining processes. The adoption of micromoulding techniques for the fabrication of transdermal drug delivery microneedles in recent years has established a new method by which composite microneedles may be manufactured. Hence, by translating pre-existing electrochemical sensing techniques used for screen printed electrodes to composite microneedles, an innovative approach for microneedle biosensing is proposed.

CHAPTER 3

Experimental Materials and Methodologies

Abstract

An overview of the experimental techniques, instruments, materials and accompanying parameters used throughout this project research are outlined here. The theoretical principles of such experimental methods are described with the perspective for use within this research. Further experimental details specific to each investigation are also included within each chapter as appropriate.

3.1 Electrochemical Materials and Instrumentation

Electrochemistry is described by the relationship of rate of flow of electrons derived by chemical changes. It becomes an invaluable qualitative and quantitative analytical tool by observing thermodynamics and electron transfer kinetics upon probing electrochemical reactions. An external power source (such as a potentiostat) is commonly used to manipulate a potential difference between electrode and solution, thus, inducing electron transfer. Heterogeneous electron transfer is often employed to investigate the detection of biological analytes by redox processes at potentials specific to the analyte of interest and experimental conditions. Complex biological media often makes analyte detection difficult with a multitude of electrochemical interferences, however, the ability to chemically or physically modify the working electrode of an electrochemical cell offers molecular specificity by adjusting potential windows and reducing/promoting surface adsorption. A variation of modification strategies has been utilised in this work and is further detailed in each chapter. The low cost of instrumentation required for electrochemical analysis is considerably advantageous over alternative laboratory techniques and, with the rapid evolution of research surrounding electrode material application and modification, it has propelled this analytical tool into a diversity of research fields including; biomedical, renewable energy, industrial and environmental.

Of the various electrochemical experiments undertaken, all available reagents were obtained from Sigma Aldrich (Dorset UK) and were of the highest grade possible unless otherwise stated. Investigations were also completed under room temperature conditions ($22^{o}C \pm 2^{o}C$), with all stock solutions prepared by Britton-Robinson buffer (acetic, boric and phosphoric acids of 0.04 M concentration) and the resulting pH adjusted by the addition of concentrated NaOH. Solutions are comprised of deionised water from an Elgastat water deioniser (Elga, UK), with potassium chloride (0.1 M) added to all buffer solutions, thereby providing sufficient electrolytes, but also defining the reference potential for pseudo references. In the cases where more complex matrices were required to test electrode response, defibrinated horse blood acquired from TSC Bioscience (Buckingham, UK) was utilised.

Electrochemical investigations were completed using a μAutolab Type III microprocessor controlled potentiostat (Eco-Chemie, Utrecht, Netherlands). Typically, a three-electrode system was employed for conducting experiments, with platinum wire as the counter electrode and a Ag|AgCl (3 M KCl) half-cell as the reference electrode (BAS Technicol, UK). On the occasion where a two-electrode configuration was used, a Ag|AgCl coated substrate (either microneedle, fibre or wire) was used as a combined counter/reference electrode. To complete the electrode setup, a plethora of materials were employed as the working electrode, including but not limited to; glassy carbon, carbon fibre and various carbon composites. Further experiment specific electrochemical cell assemblies and measurements are outlined in each chapter.

3.2 Electrochemical Cells

Electrochemical measurements are recorded using a vessel known as an electrochemical cell. A three-electrode setup is often deployed, comprised of a working electrode (WE), reference electrode (RE) and counter electrode (CE) as depicted in **Figure 3.2.1**. Conventionally, a potentiostat is used to manipulate the potential at the WE and monitored against the RE. As previously mentioned, the WE is interchangeable with different materials specific to the experiment and, since this is where the electrochemical reaction of interest occurs, the WE response is of vital importance. Conversely, the comparative chemical reaction which occurs at the RE, provides a relative constant standard potential to measure the WE against. Additionally, the counter electrode promotes a level of accuracy to the cell setup when analysing potential changes, by controlling the current flow to be distributed through the WE rather than the RE. In the scenario where a two-electrode system has been exploited, further details of cell design is explained in the appropriate chapters describing the combined counter/reference electrode used.

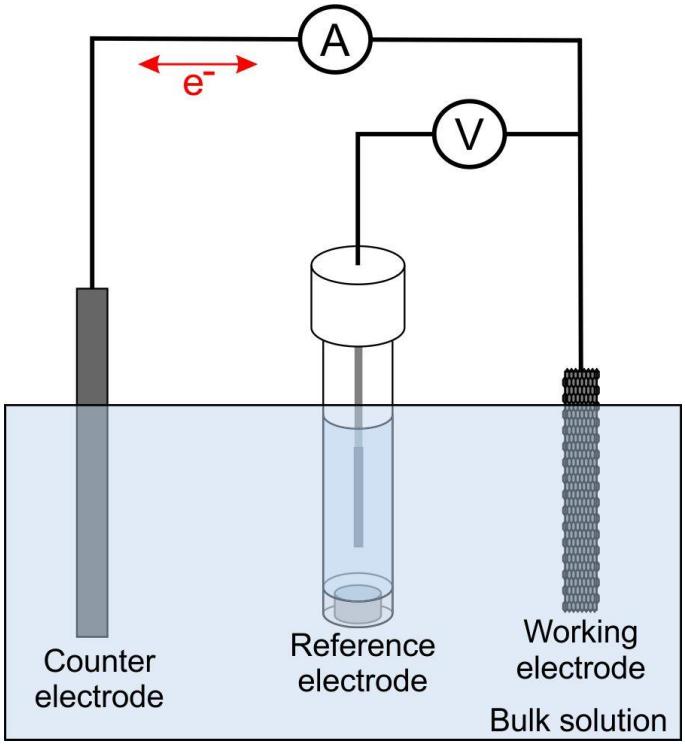

Figure 3.2.1 Typical three-electrode electrochemical cell setup.

3.2.1 Reference Electrodes

The benefit of using a reference electrode provides a constant fixed and stable equilibrium potential, allowing for control and, in the case of voltammetric sweeps, variation of the potential of the WE. The RE implements a reference point against which to compare the magnitude of potential of other electrodes within the electrochemical vessel. The assembly of the RE should enforce the electrode potential being independent of current density and of electrolyte within the cell arrangement. Throughout this work, where a three-electrode system was employed, a commercial Ag|AgCl half-cell reference electrode was used in undertaking electrochemical investigations. This type of RE is separated from aqueous solution by a porous frit, with a halide salt (AgCl) coated silver wire held in a glass sheath containing 3 M potassium chloride solution. The purpose of the porous glass membrane is to control the rate at which Cl^- may leak thereby, creating an ion conductive electrical pathway. The reference electrode fabrication is demonstrated in **Figure 3.2.2**.

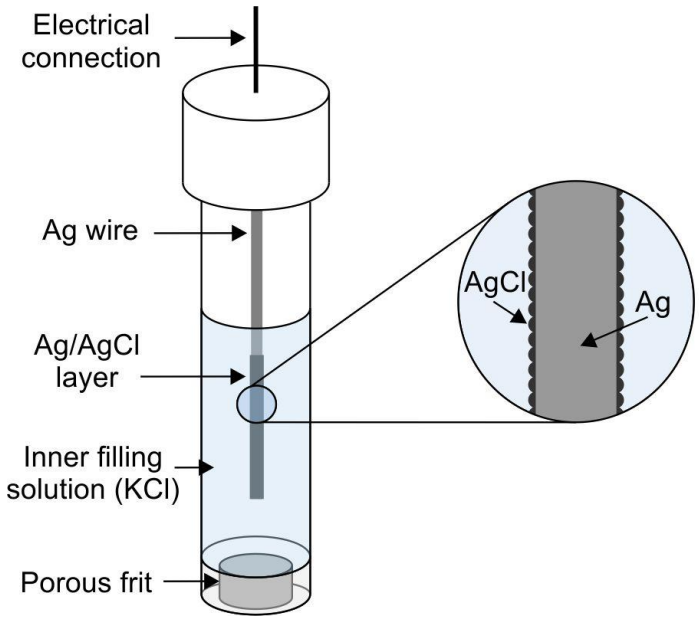

$$Cl^-_{(aq)} \mid AgCl_{(s)}, \qquad Ag_{(s)}$$

$$AgCl_{(s)} + e \;\leftrightarrow\; Ag_{(s)} + Cl^-_{(aq)} \qquad E^o = +0.222\,V$$

Figure 3.2.2 Commercial Ag|AgCl reference electrode with corresponding electrode process.

In any electrochemical cell, the flow of electrons is driven by either an oxidation or reduction reaction. The maximum potential difference between these two processes can be described by the electromotive force (emf) of the cell. The electrochemical activity which occurs in the cell is explained by the Nernst equation (Equation 3.1):

Equation 3.1

$$A + ne^- \leftrightarrow B$$

$$E = E^o - \frac{RT}{nF} ln \frac{[B]}{[A]}$$

$$AgCl_{(s)} + e \;\leftrightarrow\; Ag_{(s)} + Cl^-_{(aq)} \qquad E^o = +0.222\,V$$

Where:

E is electrode potential (Volts)

E^o is the standard electrode potential or emf for the redox couple (Volts)

R is the gas constant (8.314 JK^{-1})

T is the temperature (Kelvin)

n is the number of electrons transferred to the electrode during the reaction

F is the Faraday constant (96485 C mol^{-1})

[*A*] and [*B*] are activities of the oxidised and reduced species

When appropriate values relative to a commercial Ag|AgCl reference electrode are inserted into the Nernst equation, the potential of the electrode is determined as being directly proportional to the concentration of chloride ions. Thus, a constant chloride ion concentration is essential in maintaining a stable environment of which to provide a comparative fixed reference potential. In the event where a two-electrode system was used, it was possible to employ a combined counter/reference electrode. A well established technique of preparing an oxidised chloridised silver wire to behave as a standard Ag|AgCl reference electrode was used and is further detailed in relevant experimental chapters (Huang and Dasgupta, 1997). However, this formation does not include its own internal chloride solution and so, it is necessary to add a known concentration of chloride (0.1 M KCl) into test solutions in order to maintain a stable reference point. In doing this, there remains the assumption that whatever current being measured is so small that any influence on the combined counter/reference electrode will be negligible.

3.2.2 Working Electrodes

In electrochemical investigations, the reaction of interest takes place at the working electrode. A computer controlled potentiostat is often used to apply a potential between the reference and working electrode. Since the reference electrode is held at a fixed potential, any changes in electrode potential are due to chemical reactions occurring at the working electrode (Equation 3.2).

Equation 3.2

$$E = (\emptyset_M - \emptyset_S)working - (\emptyset_M - \emptyset_S)reference$$

Where:

E = Electrode Potential

$\emptyset_M$ = Potential of the metal phase

$\emptyset_S$ = Potential of the solution phase

However, in the event of a two-electrode system being employed, this would no longer apply as current may pass through the reference electrode. Thus, to determine the electrode potential in a two-electrode vessel, the equation should be adjusted to account for any alterations at the reference electrode (Equation 3.3):

Equation 3.3

$$E = (\emptyset_M - \emptyset_S)working + IR - (\emptyset_M - \emptyset_S)reference$$

Where:

IR = Electrical resistance of the bulk solution between the reference and counter electrode

Within this electrochemical cell setup, alterations in potential would result in unspecified changes in $(\emptyset_M - \emptyset_S)working$ alongside IR. The working electrode is no longer regulated in this scenario. Notably, in scenarios where a microelectrode has been used as the working electrode, the current flowing through the electrodes would be expected to be very small. The small current passing through the electrodes will have little to no effect on the electrocatalytic change within the reference electrode, meaning the IR can be disregarded.

A myriad of materials have been used throughout the detailed electrochemical experiments depending on their need for application. The choice of substrate used as the working electrode was dependent on fast electron transfer kinetics but also, the physical properties to yield reproducible results. A defined geometric sensing area was utilised for each working electrode to ensure accurate interpretation of voltammetric results. The materials used, pretreatment and electrode assembly for the composition of electrode designs are further specified in the experimental chapters.

3.2.3 Counter Electrodes

Counter electrodes were introduced into three-electrode electrochemical setups, with the purpose of improving accuracy when measuring potential changes. If any appreciable current passes through the reference electrode, this may jeopardise an experiment by causing fluctuation in the reference potential. The counter electrode provides an alternative route for which current (of equal magnitude but opposite sign) may flow through instead of the reference electrode. This type of electrode requires an inert material that is highly conductive, thereby not interfering with the reactions at the working electrode. Consideration to the type of reaction taking place within the cell must be given to the choice of counter electrode as well as the cost imposed and incidence of corrosion. The counter chosen should also be as large as possible to minimise the current density drawn at this electrode. From the wide variety of materials available, platinum wire (Ø 500 µM) was used as the counter electrode material throughout the investigations unless otherwise stated. Notably, where microelectrodes are concerned, the current is often of negligible magnitude having minimal effect on the reference electrode allowing the counter to be eradicated.

3.2.4 Buffer Solution

To enable the conduction of electrochemical measurements, the solution in which they are performed must provide sufficient electrolytes for which current may flow through the cell. The supporting analytes typically consist of a solvent with dissolved metal salts (or acids) or, in many of the discussed experiments, a buffer solution. The conductive electrolyte solution should be inert thereby allowing for manipulation of the analyte of interest. Incorporating a buffer solution can also be advantageous in minimising pH variations at the electrode interface. This becomes particularly beneficial when electrode processes initiate the production or depletion of protons or hydroxide ions (H^+ or OH^- ions). Predominantly in the fundamental stages, Britton-Robinson or phosphate buffered saline (PBS) were used during analysis due to the complexities of biological media.

3.3 Mass Transport

The reactions that take place within an electrochemical vessel are largely affected by electrode kinetics and the concentration of electroactive species. The rate of chemical reactions may also be affected by the mode of molecular transport of species to and from the electrode|solution interface, of which there are three types: diffusion, convection and migration.

3.3.1 Diffusion

An electrolyte concentration difference present between two points in an electrochemical cell derives a concentration gradient, forcing analyte movement from areas of high to areas of low concentration until the concentration is uniform. An electrochemical reaction occurring at the surface of an electrode will convert material typically present in the bulk solution to a new material, thus, creating a concentration difference between the analyte present at the electrode interface and the bulk solution. Over time, the new material accumulated at the electrode interface will passively move away from the electrode surface, with the initial material moving towards the electrode until equilibrium is achieved. The rate at which this occurs, otherwise known as flux, can be described by Fick's law of diffusion. Fick's first law of diffusion can be used to determine flux under steady state conditions (Equation 3.4):

Equation 3.4

$$J = -D\frac{\partial \varphi}{\partial x}$$

Where:

J = Flux of the species in mol/m^2s

D = Diffusion coefficient in m^2/s

$\partial\varphi$ = Change in concentration in mol/m^3

∂x = Change in distance in metres

The first law is based on the assumption that the flux is proportional to the gradient present. However, concentration does not always stay constant over time. Therefore, Fick's second law of diffusion depicts how the concentration is a function of both distance and time as it explains how diffusion causes the concentration to change with time (Equation 3.5).

Equation 3.5

$$\frac{\partial \varphi}{\partial t} = D\frac{\partial^2 \varphi}{\partial x^2}$$

Where:

D = Diffusion coefficient in m^2/s

$\partial\varphi$ = Change in concentration in mol/m^3

∂t = Change in distance in seconds

∂x = Change in distance in metres

3.3.2 Migration

Migration involves the transport of charged molecules across a potential gradient. Electric fields can induce electrostatic-attraction and electrostatic-repulsion, but will only affect charged species and thus, ionic solute will move in the presence of an electric field. In analytical electrochemistry, migration has little effect on the transport of electroactive species since experiments are typically carried out in a large quantity of inert electrolyte which transports most of the charge (Pletcher *et al.*, 1982).

3.3.3 Convection

The movement of molecules by density gradients or forced mechanical forces describes the mode of transport known as convection. Within electrochemistry convection may be induced by mechanically stirring or agitating the solution or by forcing it through a channel. If these mechanical forces are introduced, then convection typically becomes the primary mode of transport within the cell. However, within the investigations described here,

diffusion was the main mode of transport since it would be unrealistic to assume external mechanical forces can be combined with transdermal sensing applications.

3.4 Voltammetry

Analytical electrochemistry encompasses a number of quantitative and qualitative voltammetric techniques to gather information about a specific analyte. Voltammetry involves varying the potential subjected between the working and reference electrode over time, whilst observing the resultant current flow. From this, a voltammogram may be produced which can be interpreted to determine parameters specific to the experiment conducted such as, rate of reaction, identifying species present in the cell, and electrochemical mechanisms causing reactions. The variety of voltammetric techniques utilised throughout this work is summarised below.

3.4.1 Cyclic Voltammetry

Potentially the most common method of voltammetric analysis, cyclic voltammetry (CV), is typically used to investigate the reduction and oxidation processes of molecular species. In doing so, it becomes an invaluable tool in understanding electron transfer-initiated chemical reactions. Cyclic voltammetry involves linearly sweeping the potential at the working electrode with respect to time and repeating in a cyclic manner, thereby, generating a triangular waveform as shown in **Figure 3.4.1**. The initial potential applied to the working electrode is displayed as E_1, with no chemical reaction occurring. Once the potential is linearly swept to E_2, the reduction or oxidation process of interest has already taken place, with E_2 typically being larger than the potential required for this reaction to happen. Sweeping beyond the potential required for the reaction of interest allows the process to be recorded and plotted in its entirety. The potential sweep is then reversed upon reaching E_2 and cycled back to its primary position (E_1). Notably, the first half of this triangular waveform is akin to that of linear sweep voltammetry.

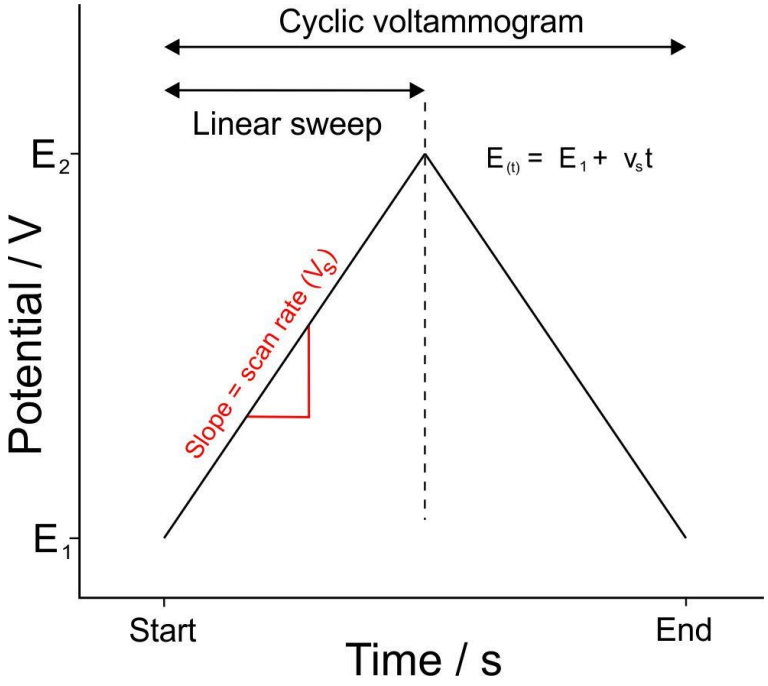

Figure 3.4.1 Triangular waveform used in cyclic voltammetry and corresponding slope for linear sweep.

The resultant voltammogram produced allows the current, which is proportional to the rate of electron transfer, to be plotted against a function of applied potential with respect to defined scanning parameters. A characteristic voltammogram detailing a reversible redox reaction is shown in **Figure 3.4.2.**

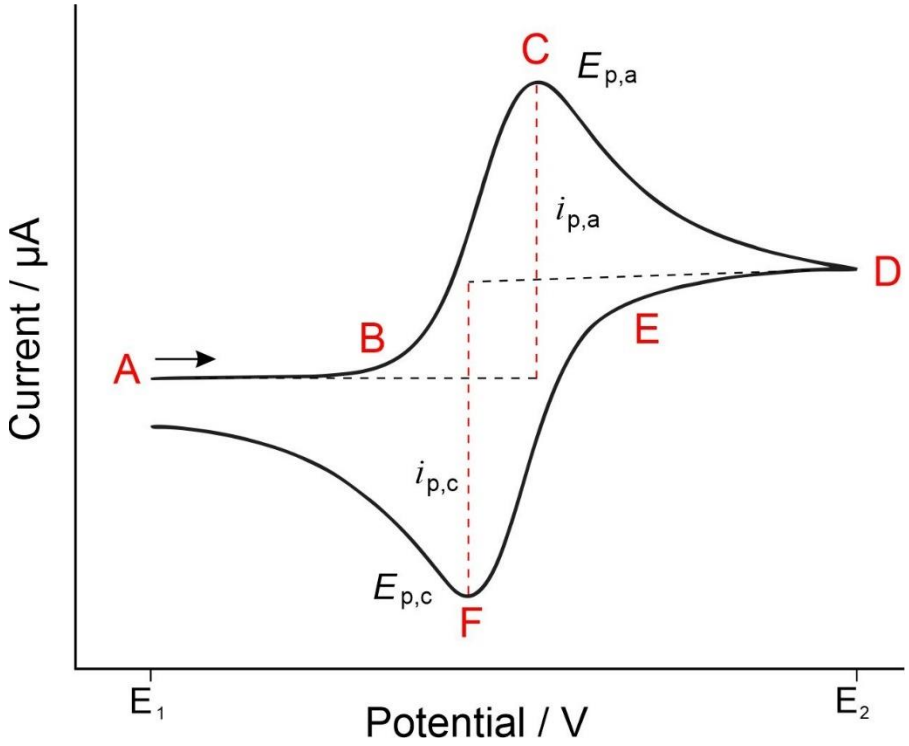

Figure 3.4.2 Expected response of a reversible redox system during cyclic voltammetry.

As previously stated, E_1 represents the initial potential state where no current flows, but as the potential is linearly increased (sweeping from left to right), current begins to flow. The potential applied to the working electrode during this time disrupts the equilibrium state allowing current to flow. The increase in current is dictated by the transport of species via diffusion from the bulk solution, thus, it proportionally increases until a peak is observed. The accumulation of solution at the electrode interface, called the diffusion layer, continues to grow with the sweeping scan therefore, minimising the flux of reactant species to the electrode. This reduction in rate of diffusion of reactant species causes a decrease in current as the scan continues past the peak observed. Upon reaching the switching potential (E_2), the scan direction is reversed, sweeping cathodically from right to left. During the reverse sweep, the product is reduced back to the starting material.

During a reversible redox reaction, a cyclic voltammogram will exhibit a number of key characteristics:

The peak voltage separation (E_p) between the oxidation and reduction peak potentials are independent of scan rate (v) described by the following equation (3.6):

Equation 3.6

$$E_p = E_{pa} - E_{pc} = \frac{59}{n} mV$$

Where:

n = the stoichiometric number of electrons involved

The peak currents (I_p) are proportional to the square root of the scan rate in a diffusible system.

$$I_p \propto \sqrt{v}$$

Finally, the peak ratio of the anodic (I_{pa}) and cathodic (I_{pc}) currents are equal to 1.

$$\frac{I_{pa}}{I_{pc}} = 1$$

Within **Figure 3.4.3.B** it can be seen that as the scanning rate at which the potential is applied increases, so too does the current response. A large factor that applies here is the instance of the diffusion layer. Since the diffusion layer increases with respect to time, if an increased scan rate is applied, this will result in a quicker rate of scan completion but, will also minimise the distance the diffusion layer moves away from the electrode. Due to the proportionality between current and flux, a larger current will be measured during a faster scan rate or, opposingly less during a slower scan rate. The linear relationship between peak current and square root of the scan rate is shown in **Figure 3.4.3.A**. The diffusion coefficient of this relationship may be calculated using the Randles–Ševčik equation (Equation 3.7).

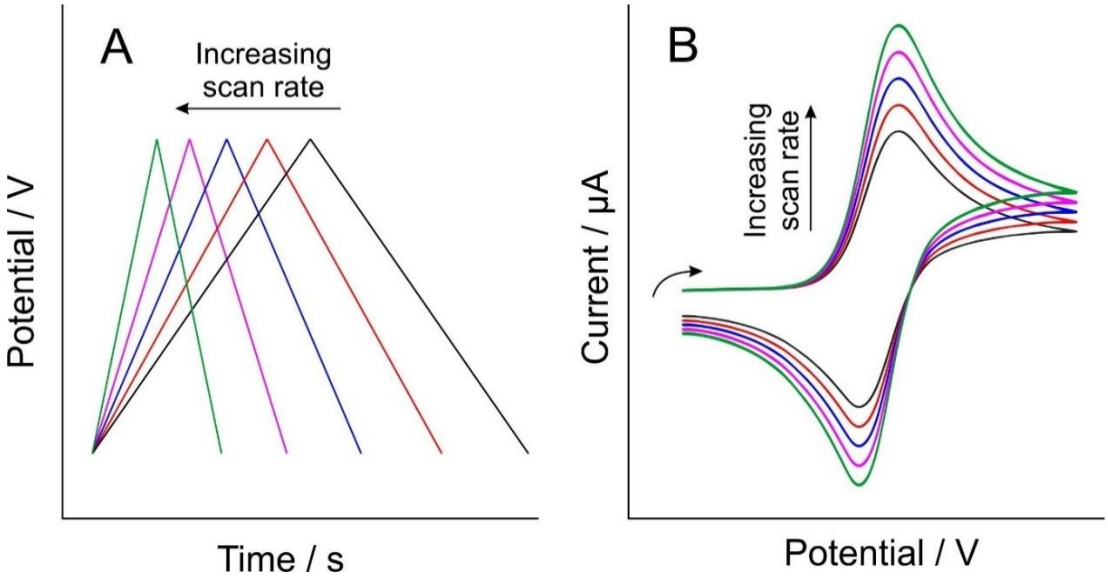

Figure 3.4.3 (**A**) Effect of scan rate on triangular waveform used during cyclic voltammetry and (**B**) cyclic voltammograms showing the effect of increasing scan rate.

Equation 3.7

$$I_p = 2.69 \times 10^5 \, n^{3/2} A D^{1/2} \, C v^{1/2}$$

Where:

I_p = Peak current

n = Number of electrons transferred

A = Electrode area in cm^2

D = Diffusion coefficient in cm^2/s

C = Concentration in mol/cm^3

v = Scan rate in V/s

The reversibility of electron transfer reactions occurring at the surface of an electrode is used to describe the state of thermodynamics of a system. A cyclic voltammogram displaying a reversible reaction is said to maintain fast electron transfer kinetics, where the forward and reverse peak currents are of the same magnitude and separated by a potential of 59 mV independent of scan rate. Where slower electron transfer is encountered, these reactions may be categorised as quasi-reversible or irreversible. An irreversible reaction is unable to maintain the equilibrium, with effectively no reconversion of the product back to reactant, thus, the magnitude of the reverse peak (relative to the forward peak) is dependent on scan

rate and will only be visible if an appreciable over-potential is used. In the case of reversible and irreversible reactions, electrode kinetics are determined relative to mass transport, however, quasi-reversible reactions are dependent on electron transfer kinetics and the rate of mass transport. While the peak current of a reversible reaction is proportional to the square root of the scan rate, the same cannot be said for a quasi-reversible system. Instead, the magnitude of the reverse peak relies on a faster scan rate and an over potential to continue the conversion of product back to reactant. **Figure 3.4.4** displays the cyclic voltammogram response for typical behaviour of a reversible, quasi-reversible and irreversible electrochemical cell.

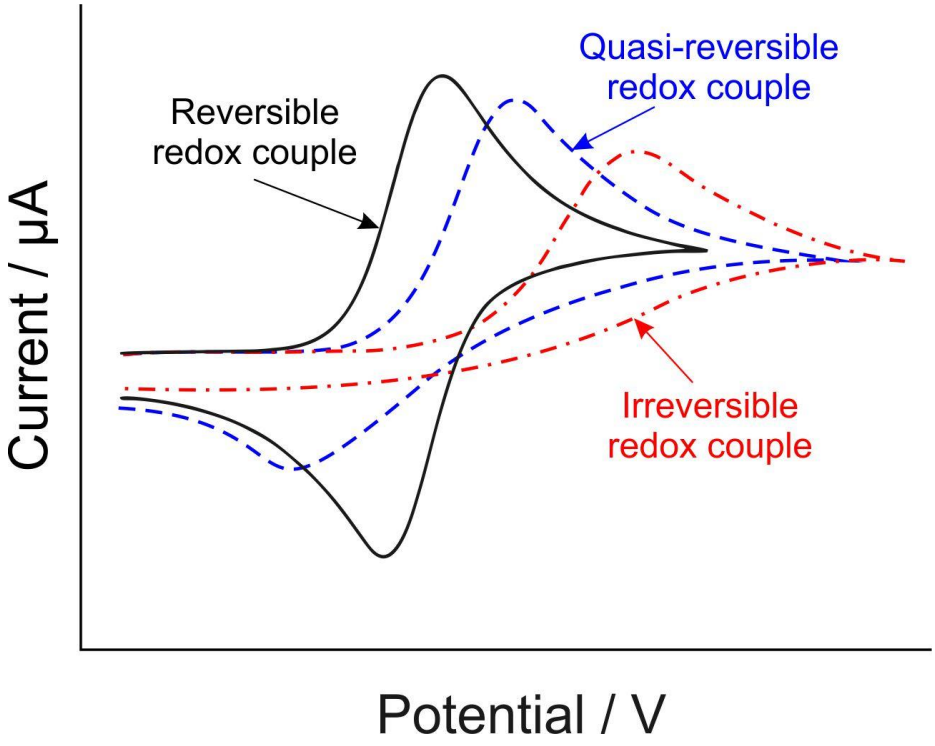

Figure 3.4.4 Cyclic voltammogram responses highlighting the effect of reversible, quasi-reversible and irreversible redox couples.

When fast electron transfer kinetics are exhibited during reactions, the peak current will always be measured at the same (or very near the same) potential. However, a greater resistance in the solution results in slower electron transfer with peak currents diminishing and broadening. This gradual increase in peak separation displays an accumulative deviation from the Nernstian response. Hence, to calculate the peak current density of a non-

reversible system, the charge transfer coefficient (α) must now be considered as follows (Equation 3.8):

Equation 3.8

$$I_p = 2.99 \times 10^5 \, n(n\alpha)^{1/2} D^{1/2} c v^{1/2}$$

As previously shown in the CV profile above, this linear relationship is characteristic of diffusion at a macroelectrode. An electrode is considered as being a 'microelectrode' when one or more of the dimensions are on the micro-scale. The decrease in geometric area of an electrode generates distinct changes in a voltammetric profile where the timescale of the experiment can significantly influence the diffusional mass transport regime and therein the response observed.

Given the classic case of oxidation or reduction of an electroactive species (i.e. ferrocyanide) in solution at a conventional macro-sized electrode at relatively fast scan rates (100 mV/s), a diffusional current flows - rising to a peak and then decaying as depletion of the electroactive materials occurs. This provides the classic "duck" shaped profile. Consider a generic spherical electrode with a radius r_O placed in a solution of the redox probe at a concentration C. The application of a potential step will alter the concentration gradient at the electrode surface and can be determined by solving Fick's second law (Equation 3.9) in spherical coordinates:

Equation 3.9

$$\frac{\partial C(r,t)}{\partial t} = D \left[\frac{\partial^2 C(r,t)}{\partial r^2} + \frac{2}{r} \frac{\partial C(r,t)}{\partial r} \right]$$

The boundary conditions for the potential step experiment are:

Equation 3.10

$$\lim_{r \to \infty} C(r,t) = C^{\infty}$$

Equation 3.11

$$C(r,0) = C^{\infty}$$

Equation 3.12

$$C(r_0, t) = \ 0$$

Where: r is the distance from the centre of the sphere, r_0 is the radius of the electrode, D is the diffusion coefficient of the redox probe and C is the concentration as a function of distance r and time t. Solving Equation 3.9 using Laplace transform techniques gives the time evolution of the current, $i(t)$, subject to the boundary conditions described resulting in Equation 3.13:

Equation 3.13

$$i(t) = \ \frac{nFADC^{\infty}}{r_O} + \ \frac{nFAD^{1/2}C^{\infty}}{\pi^{1/2}t^{1/2}}$$

It can be seen from Equation 3.13 that the current (i) contains time-dependent and time-independent terms and the relative contribution of each under conventional electrochemical timescales give rise to the differing voltammetric profiles obtained at macro and microscale electrodes. Two limiting regimes dependent upon whether the experimental timescale is short or long can be considered:

A) At sufficiently short timescales, the diffusion layer that is depleted of reactant becomes significantly smaller than the electrode radius. Thus, the spherical electrode appears planar to a molecule at the edge of this diffusion layer (**Figure 3.4.5**) and the electrode behaves like a macroelectrode.

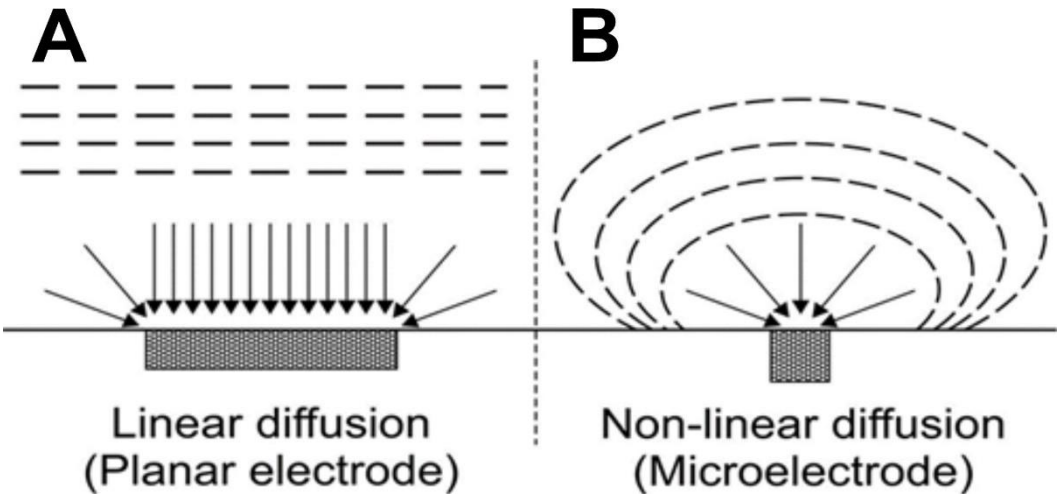

Figure 3.4.5 Schematic of diffusion fields at microelectrodes. (**A**) Short timescale linear diffusion and (**B**) Long timescale radial diffusion.

Mass transport is therefore dominated by linear diffusion to the electrode surface. At short times the first part of Equation 3.13 becomes insignificant compared to the second part due to the $t^{-1/2}$ dependence of the current. Therefore, the current decays over time in accordance with the Cottrell equation (Equation 3.14):

Equation 3.14

$$i(t) = \frac{nFAD^{1/2}C^{\infty}}{\pi^{1/2}t^{1/2}}$$

B) At long times (i.e., slow scan rates), the second term in Equation 3.13 becomes negligible and the current attains a time-independent steady-state value given by Equation 3.15:

Equation 3.15

$$i_{ss} = \frac{nFADC^{\infty}}{r_o}$$

At long times (slow scan rates), the mass transport process is dominated by radial (spherical) diffusion as illustrated in **Figure 3.4.6**. Slow scan rates therefore exhibit the classic sigmoidal shaped curve (Figure 3.4.6.A), whereas, at fast scan rates (short timescales), peaked responses which are similar to those observed at macroelectrodes are present (Figure 3.4.6.B).

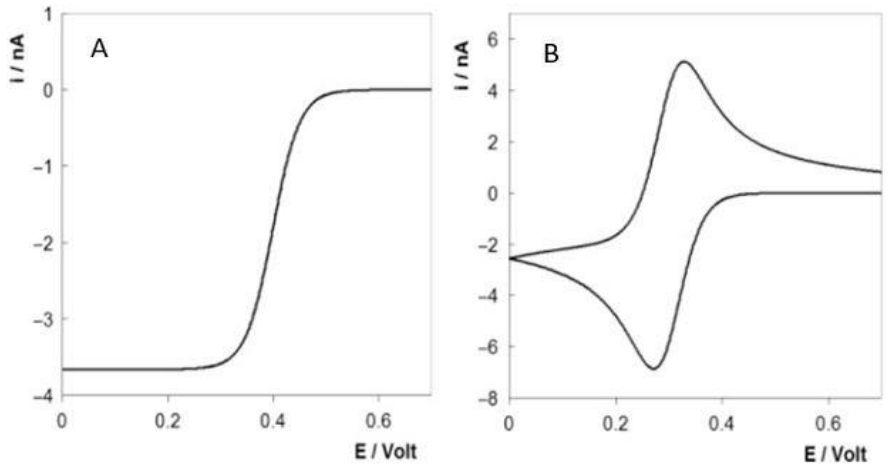

Figure 3.4.6 Effect of scan rate on the cyclic voltammetry at microelectrodes. (**A**) Scan rate is slow (0.1 V/s) and (**B**) fast scan rate (10 V/s).

The selection of a spherical electrode here provides a simple closed-form solution to the diffusion equation as the surface is uniformly accessible. A microdisk is however the most widely used geometry, but the derivation of rigorous expressions that can describe the experimental response is hindered as the surface is not uniformly accessible. Electrolysis can occur at the outer circumference of the disk, which diminishes the flux of the redox probe to the centre of the electrode. In this scenario the steady-state current is given by:

Equation 3.16

$$i_{ss} = ynFADCr_o$$

Where y is 4 and 2π for disk and hemispherical shaped electrodes, respectively.

3.4.2 Square Wave Voltammetry

Square wave voltammetry (SWV) is often used in electrochemical investigations to provide greater sensitivity in quantitative analysis. Much like cyclic voltammetry, the potential at the working electrode is swept linearly although, instead of the triangular waveform, it is swept in a staircase voltage series as shown in **Figure 3.4.7.B**. The key parameters which are characteristic of SWV are also demonstrated in **Figure 3.4.7.A**. A square wave is dependent

on two measurands, the amplitude (E_{sw}) and pulse width (t_p). The pulse width may also be described as a function of frequency where f = $1/\tau$ or f = $1/2t_p$. The square wave period (τ) is determined by the time taken to complete one cycle or staircase step. The step height (ΔE) can then be used to determine the scan rate as shown in the equation below (Equation 3.17).

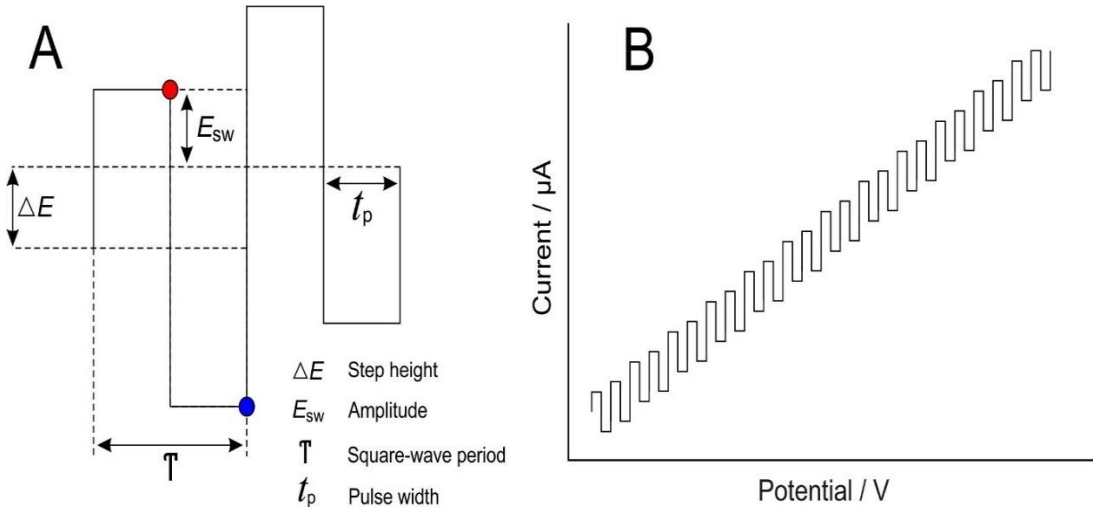

Figure 3.4.7 (**A**) Parameters of waveform used in square wave voltammetry and (**B**) staircase profile from a square wave scan.

Equation 3.17

$$\text{Scan Rate (mV/sec)} = \frac{\Delta E(\text{mV})}{\tau\ (\text{sec})}$$

The advantage of using the staircase method during a square wave period allows the current to be recorded twice, at the end of each pulse demonstrated by the red and blue dots highlighted in **Figure 3.4.7.A**. The red dot illustrates the end of the forward scan (i_f) with the blue dot symbolising the completion of the reverse current (i_r). The forward and reverse current densities are utilised to plot a square wave voltammogram which resembles one half of a cyclic voltammogram. However, it is the difference in current (Δi), calculated by $i_f - i_r$ which is plotted in the characteristic square wave voltammogram as shown in **Figure 3.4.8**.

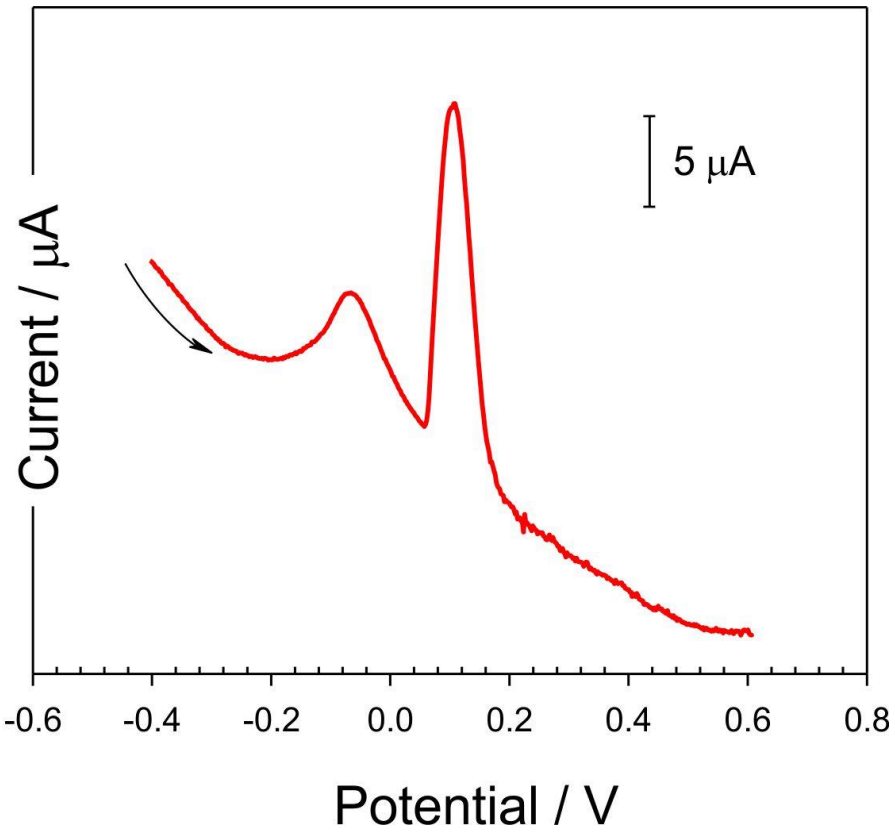

Figure 3.4.8 Typical square wave voltammogram response.

The peak observed in the square wave voltammogram above indicates a redox reaction. The magnitude of the peaks in a SWV are proportional to the concentration of analytes present and may be calculated using the equation below (Equation 3.18).

Equation 3.18

$$\Delta i_p = \frac{nFAD^{1/2}C}{(\pi t_p)^{1/2}} \Delta\psi_p$$

Where:

Δi_p = Differential peak current

n = Number of electrons

F = Faraday constant 96485 C mol^{-1}

A = Electrode area (cm^2)

D = Diffusion coefficient (cm^2/s)

C = Concentration (mol/cm^3)

t_p = Pulse width in s

$\Delta\psi_p$ = Dimensionless peak current

The highly sensitive nature of square wave voltammetry often makes it more preferable over cyclic voltammetry in electrochemical analysis. The timing of current measurements minimises background interference, contributing to its high degree of sensitivity. There is a delay in current measurement during SWV since the current is logged twice, at the end of each pulse, pausing a few milliseconds before the current is recorded. Whereas, during CV, current is measured instantly upon the applied potential. Upon changing the potential at the electrode, there is reorganisation of ions at the electrode interface, thereby producing a capacitance current. During SWV, the milliseconds in delay is vital, providing sufficient time for this capacitive current to dissipate before logging the current signal. The current of greater significance which accounts for the electron transfer to, or from, the reactive species is known as the Faradaic current. Consequently, due to the measurement delay in SWV, the capacitive current contribution towards the recorded current signal is minimal. Whereas with CV, the measured current is the sum of Faradaic and capacitive current. Thus, the minimal interference of capacitive current during SWV offers a greater advantage over CV during analysis of lower concentrations of analyte.

3.4.3 Amperometry

Another important form of electrochemical analysis includes amperometry in which the current measured or a change in current (derived by a step in potential) is utilised to gain information about the analyte under investigation as depicted in **Figure 3.4.9**. Within amperometry, the potential is stepped from a non-reactive state (E_1) to a fixed potential (E_2) for a predetermined length of time. The step in potential often induces an electrochemical change in the cell, typically an oxidation or reduction reaction generating a measurable difference in current.

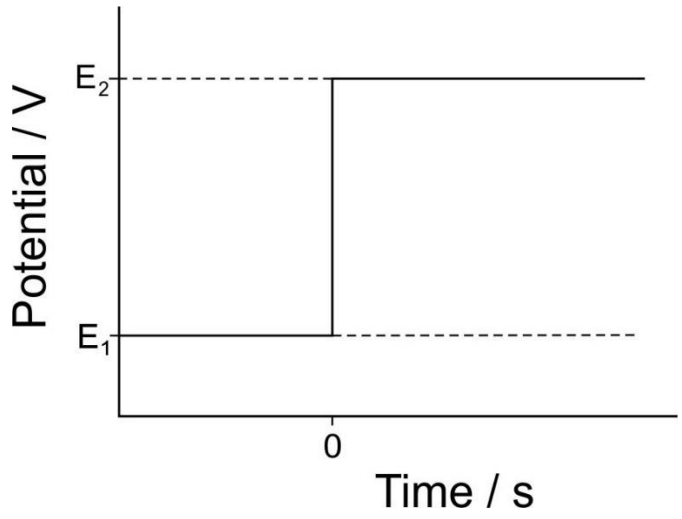

Figure 3.4.9 Step in potential characteristic of amperometric techniques.

During amperometry, the current is measured as a function of time, therefore, the shift in measurable current provides qualitative information about the reaction and the rate at which it occurred. The performance of the measured current can be described by the equation (Equation 3.19) below with a characteristic current response during amperometry represented in **Figure 3.4.10**.

Equation 3.19

$$i = \frac{E}{R_s} e^{-t/RsCd}$$

Where:

i = Current (A)

E = Electrode potential (V)

e = Electronic charge ©

t = Time (s)

Rs = Resistance of the solution (Ω)

Cd = Differential capacitance of the double layer in F

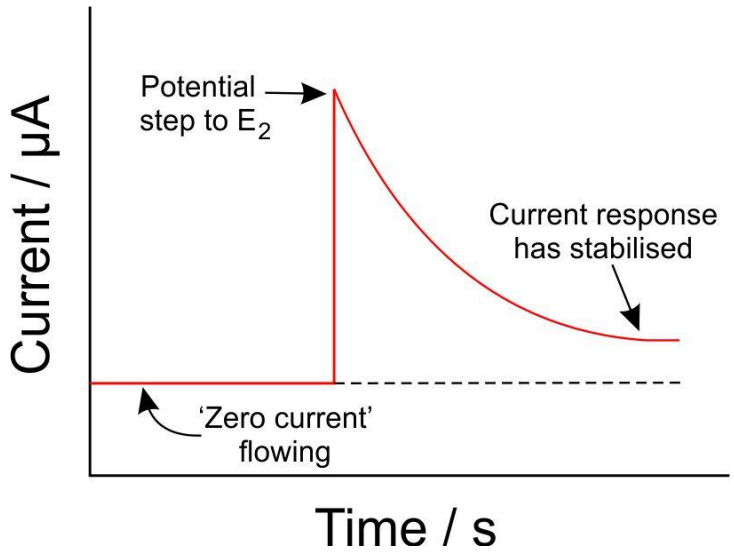

Figure 3.4.10 Typical current response encountered during amperometry.

The current response as a function of time highlights the change in concentration gradient surrounding the electrode as depicted in **Figure 3.4.11**. Further quantitative information can be gained through analysing this profile such as electrons transferred, active electrode area and diffusion coefficient.

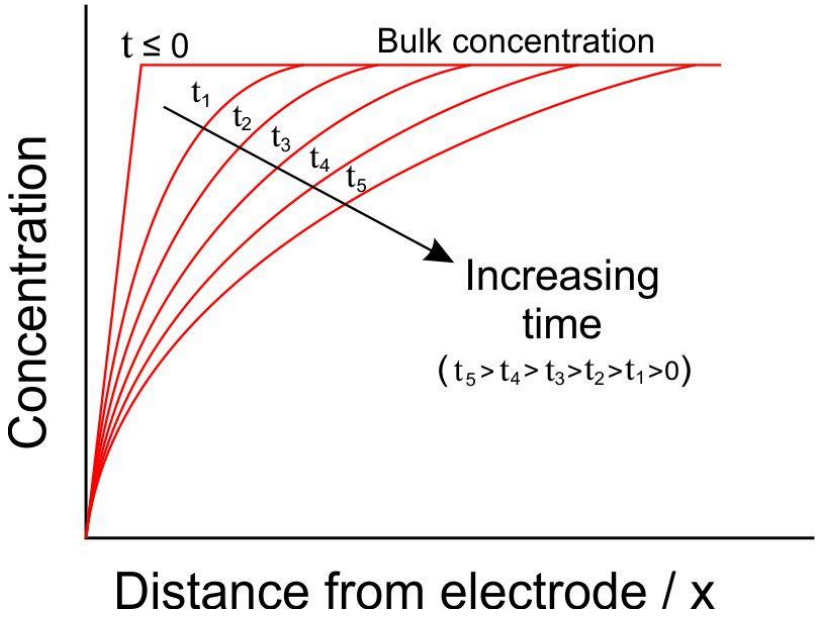

Figure 3.4.11 Relationship of increasing time on concentration profile during amperometric experiment.

As previously stated, the diffusion layer present at the electrode and concentration gradient will increase over time with the flux of reactant species towards the electrode surface decreasing over time, which causes a drop in current density over time. The decay in current density with respect to time can be evaluated by the Cottrell equation below, to determine diffusion coefficients (Equation 3.20).

Equation 3.20

$$I_f = \frac{nFAD^{1/2}c_\infty}{(\pi t)^{1/2}}$$

Where:

I_f = Faradaic current

n = Number of electrons

F = Faraday constant 96485 C mol^{-1}

A = Area of the planar electrode (cm^{-2})

D = Diffusion coefficient

c_∞ = Concentration of electroactive species (mol/cm^3)

t = Time (s)

3.4.4 Potentiometry

As an alternative to the other voltammetric methods described, potentiometry is an inexpensive, passive technique of providing information about sample composition, enabling selective detection of ions in the presence of a multitude of other substances. The electrochemical technique typically involves a working electrode and reference electrode connected by a salt bridge, and then measuring the potential difference between the working and reference electrode under static conditions over a predetermined length of time. The reference electrode is self-contained, holding a constant potential independent of the concentration of analyte in solution. Whereas the working electrode potential is dependent on the concentration of analyte in solution. The working electrode may be a metal immersed in a solution of its own ions at an unknown concentration, or, it can be an inert electrode, such as carbon, in a solution containing two ions of different oxidation states.

The selectivity towards specific ions may be further increased by exploiting perm-selective and ion-conductive membranes and through judicious choice of working electrode material. A salt bridge containing inert electrolyte is typically used to complete the electrical circuit, maintaining electrical neutrality and preventing each half-cell from rapidly reaching equilibrium. The potential difference between the two electrodes is measured using a high impedance voltmeter ensuring any flowing current is negligible. Thus, with no net current flowing in the vessel, the cell setup is effectively in equilibrium, thereby, providing quantitative information about the solution composition. A calibration curve can then be plotted by recording the potential difference of pre-determined standard additions and using the Nernst equation to calculate the unknown concentration of the analyte in solution.

3.5 Characterisation Techniques

The methods described herein outline the characterisation techniques employed to gather information on the physical and chemical composition of materials used throughout this project.

3.5.1 Scanning Electron Microscopy

Scanning electron microscopy (SEM) is a highly sensitive common imaging technique used to characterise surface morphology of materials. This method involves a focused beam of electrons being scanned across the sample specimen rather than light to produce an image. The surface morphology of the sample can be investigated upon interaction with the electron beam. In the case where a SEM has an incorporated Energy Dispersive X-Ray Spectroscope (EDX), the elemental composition present at the sample surface may also be interpreted. Prior to electrochemical investigations, many materials were considered for use as electrodes and were therefore, also observed by SEM to characterise surface topography and structural defects present. During SEM, the sample specimen is subjected to a highly focused beam of electrons (0.5 keV to 40 keV) scanned over the material in a raster pattern. Dependent on the atoms present at the material surface, they react with the incident beam and upon excitation emit secondary electrons which are utilised by the electron detector to

produce secondary electron imaging (SEI) of the surface profile. The resultant image brightness will depend on the intensity of the emitted electrons. The resolution of the image is also influenced by the conductivity of the sample, the accelerating voltage used, electron beam spot size and the distance from the sample surface.

The primary factor affecting image resolution concerns the accelerating voltage which determines the rate at which electrons are forced towards the sample. In doing so, it also manipulates the depth at which the electrons are able to penetrate the sample surface. A lower accelerating voltage will typically provide morphological information about the immediate surface, whereas a higher voltage will permeate the sample surface allowing greater definition and thus, image resolution. However, the higher resolution at higher accelerating voltages may come at the cost of increased surface temperatures due to a build-up of charge and may cause structural damage to polymeric or biological sample specimens. Additionally, sample conductivity is another important factor to consider that greatly affects image resolution. Less conductive samples are often coated with a conductive metal (such as gold or palladium) allowing the incident beam of electrons to discharge along a conductive pathway, otherwise, a build-up of charge will be prominent at the material surface since the number of electrons emitted is less than the number of incident electrons.

Tungsten is the conventional choice of filament cathode from which the incident electron beam is emitted. The process of electron beam emission known as thermionic emission, results in repeated heating and cooling of the filament which often causes degradation of the filament. Tungsten maintains a high melting point at a low cost and is therefore favourable in its application. **Figure 3.5.1** demonstrates that under vacuum, with an applied potential, the cathode emits a stream of monochromatic electrons towards the anode and is then focused downward onto the sample. Upon interaction with the sample, a myriad of signals arise including, backscattered electrons, secondary electrons, auger electrons and X-rays. These signals are collected by the detector and analysed to generate invaluable information about the surface topography and chemical composition of the specimen.

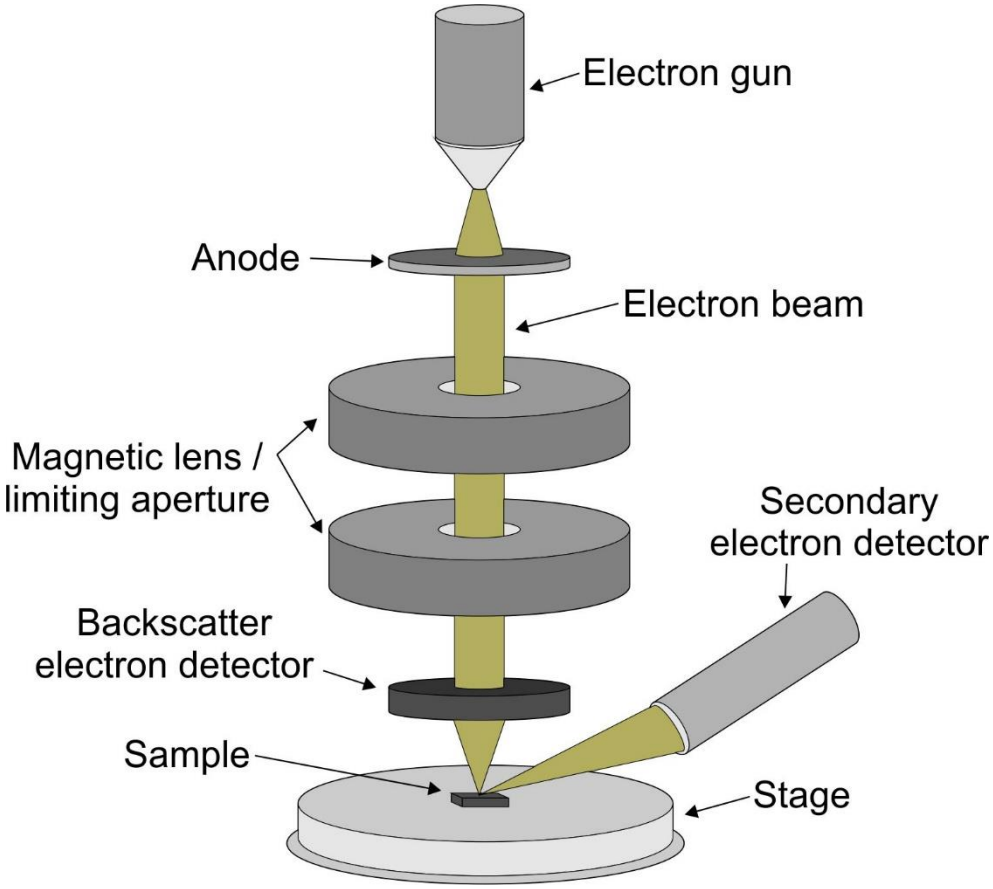

Figure 3.5.1 Electron beam pathway in scanning electron microscope.

3.5.2 X-Ray Photoelectron Spectroscopy

X-Ray photoelectron spectroscopy (XPS) is a surface sensitive quantitative spectroscopic technique used to characterise the elemental and chemical composition of materials. This spectroscopic method is non-destructive, only probing 20 nanometres (at most) into the sample. XPS utilises low mono-energetic Al Kα X-rays to excite the sample surface giving rise to emission of photoelectrons as illustrated in **Figure 3.5.2**. This process of photoemission is critical since the emitted photoelectrons are a function of their binding energies and so, possess energies characteristic of the molecular orbital and element from which they originated. Thus, an electron energy analyser can be used to determine the kinetic energy of the emitted photoelectrons. Analysis of the photoemission kinetic energy serves as the primary source of data used in XPS techniques. The binding energy and intensity of a

photoelectron peak allows the chemical state, elemental identity, and elemental quantity to be resolved. By counting the number of photoemitted electrons as a function of their energy, a spectrum representing the surface composition can be produced.

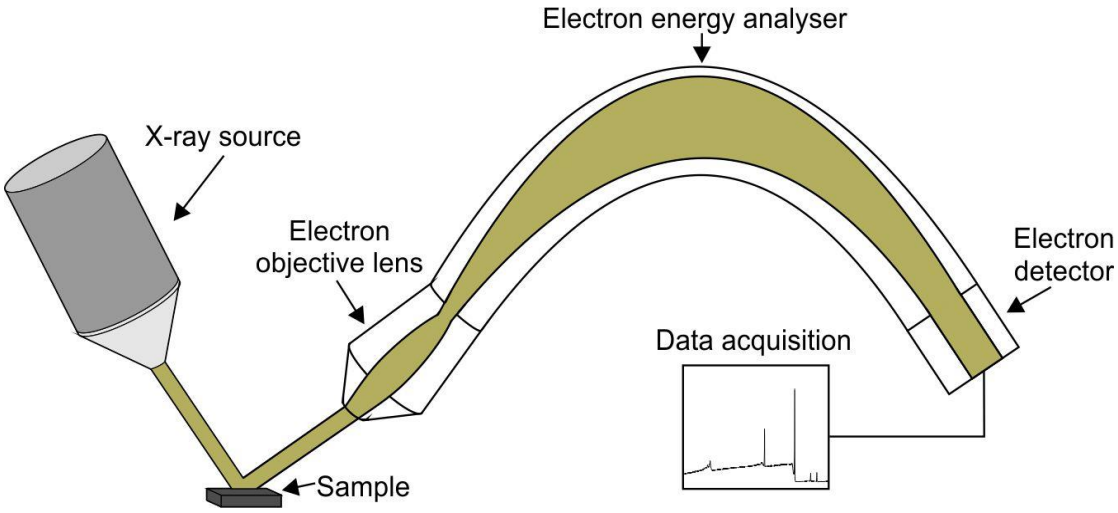

Figure 3.5.2 Electron pathway during X-ray photoelectron spectroscopic analysis.

In this project, XPS analysis was carried out using a Kratos Axis Ultra DLD Spectrometer to quantify surface composition and acquire XPS spectra. Samples excited with monochromatic Al Kα X-rays (15kV and 10mA). For analysis, wide energy survey scans (WESS) were obtained across a range of binding energies (Typically -5 to 1200 eV) and high-resolution spectra collected with at least 3 sweeps to minimise background noise (pass energy of 20 eV, 0.05 eV step size, 25 eV scan width and a dwell time of 150 ms). Typically, 3 measurements at each spot per sample were recorded and a Shirley background subtracted from the XPS spectra, which were peak fitted with high-resolution Casa XPS software. Further XPS experimental details can be found in the appropriate chapters.

3.5.3 Raman Spectroscopy

Raman spectroscopy is another non-destructive chemical analytical tool which depends on the interaction of light with chemical bonds in a material. The technique provides a structural fingerprint of the material allowing molecular identification. Raman utilises

incident monochromatic photon energy to interact with the electrons on the sample surface. With electrons having different vibrational levels, the incident energy is absorbed at the material surface and temporarily causes the surface electrons to rise to a virtual energy state. As illustrated in **Figure 3.5.3**, upon losing energy, the electrons fall back to a vibrational level again. The level which the electrons fall back to can then be categorised as Rayleigh scattering, stokes line, or anti-stokes line depending on if it was the same, higher or lower energy level than it originated from respectively. If the electrons do not fall back to the same level as before, otherwise known as inelastic scattering, then this is defined as Raman scattering. The radiation emitted during this process is collected, with the laser wavelength filtered out and scattered light forced through a monochromator to a CCD detector, providing detailed spectra which holds information about the material surface. It is important to note that the penetration depth may also be controlled by excitation wavelength and optics. In this project, Raman spectra were obtained by using a Horiba LabRAM 300 spectrometer with a HeNe laser. Further details are described in the appropriate chapter.

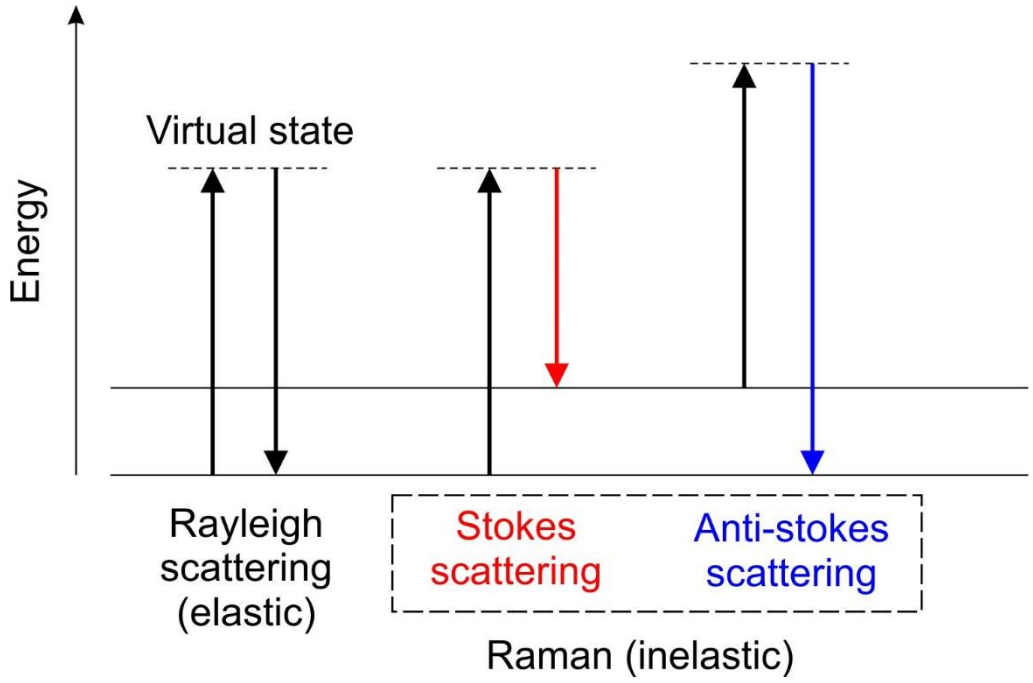

Figure 3.5.3 Virtual energy levels and corresponding category of electron scattering.

3.5.4 X-Ray Computed Tomography

Another imaging technique used during this project, computed tomography (CT), has the advantage of producing cross-sectional imagery of a sample. The technique utilises a multitude of non-destructive X-ray measurements taken from different angles, to compute dimensional slices of an object that can be reconstructed to produce a 3-dimensional construction of the scanned sample. During CT, the sample is held at a fixed point and rotated on its axis, or alternatively, as more commonly used in medical diagnostics, the X-ray tube and detector are rotated around the sample. Although this technique is known to have poor resolution compared to 2-dimensional imaging techniques, it allows the user to effectively observe the internal dynamics of a sample at the micron level. In this project CT was carried out using a SkyScan 1275 Micro-CT system (Bruker Corporation, USA). The accompanying NRecon and CTVox visualisation software allowed the reconstruction and analysis of the X-ray slices. Further experiment specific details are described in the appropriate chapters.

3.5.5 Contact Angle

Contact angle measurement is a method commonly used to assess the hydrophobicity or surface energy of a material. The molecular force of attraction on a materials surface describes the surface energy, with a high energy assuming strong molecular attraction and low energy holding weaker attractive forces. The wetting of a material can then be used to determine the hydrophobicity or surface energy of a material. When a droplet of water is subjected to a material surface, the shape of the droplet provides information on the nature of the material surface. As seen from **Figure 3.5.4**, the contour of a water droplet on a material surface can be used to categorise a material as hydrophilic or hydrophobic. Within this project, the sessile drop method was utilised, and static contact angle measurements recorded using a CAM 200 optical contact angle meter (KSV Instruments Ltd.). Further details are described in the appropriate chapters.

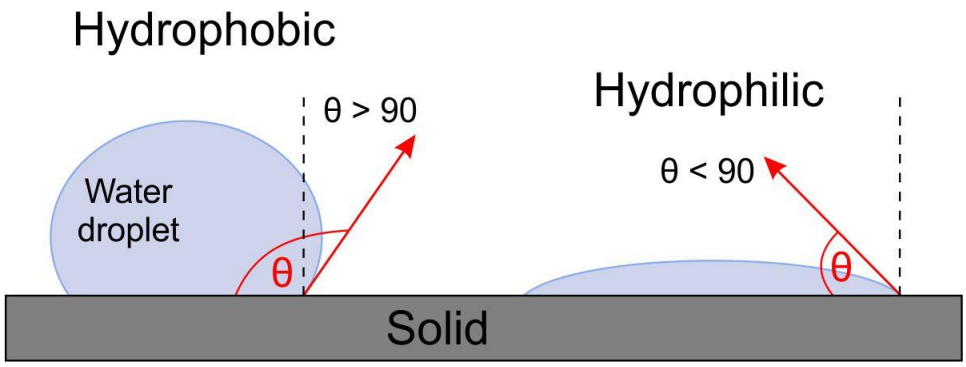

Figure 3.5.4 Contact angle of water droplet contours and corresponding hydrophobicity assessment.

3.5.6 Conductivity

Within electrochemical analysis, the choice of electrode material is often influenced by the conductivity of the material. Within this project, the formation of composite materials were investigated as working electrodes and so, the conductivity of the materials were also examined. Based on the principle that conductivity is inversely proportional to resistivity as shown below (Equation 3.21), a 2461 series SourceMeter® (Keithley) 4 point probe was used in calculating conductivity measurements of materials within this project.

Equation 3.21

$$R = \rho\frac{L}{A} \quad and \quad \sigma = \frac{1}{\rho}$$

$$\therefore \; R = \frac{L}{\sigma A}$$

Where:

R = Resistance in Ω

L = Length of path of conductance (m)

A = Cross-sectional area (m^2)

ρ = Resistivity in Ωm

σ = Conductivity in Sm^{-1}

3.5.7 Compression Testing

Compressive testing is a vital characterisation method in composite material analysis. In this project, the compressive force required to fracture composite microneedle tips were assessed. The mechanical integrity of the samples were tested using an axial load testing station (Instron 3344, Buckinghamshire, UK). A 50-N load cell was utilised with a round stainless-steel metal rod applied to the microneedle array at a rate of 0.01 mm/s until a fracture was observed. Further details are described in the appropriate experimental chapter.

3.6 Surface Modification

Throughout this project, surface modification techniques were utilised to aid characterisation or functionality. The methods used are described below.

3.6.1 Electrochemical Anodisation

Pretreatment of electrodes in electrochemistry is often used to augment their electrochemical performance. Electrochemical anodisation is an amperometric technique used to enhance electrode response by increasing oxygen functionalities present on the electrode surface. Carbon is a widely used material in electrochemistry known for its rich interfacial properties making it a highly desirable electrode material. The ability to further enhance the superficial properties of carbon by means of electrochemical anodisation is advantageous for analytical purposes. Within this project, carbon containing electrodes acting as the anode, were enhanced by amperometric oxidation (+2 V) for varying lengths of time in 0.1 M NaOH. Upon hydrogen release at the cathode and oxygen at the anode surface, this leads to a surplus of hydroxide, thereby formulating oxygen functionalities on the electrode surface. This increase in oxygen functionalities combined with the increase in edge plane sites on the electrode interface enhances electron transfer kinetics. The effects of

anodisation in conjunction with sonication of carbon fibre electrodes was also observed in parallel to investigations in this project (Casimero *et al.*, 2020).

3.6.2 Sputter deposition

As previously described, especially for SEM characterisation, where insulating materials require a conductive coating for image analysis, thin film deposition is the typical method employed. During sputter deposition, high voltage emission causes the sputter material to gravitate onto a substrate under vacuum and inert gas. The ejected sputter material is forced upon the sample resulting in a thin film layer of conductive coating (nanometre thickness). Within this project, sputter deposition was often used as a pretreatment of samples prior to SEM analysis.

CHAPTER 4

Solid State Disposable pH Electrode with Integrated Flavin Polymer-Ferrocyanide Redox Couples

Abstract

A low-cost, voltammetric method of pH sensing using disposable screen printed electrodes, integrated with a bespoke flavin derivative (10-(4-hydroxyphenyl) benzo[g]pteridine-2,4(3H,10H)-dione) has been investigated. The flavin monomer was electropolymerised onto the electrode interface by oxidation of the phenolic substituent, thereby forming a redox film at the surface, with the surrounding pH influencing the voltammetric peak positions. Electrodes modified with the flavin for utilisation as a pH probe have been characterised and an appraisal of using ferrocyanide as an internal reference is also detailed. The system response exhibits Nernstian behaviour and the inclusion of ferrocyanide as an internal standard facilitates the exclusion of silver/silver chloride reference components during the fabrication process of disposable carbon based electrodes. The flavin modified system has proven to be robust with minimal drift (<4 mV during repetitive cycling) and consistent with commercial approaches of pH sensing in more complex biological samples such as soy milk.

The work reported in this chapter was accepted for publication in:

Hegarty, C., Kirkwood, S., Cardosi, M. F., Lawrence, C. L., Taylor, C. M., Smith, R. B., & Davis, J. (2018). Disposable solid state pH sensor based on flavin polymer-ferrocyanide redox couples. *Microchemical Journal,* 139, 210–215.

4.1 Introduction

The regulation of pH is vital for the maintenance of homeostasis within the human body and the ability to preserve an acid-base balance is critical for biological processes and cell metabolism. The function of the lungs to oxygenate the blood is just one example of a biological process dependent on a systemic pH level of 7.4. Thus, the kidneys predominant role is to regulate sodium bicarbonate concentration and therefore, acid-base homeostasis (Lee Hamm, Nakhoul and Hering-Smith, 2015). A deviation outside of the pH range 7.36 and 7.44 is a sign of acidemia and alkalemia respectively and, if not compensated for, may have detrimental effects on the human body. Aside from arterial pH levels, wound and intracellular pH values are other examples of where pH can provide vital information on the function of a person's biological processes (Schneider *et al.*, 2007; Casey, Grinstein and Orlowski, 2010). For these reasons, pH sensing is highly advantageous within medical diagnostics.

Conventional methods of pH sensing include the glass membrane pH probe which has been the traditional method used in laboratory settings. Although, with recent advancements in medical technology comes the requirement of miniaturised and disposable pH sensors. Technological advancements have chartered the progression of fabrication methods, propelling the application of sensors on the nanoscale and exploiting a myriad of nanomaterials for different functionalities. Along with this, their purpose in medical diagnostics comes with the need to avoid biological contamination and therefore, the development of new methods for the cost-effective production of disposable sensor systems is highly desirable.

The limitations of the typical glass membrane electrode including, fragility, large size, temperature instability, high impedance, and its high cost for manufacture, has driven research into various alternatives such as microsensors and optical pH measurements (Magnusson *et al.*, 2013). In terms of electroanalytical techniques, significant progress has been observed in the development of pH sensitive materials for the assembly of solid state pH sensors. Multiple metal oxide electrodes have been proven to work well as pH sensitive electrodes with RuO_2, NiO, ZnO, and IrO_x often being used for bioanalytical purposes (Bause

et al., 2018). These potentiometric methods rely on the direct measurement of pH, with multiple advantages over the glass membrane electrode like cost, stability, sensing ability, response speed and mechanical strength (Qingwen, Yiming and Guoan, 1999).

Although showing benefits over the glass membrane electrode, the traditional potentiometric methods have also exhibited their own limitations of instability and high detection limits (Stred'anský *et al.*, 2000). Thus, various electroanalytical voltammetric techniques have also been explored. The primary focus of the voltammetric approaches are contingent on the observation of the oxidation peak potential of an incorporated redox species. The oxidation peak will be subject to a shift in potential (typically exhibiting Nernstian behaviour with a shift of 57 mV/pH unit) in accordance with the surrounding pH solution. Variations of pH markers incorporated into sensors have shown great success by means of surface modifiers and endogenous markers (Phair *et al.*, 2011). The integration of redox markers using surface modification has been successfully demonstrated by self-assembled monolayers, polymers bound at the electrode surface, as well as intrinsic species being directly generated at the electrode surface to monitor pH levels (Lafitte *et al.*, 2008; Xiong, Batchelor-McAuley and Richard G Compton, 2011; Anderson *et al.*, 2014). Hence, the aim of this investigation was to assess the use of disposable screen printed electrodes (SPE) integrated with a new flavin based redox marker as a sensitive, cost-effective means of pH sensing.

In this work, the potential of using a new flavin derivative as a redox marker for indirect monitoring of pH was examined. Previously, flavin compounds have been utilised in electrochemistry for a myriad of functionalities. Riboflavin, otherwise known as vitamin B_2, is a well-known compound of interest for detection within electrochemistry, but more recently has proven particularly successful in electroanalytical devices as a redox indicator (Madhuvilakku *et al.*, 2017; Yu *et al.*, 2017). The presence of two keto groups within the flavin ring of riboflavin affords its redox activity. Subsequently, the redox capabilities of riboflavin have since been utilised as electrochemical mediators, intercellular mediators and probes for immunosensors (Wu *et al.*, 2016; Celiešiūtė *et al.*, 2017; Valipour and Roushani, 2017). Here, a new flavin derivative, depicted in **Figure 4.1** comprised of a phenolic constituent has been exploited as a redox probe for pH indication. The flavin monomer was electropolymerised onto the surface of a carbon-based SPE (**I** → **II**). The benefit of the

graphitic ink layer of the electrode provides an increased surface area from which to attach the derivative, as well as unique properties such as, enhanced electrical conductivity and chemical stability (Madhuvilakku *et al.*, 2017). The indirect monitoring of pH would rely on the redox mechanism of the flavin (**II** → **III** and **III** → **II**), provided these processes are maintained post polymerisation. Voltammetric analysis of the peak position shift, abiding by Nernstian behaviour, with respect to pH variation would allow a correlation to be drawn between the monomer redox potential and subsequent pH environment, thus, acting as a redox pH probe.

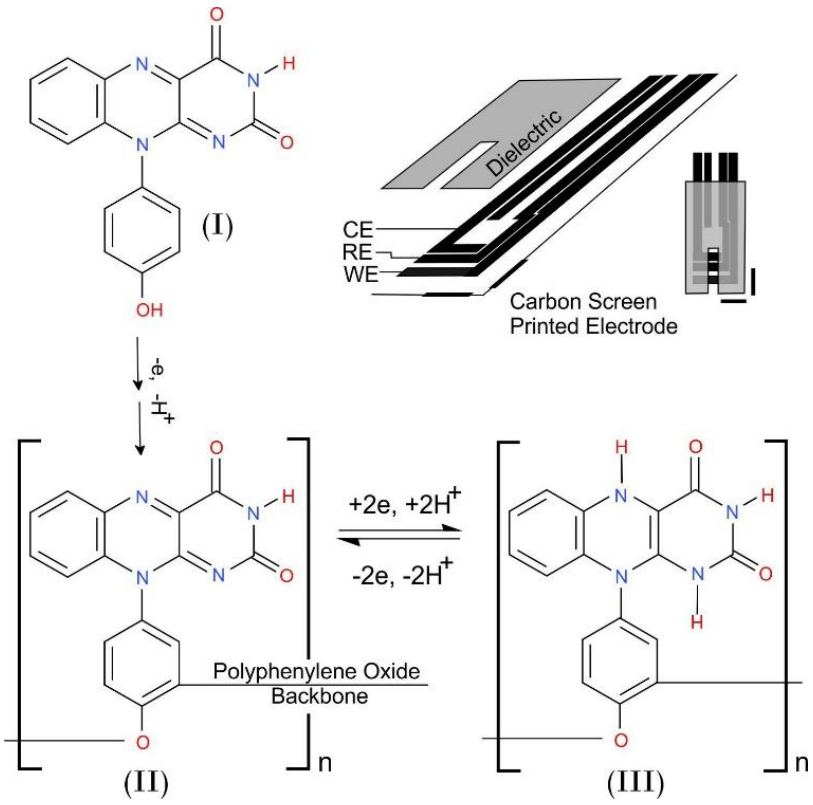

Figure 4.1 Proposed mechanism through which a flavin derivative bearing a phenolic substituent can be electropolymerised onto the electrode surface. The formation of a polyphenylene oxide chain possesses pendant flavin units capable of undergoing redox transitions (**II** → **III** → **II**). Inset: Design format of carbon-based screen printed electrodes utilised throughout.

With voltammetric analysis also comes some issues of drift and the need for recalibration. In this scenario, the reliance of the calculated pH is subject to measuring the peak positions against a stable reference electrode. Adding a silver|silver chloride reference to the disposable SPE (Inset **Figure 4.1**) in order to form a three-electrode setup would require a sufficient (and indeed constant) chloride ion concentration to be present within the sample

matrix, therefore making it just as comparable to use a pseudo-reference system. A notable method of overcoming this, is the use of an internal reference, measuring the potential difference between a pH sensitive and insensitive redox probe (Hickman *et al.*, 1991). Hence, in an attempt to rectify this, copolymerisation of a singular polymeric molecule, which contains both the pH sensitive and insensitive moieties has already been considered by Lafitte et al. (2008). Alternatively, this investigation explored the utilisation of ferrocyanide as a diffusible internal probe, providing a simpler and more attainable method of validating the electroanalytical prospect of using a flavin based redox pH probe.

As a controlled variable, a commercial silver|silver chloride (3 M KCl) half-cell reference electrode was first used in conjunction with flavin polymerised SPE in assessing various pH matrices, and the electrochemical response compared against the internal reference redox system. As any bioanalytical device may be subjected to repetitive and periodic monitoring, the reversibility, robustness, and potential drift of the system was also assessed by cycling the system through a series of pH regimes. Lastly, the accuracy of the system may be influenced by potential interferences and signal strength in a more complex biological sample, thus, soy milk was employed to test the analytical accuracy within a real sample matrix.

4.2 Experimental Details

4.2.1 Electrochemical Setup

Electrochemical measurements were recorded at $22^{o}C \pm 2^{o}C$, using a micro Autolab Type III potentiostat and a three-electrode system employed as per **Figure 4.1**. The carbon-based track of the screen printed electrode was used as the working electrode and a platinum wire functioned as the counter electrode. As previously mentioned, a commercial (BAS Technicol, UK) standard silver|silver chloride (3 M KCl) reference electrode was used as a comparison to the ferrocyanide internal reference. All chemicals used within the investigation were of the highest attainable grade, obtained from Sigma-Aldrich (Dorset, UK) and were utilised without any further purification strategies.

4.2.2 Flavin Compound and Characterisation

A Bruker Avance-III 300 MHz spectrometer operating at ambient temperature was used for the collection of ^{1}H and ^{13}C data. Tetramethylsilane (TMS) was used as the internal standard for ^{1}H NMR with deuteriochloroform ($CDCl_3$, δ_C 77.23 ppm) and deuteriodimethylsulfoxide (d_6-DMSO, δ_C 39.51 ppm) used in ^{13}C NMR investigations. Chemical shifts are quoted in ppm and coupling constants in Hertz (Hz) using the high frequency positive convention. Electrospray ionisation (ESI) mass spectra (low and high resolution) was obtained with a hybrid linear ion trap-Fourier transform mass spectrometer. Synthesis of the flavin (10-(4-hydroxyphenyl)benzo[g]pteri-dine-2,4(3H,10H)-dione) was achieved through the modification of existing methods (Cowden *et al.*, 1991; Bejugam *et al.*, 2007). The reaction pathway is summarised in **Figure 4.2** and involves the initial reaction of p-anisidine (**1**) with 2-fluoro-1-nitrobenezne (**2**) in the presence of potassium carbonate to yield 4-methoxy-2-nitrodiphenylamine (**3**). The latter was isolated at the pump in 78% yield and the crude material (**3**) reduced using zinc dust under acidic conditions. The intermediate was subsequently treated with alloxan monohydrate (**4**) in the presence of boric acid to yield the 10-(4-methoxyphenyl) benzo[g]pteridine-2,4(3H,10H)-dione intermediate in 93% yield. This was demethylated using hydrobromic acid yielding the final derivative (**5**) in 98% yield. ^{1}H NMR (400 MHz, DMSO-d_6) δ 11.40 (s, 1H), 10.06 (s, 1H), 8.16 (dd, J= 8.2, 1.5 Hz, 1H), 7.75 (ddd, J= 8.7, 7.2, 1.6 Hz, 1H), 7.60 (ddd, J=8.3,7.2,1.2Hz,1H), 7.19 (d, J=8.8Hz,2H), 7.03(d, J= 8.8 Hz, 2H), 6.86 (dd, J=8.6,1.2 Hz, 1H). ^{13}C NMR (75 MHz, d_6-DMSO) δ 160.12, 158.78, 158.78, 156.12, 152.53, 139.88, 135.22, 135.15, 135.09, 131.78, 129.28, 127.43, 126.37, 117.05. IR (ATR, cm^{-1}): 3052.32, 3151.73, 1716.20, 1666.31, 1611.52, 1527.94, 1503.20, 1191.86, 875.96, 844.29. MS (ESI) *m/z*: 307.1 [M^+]. Melting point ≥ 300 °C.

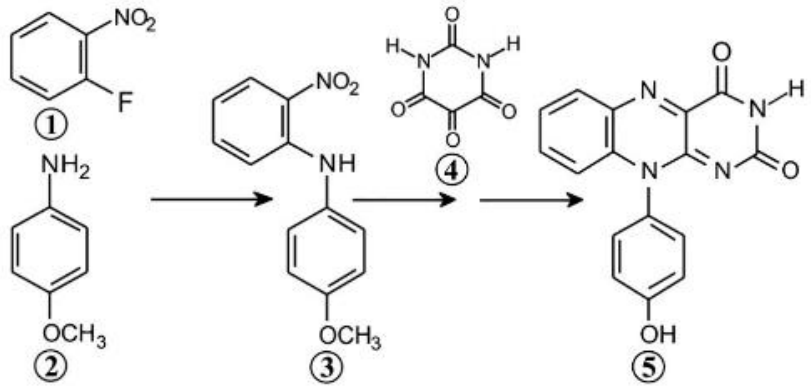

Figure 4.2 Synthetic pathway for the manufacture of the flavin monomer.

4.2.3 Electrode Fabrication

The screen printed electrodes (SPEs) were formed using a Reprint International R23 Semi-Automatic Screen printer. Carbon ink (Gwent Group C2030519P4) was pressed through stenciled stainless steel mesh (325 CL (50/30)) and onto AGFA Synaps® Offset Matt polyester substrate (450 g/m^2), creating the intended design outlined in **Figure 4.1**. Prior to sectioning, the electrodes were allowed to dry at 180^{o}C.

4.2.4 Electrochemical Anodisation

It has previously been recorded that oxidation strategies performed on carbon substrates increase the number of edge plane sites and the presence of oxygen functional groups at the electrode surface (Phair *et al.*, 2011; Casimero *et al.*, 2020). Using carbon ink on the SPEs provides the advantage of performing electrochemical oxidation to exfoliate the interfacial carbon layers and thereby, enhance electrochemical performance. Thus, electrochemical anodisation was performed on the SPEs (+2 V, 0.1 M NaOH) as a pretreatment.

4.2.5 Flavin Electropolymerisation

Polymerisation of the flavin monomer onto the electrode was performed by placing the SPE into an aqueous solution and initiating polymerisation cycles under quiescent conditions. The solution consisted of the flavin compound (150 µM) dissolved in pH 7 Britton-Robinson buffer with 0.1 M KCl as the supporting electrolyte and was degassed with nitrogen to blanket the electrochemical cell. Electropolymerisation was achieved using repetitive scan cyclic voltammetry (+0.2 V → -0.8 V → +1 V, 50 mV/s). It was observed that changes in the magnitude of the redox peak process could be attributed to the number of CV scans. Within this investigation, it was noted that 3-5 polymerisation scans were sufficient in providing well defined peak processes and so, this technique was used throughout.

4.3 Results and Discussion

It was predicted that upon employing repetitive scan cyclic voltammetry, the new flavin monomer would electropolymerise at the screen printed electrode (SPE) surface. The response of the SPE to the presence of the flavin compound (150 µM, pH 7, 0.1 M KCl) under quiescent conditions is depicted in the cyclic voltammograms shown in **Figure 4.3.1**. Sweeping the potential negatively from +0.2 V to -0.8 V, the reduction of the flavin compound (**II** → **III**) is observed at -0.408 V and upon the reverse sweep, the opposing oxidation peak (III → II) potential is shown at +0.336 V (ΔE_p = 72 mV). Another distinct feature to notice is the presence of a broad, irreversible peak at +0.82 V, which can be attributed to the oxidation of the phenolic substituent (I → II) within the flavin compound. Notably, sweeping the potential to sufficient magnitude at which to oxidise the phenolic component is deemed necessary to induce polymerisation. Successful electropolymerisation of the flavin derivative is observed by the increasing magnitude of flavin redox peaks upon each scan, indicative of material accumulation at the electrode surface. In addition to this, the magnitude of the anodic peak, representative of phenolic oxidation, will decrease with successive scans, which is characteristic of polyphenol formation (Belhadj Tahar and Savall, 2009; Santos *et al.*, 2019; Kiss *et al.*, 2020).

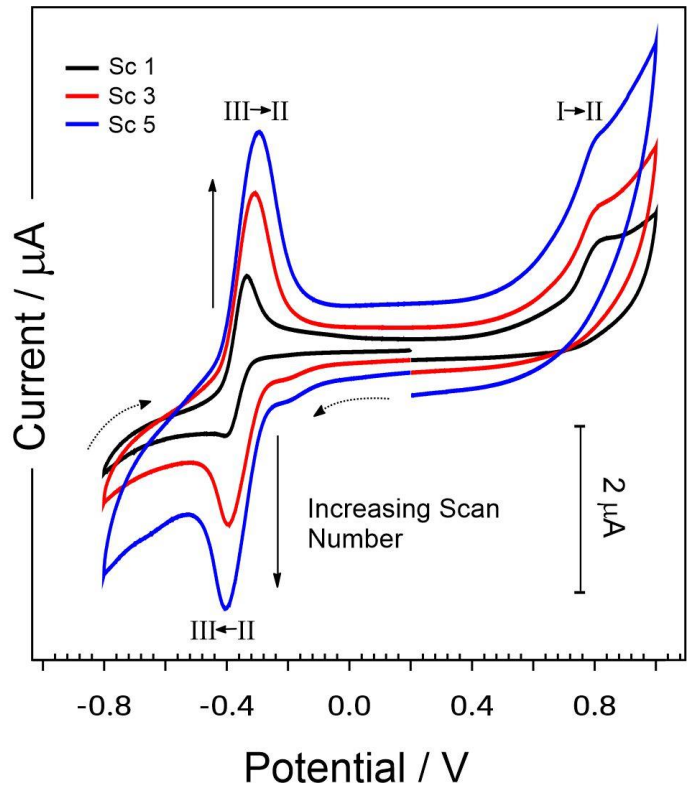

Figure 4.3.1 Cyclic voltammograms depicting the response of the carbon-based screen printed electrode to the flavin monomer (150 µM) in pH 7 buffer with 0.1 M KCl (scan rate 50 mV/s) after 5 electropolymerisation scans.

To determine the influence of pH on the flavin modified electrode response, square wave voltammetry was used, providing a more accurate analyses of oxidation peak potentials. Where previously electropolymerisation was performed under quiescent conditions to enhance redox peak resolution, nitrogen degassing was not used during square wave voltammetric analysis. This decision was based on impracticalities when applied to point of care diagnostic sensing, where the need for degassing would defeat the purpose of efficient, cost-effective disposable biosensing. Thus, the following square wave voltammograms were recorded in ambient air, with the assumption that the interference of oxygen reduction on the measured anodic peak would be minimal.

The response of flavin modified SPEs to various pH matrices are presented in the square wave voltammograms in **Figure 4.3.2**. The polymerised flavin monomer is instantaneously reduced (**II** → **III**) once the square wave scan is initiated at -0.6 V. A more negative potential increases the likelihood of bubble formation (hydrogen evolution) at the electrode surface, especially in acidic environments, effectively jeopardising the interfacial pH of the electrode

and producing a false response. As the potential sweep continues, a prominent oxidative peak is ascertained. Since the observed peak is without competing redox processes, this peak measurand can be attributed to the oxidation of flavin (**III** → **II**). From **Figure 4.3.2**, as predicted, the peak potential shifts in correlation with pH change, exhibiting near Nernstian behaviour (57 mV/pH unit).

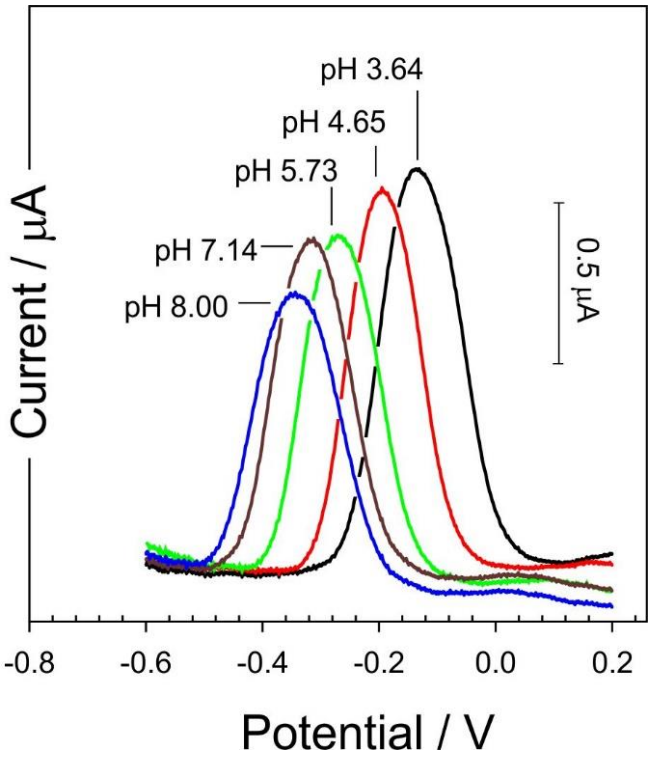

Figure 4.3.2 Square wave voltammograms representing the response of flavin modified screen printed electrodes towards varying pH buffer solutions.

As a means of validating the reversibility of the system, the SPEs were subjected to a further two cycles of sensing within the pH matrices, and the square wave voltammograms documented. **Figure 4.3.3.A** details the effect of pH detection throughout the three consecutive cycles, where minimal drift of the peak potentials (<3 mV) and reversibility of the flavin redox processes are observed. However, as shown in **Figure 4.3.3.B**, the oxidative peak current can be seen to decrease to 25% of the original magnitude after 68 successive scans. Thus, the robustness of the system is compromised by the oxidation peak failing to reach the same magnitude upon successive scans, expressing a loss of immobilised flavin from the electrode surface.

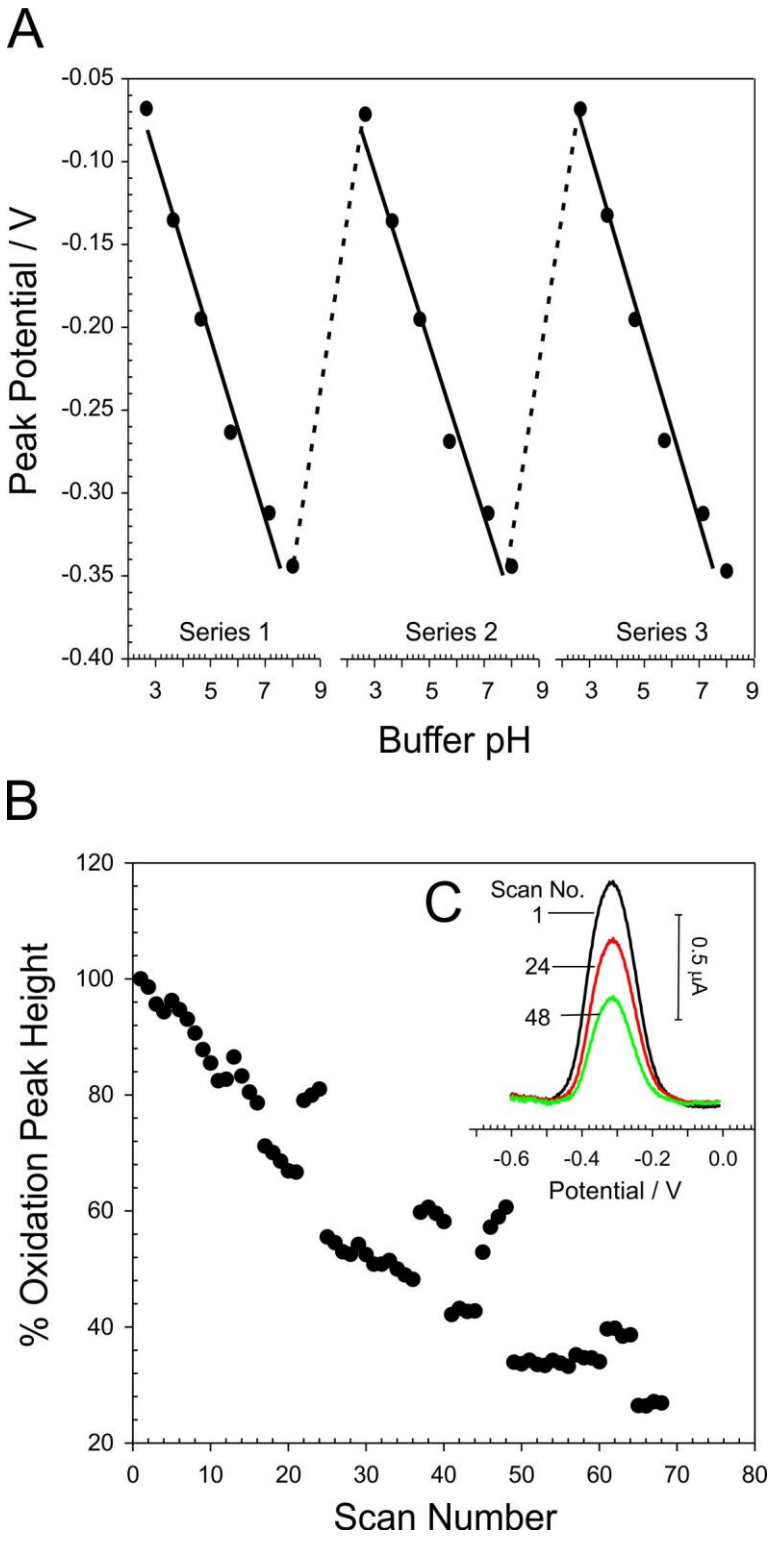

Figure 4.3.3 (**A**) Effect of consecutive cycle scans in varying pH on the flavin oxidation peak potential demonstrating reversibility of the system and (**B**) the influence of repetitive scans on the magnitude of the current response. (Inset (**C**) SWV visual depiction of diminishing current response)

The apparent curtailed response of the flavin after repetitive scans may be associated with the backbone of the flavin polymer, constructed by short phenolic spacers. The resultant

steric hindrance present in the polymeric backbone at the time of formation may cause the formation of oligomers, rather than a blanket network of polymeric chains through which the redox groups are attached to the electrode interface. Additionally, impurities may be introduced during the flavin film formation at the electrode surface. This is caused by doping intrinsic to the electrolyte used during the polymerisation process, thereby modulating the electrical properties of the film formation, and may also contribute to a diminished flavin response after numerous scans. Parallel to this, inconsistencies in the composite material of the SPEs can also obstruct the immobilisation of the flavin polymer, again forming segregated clusters rather than a network of polymeric film. Notably, increasing the number of polymerisation scans in pursuit of establishing an increased presence of flavin polymer had little to no effect on maintaining the magnitude of redox activity.

Despite a diminished redox peak magnitude, the correlation between oxidation peak shift and pH is maintained with minimal drift as shown in **Figure 4.3.3.A**. Unlike quinone based systems, where common electroactive interferences such as ascorbic acid and uric acid are expected to obscure peak processes with overlapping signals, the oxidation peak of the immobilised flavin occurs approximately 700 mV from ascorbate (pH 7). Evidently, the flavin redox mechanism lies in a region free from such interventions, therefore, making the flavin oxidative peak process an ideal system for calculating pH levels. However, applying this assumption of interference is dependent on the surrounding environment, where natural flavins present in a different sample matrix may cause overlapping signals.

Although, the voltammograms from **Figure 4.3.2** were analysed to exhibit Nernstian behaviour, it should be considered that they were recorded using a commercial Ag|AgCl half-cell reference. Whereas, if a solid state silver|silver chloride reference were used, the peak positions would be more susceptible to fluctuations in chloride ion concentration (Valipour and Roushani, 2017). In an attempt to counteract this issue, ferrocyanide was employed as a diffusible internal probe, insensitive to pH changes. It is expected that fluctuations in chloride activity will have mutual effect on the peak positions of both flavin and ferrocyanide oxidation. This would allow the pH sensitive flavin oxidation peak to be measured in correspondence with the oxidation peak process of ferrocyanide. In principle, the analytical signal can be derived from the peak separation of the two oxidative peaks, thereby, acting as an internal standard and eliminating the issues associated with analysing the standalone

flavin peak position. In addition to removing the complication of chloride concentration, it would also aid the fabrication process of the disposable strips by excluding the cost of silver ink application.

The incorporation of ferrocyanide as an internal probe to the flavin polymerised SPE system and its response to varying pH regimes are detailed in the square wave voltammograms shown in **Figure 4.3.4**. From the square wave voltammograms, it can be seen the ferrocyanide oxidative peak occurs at +0.187 V with minimal drift observed upon varying pH level (±6 mV). Again, the flavin modified SPE, with the integrated ferrocyanide probe, exhibits a near Nernstian response: E_{pa} = 0.057 (±0.004) V; pH – 0.167 (±0.0178) V; N = 15; R^2 = 0.991 (error estimations are inclusive of fluctuation in ferrocyanide peak position and is based on 95% confidence limit assessments).

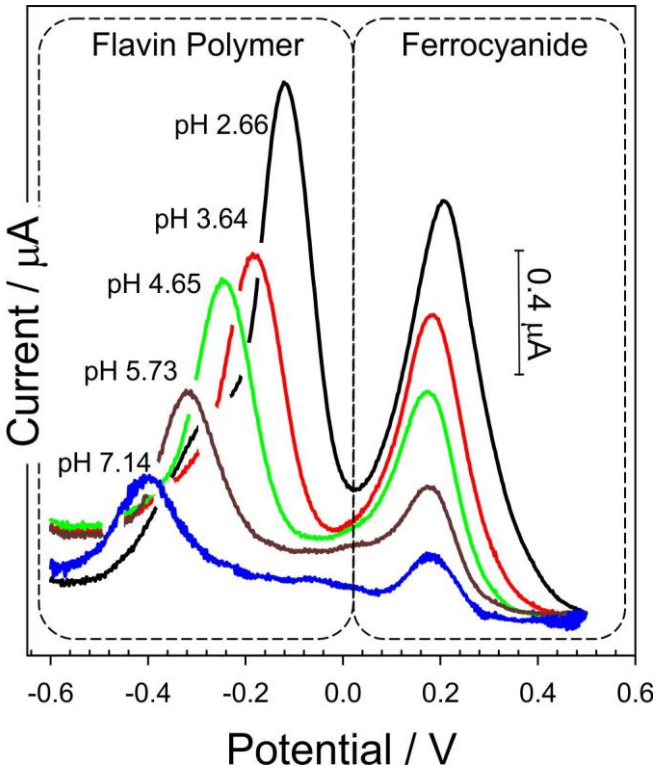

Figure 4.3.4 Square wave voltammograms showing the flavin modified screen printed carbon electrode response to varying pH with an internal ferrocyanide reference.

A more detailed quantitative evaluation of the ferrocyanide internal standard SPE system is illustrated in **Figure 4.3.5**. The use of a commercial silver|silver chloride reference is

compared against the disposable SPE system. Both systems were based on the response of flavin oxidation in varying pH, measured against either the commercial half-cell reference electrode, or, calculated by the peak separation from the internal ferrocyanide probe. Both systems were subjected to three measurements each, and the average displayed in **Figure 4.3.5,** where the error bars are of negligible magnitude (1-2 mV) and therefore, cannot be seen on the scale used. Near Nernstian behaviour was exhibited by both systems and trivial deviation observed in their gradients across the examined pH regime. Thus, the ferrocyanide internal probe approach has been demonstrated as a feasible alternative to the traditional commercial reference electrode.

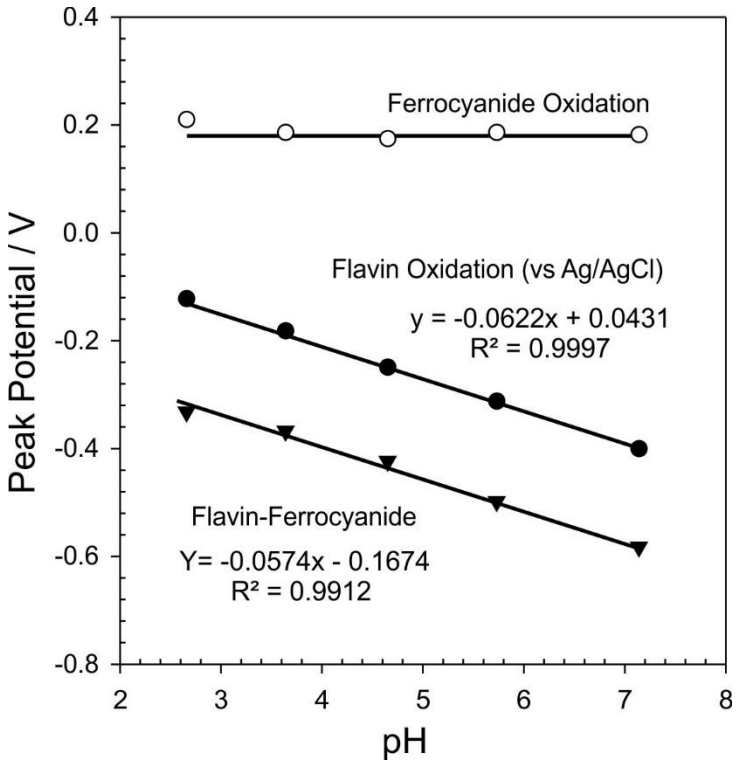

Figure 4.3.5 Comparison of pH influence on oxidative peak position of a screen printed electrode system with and without internal ferrocyanide standard.

Durability is an essential characteristic of disposable electrodes when applied to the field of point of care diagnostics and so, performance repeatability and inter electrode reproducibility were examined, as indicated in **Figure 4.3.6**. To assess the repeatability of the flavin modified SPEs, the same operator cycled the same electrode through 10 measurements in pH 6 buffer, with the electrode response recorded and their peak separation evaluated. Inter electrode reproducibility was also assessed using the same

method, but with 5 separate electrodes and 5 measurements taken. Repeatability and inter electrode %RSD of the flavin modified SPEs were found to be 1.03% and 1.65% respectively, corroborating the robust nature of the fabrication process and analytical capabilities of the electrodes.

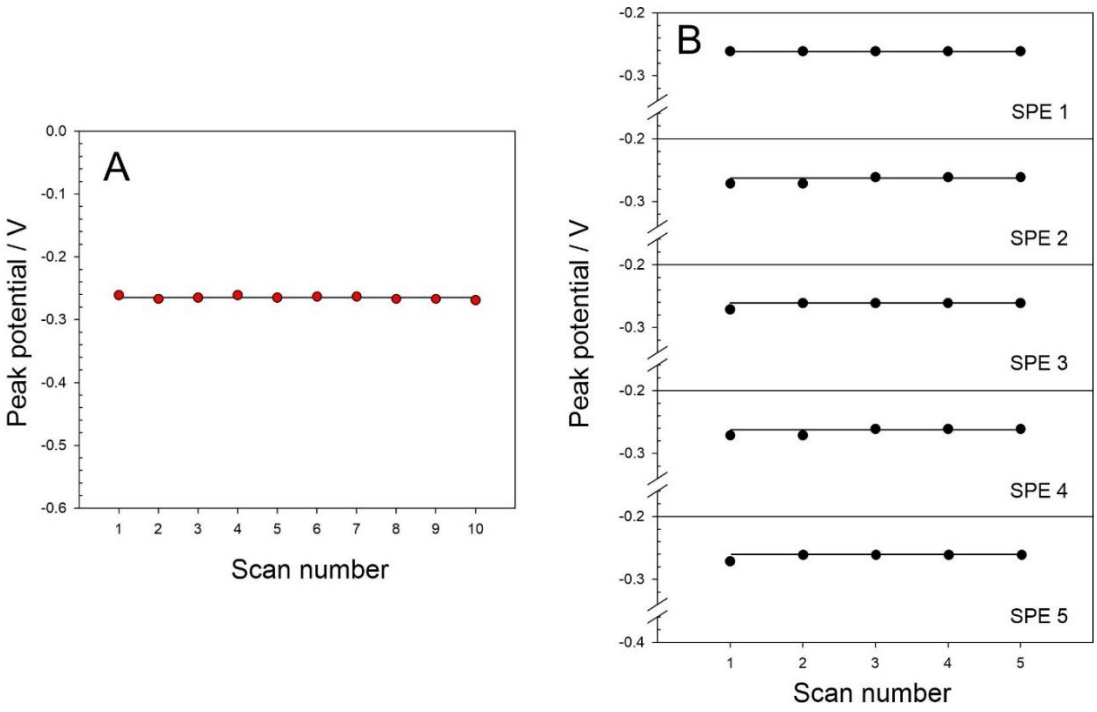

Figure 4.3.6 (**A**) Examining flavin modified screen printed electrode repeatability and (**B**) interelectrode reproducibility by examining peak potential variance.

The analytical performance of the flavin modified electrodes have been demonstrated in pH buffer solutions. Although, it was noted that pH buffers are free from common electroactive interferences and therefore, would not take into account natural flavins that may be present in biological samples. Thus, the accuracy of the system within more complex sample matrices were appraised in soy milk. Soy milk products have been established as a significantly complex sample model, containing isoflavones, protein and a fluctuant amino acid and carbohydrate profile (Chen *et al.*, 2017). Fermenting soy milk has recently proven as an economical alternative to fermented cow's milk, but more importantly has been identified as a key component for nutrition (Niamah, Sahi and Al-Sharifi, 2017). The fermentation of soy products with probiotic bacteria has been propounded as a method to increase bio-effectiveness and availability of soy constituents (Lee *et al.*, 2013). The process of soy fermentation is pH dependant and so, regulating pH is a critical factor in maintaining

product specifications (Dashper *et al.*, 2012; Chen *et al.*, 2017). Hence, it was envisaged that soy milk would prove a challenging and intricate testing sample for the flavin modified SPE system containing the internal ferrocyanide probe. The response of the flavin modified SPE sensor system with, and without the internal ferrocyanide standard are compared in **Table 4.3.1** alongside measurements recorded using a commercial glass pH probe. The evaluation of pH using the SPE system with and without the ferrocyanide probe was shown to be consistent with the glass pH probe and comparable to glass pH probes, where the error of a typical commercial laboratory probe is approximately ± 0.25 pH (Mettler Toledo, 2015). Although greater error was evident using the internal standard SPE method, this can be attributed to slight variation in peak position of the internal ferrocyanide reference. Nonetheless, the SPE system proved an invaluable electrochemical analytical tool even in complex biological media, free from electroactive interferences and ambiguities in signal strength.

Table 4.3.1 Response of flavin modified screen printed carbon electrode systems in commercially available soy milk samples.

Milk sample	Actual pH	Method	Mean pH	Error*
Soy sweetened	6.66	Flavin peak	6.75	± 0.076
		Flavin-ferro	6.79	± 0.239
Soy unsweetened	6.82	Flavin peak	6.80	± 0.072
		Flavin-ferro	6.88	± 0.233

*Error estimated at 95% confidence interval

4.4 Conclusions

From the investigation, the flavin derivative was shown to be successfully electropolymerised onto the carbon tracks of the screen printed electrode and generated significant redox peaks, obeying Nernstian behaviour over the pH range 3 to 8. The flavin modified electrode response exhibited pronounced redox peaks, which lie in a potential window free from common impeding electroactive species. Upon cycling the system through pH regimes, the derived pH measurement remains consistent with minimal drift, however, peak signal strength dwindles with repetitive scanning. Although, it is noteworthy that the

peak response was still valid and measurable even after 68 scans. While a diminished signal intensity could prove problematic for continuous monitoring applications, the disposable SPE design purpose is intended for single shot analysis and therefore, should escape the ambiguity of loss in signal strength. The constraints associated with the use of reference electrodes in voltammetric analytical approaches has long been established. Here, the use of an internal standard by means of a ferrocyanide pH insensitive probe was shown to be a feasible alternative and the accuracy of the system illustrated – with and without a silver chloride reference.

CHAPTER 5

Construction of Microneedle Array Sensors Based on Carbon Nanoparticle Composites

Abstract

Micromoulding techniques were used to manufacture conductive composite microneedle arrays consisting of carbon nanoparticles dispersed throughout a polystyrene binder. Mechanical force testing of the composite microneedles were used to examine their capability for skin penetration and assess the subsequent risk of needle-stick injuries. X-ray photoelectron spectroscopy and contact angle measurements have been analysed to describe the effect of electrochemical anodisation on the interfacial properties of the composite arrays. Anodisation was shown to be effective in enhancing electrochemical performance through a considerable increase in oxygen functionalities present on the microneedle surface. Validation of the system within a complex biological sample was assessed by detection of uric acid in horse blood. The adaptable methodology of fabricating microneedle arrays detailed here, can be tailored through the composite nature of the micromoulding procedure. This offers a rapid prototyping approach in the absence of high precision machinery to produce carbon-based sensors and opens a surplus of opportunities for other biomedical sensing applications.

Publications resulting from the work presented in this chapter:

McConville, A., **Hegarty, C.**, & Davis, J. (2018). Mini-Review: Assessing the Potential Impact of Microneedle Technologies on Home Healthcare Applications. *Medicines*, 5(2), 1–15.

Hegarty, C., McKillop, S., McGlynn, R.J., Smith, R.B., Mathur, A., Davis, J. Microneedle array sensors based on carbon nanoparticle composites: interfacial chemistry and electroanalytical properties. *J Mater Sci*. 2019;54(15):10705–14.

5.1 Introduction

Hypodermic needle injection is an invaluable method for therapeutic drug delivery for those drugs that otherwise cannot be taken orally. Likewise, hollowbore needles are a critical tool in performing phlebotomy on a patient requiring blood analysis. Despite their establishment as a fundamental tool in medicine, these sharps come with some major drawbacks. The potential of a needle-stick injury (NSI) has become a normalised hazard to healthcare workers, mostly due to improper use and disposal of sharps. The annual risk of a healthcare worker sustaining a needle-stick injury can be as high as 80% (Lee *et al.*, 2005). Notably, the incidence of NSIs is considerably higher in developing countries, where 75% of cases are not reported (Goel *et al.*, 2017). In addition to incurring a percutaneous injury, this increases the risk of transmission of blood borne pathogens (BBP). As reported by the US Centers for Disease Control (CDC), approximately three million healthcare workers are exposed to blood and bodily fluids as a result of an NSI annually (Sriram, 2019). Aside from needlestick injuries, the predominant use of sharps in medicine maintains a myriad of other disadvantages. The process of puncturing the skin with a needle can be painful and distressing for many patients. Thus, phlebotomy and needle injection often prove to be difficult procedures, especially in paediatrics and for patients presenting with needle phobia (McMurtry *et al.*, 2015; Orenius *et al.*, 2018). Furthermore, for patients who require routine sampling, such is the case for diabetic patients, there is a prevalent increase of insulin needle reusage, which can lead to infection and tissue scarring (Becton Dickinson, 2006). Unsurprisingly, there have been multiple interventions in medical technology attempting to overcome the safety hazards and needle phobia associated with routine medical procedures.

Transdermal drug delivery by method of microneedle (MN) patches has accumulated considerable attention over the past few decades (Prausnitz, 2004). Originally used as a minimally invasive technique in facilitating drugs to overcome the stratum corneum (SC) layer of the skin, they now offer a pain free approach of injecting high molecular weight drugs by the micron sized projections that penetrate the skin (Donnelly and Larrañeta, 2018; Ita, 2018a; Rzhevskiy *et al.*, 2018). The relative sizes of a typical MN array (200(b) x 500(p) x 700(h) µm) are compared to a conventional hollowbore syringe in **Figure 5.1.1.A** with a more detailed image of the needle projection shown in **Figure 5.1.1.B**.

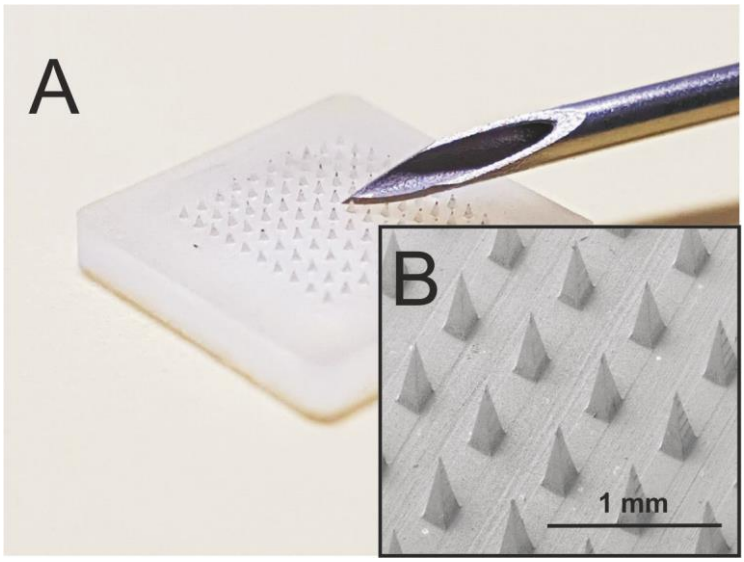

Figure 5.1.1 Comparison of a typical silicone microneedle array against conventional hollowbore syringe needle (**A**) and a more detailed electron microscopic image of the silicone microneedle patch (**B**) consisting of 100 (200(b) x 500(p) x 700(h) µm) needles.

A diverse range of concepts have previously been explored in fabricating MN masters, although, the common trend here surrounds lithography or etching of silicon wafers and computer numerical control (CNC) milling of metallic blocks such as aluminium (Moga *et al.*, 2013; Lutton *et al.*, 2015; Chiaranairungroj, Pimpin and Srituravanich, 2018; Ribet, Stemme and Roxhed, 2018). The construction of microneedle masters has been extensively reviewed, and it should be noted that the material of the workhorse template consistently used in the production of MN masters, is almost invariably designed from polydimethylsiloxane (PDMS) (Lim *et al.*, 2018). With advancing technology and the ever increasing the availability of PDMS moulds, there is no longer a requirement to possess the high specification equipment necessary to produce MN masters (Zhu *et al.*, 2009; Cha *et al.*, 2014). The accessibility of PDMS moulds which cater for an assortment of needle designs have since initiated intrigue in generating new MN formulations and expanding their design purpose. Adapting the material composition within the PDMS moulds has not only provided great benefits for therapeutic drug delivery, but has also established an opportunity to produce MNs for sensing applications. With relation to electrochemical MN sensing arrays, great progress has been observed for glucose monitoring applications however, they often rely on a metal coating (Au or Pt) deposited onto a preformed MN array (Sharma *et al.*, 2016; Chinnadayyala, I. Park and Cho, 2018; Kim *et al.*, 2019).

Traditionally, microneedle applications have been heavily focused on transdermal drug delivery. However, the potential of using commercial PDMS moulds to construct MNs from a conductive composite material could pave the way for rapid prototyping of simplistic, cost-effective microneedle biosensors, and eliminate the costs associated with high precision machinery in producing MN masters (Sharma *et al.*, 2016). The composite MN approach was originally examined by constructing conductive palladium|polycarbonate MN arrays and was shown to be a promising fabrication method for electrochemical sensing (McConville and Davis, 2016). Alternatively, the prospect of producing carbon-based MN arrays could be highly advantageous, and facilitate the adoption of established electroanalytical methods based on carbon electrodes, hence, pioneering new methods of transdermal sensing. More poignantly, the large overpotential necessary to induce the hydrogen evolution reaction at carbon makes it an ideal material for electroanalytical investigations, providing a larger potential window than would be available using conventional electrode materials such as gold or platinum (Sharma *et al.*, 2016; Chinnadayyala, I. Park and Cho, 2018; Kim *et al.*, 2019). Another benefit of exploiting carbon, is the nature of structural chemistries exhibited at its surface, where the presence of endogenous quinones may be functionalised for catalytic capabilities (Anderson *et al.*, 2014). Furthermore, the assortment of interfacial carboxylic acid groups at the carbon surface has the potential to facilitate carbodiimide bonding of biomolecules such as enzymes or antibodies (Brownlee *et al.*, 2018; Desai *et al.*, 2018).

Whilst polymeric MNs, for the purpose of transdermal drug delivery, have recorded challenges with penetrating through the stratum corneum due to the inherent elasticity of the skin, the physical properties of the polymeric constituent play a vital role (Singh *et al.*, 2019). Many of these polymer drug delivery MNs require characteristics that facilitate controlled drug release. Whereas, the sole purpose of the polymer within this context is to serve as a binder for the conductive nanoparticles, and provide structural stability for transdermal penetration. It could be envisaged that an increase in the conductive nanoparticles in the composite MNs would increase conductivity, however, it has previously been noted that a compromise is necessary in maintaining architectural integrity (McConville and Davis, 2016; Hegarty, McConville, *et al.*, 2019).

Hitherto, the force required for minimally invasive MN puncture has been estimated as being less than that needed to push an elevator button (<10 N), with a closer examination

documenting a force less than 0.03 N for reliable insertion through skin, although, this is of course subjective to needle geometry and material properties (Henry *et al.*, 1998; Olatunji *et al.*, 2013). Such small forces are clearly advantageous from the perspective of clinical application, hence, their potential for countering needle phobia and reducing the incidence of NSI events has long been recognised. However, it is also possible that they could pose a safety issue when applied within the home and by non-experts, where the careless positioning of the MN array could lead to their accidental application. This obviously poses a dilemma in that if the MNs are discarded, MNs which have been used for previous transdermal application, any subsequent penetration raises the possibility of BBP transmission. The situation is further complicated by the relatively benign nature of the MN array, and, where the painless nature of the application could mean that any accidental MN application could go unnoticed and hence, treatment delayed. A health advisory notice was recently announced by Public Health England relating to the risk of BBP transmission from the cosmetic application of facial microneedling systems (Public Health England, 2017).

Some evidence for the potential inadvertent application of MNs can be obtained from an everyday source – the common garden nettle (**Figure 5.1.2.A** and **5.1.2.B**). The latter, Urtica dioica, will have resonance with many childhood experiences, where the slightest causal contact with its leaves can lead to a stinging sensation. The latter is due to a perfusion of microneedles on the leaf surface capable of injecting a cocktail of chemical irritants. The needles, composed largely of silica, are highlighted in **Figure 5.1.2.C** and **Figure 5.1.2.D,** where the spherical end cap is displaced upon contact, revealing the hollow microneedle. It could be imagined that a similar experience with a MN of not too similar size, but without the noxious cocktail, could occur painlessly.

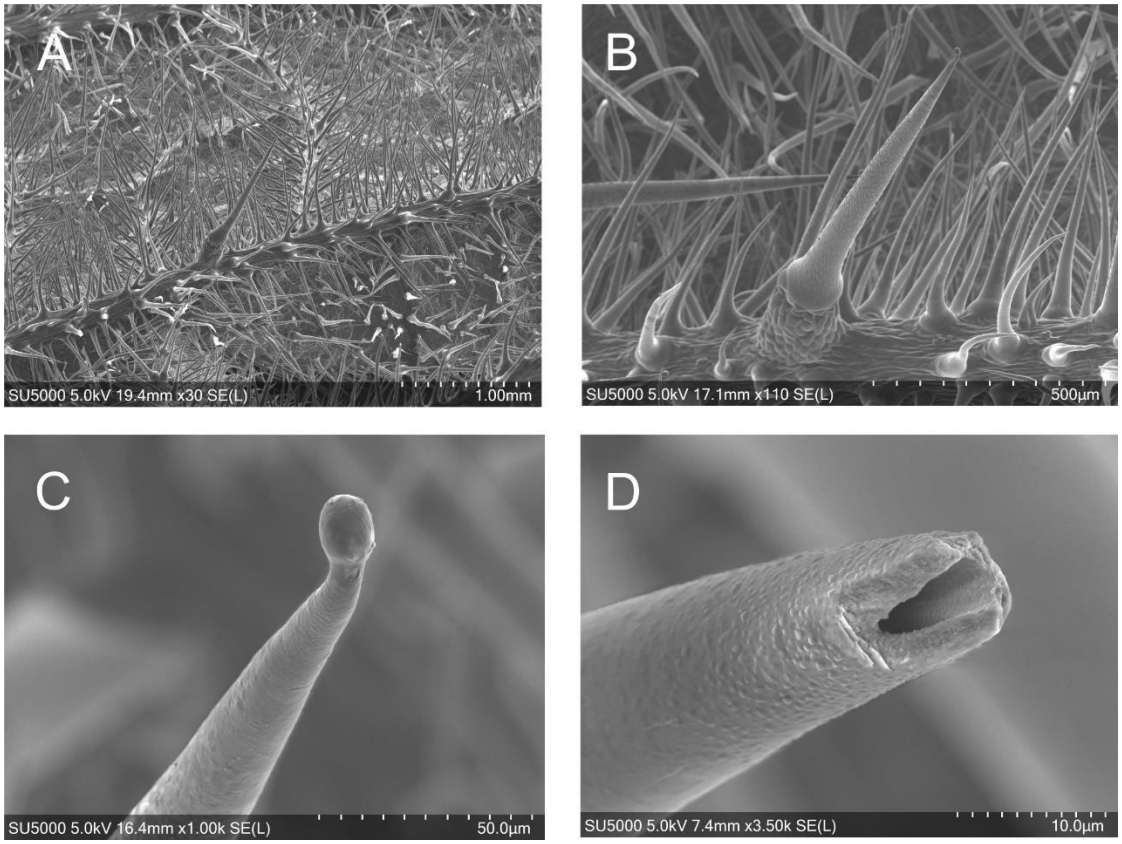

Figure 5.1.2 Scanning electron microscopy images of Urtica dioica (the common garden nettle) (**A, B**) and individual microneedles protruding from the surface of the nettle (**C, D**).

Within this investigation, a preliminary study was conducted to assess the possibility of accidental MN injury resulting from the hands/limbs being in contact with a MN patch left on a solid surface. A number of simulated scenarios involving workplace/domestic actions were undertaken, and the forces applied between surface and the human subject measured to determine if these standard movements would be sufficient for accidental and/or intentional MN puncture. Thus, this observational study of typical movements within an engineering laboratory may also be used in conjunction with mechanical fracture testing to ascertain whether microneedle fabrication in a laboratory setting has cause for concern, but also in the wider context of their applications within clinical or domestic environments (McConville, Hegarty and Davis, 2018).

The second component of the study was to investigate the suitability of conductive carbon composite MN arrays as the basis of an electroanalytical sensor. The granular structure of carbon particles is anticipated as a possible hindrance to mechanical integrity of the

microneedle design. Therefore, the incorporation of nanoparticles is essential for efficient dispersion throughout the polymeric component of the composite MN. Thus, microneedles were fabricated from carbon nanoparticle-polystyrene composite, with the modification of interfacial properties examined as a means of enhancing sensing capabilities.

The performance of the MN system was examined through the electroanalytical detection of uric acid, which is an accepted biomarker used in clinical diagnostics of cardiovascular disease, kidney function and stroke among others (El Ridi and Tallima, 2017; Kumagai *et al.*, 2017; Zhong *et al.*, 2017; Kei *et al.*, 2018). There is a vast network of literature surrounding electroanalytical detection of uric acid, as the biomarker continues to be at the forefront of diagnostic research using 2D carbon-based nanomaterials and other catalytic particulates (Baig, Rana and Kawde, 2018; Raymundo-Pereira *et al.*, 2018; Azzouz *et al.*, 2019). Therefore, the MN response to urate present within a biological sample (horse blood) was critically examined for potential use as a transdermal sensor, as well as the material characteristics of the fabricated MN arrays.

5.2 Experimental Details

5.2.1 Materials

Carbon nanopowder (< 100 nm) and polystyrene pellets (MW 192000) were obtained from Sigma-Aldrich (Dorset, UK), along with all other chemicals used in the investigation, were of the highest attainable grade and were utilised without further purification strategies. Defibrinated horse blood was acquired from Fischer Scientific (Thermo Scientific Oxoid 100 mL) and used upon receipt. Britton-Robinson buffers (acetic, boric and phosphoric acids) were used throughout, unless mentioned otherwise. Silicone microneedle templates were procured from Micropoint Technologies Pte Ltd (Singapore), and consisted of a 10 x 10 array of pyramidal shaped needles (200 µm base x 500 µm pitch x 700 µm height).

5.2.2 Instrumentation

Electrochemical measurements were recorded at 22°C ± 2°C, using a micro Autolab Type III potentiostat and a three-electrode system employed. The microneedle array was employed as the working electrode, with a platinum wire and commercial silver|silver chloride (3 M KCl, BAS Technicol, UK) used as the counter and half-cell reference electrodes respectively.

The conductivity of the microneedle arrays were calculated using a 2461 series SourceMeter® four-point probe (Keithley), with the average conductivity of an unmodified MN array measured as 1575.2 ± 96 Sm^{-1} (n = 5). Static contact angle measurements were taken using the sessile drop method (5 µL of deionised water as probe liquid) and a CAM 200 optical contact angle meter (KSV Instruments Ltd.). Left and right contact angles were then determined from the high-resolution CCD camera images using drop shape analysis.

X-ray photoelectron spectroscopy (XPS) of the MN arrays before and after electrochemical anodisation was performed using a Kratos Axis Ultra DLD Spectrometer. Analysis of spectra was completed under typical parameters of 15 kV and 10 mA (150 W) at an operating pressure lower than $6x10^{-8}$ Pa using monochromated Al Ka X-rays (*hv* = 1486.6 electron volts (eV)). A hybrid lens mode was used (electrostatic and magnetic) during analysis, with a 300 µm x 700 µm analysis area at a take-off angle (TOA) of 90° relative to sample surface. Wide energy survey scans (WESS) were collected across a range of – 5 to 1200 eV binding energy (BE), with a pass energy of 160 eV and step size of 1 eV. High-resolution spectra were collected with a pass energy of 20 eV, a 0.05 eV step size, a 25 eV scan width, a dwell time of 150 ms and at least 3 sweeps to reduce the signal noise. A Kratos charge n95eutraliser system with a filament current between 1.8 and 1.95 A, a charge balance of 3.3 – 3.6 V and a filament bias of 1.3 V was used for all samples. Charging effects on the BE positions were adjusted by setting the lowest BE for the C1s spectral envelope to 284.8 eV, which is commonly accepted as adventitious carbon surface contamination. Three measurements were taken per sample, with a Shirley background subtracted from each XPS spectra. The peak areas of the most intense spectral lines for each elemental species were used to determine the percentage atomic concentration. Peak fitting of high-resolution spectra was carried out using Casa XPS software.

5.2.3 Preparation of Microneedles

Carbon nanoparticles and polystyrene beads were mixed at a 1:1 ratio, then dissolved and stirred in cyclohexanone (MW 98.14 g/mol) for approximately 2 hours or until a homogenous solution was formed. For the preparation of microneedles detailed in this thesis, 2 mL of solvent was used for every 0.3 g of polymer. Solubilising this volume of polymer was a compromise for the time taken to form a homogenous solution and the volume required for the number of silicone moulds for the investigations within this thesis. The 1:1 ratio has previously been determined to be the optimal formation, as varying the carbon component beyond this either leads to poor conductivity or decreased mechanical integrity. The mixture was then suspended into the silicone templates with a carbon fibre stub inserted at the base plate to ease electrical connection. The templates were placed in a vacuum oven at 30 °C, the pressure increased to 1000 mbar and upon reaching the desired pressure, the air was released again. The pressure increase was to ensure packing of the homogenous solution at the microneedle tips and drawing air out of the mixture, ensuring sharp needle tip formation. If necessary, after vacuuming the templates were topped up with more of the homogenous mixture, ideally overflowing the template to account for solvent evaporation. The templates were then left at room temperature to allow solvent evaporation (over 48 h), thereafter, the microneedle arrays could be carefully withdrawn from the templates. The typical morphology of a 1:1 (wt) carbon|polystyrene composite MN array obtained from the silicone templates (Micropoint®) is depicted in **Figure 5.2**. The geometric electrode area (0.49 cm2) was defined by coating the baseplate and non-needle surfaces with enamel, acting as a dielectric material and left to dry for approximately 6 hours.

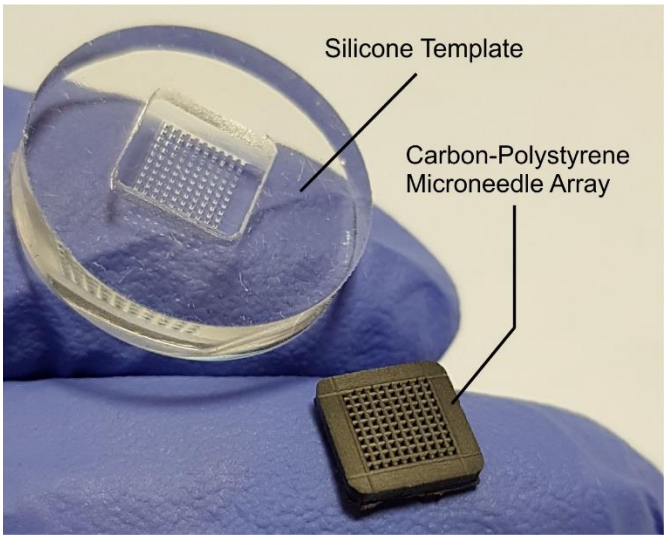

Figure 5.2 Silicone template employed for fabricating 10 x 10 array microneedle and example array consisting of (100 x (200(b) x 500(p) x 700(h) µm) needles.

5.2.4 Preliminary Posture-Force Assessment

In order to record force application, a force plate (FP-BTA, Vernier Software & Technology, USA) was employed in conjunction with a Go!Link® single-channel USB interface and accompanying Logger Lite software from the same supplier. The force plate was positioned on a lab bench, adjacent to a chair upon which 28 participants, both male and female, of ages 19 – 47, were instructed to sit. Once comfortable, the participants were asked to take up a number of postures that simulated the type of contact likely to arise within a conventional laboratory setting. The subject's hands/wrist or forearm were placed on the force plate, measured at rest, and then asked to transfer weight to their hand in order to move from the chair to a standing position. The actions were performed in triplicate with a force-time measurement recorded on each occasion – typically over a 10 second period. Finally, data was exported from Logger Lite to Excel 2016 (Microsoft, USA) for statistical analysis. The Force Plate study was approved by the Ulster University Faculty of Computing and Engineering Ethics Filter Committee (Ref: 20170911 17.46). A total of 28 healthy volunteers (researchers and students) from within the School of Engineering were recruited with the cohort covering an age range of 19-47 years.

5.2.5 Fracture Testing

The mechanical force necessary to fracture the composite microneedle systems was examined using an axial load test station (Instron 3344, Buckinghamshire, U.K.). A 50 N load cell was employed, along with a stainless-steel metal rod (Ø = 10 mm), which was applied to the needle surface of the MN array at a rate of 0.01 mm/s until a fracture was evident. The MN was fixed to the bottom plate of the testing station to prevent deflection, and fracture of the needles was confirmed by observation through an optical microscope and force/displacement graph in real time. The effect of mechanical compression testing on the MNs was also later inspected using electron microscopy.

5.3 Results and Discussion

5.3.1 Evaluation of Fabrication Methods

Composite microneedles have previously been formed by casting a mixture of metallic particles (typically Pd) in a polymer/dichloromethane (DCM) solution into a silicone mould (McConville and Davis, 2016). The design of the silicone template determines the geometry of the resultant MN array. A composite MN patch consisting of conductive metallic particles homogenously dispersed throughout the polymeric binder is then formed upon evaporation of the DCM solvent. Here, the objective was to distribute carbon nanoparticles (< 100 nm) throughout a polystyrene binder, thereby facilitating electrical conductivity from needle tip through to MN base plate. The MN design concept is depicted in **Figure 5.3.1**, where connection to an external potentiostat was accomplished via connection from the back of the base plate.

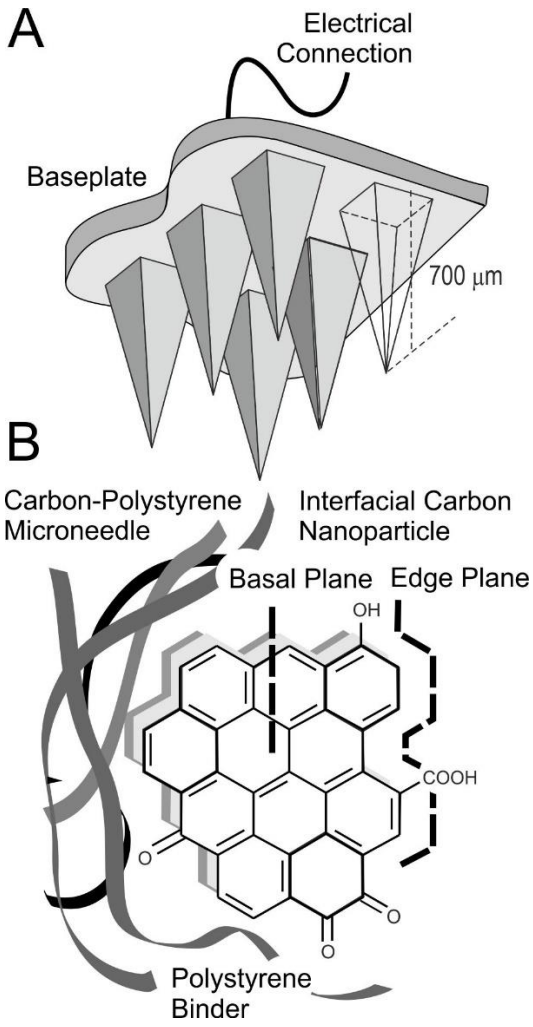

Figure 5.3.1 (**A**) Microneedle geometry and (**B**) interfacial structure of conductive carbon nanoparticles bound within the microneedle array.

Initial attempts to produce MNs composed of carbon nanoparticles in a polycarbonate|DCM mixture were found to yield substandard arrays, where the structural integrity of the needles and baseplate was visibly compromised as shown in **Figure 5.3.2**. Hence, an alternative polymeric binder, polystyrene, was used for the remainder of the investigation. It was also decided to refrain from using DCM as the solvent to prevent any damage to the silicone template, thus, cyclohexanone was deemed sufficient in dissolving the polystyrene polymer. The increased boiling point of the cyclohexanone greatly eased the handling and subsequent casting of the mixtures in comparison to rapid evaporation characteristics of the DCM.

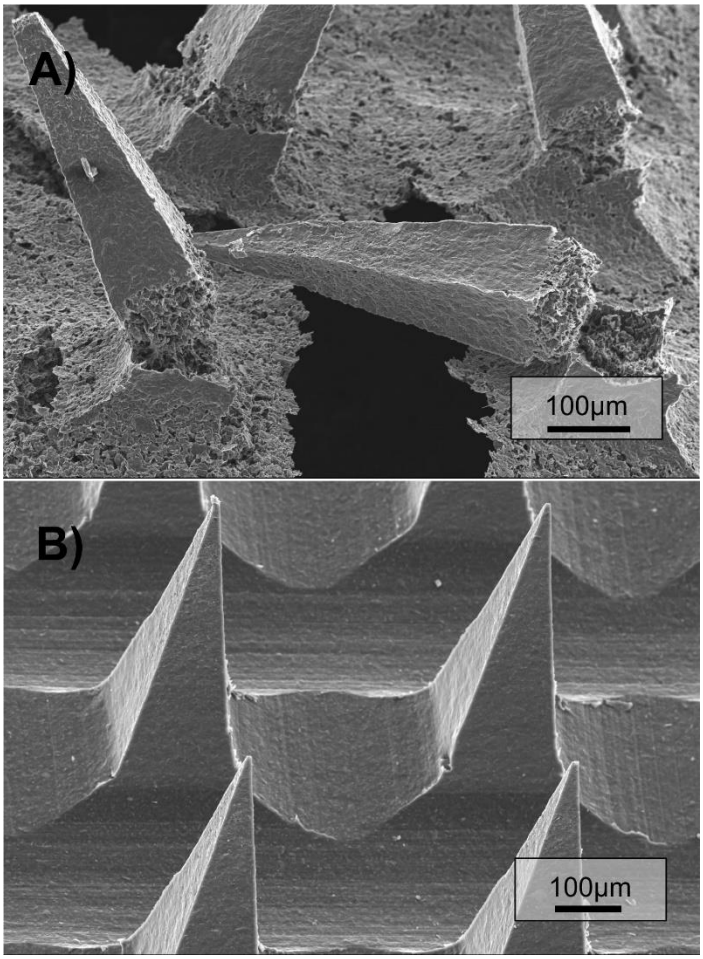

Figure 5.3.2 (**A**) Scanning electron micrographs detailing morphology of microneedles composed of carbon nanoparticles within a polycarbonate|DCM mixture and (**B**) a polystyrene|cyclohexanone mixture.

The presence of graphitic carbon is anticipated at the interface, maintaining a range of functionalities and surface defects although, it is expected to mostly consist of basal plane formation highlighted in **Figure 5.3.1**.**B** The lack of active edge plane sites, exhibited by a basal plane structure at the interface, may pose as a deterrent to electron transfer kinetics for electroanalytical detection of biomolecular species such as uric acid (Dutt *et al.*, 2005). Exfoliation of solid carbon structures such as screen printed electrodes and carbon fibres by electrochemical anodisation is a method proven to enhance electroanalytical performance (Phair *et al.*, 2011; Anderson *et al.*, 2014). Application of this method may be beneficial to electron transfer kinetics but, it was considered that such processes may also be detrimental to the needle microstructures.

5.3.2 Preliminary Force Plate Study

A preliminary observational study of general behaviour within a typical laboratory served to identify actions that would, if a discarded MN patch (similar to those highlighted in **Figure 5.3.2.B**) were present, lead to a possible needle-stick event. The latter requires the physical placement of skin on a work surface and, as such, hands and arms – resting, leaning or manipulating equipment on a bench represented the most probable targets. Six scenarios, detailed in **Table 5.3.1**, were investigated and the forces resulting from surface contact appraised. In general, the subject may be in a sitting position, and either casually resting their arm on the work surface (1), or, using their hand/wrist, raise their body from the seated to standing position (2). The force exerted on the work surface was determined using force plate measurement. A selection of the typical force profiles for some of the simulated activities are detailed **Figure 5.3.3**.

Table 5.3.1 List of six scenarios used to model typical forces exerted on a workbench.

Position number	Motion
1	Hand – Leaning on table
2	Hand – Sitting to standing position 1 hand
3	Hand – Sitting to standing position 2 hands
4	Forearm/Wrist – 2 arms resting on table
5	Forearm/Wrist – Sitting to standing
6	Elbow – Leaning on table

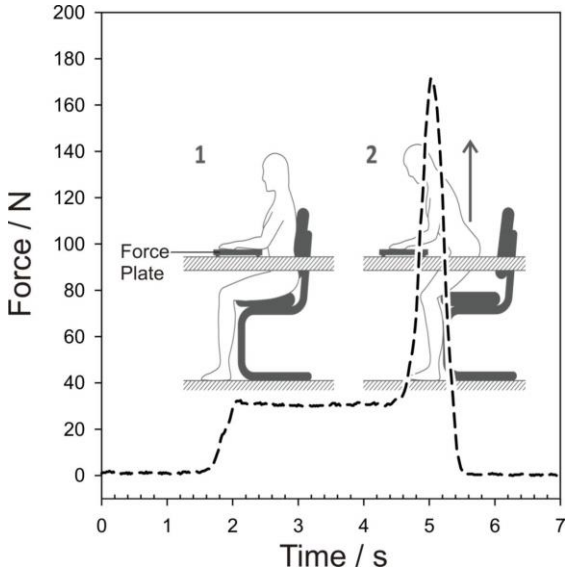

Figure 5.3.3 Example of force profile recorded in real-time as a consequence of using motion 3 to raise the subject from a seated (1) to standing (2) position.

A breakdown of the force distribution for each activity among the sampled cohort is detailed in **Figure 5.3.4**. Numerous studies have examined the insertion of microneedles, and it is generally regarded that thumb pressure applied to the back of the patch is sufficient to induce skin puncture. According to previous studies, which have recorded forces necessary for skin puncture to be less than that needed to push an elevator button (<10 N), it is clear from the results, shown in **Figure 5.3.4**, that each activity exerts forces that would be more than sufficient to penetrate skin (Henry *et al.*, 1998).

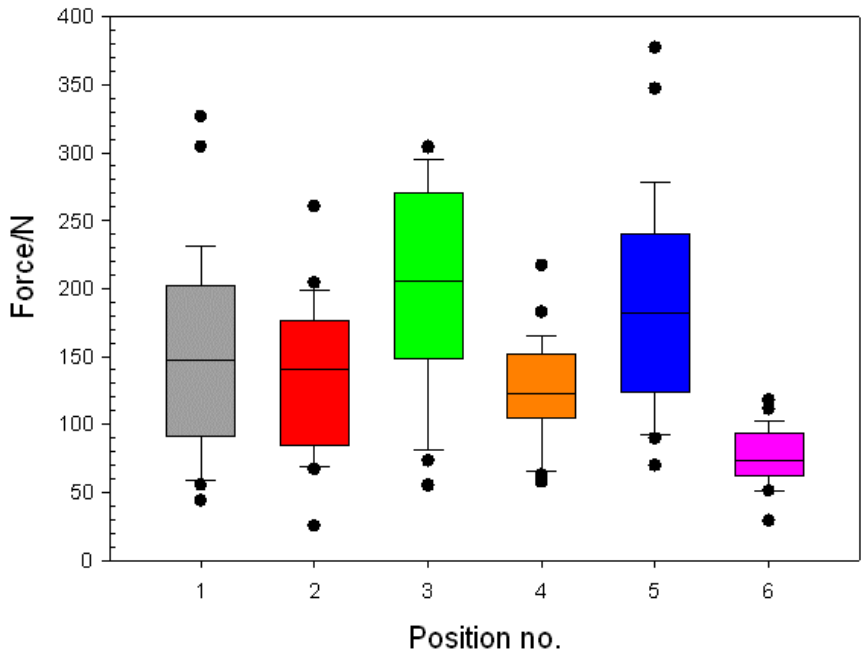

Figure 5.3.4 Variation in applied force recorded for each motion among sampled cohort (Based on sample of 28 volunteers).

5.3.3 Compressive Force Testing

The mechanical force necessary to fracture the composite MN arrays was determined by compression, with the mean axial force required to fracture the MN tips assessed as 11.35 N ± 0.91 N (n = 5), equating to 0.1 N per needle. A representative example of this testing is shown in **Figure 5.3.5**, where the point of fracture occurs at 12.55 N. This coincides with a previous study of hollow polymeric needles requiring a 0.27 N force to produce a needle fracture (Nicholas *et al.*, 2018). It's anticipated that the introduction of carbon particles to the composite system contributes to an increased fragility of the microneedle structure. However, it should be noted that needle geometry, particular needle tip width, holds great influence over the force necessary for needle puncture (Davis *et al.*, 2004). Despite this, the fracture force of the carbon|polystyrene MN lies comfortably outside the range required for reliable insertion through the skin (0.028 – 0.03 N) (Olatunji *et al.*, 2013). The effect of compression on needle structure was later observed by SEM as seen in **Figure 5.3.5**, which corroborates with previous studies of metallic hollow needles, where the continuation of axial force after fracture begins to crush the needle (Davis *et al.*, 2004). As evidenced from

the scanning electron micrographs (**Figure 5.3.2** and **Figure 5.3.5**), the microneedles in this study present with a high aspect ratio and an average tip width of 2.5 µm (n = 10). It should also be noted that it is possible to acquire templates capable of producing needles of various heights, typically 200 to 1000 µm in height, which of course may affect aspect ratio and tip width, however, for the purpose of this investigation, a fixed needle height of 700 µm was used throughout.

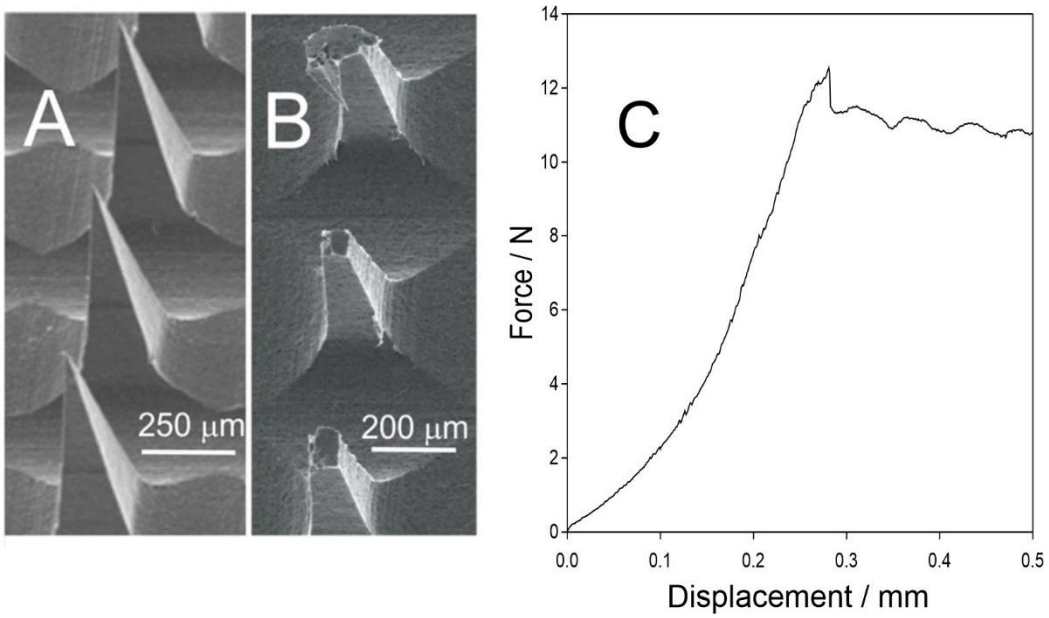

Figure 5.3.5 Scanning electron microscope images of carbon-polystyrene microneedles before (**A**) and after (**B**) compression testing, along with a representative example of the force/displacement graph from one microneedle array sample (**C**).

Considering the preliminary study of general behaviour in a laboratory setting, the typical forces exerted on a worktop bench were shown to be more than sufficient for MN penetration through skin. Although the magnitude of the force required to fracture the needles was considerably less, it's important to acknowledge the difference in material properties between skin and the stainless-steel rod driven into the needle face of the MN array (Davis *et al.*, 2004). Thus, it can be assumed the structural integrity of the composite needles proposed here would be more than adequate for skin penetration. Whilst this invokes the threat of NSIs within the lab, the actual risk of BBP transmission by a solid MN would be relatively low given the small surface area of the needle compared to a conventional hollowbore needle (Martin *et al.*, 2017; McConville, Hegarty and Davis, 2018). It is also important to consider other mitigating factors that will improve safety within the

lab, of which the wearing of gloves is an obvious safeguard. Preliminary experiments indicated that the MN could penetrate through stretched latex and nitrile. This is highlighted in **Figure 5.3.6**, where electron micrographs reveal the penetration of the needle tips through a section of nitrile glove (previously held taut over a rubber block).

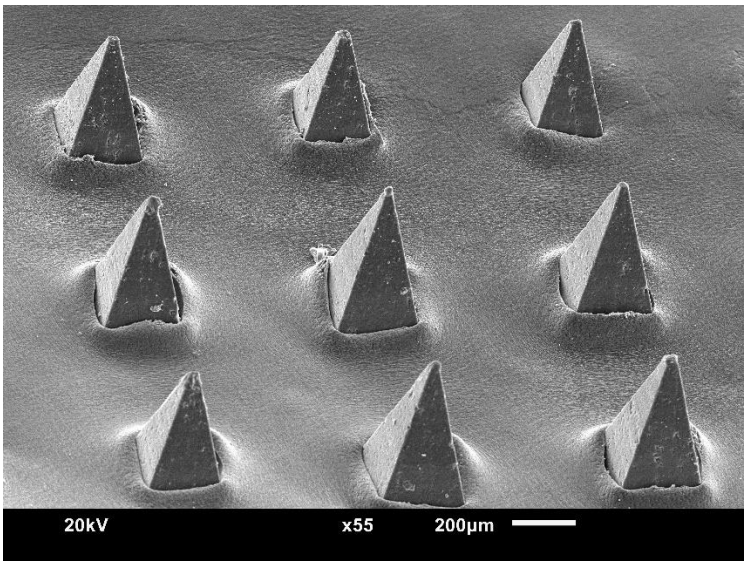

Figure 5.3.6 Scanning electron micrograph highlighting the ability of microneedles to penetrate through a nitrile glove segment.

The puncture of the common safety glove, as highlighted in **Figure 5.3.6**, indicates that the needle length is greatly reduced, such that only the tips protrude, but this will obviously depend on the dimension of the original MN array. A secondary safety feature inherent to the wearing of gloves relates to a wiping function, whereby, the close contact between the nitrile (or latex) with the MN surface also aids in the removal of contaminants (i.e. blood). This can be inferred from the electron micrograph in **Figure 5.3.6,** where there is close physical contact between the nitrile and the individual needles. The possible cleaning action upon initial penetration (I->II) and a proposed second NSI (III->IV) is highlighted in **Figure 5.3.7**.

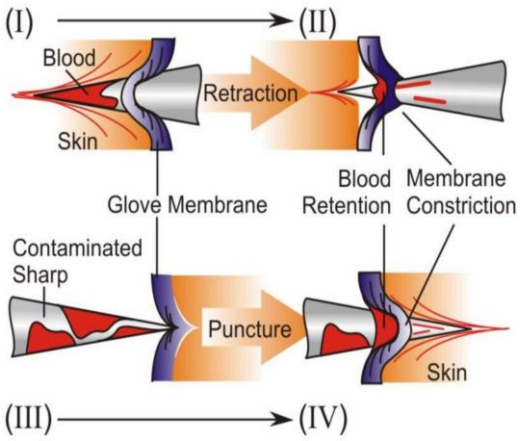

Figure 5.3.7 Proposed cleaning effect of conventional nitrile gloves preventing accidental transmission of contaminants during a needle-stick injury. Where (I->II) represents the initial penetration of clean microneedle and (III->IV) penetration of a contaminated microneedle.

There are clear benefits to the wearing of gloves when handling MNs, but their use in domestic situations will depend on the context in which the MNs are applied. It is clear that the small dimensions of the array present less risk, but are not necessarily benign and caution is still required.

5.3.4 Electrochemical Evaluation

Unmodified carbon|polystyrene microneedle responses to uric acid in pH 7 buffer are shown in the square wave voltammograms in **Figure 5.3.8.A**, where a broad oxidation peak is observed at +0.6 V and increases in correlation with increasing concentration of urate. When the same MN array is subjected to five minutes of electrochemical anodisation and the samples re-run, the oxidative peak can be seen to shift to +0.3 V, with a dramatic increase in magnitude. This is attributed to the exfoliation of carbon at the electrode interface, exposing more edge plane sites (**Figure 5.3.1**), which increases the presence of oxygen functionality groups and, thereby, enhances the electron transfer kinetics. The limit of detection represented by the MN array was calculated to be 2.85 µM (based on 3.3 S_b/m) which, relative to other forms of electrochemical detection, is in the lower range of detection limits (WitkowskaNery, Santhiago and Kubota, 2016; Azeredo *et al.*, 2020) The microneedle response also demonstrates the capability to detect within uric acid concentrations within

biofluids, as typical concentration of uric acid found within human blood plasma ranges from 100 to 250 µM. The sensitivity of the MN electrode system, 361 µA mM^{-1} cm^{-2}, was shown to be competitive with literature reports providing comparative data, without undergoing any further complicated modifications (Ali *et al.*, 2018; Foroughi, Rahsepar and Kim, 2018).

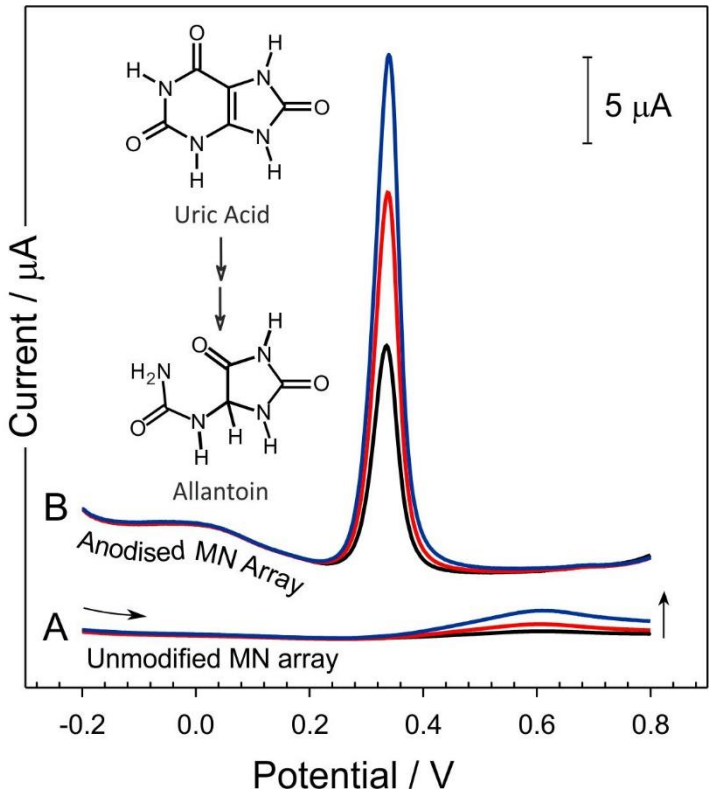

Figure 5.3.8 Square wave voltammograms showing response of a carbon nanoparticle-polystyrene microneedle to varying uric acid concentrations in pH 7 buffer before (**A**) and after (**B**) electrochemical anodisation at +2 V in 0.1 M NaOH.

Further investigation of the carbon-based interface was conducted using high-resolution X-ray photoelectron spectroscopy (XPS). The C 1 s profile of the carbon|polystyrene MNs before, and after anodisation are detailed in the spectra in **Figure 5.3.9.**

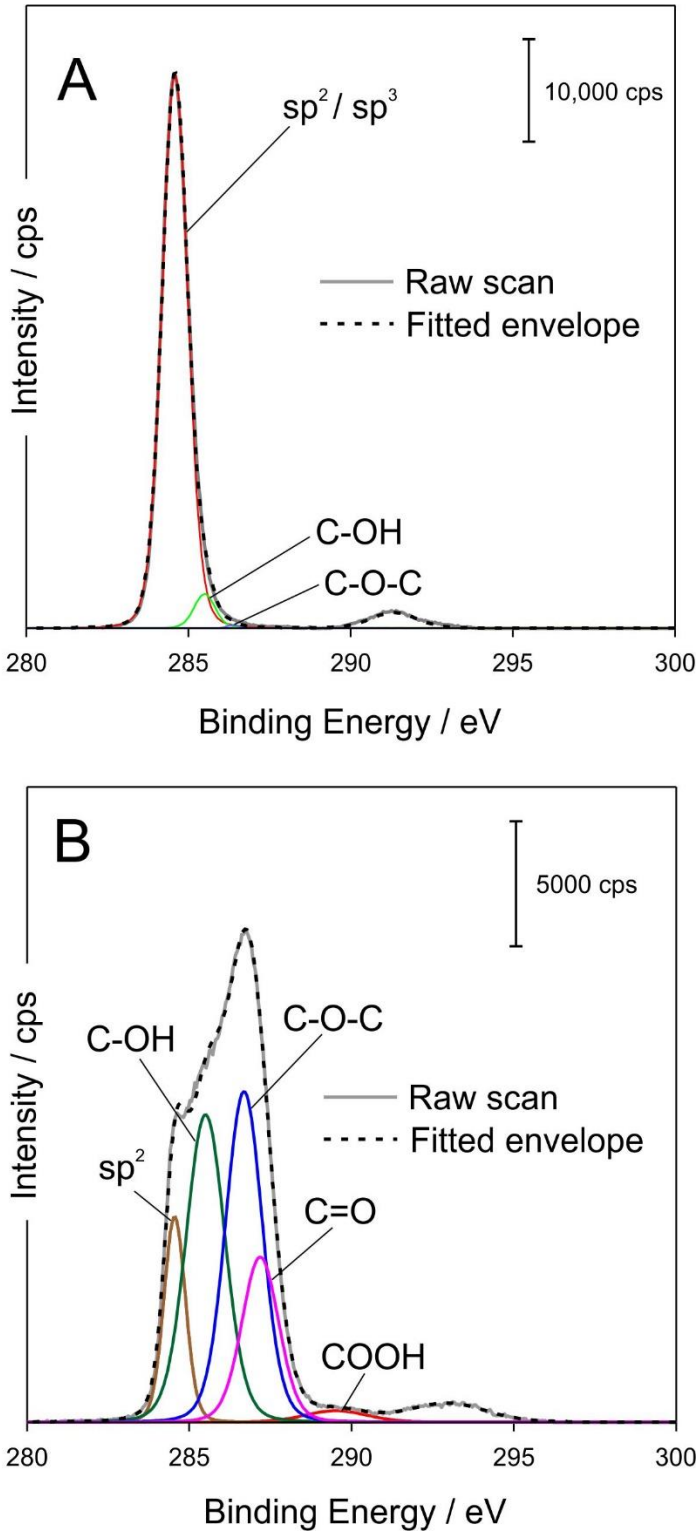

Figure 5.3.9 XPS spectra of carbon-polystyrene microneedle electrode surface before (**A**) and after (**B**) electrochemical anodisation at +2 V in 0.1 M NaOH.

On observing the XPS data obtained, a significant increase in oxygen functionality is exhibited at the carbon electrode surface post anodisation when compared to the relatively simplistic

spectra displayed by the unmodified MN. Another distinct difference in the spectra is the decrease in magnitude of the sp^2 peak after anodisation, which can be primarily attributed to the oxidation of the carbon present at the composite interface. Notably, sp^2 and sp^3 moieties will both be present at the interface however, differentiating between them is impractical under the operating conditions used.

Despite the decrease in magnitude of the sp^2 signal, it is well pronounced in both spectra, and can be largely attributed to the non-conductive polymeric binder possessing unreactive aromatic rings which are unlikely to change after anodisation. A further detailed investigation of the surface composition is detailed in **Table 5.3.2**, highlighting the increase in various oxygen functionalities enabled post electrochemical anodisation, which coincides with previous studies (Anderson *et al.*, 2014; Casimero *et al.*, 2020).

Table 5.3.2 XPS data highlighting the change in carbon-oxygen functionalities present on the microneedle surface before and after electrochemical anodisation at +2 V in 0.1 M NaOH.

	Peak Position / eV	% Composition	
		Unmodified MN	Anodised MN
C 1s			
Sp^2	284.57	73.4	13.0
C-OH	285.50	12.7	28.9
C-O-C	286.52	10.3	31.8
C=O	287.50	0.0	19.3
COOH	289.13	0.0	2.5
Pi to Pi*	292.11	3.7	4.5
O 1s			
C=O	531.47	3.7	1.4
C-O	532.47	59.1	24.5
C-OH	533.80	19.4	24.1
Absorbed Water	534.14	17.8	50.0

*Mean values based on 3 replicate measurements

As demonstrated by the XPS spectra, there is a significant lack of carbon-oxygen functionalities at the MN interface. Thus, it was anticipated the composite material would express an appreciable hydrophobic status. Upon anodisation, the MN array displays innumerable polar groups, and, a high degree of intercalated water, which can be expected to substantially increase hydrophilicity. The contact angle for the polystyrene constituent

used in the formation of the MN arrays was assessed by solvent casting onto a planar silicone sheet, lacking needle protrusions and was measured as 88.7° ± 0.9° (n = 6), coinciding with previous studies of the material (Extrand and Kumagai, 1997; Thomas *et al.*, 2008). Carbon-polystyrene films were then examined before and after electrochemical anodisation, providing angles of 98.1° ± 0.81° and 95.2° ± 2.9° (n = 6), respectively. While anodisation was expected to greatly improve surface wetting, the incorporation of carbon nanoparticles has the greater effect of increasing hydrophobicity compared to the singular polymeric component. The introduction of microneedles on the surface only further increased hydrophobicity, as an unmodified and anodised carbon|polystyrene composite MN displayed angles of 115° ± 7.7° and 108° ± 1.3° (n = 6), respectively. This can be observed by contact angle imaging shown in **Figure 5.3.3**, accentuating the hydrophobicity exhibited by the MN system.

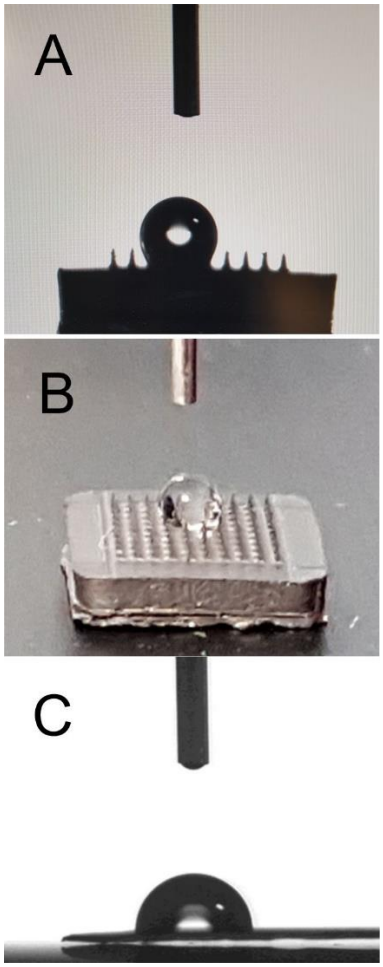

Figure 5.3.10 Contact angle measurement being analysed on an unmodified carbon-polystyrene microneedle (**A, B**) and an unmodified carbon-polystyrene film (**C**).

5.3.5 Electroanalytical Performance

An exploratory assessment of the viability of using the anodised MN array as an analytical sensor within biological fluids was completed using defibrinated horse blood (HB) as the testing media. Urate is an established key biological marker and a naturally occurring product which can be found in horse blood (Räsänen *et al.*, 1996). Thus, uric acid concentration analysis within HB was performed using a MN sensing system based on a standard addition protocol, where known volumes (50 µL) of standard urate solution (0.01 M) were added to the testing media (10 mL). Square wave voltammograms exhibiting anodised MN response to increasing concentration of urate in HB are displayed in **Figure 5.3.11**. A prominent oxidation peak is detected as a result of urate oxidation in the HB and the current response increases in accordance with increasing uric acid concentration added (the standard addition) to the HB media. The typical reference range for urate in HB plasma falls within 30-250 µM and is dependent on the health and activity of the animal (Adamu *et al.*, 2012). Of the defibrinated HB used in this investigation, the MN system detected a 155 µM concentration of uric acid.

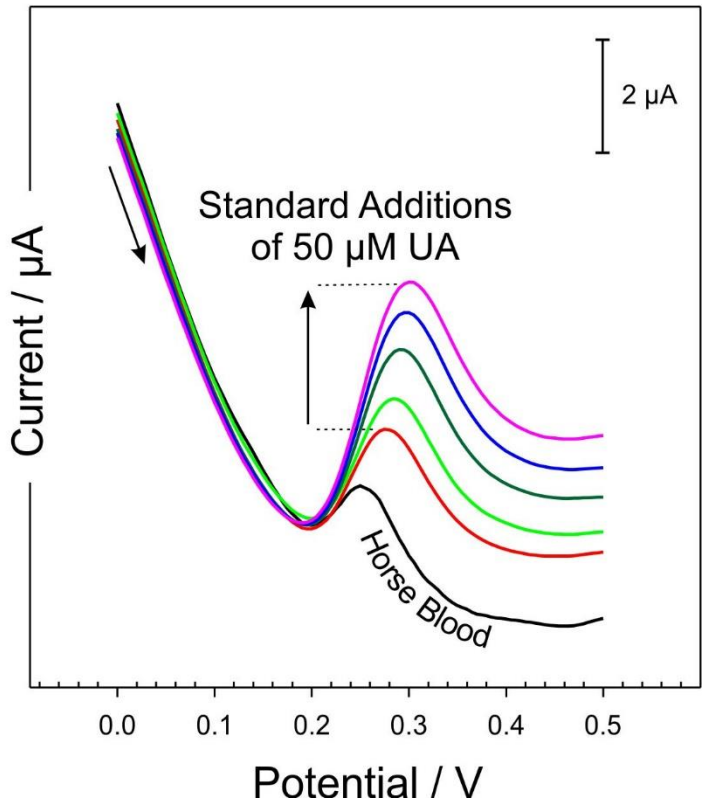

Figure 5.3.11 Square wave voltammograms depicting the anodised microneedle response in horse blood before and after standard additions of 50 µM of uric acid.

Although the MN system exhibited a clearly defined and identifiable peak process for the oxidation of urate within the biological media, a slight peak shift is recognised with increasing additions of standard urate and can be attributed to accumulative fouling of the electrode surface. This is not an uncommon issue, as previously realised by Phair and coworkers, where carbon screen-printed electrodes were subject to surface contamination by proteins and macromolecules when performing in whole blood samples (Phair *et al.*, 2011). Hence, the scanning window as shown in **Figure 5.3.11** was conditioned to 0 to +0.5 V, in an attempt to diminish fouling of the electrode surface by the oxidation of components such as tyrosine or tryptophan present within the sample matrix. These are known to form oligomeric/polymeric deposits that can significantly influence the voltammetric profiles on repetitive scanning. Despite restricting the scanning window parameters, peak shifting was still evident, and it was calculable that although minimising the effect of tyrosine and tryptophan oxidation, the MN electrode was vulnerable to passive adsorption of proteins. This was investigated as shown in **Figure 5.3.12**, where the current magnitude representative

of Urate oxidation within HB was reviewed over 14 consecutive scans. The peak height percentage is visibly reduced with increasing scan number, which could be expected due to the accumulation of fouling at the electrode surface. This was then confirmed through XPS analysis of proteinaceous material present at MN surface after their use in HB as shown in **Figure 5.3.13**. The N 1s and S 2p spectra shown in **Figure 5.3.13.A** and **Figure 5.3.13.B** respectively, are markedly different to those MN arrays which had not been immersed in HB. The distinct features in the N and S spectra of the anodised MNs, exposed to HB for 30 mins, are characteristic of amide and thiol/disulphide functionalities, common to the peptide macromolecules in the HB assumed to be adsorbing to the MN surface. Likewise, with the unanodised MNs, similar profiles were observed in the MNs before and after immersion in HB for the same period of time, with negligible difference in percentage content compared to the anodised MN. Hence, the expected fouling of the electrode surface is coherent with the accumulation of peptide moieties, in the form of amide N and thiol groups at the MN surface.

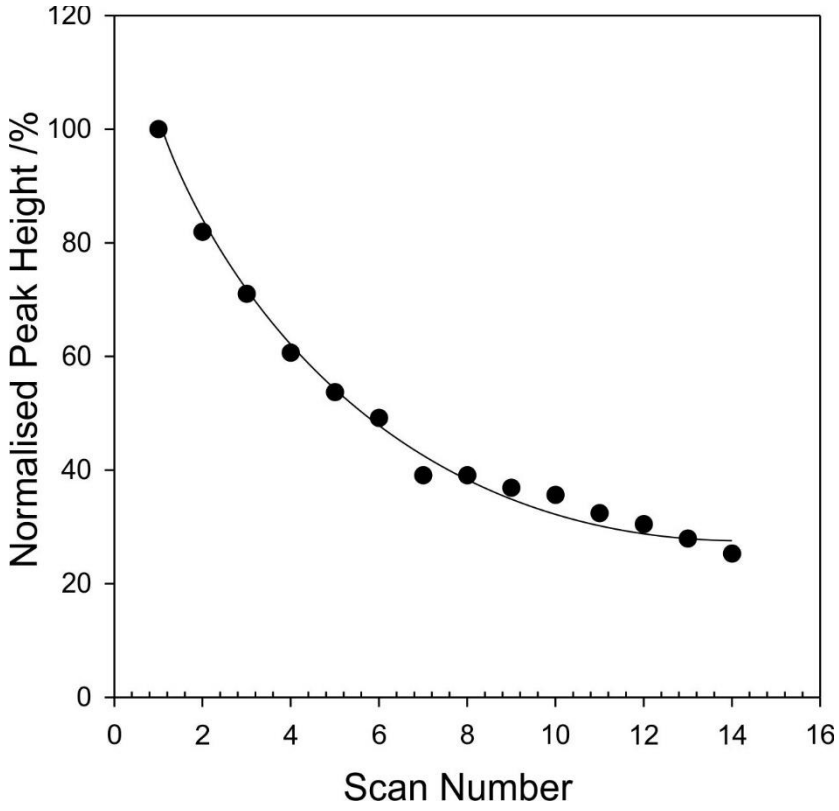

Figure 5.3.12 Visualisation of decreasing urate oxidation peak magnitude response of an anodised carbon-polystyrene microneedle in horse blood with increasing scan number.

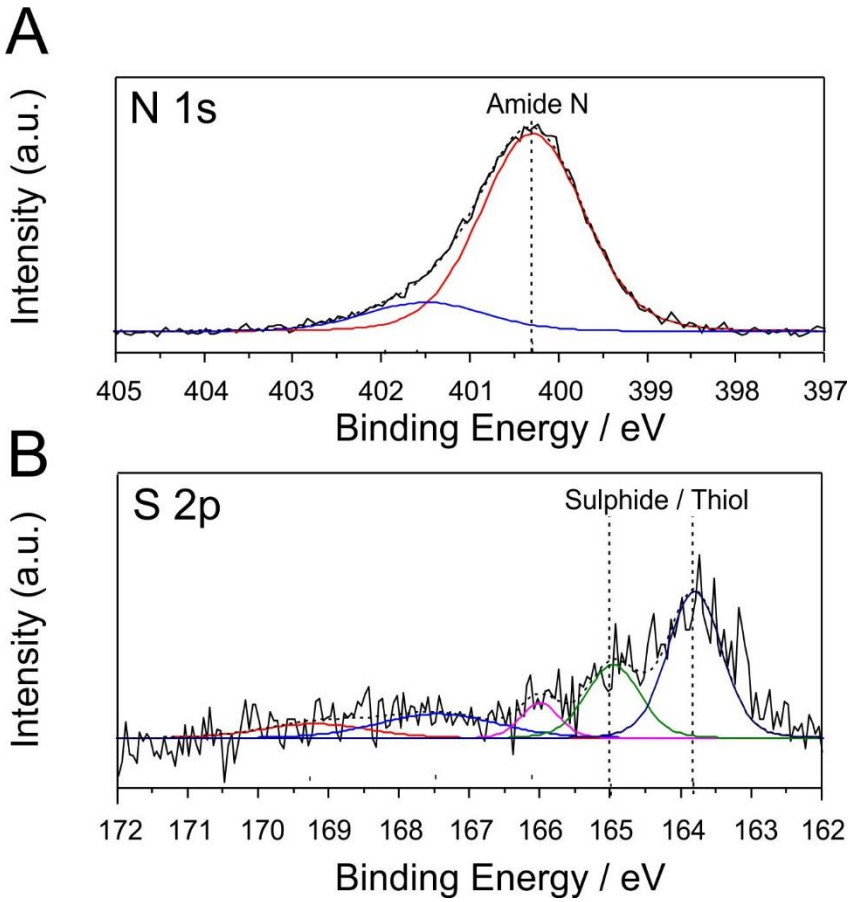

Figure 5.3.13 XPS spectra detailing the N 1s (**A**) and S 2p (**B**) profiles after immersion of the carbon-polystyrene microneedle in horse blood for 30 min.

From this investigation, it is clear that whilst the MNs are responsive in complex biological media, and, have exhibited competitive analytical performance with conventional carbon electrodes, fouling remains an issue, particularly with repeating scans or long measurement periods. Electrode fouling is an ongoing issue within analytical electrochemistry, where the various carbon surface chemistries are ideal for encouraging favourable interactions leading to agents adhering to electrode surfaces (Hanssen, Siraj and Wong, 2016). Thus, utilising microneedles for transdermal operations will be disadvantaged by these issues of fouling. Although the instance of single use electrodes or short measurement times will alleviate these issues to an extent, permselective barriers such as Nafion® may still be necessary for longer measurement scans in the absence of a permanent solution.

Regardless of the consequential fouling exhibited by the MN arrays, the anodisation process has proven to generate a myriad of oxygen functionalities on the MN interface, thereby greatly enhancing electroanalytical performance. The resultant formation of interfacial functionalities, however, do not display any surface morphological differences to the unmodified composite MN arrays upon SEM examination shown in **Figure 5.3.2**. Urate analysis is a long-standing point of interest which has seen considerable attention into researching electrode modification strategies, some of which are illustrated in **Table 5.3.3**. Despite anodisation not positioning this particular electrochemical approach as having a competitive edge in terms of detection limit, it is still considered advantageous in advancing sensing technology, due to the facile method of electrode manufacture and modification. Additionally, many of the procedures described in **Table 5.3.2** would be deemed unsuitable for transdermal application.

Table 5.3.3 Electrode modification strategies employed in the detection of urate.

Electrode	**Electrode modifier**	**LoD (µM)**	**Sensitivity ($\mu A\ mM^{-1}\ cm^{-2}$)**
GCE (He *et al.*, 2018)	Polyglycine/GR	0.061	
Au/IDA (Abellán-Llobregat *et al.*, 2018)	Herringbone CNT	15	
CSPE (Ali *et al.*, 2018)	Uricase ZnO QDs	23	4.0
Al (Sha, Vishnu and Badhulika, 2019)	MoS_2	1.17	
CSPE (Ji *et al.*, 2018)	GR/Au NPs	5.4	
GCE (Zhang *et al.*, 2018)	$ZnCl_2$-CF	0.11	
GCE (Zhao *et al.*, 2019)	MoS_2rGO	0.74	
CF (H. Yang *et al.*, 2019)	Pt NPs/Au-Sn Alloy	0.67	280
GCE (Foroughi, Rahsepar and Kim, 2018)	N Doped GR	0.13	2064
GPE (Kumar *et al.*, 2018)	$XFeO_3$ NPs (X = La,Ce etc.)	0.2	
GPE (Biswas *et al.*, 2018)	TiO_2 NPs	0.07	
C-PS MN (This work)	**Anodised**	**2.85**	**361**

GCE glassy carbon electrode, GPE graphite paste electrode, CSPE carbon screen-printed electrode, CF carbon fibre, IDA interdigitated array, GR graphene, rGO reduced graphene oxide, CNT carbon nanotube, QDs quantum dots, NPs nanoparticles

5.4 Conclusions

Fabrication methods for microneedle systems largely depend on expensive high precision machinery to produce templates which can then be modified by deposition of metallic layers. Here, a process of forming composite material microneedles through inexpensive micromoulding methods, which can easily be replicated in traditional laboratory settings was described. The mechanical properties of the composite MNs were investigated with respect to fracture, and their ability to penetrate skin without damage. The health and safety aspects of their production and use were also investigated. They were shown to be capable of skin puncture and moreover, at a reduced risk of needle stick injury compared to conventional sharps.

The attractive capability of incorporating a vast number of materials by this method also facilitates a plethora of surface rich functionalities which can be invoked. An exemplar model of this includes the carbon-based system detailed in this investigation, where electrochemical anodisation greatly improved analytical performance and promotes a range of detection methodologies now accessible to transdermal sensing. This development has enabled a platform from which new channels of transdermal sensing can stem.

CHAPTER 6

Design of Composite Microneedle Sensor Systems for the Measurement of Transdermal pH

Abstract

Composite microneedle arrays composed of carbon nanoparticles dispersed in a polystyrene binder fabricated by a micromoulding process are described and their application as a transdermal pH sensor evaluated. The generation of quinone functionalities endogenous to the interfacial carbon nanoparticles at the electrode surface was increased by electrochemical anodisation. Thus, these pH sensitive oxo-groups were exploited to form the basis of an indirect pH microneedle sensor. The oxidative peak process attributed to hydroquinone oxidation displayed Nernstian behaviour by shifts in peak potential relative to the surrounding pH. The electroanalytical capability of the microneedle system was critically assessed using tomato as a complex transdermal sample matrix, with the effect of penetration depth on the analytical response evaluated. Given the complex nature of the tomato sample, the sensor system exhibited a comparative and corroborative response to that of a commercially available pH probe, whilst also demonstrating its potential for sensing an extensive range of electroactive markers.

The work reported in this chapter was accepted for publication in:

Hegarty, C., McConville, A., McGlynn, R. J., Mariotti, D., & Davis, J. (2019). Design of composite microneedle sensor systems for the measurement of transdermal pH. *Materials Chemistry and Physics*, 227(August 2018), 340–346.

6.1 Introduction

Initial production of microneedles has predominantly focused on micromachining and photolithographic fabrication techniques, however, polymeric based MNs have consequentially sparked interest in new design concepts for drug delivery and sensing capabilities (Anderson *et al.*, 2019). Moreover, sputtering of metallic layers onto these polymeric structures, thereby allowing conductivity for sensing approaches, has since evolved to the prospect of incorporating conductive/catalytic particles within a composite system, further expanding sensing applications (Apollo *et al.*, 2015; Zhou *et al.*, 2017; Ciui *et al.*, 2018). The availability of silicone moulds has seen MN applications branch into diagnostic sensing, mainly by extraction of interstitial fluids followed by secondary in vitro analysis (Chang *et al.*, 2017; Samant and Prausnitz, 2018). More recently, the convenience of this micromoulding approach has generated a new wave of wearable sensors based on in situ monitoring of biomarkers (Anastasova *et al.*, 2017; Chinnadayyala, I. Park and Cho, 2018; Chinnadayyala, K. D. Park and Cho, 2018). From here, the attractiveness of utilising MNs within a closed loop system has only further increased research activity of MN sensing applications in recent years (Rawson *et al.*, 2018). The potential of integrating carbon nanoparticles within a polymeric composite microneedle system could further diversify sensing application opportunities, due to the wide potential window associated with interfacial carbon and simple modification strategies. The aim here is to build on the initial microneedle design described in Chapter 5, but expands the work to investigate the fabrication of a carbon|polymer composite microneedle system and its modification to be responsive to pH. This extends the work initially described in Chapter 4, but seeks to exploit the functionalities inherent to the carbon particles rather than rely on modification with an engineered flavin.

There has been extensive research into electrodes composed of particulate carbon, dispersed within a curable resin (Lawrence, Thompson, *et al.*, 2002; Lawrence *et al.*, 2007), and their attractive applicability for enzyme based biosensing (Harper and Anderson, 2010; Eliana and Bojorge, 2011; Riyanto, 2016). The performance of these carbon composite electrodes are reminiscent of microelectrode arrays, with surface characteristics which can be appropriately renewed by 'polishing', making them highly desirable diagnostic substrates (Ramírez-García *et al.*, 2002; Li *et al.*, 2017). Screen printed electrodes (SPEs) in particular

have been established as exemplar invaluable substrates that are easily manipulated for the detection of a diverse range of biomarkers (Arduini *et al.*, 2016; Trojanowicz, 2016) and were exploited within Chapter 4 of this thesis. Despite significant developments in carbon formulations, there has been a lack of translating this to microneedle technology, thus, there is a prime opportunity in this field with considerable benefits over planar substrates. Conventional systems are principally based on pin-prick procedures for acquiring capillary blood and are often associated with pain, which in turn, correlates to compliance issues (McConville, Hegarty and Davis, 2018). Microneedle systems have shown great success over these traditional procedures, offering a minimally invasive method of penetrating the skin whilst avoiding the dermal nerve network, thereby, making them virtually painless (Waghule *et al.*, 2019). This effectively has sparked the revolution of vaccination procedures, especially in paediatrics, where needle phobia is rife, resulting in a momentous increase in treatment compliance (Rejinold *et al.*, 2016). Since the proposed sensing MN arrays maintain similar dimensions, a shift towards MN sensing is anticipated in future designs of diagnostics, benefiting from pain-free administration.

A representation of the basic composite MN system design adopted in this investigation is shown in **Figure 6.1.1**. The structural integrity is provided by the polystyrene, and the conductive nature maintained by the presence of carbon particles within the body of the microneedle array. The proposed sensor consists of two separate MN arrays; one to serve as the sensing electrode and the other as the reference electrode. The latter is distinctly different by virtues of the incorporation of silver. This is achieved either by silver nanoparticles included in the composite formulation, or, as an electrodeposited layer. In both cases, the presence of silver and its subsequent chloridisation was intended to serve as a silver|silver chloride pseudo reference (Sharma *et al.*, 2016).

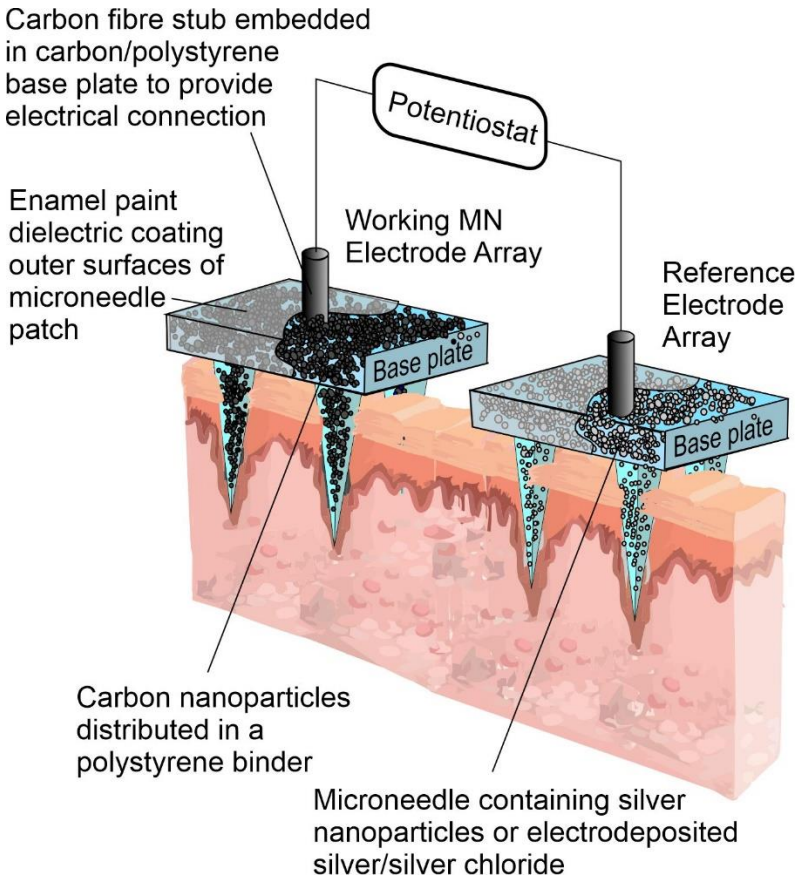

Figure 6.1.1 Proposed carbon loaded polystyrene microneedle sensing system design.

Carbon is often used in voltammetric analysis for the advantage of having a wide potential window, however, the basal plane structures characteristic of carbon particulate typically require large over potentials, effectively reducing selectivity and sensitivity. Exfoliation of interfacial carbon has been shown to be successful in exposing more edge plane sites and creating interfacial oxygen functionalities. This was previously shown to significantly enhance the response to urate in Chapter 5. Electrochemical anodisation of carbon electrodes has previously been confirmed by XPS to modify their chemical functionality with a reported increase in oxygen functionalities found within the carbon interfacial structures as illustrated in **Figure 6.1.2** (Anderson *et al.*, 2014; Casimero *et al.*, 2020). This results in a dramatically improved electroanalytical performance by improving susceptibility to surface wetting and increasing electron transfer kinetics. As shown in **Figure 6.1.3**, this work intends to utilise the benefits of electrochemical anodisation on carbon based composite MN arrays to derive an increase in endogenous quinone functionalities. Quinones have long been associated with the fundamental workings of pH sensors that exploit their proton dependent nature, correlating their oxidative peak shifts with changes in pH (Lafitte *et al.*, 2008; Musa

et al., 2012). Hence, an increased population of endogenous quinones trapped within the interfacial carbon structures of the microneedle arrays could be anticipated to facilitate an indirect means of recording pH measurements, essentially creating a facile method of producing a reagentless transdermal pH sensor. In this investigation, the electroanalytical performance of the composite microneedle arrays were critically analysed by examining the pH of tomato exocarp (outer skin) and the underlying mesocarp (fleshy interior). This form of validation avoided ethical issues whilst still providing a transdermal model (**Figure 6.1.1**). The latter has the added advantage of easily excising the exocarp for electron microscopy and computerised tomography investigations.

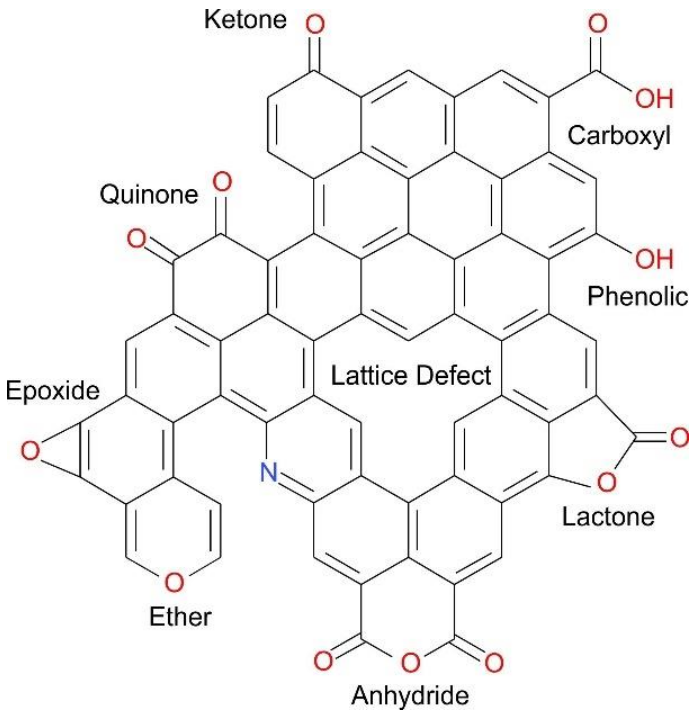

Figure 6.1.2 Summary of various oxygen functionalities present on the surface of carbon-based microneedles.

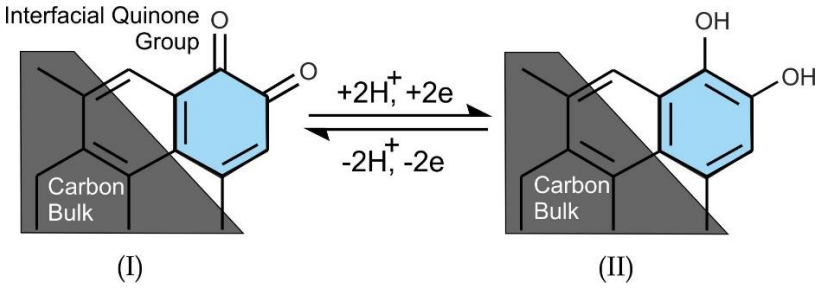

Figure 6.1.3 An example of typical quinone structures present on the MN surface associated with embedded carbon particles and their resultant redox transformations.

6.2 Experimental Details

6.2.1 Materials and Instrumentation

Carbon nanopowder (< 100 nm) and polystyrene pellets (MW 192000) were obtained from Sigma-Aldrich (Dorset, UK), along with all other chemicals used in the investigation, were of the highest attainable grade and were utilised without further purification strategies. Britton-Robinson buffers (acetic, boric and phosphoric acids) were used throughout unless mentioned otherwise. Silicone microneedle templates were procured from Micropoint® Technologies Pte Ltd (Singapore) and consisted of a 10 x 10 array of pyramidal shaped needles (200 µm base x 500 µm pitch x 700 µm height).

Electrochemical measurements were recorded at 22°C ± 2°C, using a micro Autolab Type III potentiostat. Where a three-electrode system was employed, the microneedle array served as the working electrode, with a platinum wire and commercial silver|silver chloride (3 M KCl, BAS Technicol, UK) used as the counter and reference electrodes, respectively. As the investigation progressed, a two-electrode system was utilised, with the microneedle array acting as the working electrode and a silver loaded microneedle exploited as a combined counter and pseudo reference electrode. In the case where a three-electrode configuration is used, little to no current passes through the reference electrode, thereby, maintaining a reference potential. However, in the two-electrode setup, the silver modified MN must serve as both the counter and reference electrode, thus, making it susceptible to current

passage. Despite reducing the complexities of electrochemical cell design, the two-electrode configuration may be limited by reference instability, which is also explored in this work.

X-ray microtomography images were obtained using a SkyScan 1275 Micro-CT system (Bruker Corporation, USA), at a rotation angle increment of 0.20° and an average of 3 frames per increment. Reconstruction and analysis of the subsequent imaging was performed using the accompanying NRecon and CTVox visualisation software respectively. The conductivity of the microneedle arrays were calculated using a 2461 series SourceMeter® four-point probe (Keithley), with the average conductivity of an unmodified carbon|polystyrene MN array measured as 1575.2 ± 96 Sm^{-1} (n = 5).

X-ray photoelectron spectroscopy (XPS) of the MN arrays, confirming the deposition of silver on the electrode surface, was performed using a Kratos Axis Ultra DLD Spectrometer. Analysis of the spectra was completed under typical parameters of 15 kV and 10 mA (150 W) at an operating pressure lower than $6x10^{-8}$ Pa using monochromated Al Ka X-rays (*hv* = 1486.6 electron volts (eV)). A hybrid lens mode was used (electrostatic and magnetic) during analysis, with a 300 µm x 700 µm analysis area at a take-off angle (TOA) of 90° relative to sample surface. Wide energy survey scans (WESS) were collected across a range of - 5 to 1200 eV binding energy (BE), with a pass energy of 160 eV and step size of 1 eV. High-resolution spectra were collected with a pass energy of 20 eV, a 0.05 eV step size, a 25 eV scan width, a dwell time of 150 ms and at least 3 sweeps to reduce the signal noise. A Kratos charge neutraliser system with a filament current between 1.8 and 1.95 A, a charge balance of 3.3 – 3.6 V and a filament bias of 1.3 V was used for all samples. Charging effects on the BE positions were adjusted by setting the lowest BE for the C1s spectral envelope to 284.8 eV, which is commonly accepted as adventitious carbon surface contamination. Three measurements were taken per sample, with a Shirley background subtracted from each XPS spectra. The peak areas of the most intense spectral lines for each elemental species were used to determine the percentage atomic concentration. Peak fitting of high-resolution spectra was carried out using Casa XPS software.

Raman spectroscopy analysis was performed under ambient conditions using a Horiba LabRAM spectrometer, which has a focal length of 300 mm, offering a spectral resolution of

2-4 cm^{-1}. A helium-neon (HeNe) laser was employed at an excitation wavelength of 632 nm, using 50 X optical lens to illuminate the sample surface, providing an estimated spot size of 30 µm (10% filter, laser power 2.59 W (25.9×10%)). The carbon|polystyrene composite samples were analysed over a spectral range of 100-3500 cm^{-1}, accumulating 5 slices (energy per slice 38.85J) to cover the range, with 5 spots per sample.

6.2.2 Preparation of Microneedles

Basic unmodified carbon|polystyrene microneedles, forming the basis of the working electrode used within this study, were prepared in accordance with the procedure outlined in Chapter 5.

6.2.3 Preparation of Silver Modified Microneedle Pseudo Reference

Electrochemical deposition of silver on the predominately carbon MN electrode surface was achieved using chronoamperometric methods, where the electrode was held at -1 V for 60 s in an aqueous solution of 0.01 M $AgNO_3$ (in 0.1 M HNO_3). Upon removing the electrode from the solution, it was rinsed with deionised water before immersing in 0.1 M KCl, at which point the electrode was subjected to a single cyclic voltammogram sequence (-0.8 V to +0.8 V, 50 mV/s). In doing so, the electrodeposited layer of silver on the electrode surface becomes oxidised, creating a layer of silver chloride.

6.3 Results and Discussion

The carbon-based composite microneedle response towards ferrocyanide (2 mM, 0.1 M KCl, 50 mV/s) pre- and post anodisation is depicted in the cyclic voltammograms in **Figure 6.3.1**. A dramatic improvement in MN response with relation to peak process definition and a reduced peak separation (ΔE_P = 360 mV) is recognised after electrochemical anodisation. Despite the smaller peak separation after anodisation, the large polymeric proportion

making up the composite nature of the MN, contributes to an elevated internal resistance of the system, resulting in a higher peak separation than expected for the ferro-ferricyanide couple (McConville and Davis, 2016). The drastic change in electrochemical response upon anodisation can be attributed to the exfoliation of the carbon interface, exposing more edge plane sites, and facilitating an increased population in oxygen functionalities, which, as a result, greatly improves electron transfer kinetics. In marked contrast, the substandard response of the unanodised MN towards ferrocyanide is coherent with previous investigations of carbon-based electrodes, where the surface is largely composed of basal plane features thus, impeding electron transfer kinetics (Phair *et al.*, 2011). However, within such studies, the electrode response towards ruthenium hexamine was demonstrated to be of much higher quality than ferrocyanide (Cline, McDermott and McCreery, 1994). As shown in **Figure 6.3.1**, this investigation was consistent with these studies, presenting a superior MN response towards ruthenium hexamine and minor differences pre- and post anodisation.

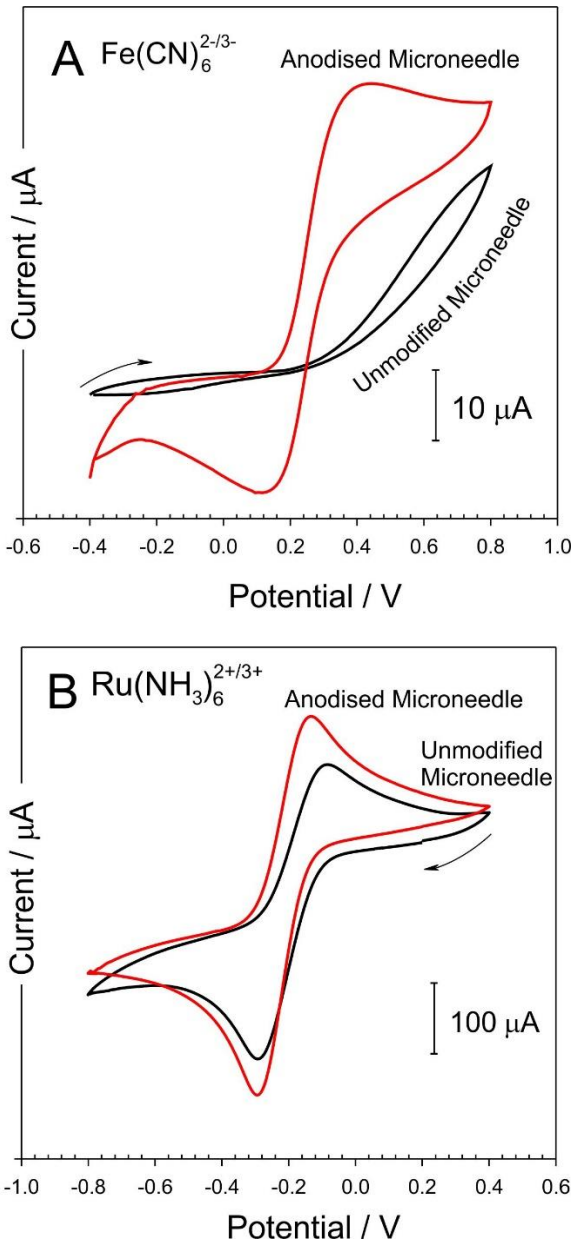

Figure 6.3.1 Cyclic voltammograms detailing the response of carbon-polystyrene microneedles (single MN array as WE) before and after electrochemical anodisation towards 2 mM ferrocyanide (**A**) and 2 mM ruthenium hexamine (**B**) (Scan rate in both: 50 mV/s).

Whilst an increase in the proportion of carbon nanoparticles added to the composite mixture could be foreseen as reducing the internal resistance of the system, and improve electroanalytic response accordingly, this comes at the cost of jeopardising the structural integrity of the MN arrays. Although the carbon nanoparticles facilitate a conductive pathway intrinsic to the MNs, they possess no adhesive traits. Thus, polystyrene serves as a constituent in which to secure the conductive nanoparticles, but also, fundamentally

maintains structural integrity and mechanical strength for dermal penetration. It has been recorded that a contribution of polystyrene less than 50% will permit MN formation with a visibly granular morphology. In addition to this, it has previously been evidenced that MN surface topography may also be influenced by the size of the conductive nanoparticles incorporated within the polymer matrix (McConville and Davis, 2016). It also could be argued that, in some contexts, a granular microstructure is preferable over a largely flush surface, providing an increase in interfacial defects, however, this comes at the expense of inherently brittle needle construction.

Raman spectroscopy was also used as a means of assessing the surface chemistries of the electrode post anodisation and is presented in **Figure 6.3.2**, where the spectra are normalised to the G-band maximum intensity for the purpose of this investigation. From the obtained spectra, a modest increase in sp^2 lattice disorder is represented by the increase in the D-band and corresponding 2D (G') band with increasing anodisation time. This documented increase in disorder in relation to electrochemical anodisation time is consistent with previous studies, which have found a rise in the presence of lattice defects upon oxidising carbon fibres (Liu *et al.*, 2010; Casimero *et al.*, 2020). Another feature evident from the spectra is the loss of carbon at the electrode-solution interface. An accepted compromise of the composite nature of the MNs is that there will be carbon nanoparticles present at the surface, which will inevitably be loosely bound to the structure. The loss in carbon can be attributed to these carbon particles disbanding from the interface as a direct result of the electrolytic evolution of oxygen upon anodisation, therefore, exposing more of the polystyrene constituent at the surface. This theory is coherent with the presented Raman spectra, which displays peaks corresponding to the elemental composition of polystyrene that become more pronounced with increasing anodisation time. Additionally, the population of OH functionalities becomes more prominent in correlation with anodisation time, which coincides with the envisaged redox transformations presented in **Figure 6.1.3**, contributing to the elevated electron transfer kinetics in **Figure 6.3.1**.

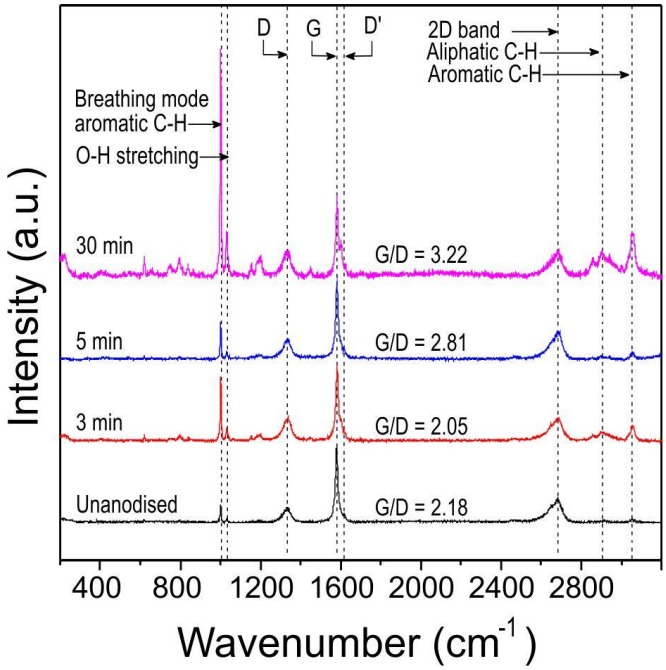

Figure 6.3.2 Raman spectra displaying the effect of electrochemical anodisation at +2 V in 0.1 M NaOH for varying lengths of time on the interfacial chemistries of the carbon-polystyrene microneedle surface.

6.3.1 Characterisation of Silver Modified Microneedle Pseudo Reference

To utilise a dual MN configuration for sensing capabilities, a carbon|polystyrene microneedle was modified with a silver|silver chloride layer to act as a pseudo reference microneedle. The accumulation of silver at the microneedle surface was observed by SEM/EDX and XPS analysis as shown in **Figure 6.3.3** and **Figure 6.3.4** respectively. From the SEM imaging (**Figure 6.3.3.A**), a significantly different surface topography is evident as a direct result of the silver deposition layer. This is also confirmed by the accompanying EDX spectra (**Figure 6.3.3.B**), showing peaks corresponding to the elemental composition of the deposited layer. The XPS spectra (**Figure 6.3.4**) provides further confirmation of the MN surface being metallised with silver, with the emerging peaks post electrodeposition relating to the elemental composition of silver and the percentage atomic concentration of silver recorded as 4.8%. The derived silver-silver chloride pseudo reference was later electrochemically characterised by potentiometric methods using incremental chloride concentrations and produced a -58.9 mV per decade chloride ion response which coincides with Nernstian behaviour (Sharma *et al.*, 2016).

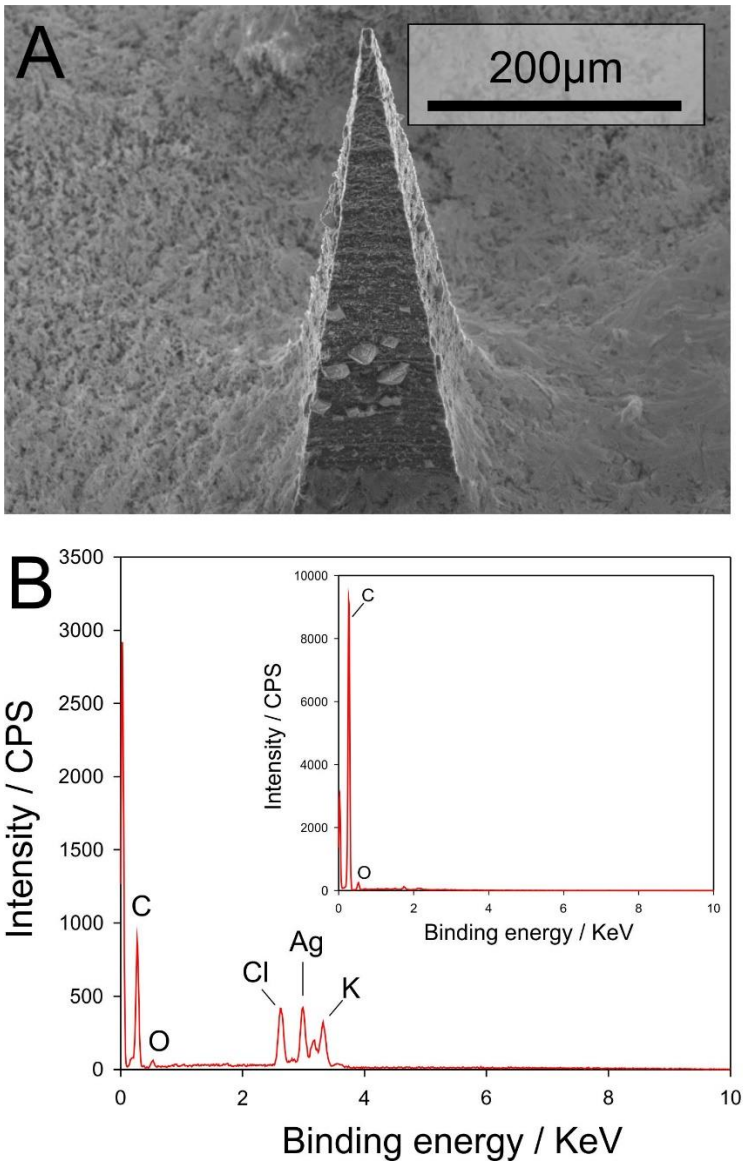

Figure 6.3.3 (**A**) Scanning electron micrograph of carbon-polystyrene microneedle after electrodeposition of silver and (**B**) accompanying EDX spectra confirming surface chemistries corroborating with silver-silver chloride deposit. Inset: Control EDX spectrum of carbon-polystyrene MN before silver deposition.

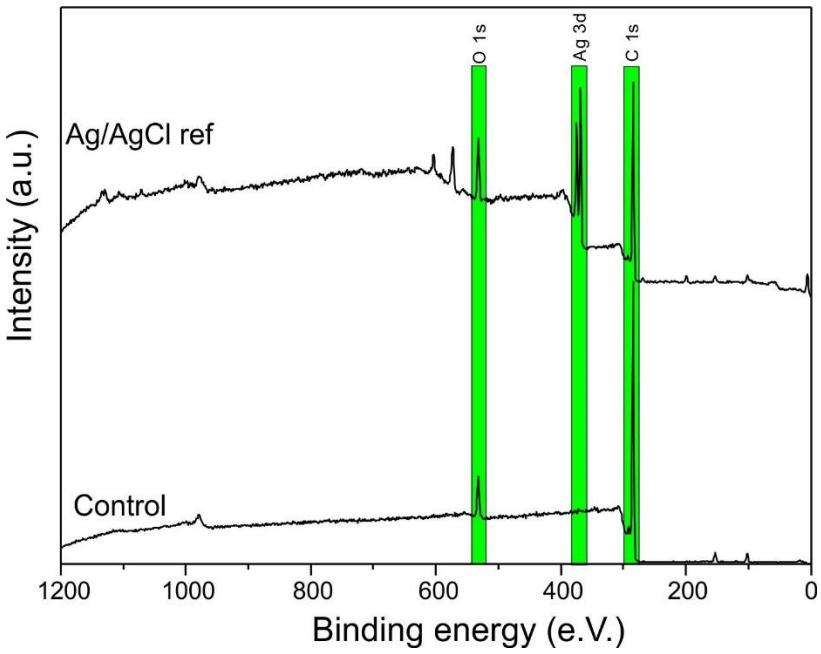

Figure 6.3.4 XPS spectra identifying presence of silver on modified MN compared to absence of Ag 3d double peak in unmodified carbon-polystyrene MN.

6.3.2 Microneedle pH Response

Exploiting the microneedle as a pH sensor relies on the immediate reduction of the quinone species (I → II, **Figure 6.1.3**) trapped in the carbon nanoparticulate at the electrode-solution interface. Upon sweeping the electrode potential to more positive values, the quinone groups become re-oxidised (II → I, **Figure 6.1.3**). The recorded potential of the observed quinone oxidation peak process is dependent on pH, thus, making it an ideal marker for the indirect measurement of pH (Lafitte *et al.*, 2008; Xiong, Batchelor-McAuley and Richard G. Compton, 2011; Hegarty *et al.*, 2018) The highly sensitive differential technique, square wave voltammetry, was strategically used for analysing peak positions, given the delicate nature of fluctuations in peak processes. Square wave voltammograms in **Figure 6.3.5** detail the composite MN response to varying pH buffers. Well defined peak processes are evident, corresponding to the re-oxidation of the interfacial hydroquinone groups back to quinones. Another conspicuous feature of the square wave voltammograms is the clear shift in oxidative peak position with pH which displays Nernstian behaviour (E_{pa}/V = −0.0575 pH + 0.4107; n = 6, R^2=0.999), indicating the transmission of equivalent number of protons and electrons involved in the electrochemical reaction. This corroborates with previous studies

documenting Nernstian response of electrodes with pH sensitive quinoid moieties covalently bonded at the solution interface (Lafitte *et al.*, 2008; Musa *et al.*, 2012).

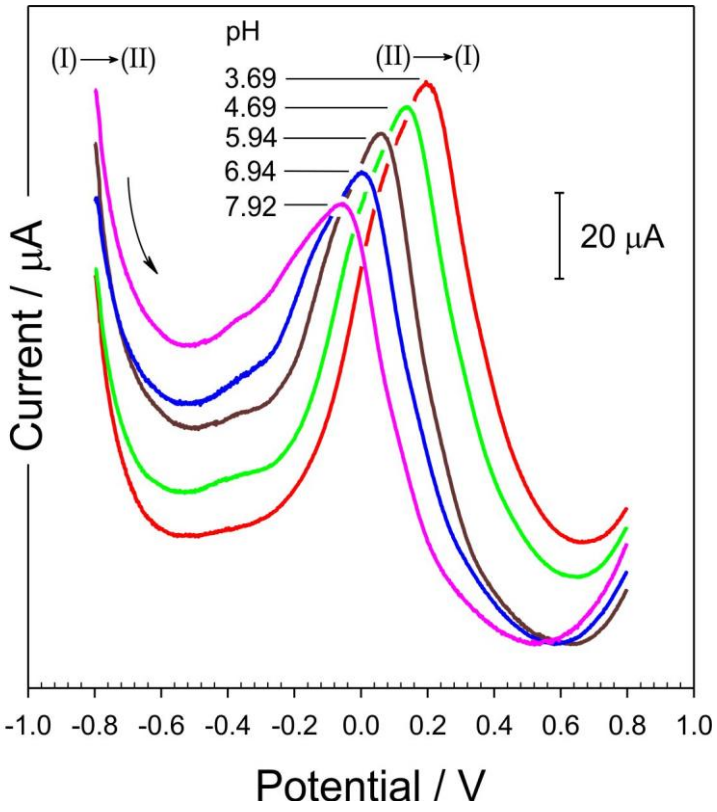

Figure 6.3.5 Square wave voltammograms showing the response of carbon-polystyrene microneedle arrays in Britton-Robinson buffers of varying pH.

The stability of the MN to serve as a working and reference electrode was examined using a dual MN configuration subjected to repetitive cycling of 15 scans in pH 3 Britton-Robinson buffer, with **Figure 6.3.6** encapsulating the peak current and peak potential recorded for each scan. Any instability in the MN pseudo reference would be signified by dramatic inconsistencies in peak potential. However, through the course of repetitive cycling, minimal drift in peak potential is exhibited by the dual system (E_p = 0.178V ± 1 mV; Std Dev = 0.0036; n = 15). Furthermore, negligible deviation in peak current (I_{pa} = 2.48 µA ± 0.02 µA; n=15) is also displayed, indicating that the administration of electrochemical anodisation as a MN pretreatment, which is necessary for the formation of endogenous quinone groups (**Figure 6.1.3**), does not jeopardise MN stability in the process.

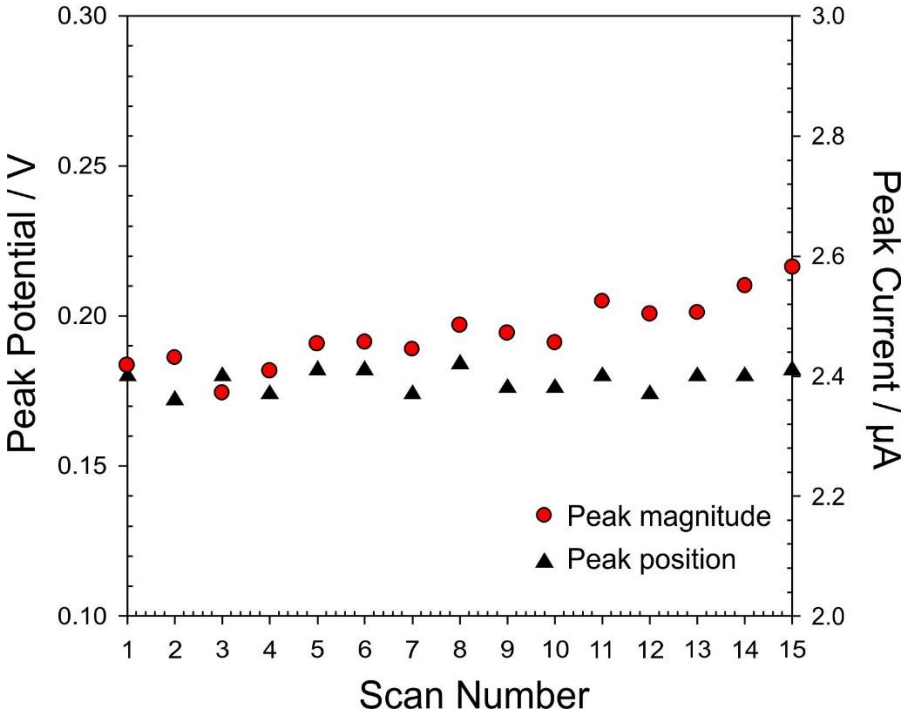

Figure 6.3.6 Effect of repetitive scans on oxidative peak position and magnitude of a dual microneedle array setup in pH 3.

An influential characteristic of voltammetric pH sensing is the significance of peak potential over current magnitude since the obtained current response is confined by electrode surface area. While the square wave voltammograms recorded in **Figure 6.3.5** are representative of MNs immersed in pH buffer, where the entire microneedle structure is in contact with the solution. In the case of transdermal application however, MN penetration depth becomes a critical consideration as the effective electrode area will change with insertion. Increasing the depth to which needles puncture the skin inevitably increases the degree of MN surface interaction with electrolyte, and can therefore be expected to increase the current signal response. This theory was investigated by limiting the achievable needle penetration depth into membranes of defined thickness. Microneedles were inserted into a soft cellulose filter membrane saturated with pH 7 buffer and fixed to a glass surface, thereby, restricting the active surface area to the membrane thickness. **Figure 6.3.7** shows square wave voltammograms depicting the MN response to single and double (180 µm and 260 µm thickness respectively) layer membranes, highlighting the anticipated surge in magnitude of current response for the double layer membrane.

Other studies have instigated the use of the same electrode for pH analysis and as a working electrode for near-simultaneous electroanalysis of biomarkers, where the current response is relative to concentration (Lu and Compton, 2014). Whilst this would be an admirable additional feature, relying on fluctuations in current response would prove an obstacle for MN transdermal voltammetric sensing. Nonetheless, the significance of the current in this study is secondary to discerning the peak potential of the oxidative process. Despite the contrast in peak currents presented in **Figure 6.3.7,** the peak position remains unequivocally static irrespective of the penetration depth.

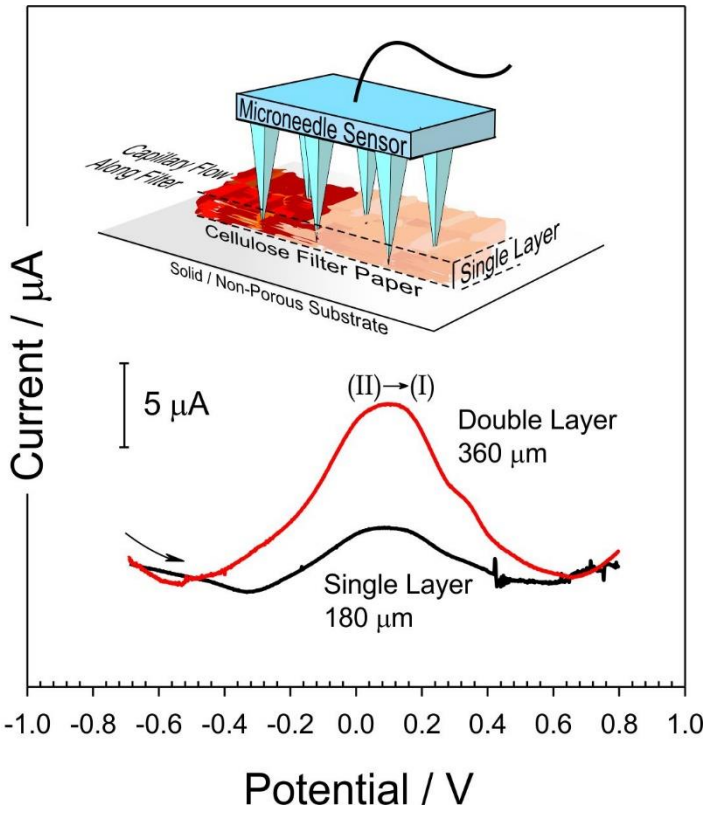

Figure 6.3.7 Microneedle sensor setup and resultant square wave voltammograms detailing the influence of penetration depth on peak magnitude and peak position of a single carbon-polystyrene microneedle array sensing pH 7 buffer.

6.3.3 Transdermal Analysis of Tomato Skin pH

The electroanalytical performance of the microneedle system in an authentic sample was critically assessed by evaluating the pH of tomato mesocarp upon puncturing the exocarp. Scanning electron microscopy images are shown in **Figure 6.3.8** of composite microneedles before and after penetration into tomato mesocarp, where the flesh has been removed from the exocarp for the purpose of highlighting the puncturing capability of the needles. The webbing microstructures visible in **Figure 6.3.8.C** are an established characteristic of tomato skin, showing defined contours of cell wall structures, vital for adhesion to the waxy cuticular membrane (Li *et al.*, 2014).

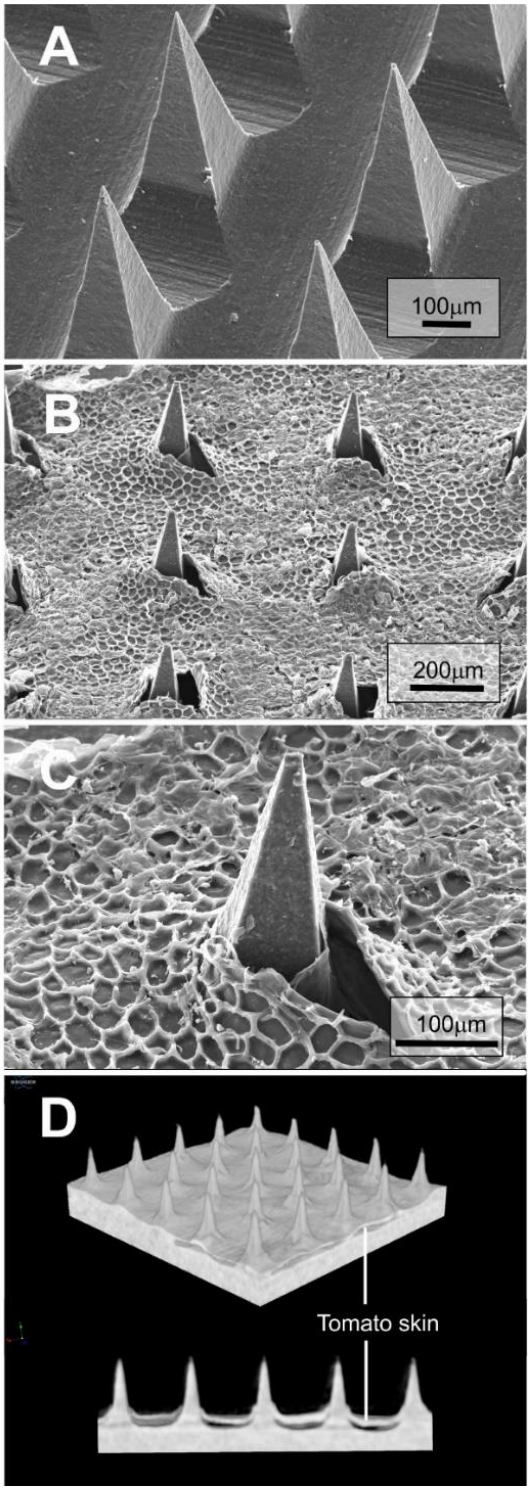

Figure 6.3.8 Scanning electron micrographs of carbon-polystyrene microneedle array before (**A**) and after (**B, C**) insertion into tomato. CT scanning image of the array after penetrating the tomato (**D**).

Another view of assessing the MN piercing capability is represented by the micro computerised tomography (CT) x-ray scanning images shown in **Figure 6.3.8.D**. Cross-sectional perspectives of the CT imaging also provides the opportunity to examine the

internal needle structure, where the images give assurance that there is a lack of fissures or voids in the main body of the MNs. It is acknowledged that extensive handling and manipulation is necessary in the preparation of obtaining high resolution electron microscopy and CT scanning images. From the images shown in **Figure 6.3.8**, the needles are shown to maintain their structural integrity after acquiring the necessary images. At a glance, it could be said that the SEM imaging presents the MNs as only penetrating the tomatoes at a rather shallow depth since only the needle tips are visible. Although, this perception is contradicted by the CT imagery, where the needles exhibit a generous depth of insertion. While micro CT scanning is performed at atmospheric pressure, the high vacuum required in sample preparation (Au/Pd sputtering), as well as the heat generated at the sample surface during SEM analysis is accountable for dehydrating the tomato cytoplasm and the subsequent cuticular shrinkage (Li *et al.*, 2014). Undoubtedly, the hole diameter will increase with needle puncture as the pyramidal shape broadens towards the base. This is evident in the resultant holes formed by MN puncture, where they appear larger in the SEM image than the needle protruding from them. Hence, it can be assumed that the tomato cuticle has raised upwards upon shrinking during the SEM process.

The electroanalytical performance of the MNs assessing tomato skin pH was performed using both a dual MN system and a conventional three-electrode configuration as shown in **Figure 6.3.9**. Similar to a standard potentiometric pH electrode, a two-point calibration system was used throughout. The dual MN system utilised a composite MN array as a working electrode and a silver modified MN as a pseudo reference as indicated in **Figure 6.1.1**. The typical three-electrode approach employed a MN as the working electrode, a platinum wire as the counter and a commercial Ag|AgCl half-cell as the reference electrode. A commercial HALO® (HI-14142) wireless flat pH probe was then used for comparison to validate the response of both approaches. Square wave voltammograms outlining the MN response (two-electrode setup) to pH 3.13 and pH 7.22 buffers forming the basis of the two-point calibration are presented in **Figure 6.3.9.A**. A broad oxidation peak is observed at +0.204 V and -0.013 V for pH 3.13 and pH 7.22 buffers respectively, which coincides with the single MN response described in **Figure 6.3.5**.

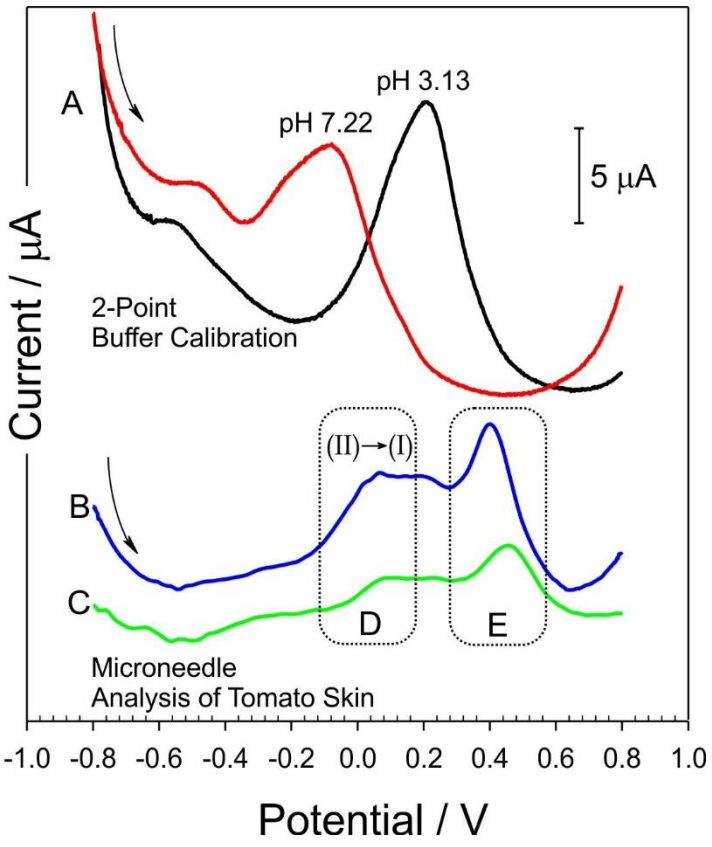

Figure 6.3.9 Square wave voltammograms determining 2-point calibration (**A**) (in pH 3.13 and pH 7.22 Britton Robinson buffer) and the single (**B**) and dual (**C**) MN sensing systems response towards tomato pH. The quinone analytical region (**D**) and a secondary oxidation process (**E**) are also highlighted.

The dual MN and single MN (three-electrode) system responses, after puncturing through the tomato exocarp, are also detailed in **Figure 6.3.9** as scans B and C respectively. A distinct difference between the MN response to simple pH buffers and the scans obtained from tomato are recognised, which can be expected given the increased complexity of the tomato sample. Despite the increased ambiguity of the MN response to the tomato matrix, the oxidation peak processes of the endogenous hydroquinone groups (II →I) are still visible and highlighted in **Figure 6.3.9.D**. A second oxidative process is also evident (**Figure 6.3.9.E**) in the response to tomato, which was lacking in the pH buffer response and can be attributed to the intrinsic electroactive components of the tomato sample (Lawrence, Beckett, *et al.*, 2002). Even with the unidentified species generating the secondary peak process, it should be noted that the advantage of the low oxidative potential of the endogenous quinones still facilitate the unambiguous interpretation of tomato skin pH. A similar scanning profile (**Figure 6.3.9.B**) is exhibited by the single MN (three-electrode configuration) response to

that of the dual (**Figure 6.3.9.C**) system. The pH evaluated by the MN responses was calculated using the linear regression equation obtained from the 2-point calibration (E_{pa}/V = −0.0484 pH + 0.394). The resultant MN acquired pH calculations are compared to the commercial pH probe measurements in **Table 6.3**.

Table 6.3 Comparative data showing measured tomato pH using MN system (single and dual) against a commercial pH probe.

System	Actual pH	Calculated pH	N
Dual MN (2 Electrode)	4.52	4.77	5
Single MN (3 Electrode)	4.43	4.48	5

The single MN array within a three-electrode setup exhibits a comparable response with the commercial pH probe, evaluating the tomato skin pH to be within 0.1 pH. This demonstrates the capability of the endogenous quinone functionalities embedded in the interfacial carbon particles to perform as an indirect pH sensor. The dual MN system however, displays a larger disparity with the commercial probe, which is most likely concerned with the nature of the pseudo reference. Where the three-electrode setup employs a conventional Ag|AgCl reference with an internal chloride concentration, which enables the maintenance of a stable reference potential, the dual setup relies on the silver modified MN depending on the intrinsic chloride ion concentration of the tomato. Thus, it is susceptible to fluctuations in chloride concentration which deviate from the concentration used in the calibration pH buffers. With the simpler pseudo reference employed in the dual system, it should be noted that the recorded pH is still within range of the actual tomato pH. For future designs, one solution to this considers the incorporation of an internal reference system, insensitive to pH, based on the co-immobilisation of a redox species onto the electrode interface. Previous studies encountering similar issues with fluctuating chloride concentrations have demonstrated success using systems based on ferrocene/ferrocyanide (Lafitte *et al.*, 2008; Hegarty *et al.*, 2018). Although, the integration of such species would further complicate the MN manufacturing process, hence, the application purpose and necessary accuracy should be contemplated in the design phase.

Although microneedles have previously been utilised as sensing applications within plant physiology (Jeon *et al.*, 2017; Baek *et al.*, 2018), this is the first documented use of composite arrays showcased as a voltammetric sensor. Whilst the scope of this particular investigation was to examine the application of the MN system as a pH detection unit, the electroanalytical capability of the system expands beyond this purpose. This is recognised by the MN response to tomato depicted in **Figure 6.3.9**. The wide potential window established by the incorporation of carbon provides a platform from which to tailor analysis towards a range of electroactive species. Thus, this type of micro-sensing device offers an attractive alternative to the fundamentally flat sensing surface available in the form of screen printed electrodes (Arduini *et al.*, 2016; Trojanowicz, 2016; Li *et al.*, 2017).

6.4 Conclusions

Microneedle sensing leverages a myriad of advantages over traditional screen printed electrodes, with the composite nature of the patches accommodating the translation of existing electrochemical techniques to this new formulation. The low-cost production provided by the micromoulding fabrication process facilitates rapid prototyping of sensors that can be easily manipulated during development. Hence, whilst this carbon|polystyrene system has been proposed as a pH sensing unit, the electrochemical characterisation exhibits a wide potential range which promotes the versatile functionality of a composite structure. Here, the MN arrays have demonstrated piercing potential into tomato mesocarp and, in doing so, could lay strong foundations for application within a host of biomedical sensing applications.

CHAPTER 7

Composite Microneedle Arrays Modified with Palladium Nanoclusters for Electrochemically Controlled Drug Release and Electrocatalytic Detection of Peroxide

Abstract

Conductive composite microneedles fabricated by a rapid prototyping method, modified with palladium nanoclusters has been described. A micromoulding technique was utilised, which allowed the composition of carbon nanoparticles to be dispersed within a cellulose acetate phthalate (CAP) or polystyrene binder to form a 10 x 10 array of microneedles The exploitation of the composite systems utilised as an electrochemically controlled drug release mechanism and as an electrocatalytic peroxide detection system was examined. Modification of the microneedles with palladium was investigated as a means of enhancing the hydrogen evolution reaction (HER) and improving the response towards the detection of peroxide. Exploitation of the HER process and manipulation of changes in local pH at the electrode surface enabled swelling of the needle structure, thereby, facilitating electrochemically controlled release of a model drug formulation contained within the needle framework. Electrochemical anodisation of the carbon constituent within the carbon-polystyrene MN array increases the concentration of interfacial carboxyl moieties which then facilitated the passive entrapment of Pd^{2+} ions. Subsequent electroreduction of the Pd^{2+} ions converts the surface to a fundamentally electrocatalytic interface consisting of Pd metal, which is highly sensitive to peroxide (–0.3 V: 49.7 ± 2.8 $\mu A \cdot mM^{-1} \cdot cm^{-2}$; –0.5 V: 102.1 ± 2.32 $\mu A \cdot mM^{-1} \cdot cm^{-2}$).

Publications resulting from the work presented in this chapter:

Hegarty, C., Mckillop, S., Dooher, T., Dixon, D., & Davis, J. (2019). Composite Microneedle Arrays Modified with Palladium Nanoclusters for Electrocatalytic Detection of Peroxide. *IEEE Sensors Letters*, 3(9), 1–4.

Anderson, A., **Hegarty, C.**, Casimero, C. & Davis, J. (2019). Electrochemically Controlled Dissolution of Nanocarbon-Cellulose Acetate Phthalate Microneedle Arrays. *ACS Applied Materials and Interfaces*, pp. 35540–35547.

7.1 Introduction

It has already been noted in previous chapters that microneedle (MN) systems are increasingly regarded as providing a step change in drug delivery mechanisms offering many advantages over more traditional oral and syringe-based strategies (Prausnitz, 2004; Cheung and Das, 2014; Pandey *et al.*, 2019). The main remit of this project was to examine how these technologies could be translated to sensing applications and initial designs have been highlighted in Chapters 5 and 6. Given that the latter have demonstrated that conductive MN are possible and that useful electroanalytical information can be extracted, a second query arose which related to the possibility of exploiting the conductive nature of the MN as a means of controlling the release of drugs. Hence, the approach that was explored within this investigation surrounds the use of cellulose acetate phthalate (CAP), as indicated in **Figure 7.1.1**, to be utilised as the polymeric binder which would maintain the structural integrity of the microneedles. As opposed to inert polymer-based MN systems composed of polycarbonate or polystyrene, CAP is a pH dependent polymer and is therefore regularly exploited as an enteric coating for oral drug tablets and capsules (Liu *et al.*, 2011; Kelley *et al.*, 2012; Wong *et al.*, 2017). Utilisation of the pH sensitivity of the polymer for controlled drug release has previously been reported, however, this has typically been in the form of a film coating a drug loaded capsule (Anderson, McConville and Davis, 2015). The dissolution of a CAP polymer coating, encapsulating a drug reservoir will occur in an alkaline environment such as the small intestine, thereby, preserving acid-labile drugs or the stomach from irritants. The carboxylic acid groups contained in the CAP facilitate this process by becoming un-ionised in acidic conditions (rendering it stable in the stomach), but, ionised in the higher pH environment of the colon, where the coating begins to dissolve, thus, exposing the internal drug to be released (Liu *et al.*, 2011). The pH of human blood ranges between pH 7.35 and pH 7.45, thus, it is assumed that this same process could apply when penetrating microneedles composed of the same polymer through the skin to come into contact with the higher pH contained in the blood.

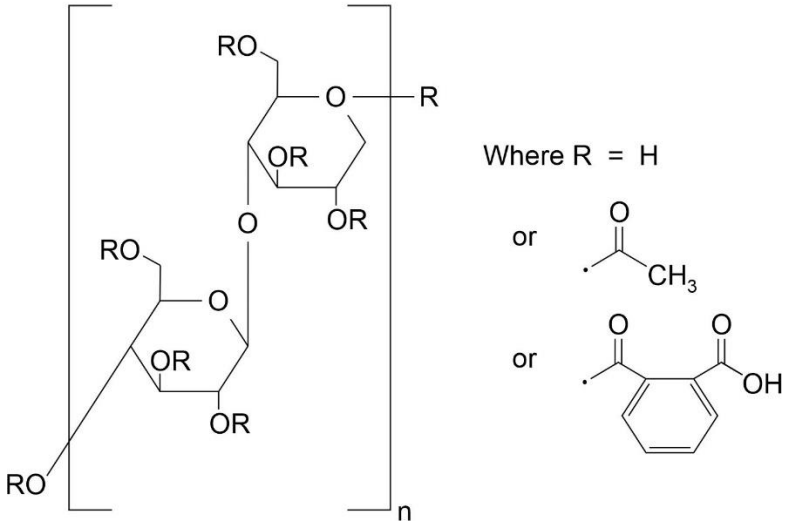

Figure 7.1.1 Structure of cellulose acetate phthalate chemical used as binder within the composite microneedle casting formulation.

Henceforth, carbon nanoparticles would be dispersed within the CAP binding polymer to fabricate a composite microneedle array where dissolution or swelling of the CAP is achieved by changes in local pH. Alternatively, the incorporation of conductive nanoparticles provides the opportunity to manipulate the morphology of the CAP polymer by electrochemical means. It could be anticipated that application of a sufficient reducing potential, would cause a cathodic reaction at the electrode surface inducing the hydrogen evolution reaction (HER), thereby, causing an increase in local pH (Anderson, McConville and Davis, 2015; Dubouis and Grimaud, 2019). Thus, this mechanism would support the ideal concept of controlled drug release, where a drug formulation would be preserved within the MN structure and exploitation of electrochemically induced dissolution of the CAP would expose the drug to be released. The theoretical principle for the proposed electrochemically controlled drug release strategy is outlined in **Figure 7.1.2**. In recent years, there has been a converging interest surrounding dissolvable and swellable microneedles for transdermal drug delivery applications, some of which are comparable to the concept idealised here, however, the main drawbacks are that they are largely passive techniques and lack control of drug dosage (Larrañeta *et al.*, 2016; Ita, 2018b; Tarbox *et al.*, 2018). In light of this, the investigation described here evaluates the functionality of integrating conductive nanoparticles to enable a controlled release operation and critically examines the constraints which would arise for transdermal applications.

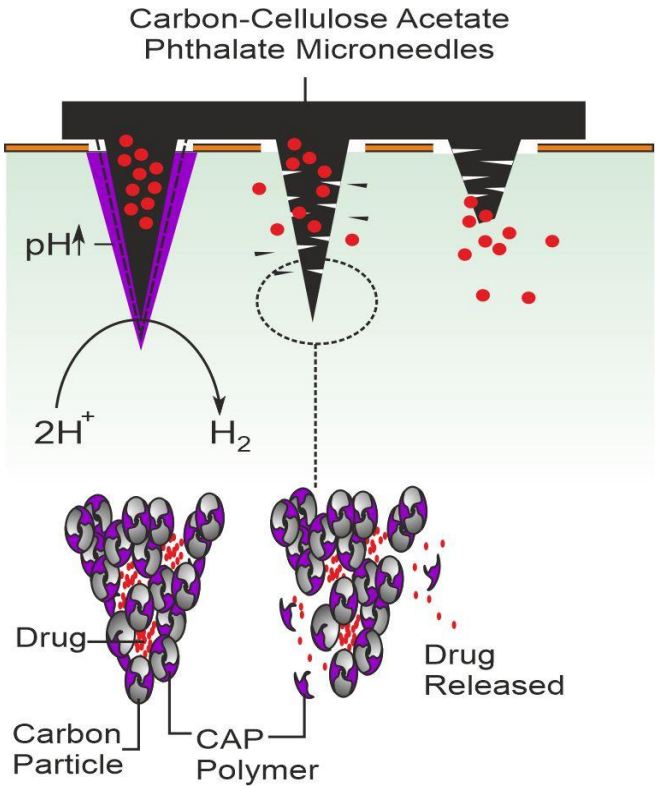

Figure 7.1.2 Proposed mechanism for electrochemically induced drug release of carbon-cellulose acetate phthalate microneedles.

7.2 Experimental Details

Carbon nanopowder (< 100 nm), cellulose acetate phthalate granules (MW 2534) and polystyrene pellets (MW 192000) were obtained from Sigma-Aldrich (Dorset, UK), along with all other chemicals used in the investigation, were of the highest attainable grade and were utilised without further purification strategies. Britton Robinson buffers (acetic, boric and phosphoric acids) were used throughout unless mentioned otherwise. Silicone microneedle templates were procured from Micropoint® Technologies Pte Ltd (Singapore) and consisted of a 10 x 10 array or pyramidal shaped needles. Electrochemical measurements were recorded at 22°C ± 2°C, using a micro Autolab Type III potentiostat. A three-electrode system was employed, with the carbon-polymer microneedle array serving as the working electrode, a platinum wire as the counter and a commercial silver|silver chloride (3 M KCl, BAS Technicol, UK) as the reference electrode.

7.2.1 Microneedle Fabrication

7.2.1.1 Cellulose Acetate Phthalate - Carbon Microneedles

Much like the fabrication of the carbon-polystyrene microneedles, the cellulose acetate phthalate-carbon MNs were composed by adding carbon nanoparticles and the CAP polymer at a 1:1 ratio into a 2 mL volume of cyclohexanone (MW 98.14 g/mol) solvent. The mixture was allowed to stir for approximately 2 hours where the polymer would dissolve and a homogenous solution was formed, with the carbon nanoparticles disperse throughout the polymer. The solution was then cast into the silicone templates (200 µm base x 200 µm pitch x 350 µm height or 200 µm base x 500 µm pitch x 700 µm height) and the templates placed in a vacuum oven at 30 ^{o}C and the pressure increased to 1000 mbar. Once the desired pressure was reached, the air was released again, and the templates removed. If deemed necessary, the templates would be topped up with more of the homogenous mixture, ideally overflowing the template to account for solvent evaporation. Alternatively, in the case of forming Toluidine Blue (TBO) loaded MNs, the templates would have been loaded with an initial coating of carbon-CAP (to allow for a conductive electrode interface) and at this point (after vacuuming), topped up with a second homogenous carbon-CAP solution containing 5% TBO. The templates were then left at room temperature to allow for solvent evaporation (over 48 h), thereafter, the microneedle arrays could be carefully withdrawn from the templates.

7.2.1.2 Carbon - Polystyrene Microneedles

Basic unmodified carbon-polystyrene microneedles (200 µm base x 500 µm pitch x 700 µm height), forming the basis of the working electrode used in the latter half of this investigation, were prepared in accordance with the procedure outlined in Chapter 5.

7.2.2 Microneedle Modification

7.2.2.1 Cellulose Acetate Phthalate - Carbon Microneedles

A thin coating of palladium on the carbon-CAP MN surface was achieved by sputtering a layer of Pd/Au (80:20) at 30 mA for 3 min using an Emitech K500X Sputter Coater (Quorum Technologies Ltd., England). X-ray photoelectron spectroscopy (XPS) analysis of the Pd sputtered MN samples before and after modification with cysteine was performed using a Kratos Axis Ultra DLD Spectrometer. Analysis of spectra was completed under typical parameters of 15 kV and 10 mA (150 W) at an operating pressure lower than $6x10^{-8}$ Pa using monochromated Al Ka X-rays (*hv* = 1486.6 electron volts (eV)). A hybrid lens mode was used (electrostatic and magnetic) during analysis, with a 300 µm x 700 µm analysis area at a take-off angle (TOA) of 90^{o} relative to sample surface. Wide energy survey scans (WESS) were collected across a range of 0 to 1300 eV binding energy (BE), with a pass energy of 160 eV and step size of 1 eV. High resolution spectra were collected for Pd 3d, C 1s, N 1s, O 1s, and S 2p at a pass energy of 20 eV. A Kratos charge neutraliser system with a filament current between 1.7 and 2.1 mA at a charge balance of 3.0 – 3.6 V was used for all samples. Three measurements were taken per sample, with a Shirley background subtracted from each XPS spectra. The peak areas of the most intense spectral lines for each elemental species were used to determine the percentage atomic concentration. Peak fitting of high-resolution spectra was carried out using Casa XPS software.

7.2.2.2 Carbon – Polystyrene Microneedles

Electrochemical anodisation is an established method for increasing the population of oxo-groups on carbon-based surfaces as reported in Chapter 6. In this case, anodisation (+2 V, 0.1 M NaOH) was performed on the carbon-polystyrene composite MNs to promote exfoliation of interfacial carbon on the needle surface and increase the resulting generation of endogenous carboxyl groups, to be exploited as a means of capturing palladium ions (Hegarty, McKillop, *et al.*, 2019). X-ray photoelectron spectroscopy (XPS) of the MN arrays,

confirming the modification of interfacial chemistries on the MN surface, was performed using a Kratos Axis Ultra DLD Spectrometer. Analysis of spectra was completed under typical parameters of 15 kV and 10 mA (150 W) at an operating pressure lower than $6x10^{-8}$ Pa using monochromated Al Ka X-rays (*hv* = 1486.6 electron volts (eV)). A hybrid lens mode was used (electrostatic and magnetic) during analysis, with a 300 μm x 700 μm analysis area at a take-off angle (TOA) of 90° relative to sample surface. Wide energy survey scans (WESS) were collected across a range of 0 to 1200 eV binding energy (BE), with a pass energy of 160 eV and step size of 1 eV. High-resolution spectra were collected with a pass energy of 40 eV, a 0.05 eV step size, a 25 eV scan width, a dwell time of 150 ms and at least 3 sweeps to reduce the signal noise. A Kratos charge neutraliser system with a filament current between 1.8 and 1.95 A, a charge balance of 3.3 – 3.6 V and a filament bias of 1.3 V was used for all samples. Charging effects on the BE positions were adjusted by setting the lowest BE for the C1s spectral envelope to 284.8 eV, which is commonly accepted as adventitious carbon surface contamination (NIST, 2012). Three measurements were taken per sample, with a Shirley background subtracted from each XPS spectra. The peak areas of the most intense spectral lines for each elemental species were used to determine the percentage atomic concentration. Peak fitting of high-resolution spectra was carried out using Casa XPS software.

7.2.3 Biocompatibility

Skin irritation (DIN EN ISO 10993-10:2014) and cytotoxicity (DIN EN ISO 10993-5:2009) biocompatibility studies of the cellulose acetate phthalate-carbon microneedles were completed under GLP conditions by Bioserv Analytik Un Medizinprodukte GMBH (Rostock, Germany). Young female albino rabbits which were considered healthy and at a weight no less than 2 kg were used for skin irritation assessment in accordance with ISO recommendations. Prior to testing, the rabbits were immunised against myxomatosis and RHD, and were also subject to acclimatisation, by being caged for at least 5 days before testing. In preparation for skin irritation testing, the fur on the rabbits back was clipped on either side of the spinal column (10 x 15 cm) 4 hr before commencing the testing procedure. Gauze patches (25 x 25 mm), serving as the control, and the test material (C-CAP) were then applied to the clipped skin. The testing sites were covered with a nonocclusive gauze and wrapped in an occlusive bandage for a testing period of 4 hours. Upon completion of the

test, all dressings were removed from the skin, which was then rinsed with warm water and blown dry. Examination of the application sites were scored with relation to extent of erythema, edema formation and eschar with the testing sites monitored at 1, 24, 48 and 72 hr after removal of the dressings. No skin irritation was recorded at any point over the course of the 72 hr period.

For cytotoxicity assessment, 6 cm^2 of the testing material (C-CAP) was compared against positive (Dimethyl sulfoxide (DMSO)) and negative (polypropylene) control samples. Extracts were processed with gentle shaking at 37 ^oC for 24 hr, in line with ISO 10993-12:2012, using Dulbecco's Modified Eagle Medium with 10% foetal calf serum (DMEM-FCS). In accordance with ISO 10993-5:2009, cell cultures were prepped using L929 cells (ATCC CCL 1, NCTC clone 929, connective tissue mouse) and the cells grown in DMEM-FCS at 5% CO_2 in a humidified incubator at 37 ^oC. Prior (24 hr before) to cytotoxicity assessment, cells were harvested using a trypsin/EDTA solution and resuspended in a fresh solution of DMEM-FCS, with the cell density adjusted to 1.75 x 10^5 cells/mL. A tissue culture plate was then inoculated with 1 mL of the cell suspension and incubated again for 24 hr to form a sub-confluent monolayer. Serial dilutions of the C-CAP extract were then prepared using DMEM-FCS as the dilutent to provide concentrations of 100, 66, 44, 30 and 20%, where (after removal of the culture medium) each dilution extract was then tested in triplicate by pipetting 1 mL aliquots into the respective cell culture wells and placed in incubation for 24 hr before assessment. The qualification of each cell culture plate was inspected using microscopy and graded in terms of reactivity (0: no growth inhibition or cell lysis, 4: almost complete eradication of cell layers). Quantification of the cell layers were also examined by staining with 0.25% crystal violet, washed, dried and the cell bound stain extracted using 33% glacial acetic acid. A microplate reader was employed to examine the dissolved stain samples at a wavelength of 550 nm. Absorbance of each sample was tested in triplicate and the mean value compared against the negative control (polypropylene) sample, which was estimated at 100% cell growth. From this, relative inhibition of cell growth (ICG) was calculated (%ICG = 100-($100 \cdot A_{550\ test}/A_{550\ negative\ control}$)) and assessed in accordance with ISO 10993-5:2009, whereby an ICG higher than 30% is considered as a cytotoxic effect. All testing extract solutions from this study were below the threshold and throughout the overall cytotoxicity assessment, the material did not present with any relevant toxicological or biological damage of the sub-confluent monolayer of the L929 cells in line with testing conditions of DIN EN ISO 10993-5:2009.

7.3 Results and Discussion

7.3.1 Cellulose Acetate Phthalate – Carbon Microneedles

Scanning electron micrographs are presented in **Figure 7.3.1**, which detail microneedle arrays (200 µm base x 200 µm pitch x 350 µm height) composed of solely CAP polymer, where the needles presented as stable and intact in pH buffer solutions which were acidic or neutral. However, once exposed to more alkaline solutions the CAP MN structure begins to deteriorate and the dissolution process commences. This is evidenced in **Figure 7.3.1**, where the CAP MNs have been immersed in pH 8 (Britton Robinson) buffer solutions for increasing time intervals (3 and 5 mins) and the needle definition degrades with increasing time.

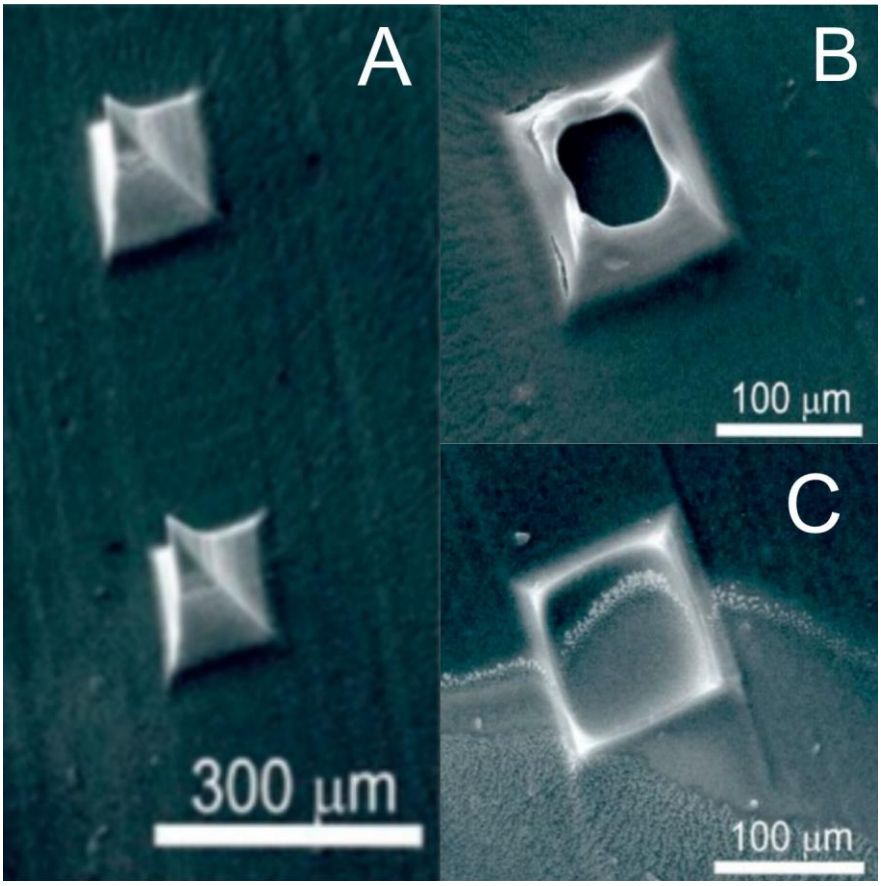

Figure 7.3.1 Scanning electron micrographs of pure CAP MNs (200 x 200 x 350 µm) after exposure to pH 8 Britton Robinson buffer for (**A**) 0, (**B**) 3 and (**C**) 5 min.

This procedure was repeated again, but with the integration of carbon nanoparticles into the MN casting formulation. Scanning electron micrographs displaying the effects of pH 8 buffer before and after 1 min are shown in **Figure 7.3.2**. Given previous records of particulate introduction into MN systems causing features of defects or granularity, it could have been expected that the carbon nanoparticles may have had a similar effect here (McConville and Davis, 2016). However, (prior to exposure to the alkaline solution) the surface topography of the C-CAP composite MN (**Figure 7.3.2.A**) presented as relatively smooth, with no granularity or major disruption of the needle surface. As seen in **Figure 7.3.2.B** and **Figure 7.3.2.C,** exposure to the pH 8 buffer induced the dissolution of the CAP layer and, although the fundamental needle structure is maintained, the surface morphology was disrupted. Disintegration of the CAP layer exposes the residual carbon foundation structure, which presents with a rugged, platelet like carbonaceous surface (**Figure 7.3.2.C**). Continued immersion of the C-CAP MNs in the alkaline buffer further jeopardises the structural integrity of the needles by proceeding with the degradation and ultimately, the disappearance of the needles, similar to the progression identified in the pure CAP MN systems (**Figure 7.3.1.B,C**).

Piercing capability of the C-CAP microneedles penetrating tomato skin was assessed by scanning electron microscopy (**Figure 7.3.2.D,E**) and their ability to maintain needle structure after puncture examined by computerised tomography (CT) (**Figure 7.3.2.F**). Similar to the process in Chapter 6, the tomato flesh was excised from the exocarp to facilitate close inspection of the needles after puncture. As previously recognised in Chapter 6, the web-like microstructures featured in **Figure 7.3.2.F** are characteristic of cell-wall structural contours necessary for adhesion to the waxy cuticular membrane (Li *et al.*, 2014). The benefit of using CT scanning allows sectional imaging of the MN array demonstrating that the capability of the needles to puncture at a sufficient depth, but also, that the internal needle structures were free from fissures and voids.

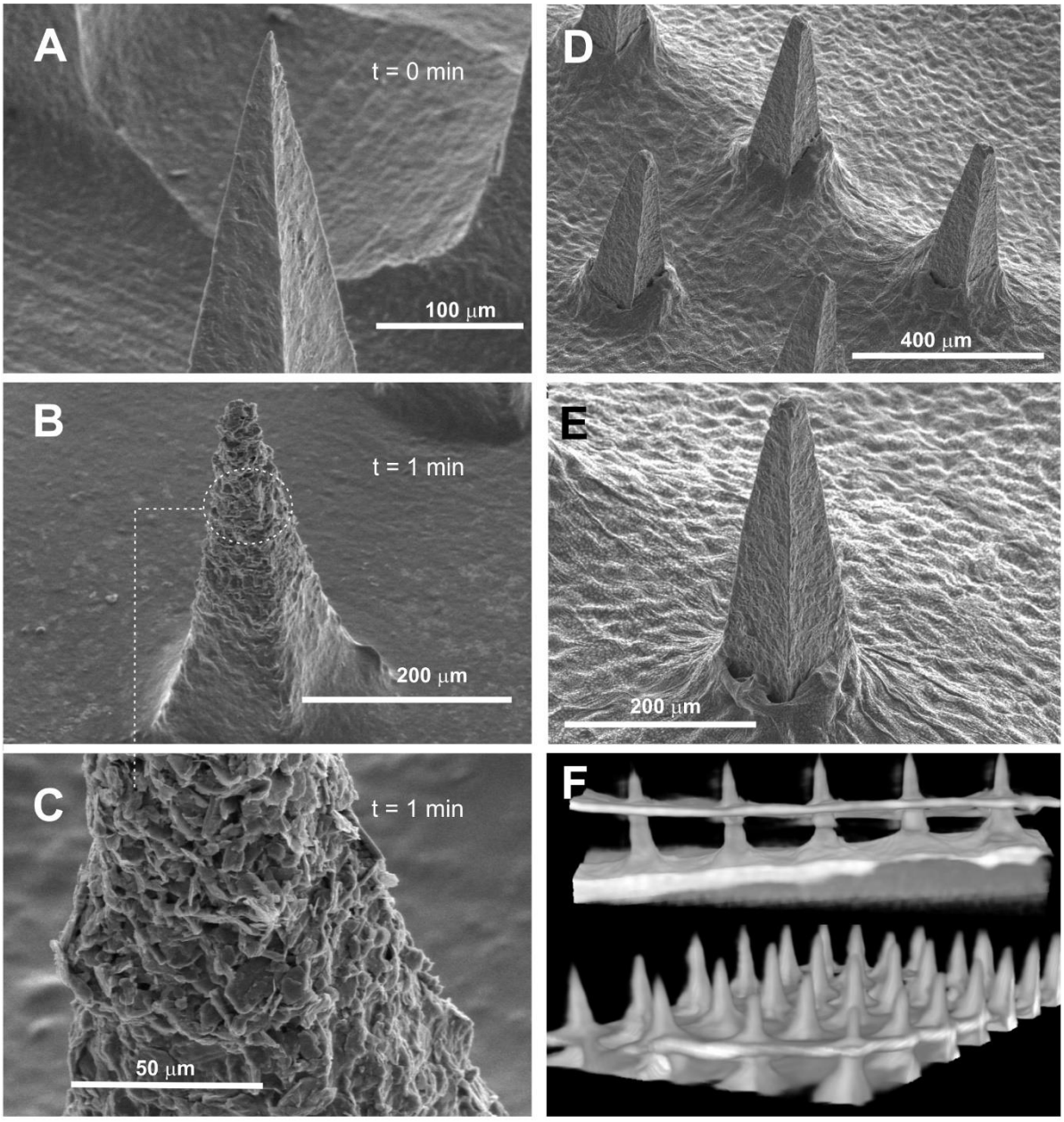

Figure 7.3.2 Scanning electron micrographs of carbon-CAP MNs (200 x 500 x 700 μm) before (**A**) and after (**B**) 1 min exposure to pH 8 Britton Robinson buffer, with CAP dissolution highlighted (**C**). Scanning electron microscopy (**D,E**) and computerised tomography (**F**) imaging of the microneedles penetrating through de-fleshed tomato exocarp.

7.3.2 Electrochemically Induced Dissolution of CAP

The hydrogen evolution reaction has been extensively researched with relation to fuel cell reactions and water splitting over the past five decades (Zhang *et al.*, 2016). Carbon

supported platinum has been the common material choice for electrocatalysis in low temperature fuel cells. However, palladium has recently garnered attention as an alternative to the platinum catalyst, providing it is cheaper (thereby reducing the cost of fuel cells) and at least fifty times more abundant in the earths supply than platinum (Antolini, 2009; Lin and Lasia, 2017). Since electrocatalysis is predominantly a surface effect, the catalyst is required to have the highest possible surface area, thus, the active phase is often dispersed on an inert conductive substrate with a high surface area (Kibler, 2008; Lin and Lasia, 2017). Hence, palladium has previously been employed as a catalyst to enhance the HER process, as a coating or in the form of clusters on many carbon based materials (such as graphene, graphite, carbon nanotubes) (Ghasemi *et al.*, 2015; Bhowmik, Kundu and Barman, 2016; Ramakrishna *et al.*, 2016) and various other nanoparticle systems acting as the high surface area supporting conductive element (Jović *et al.*, 2017; Zheng *et al.*, 2019). Palladium has since been proven as an ideal catalyst, occurring with little to no activation barrier and a facile means of hydrogen sorption and desorption (Nakatsuji and Hada, 1985). However, the mechanism proposed here revolves around exploiting the change in local pH as a consequence of electrolysis rather than capitalise on the hydrogen that is produced.

As carbon is known to be a poor catalyst for the HER process, it was envisaged that the application of Pd to the surface would facilitate an improved response and so, the C-CAP MN surface was sputtered with a thin layer of palladium. This would provide the platform to decipher if the presence of the metallic catalyst would enhance not only the sensing application of the MN system, but also the HER process which would be used to maintain the dissolution and/or swelling of the needles as proposed in **Figure 7.1.2**. The cyclic voltammograms presented in **Figure 7.3.3.A**, detail the response of the Pd modified C-CAP MN towards ferrocyanide.

As evidenced by the cyclic voltammograms (**Figure 7.3.3.A**), the addition of a metallic Pd layer to the C-CAP MNs greatly improved electron transfer kinetics, thereby improving MN response towards ferrocyanide complimented by the improved peak separation and definition. Despite this, the greatest improvement in electrochemical performance was instigated by the addition of an adsorbed layer of cysteine to the Pd modified C-CAP MNs as presented in **Figure 7.3.3.A**. Cysteine has been shown to adsorb very strongly to surfaces containing gold or platinum metals due to the thiol functionalities present on the sulfur-

containing amino acid (Qingwen *et al.*, 2001). Surfaces predominantly containing palladium have also been demonstrated to successfully adsorb cysteine with the intent of improving electrochemical performance, where it has been postulated that the cysteine facilitated enhancement occurs through the removal of surface oxides (Feliciano-Ramos *et al.*, 2010). This was expected due to the properties of Pd being comparatively similar to platinum, the Pd lattice being smaller than gold and, in addition to this, it is highly reactive to sulfur (Christopher Love *et al.*, 2003; Feliciano-Ramos *et al.*, 2010). Therefore, it was speculated that the incorporation of a self-assembling monolayer (SAM) of cysteine would advance the catalytic behaviour of the Pd modified MN surface. The incorporation of a SAM of cysteine to the Pd modified C-CAP MNs was examined by XPS analysis as shown in **Figure 7.3.3.B** and was confirmed by the S 2p peaks before and after modification.

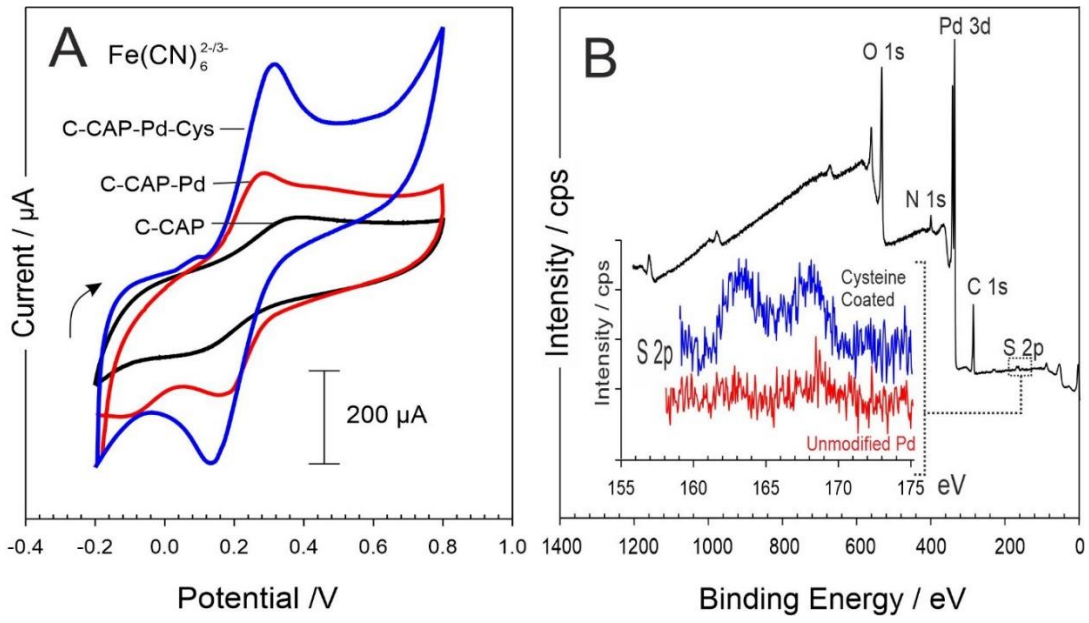

Figure 7.3.3 (**A**) Cyclic voltammograms detailing response of C-CAP MN towards ferrocyanide (2 mM in 0.1 M KCl) before and after modification with palladium and cysteine (Scan rate: 50 mV/s). (**B**) XPS spectra confirming the C-CAP-Pd microneedles modification with self-assembling monolayer of cysteine.

The cyclic voltammograms presented in **Figure 7.3.3.A**, demonstrate the capabilities of the Pd-cysteine modified C-CAP MNs to serve as both the actuator and sensing unit combined. Although, a major limitation of this proposed synergy involves the large reducing potential which is essential to induce the HER process, and therefore, drug release. This would result

in the desorption of the cysteine as a consequence of reducing the Pd-thiol bond and, effectively eradicating the cysteine promoted influence on the kinetics of the drug release. In light of this, the additional cysteine modification process was excluded from the ensuing investigations within this study regarding MN dissolution. Depicted in **Figure 7.3.4** are linear sweep voltammograms representative of C-CAP and Pd modified C-CAP microneedle responses to under two divergent pH buffer regimes. Notably, the modification with Pd has an indisputable effect on the MN response in both comparative pH solutions.

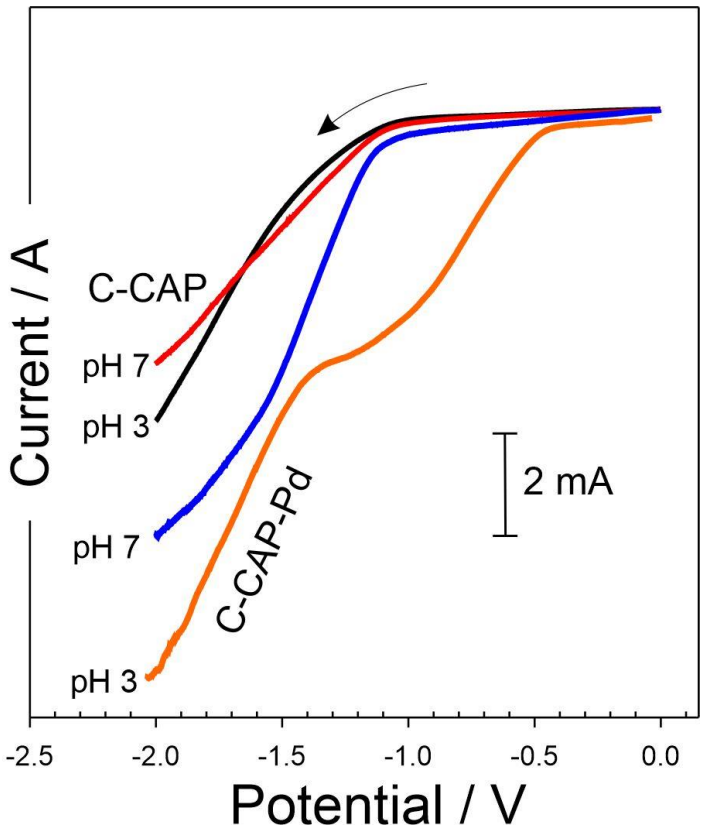

Figure 7.3.4 Linear sweep voltammograms depicting response of C-CAP microneedles in pH 7 and pH 3 Britton Robinson buffers before and after modification with palladium (Scan rate: 50 mV/s).

The next progressive step within this investigation was to evaluate the microneedle capability for controlled swelling and/or dissolution. To do this, a model skin mimic was constructed, where a parafilm™ layer (~ 100 µm thick) was employed to serve as the epidermal layer and placed on top of (previously prepared) calcium alginate gel containing ferrocyanide (2 mM). The pH of the gel was controlled to preserve the needles from unintended dissolution. Only upon successful puncture of the needles through the parafilm,

with the application of thumb pressure, would the needle interface contact the underlying gel matrix (McConville and Davis, 2016). A Pt counter and commercial reference (3 M NaCl, Ag|AgCl) electrode were employed to complete the electrochemical cell by insertion into the gel. The inclusion of ferrocyanide within the matrix was utilised to appraise the functional integrity of the needles. Cyclic voltammograms were documented before subjecting the MNs to a reducing potential which would be used as the control. Theoretically, it was envisaged that the application of a reducing potential would increase the local pH. Hence, initiating the swelling/dissolution of the CAP polymer holding the needle structure, which would in effect, change the surface area of the needles. By changing the electrode surface area, this could be examined by fluctuation in peak magnitude response to the ferrocyanide contained in the gel. Therefore, cyclic voltammograms detailing the MN response to ferrocyanide were taken before and after each step in cathodic potential. These cyclic voltammograms are displayed in **Figure 7.3.5**, representative of the Pd modified C-CAP MN response to the ferrocyanide within the alginate gel matrix before and after the application of a -2 V potential. The control response of the MN before application of the cathodic potential is coherent with the response recorded in **Figure 7.3.3**.

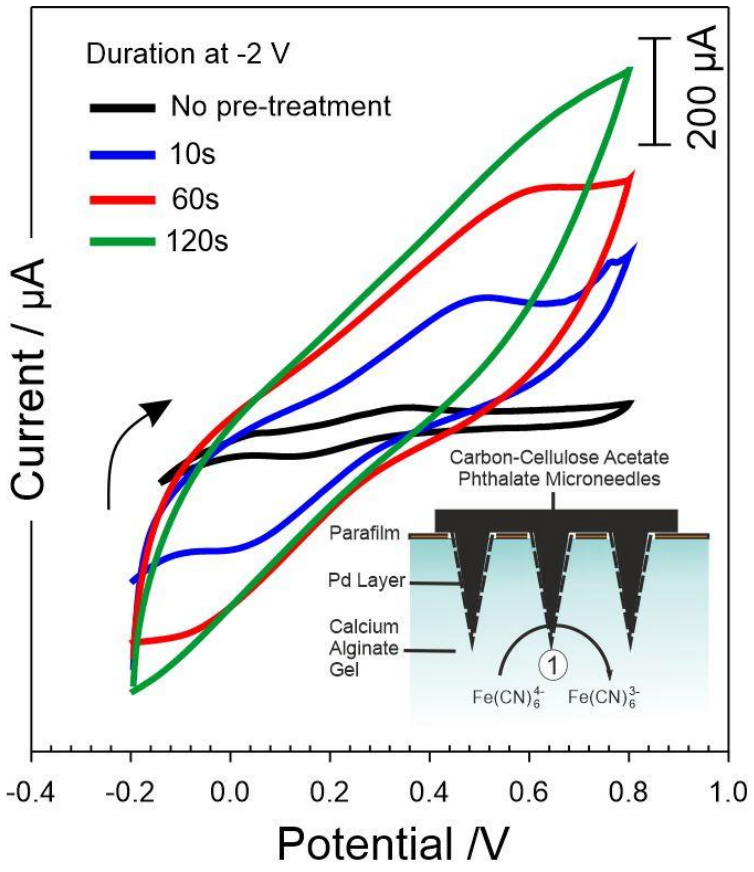

Figure 7.3.5 Cyclic voltammograms showing the response of C-CAP-Pd MNs towards ferrocyanide (2 mM) before and after imposing a reducing potential (-2 V) at the electrode surface for varying periods of time (Scan rate: 50 mV/s).

As observed in **Figure 7.3.5**, the voltammetric signal response undertakes a dramatic transformation with the initiation of the HER, losing the characteristic peak processes. This can be attributed to the swelling mechanism of the CAP polymer, whereby the special separation between the carbon nanoparticles will have increased and consequently, so too will the resistance of the needle framework. This hypothetic reasoning was confirmed by placing the MN arrays in a controlled buffer solution (pH 6 Britton-Robinson buffer), applying a reducing potential (of -1 and -2 V) and observing the swelling/dissolution effect by electron microscopy. The scanning electron micrographs depicting this mechanism are represented in **Figure 7.3.6**. The electron microscopy imaging accentuates the progressive degradation of the needle structure after the imposition of varying cathodic potentials (-1 and -2 V) for a 30 s duration. The disintegration of the CAP binder and loss of needle framework is evident after application of the -1 V cathodic potential which is analogous to the imaging previously documented in **Figure 7.3.2.B**. Subjecting the MN arrays to -2 V for 30 s however, results in near eradication of the needle. Upon observing the voltammograms in **Figure 7.3.5**, a

substantial increase in resistance occurs from inducing a cathodic potential for a relatively short duration, illustrating that the swelling of the CAP binder materialises without hesitation. Although, for total dissolution and deterioration of the needle structure, a larger and more forceful reducing potential is necessary. Even after complete eradication of the needle framework (**Figure 7.3.6.C**), a signal response is still detected as seen in **Figure 7.3.5**, which can be accredited to the persistent electroactivity of the base plate.

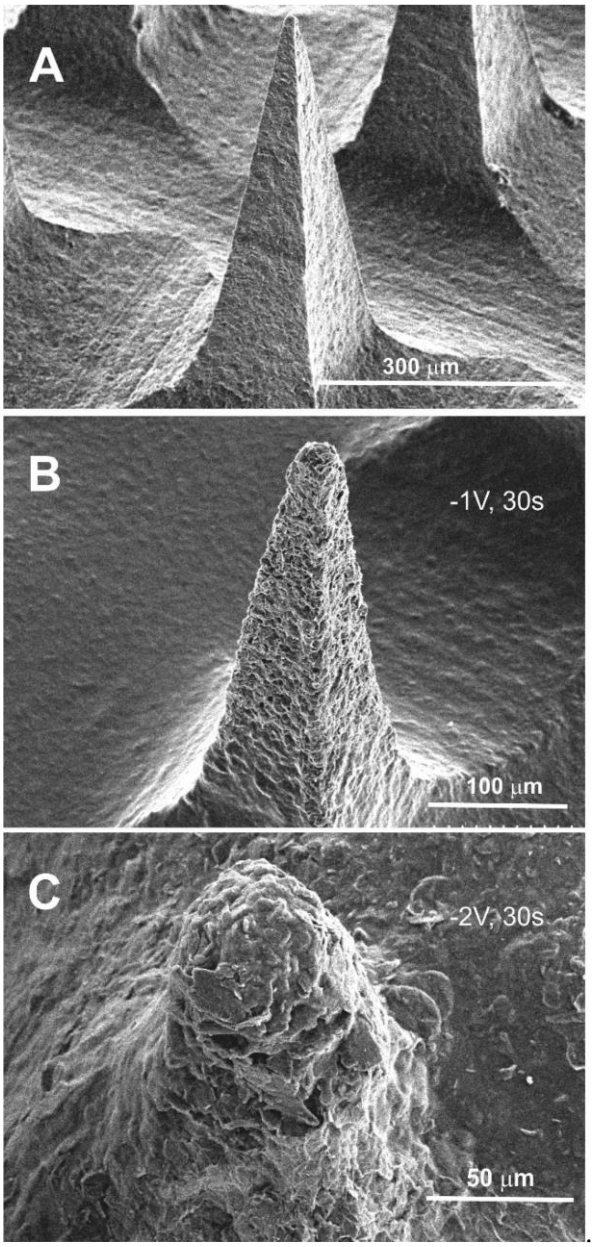

Figure 7.3.6 Scanning electron micrographs highlighting the morphological effects before (**A**) and after imposing a reducing potential of (**B**) -1 V for 30 s and (**C**) -2 V for 30 s to the C-CAP-Pd microneedles (200 x 500 x 700 μm).

7.3.3 Electrochemically Controlled Release of Model Drug

The mechanism of electrochemically controlled release was evaluated using a model drug discharged within a gelatin formulation, to resemble drug transport into the skin. The gelatin matrix was maintained at pH 4.02, preventing unintended dissolution of the CAP and preserving the MN structural integrity. This of course is not representative of a pH which would be found in the human body but is used as a control to show that the microneedle only dissolves due to the influence of an increased pH thereby, demonstrating proof of principle. A layer of parafilm was again placed over the gelatin matrix, serving as a skin mimic, ensuring drug release exclusively occurred through the needles which successfully penetrated through the film and not through contact with the baseplate. Toluidine Blue (TBO) was employed as the model drug which would be easily introduced to the C-CAP composition and then be visually monitored by blue coloration (λmax = 630 nm). Inducing a cathodic potential at the MN electrode surface was expected to induce the HER process. Thereby increasing the local pH, where dissolution of the CAP would commence and the TBO would be discharged into the gelatin matrix. The MN array encompassing TBO was rinsed with acid upon removal of the gelatin in an attempt to expel extraneous TBO. The Mn was then pierced into fresh gelatin and left to sit. With no blue coloration indicated, this confirmed that the model drug (TBO) was contained within the MN framework. **Figure 7.3.7** highlights the impact of imposing a cathodic potential to the MN, where the progression of blue coloration is attributed to the release of TBO with increasing duration of the HER process.

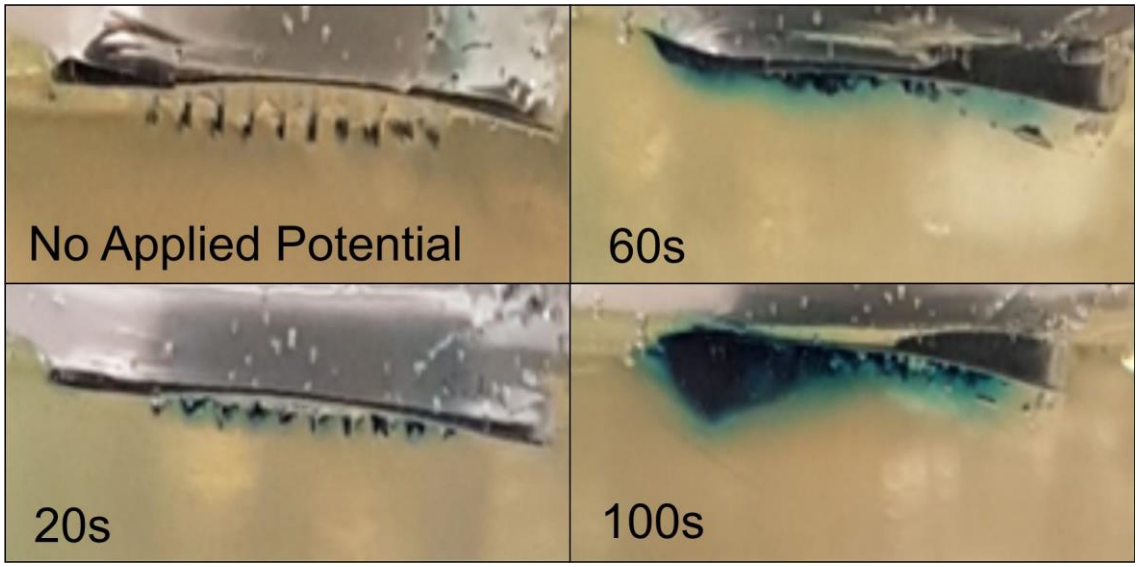

Figure 7.3.7 Imaging representative of a TBO loaded C-CAP-Pd microneedle (200 x 500 x 700 µm) pierced into a gelatin matrix (pH 4.02). The increasing time (0-100 s) for which the cathodic potential (-2 V) is held at the electrode sees the accumulative release of TBO (blue coloration).

TBO was released from the needles and discharged into the gelatin by imposition of a large cathodic potential of -2 V, where changing the local pH at the electrode interface accelerated the dissolution of the CAP binder. A major limitation of this electrochemical strategy is the rapid disintegration of needle structure (**Figure 7.3.6.C**). An alternative, less vigorous method, with less negative potentials may also be used as seen in **Figure 7.3.6.B**. Controlled release of the TBO model was also investigated by implementing a -1 V potential step for a period of 3 min and activated repetitively in pH 5 buffer over a duration of 40 min. After each 3 min period, the solution was sampled and examined by conventional colorimetry (TBO λmax = 632 nm; ε = 30 000 M^{-1} cm^{-1}) (Saha *et al.*, 2018). For comparison, a TBO containing MN array was left in contact with the buffer and no potential applied to serve as the control with the absorbance depicted in **Figure 7.3.8**. Without the implementation of a cathodic potential, the MN exhibited little to no release of the TBO model drug. The MN with repeated application of -1 V however, displayed continuous discharge of the TBO. The recorded yield per cycle is presented in **Figure 7.3.8.B** and illustrates an increasing yield with each accumulative cycle before falling to zero, where it is inferred that the needles have completely dissolved. The concentration of model drug falling within the nanomole region was expected and can be attributed to the proportional capacity of the needles.

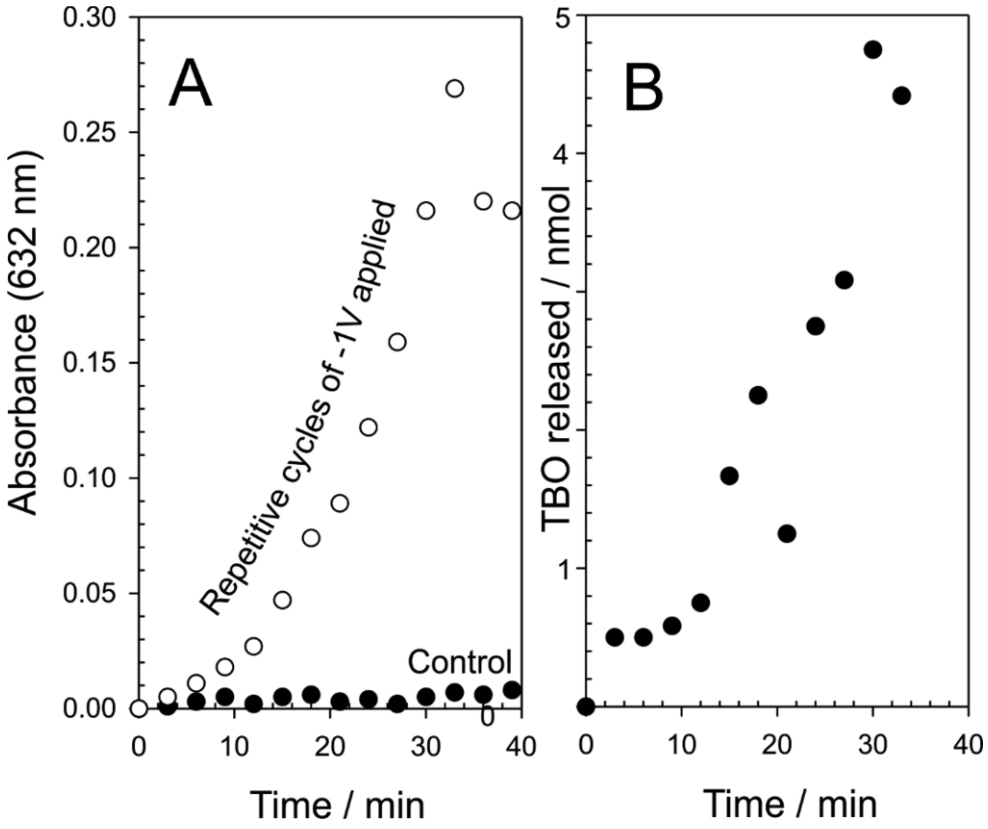

Figure 7.3.8 The effective release of TBO from a C-CAP-Pd microneedle into pH 5 Britton Robinson buffer through repetitive application of reducing potential (-1 V, 300s) (**A**) and the corresponding yield of TBO obtained per cycle (**B**).

The ability to synergise a conductive and dissolving polymer within one micromoulded composite MN array was demonstrated to be advantageous here and has potential to be applied to a variety of biosensing and drug delivery applications (Cheng *et al.*, 2019; Dharadhar *et al.*, 2019). The additional modification with palladium was easily accomplished, utilising standard methods traditionally employed for coating SEM samples. The introduction of the Pd layer exhibited significant improvement to the electrochemical performance of the system. Despite this, the significance of this investigation was to control the integrity of the microneedles by controlling the cathodic potential imposed at the needle surface. Exchanging the TBO for a suitable drug would be easily achieved with the C-CAP formulation during the MN casting process. Although, a constraint for this method and for many transdermal drug delivery MNs is the drug yield, limiting the system to low yield, high potency agents (Dharadhar *et al.*, 2019). Another point to note considers the reducing potential required to initiate the swelling/dissolution process, which, potentially could also reduce functional groups within the drug (such as nitro groups). Thus, this effect should be

contemplated to ensure the therapeutic agent does not become negligently modified as a secondary repercussion of the release mechanism. The design of the composite MN array also leaves the system vulnerable to possible fragmentation or loss of carbon and palladium particulates. Notwithstanding this, the micron sized needles penetrate at a relatively shallow depth and any residual particulate will most likely be displaced through shedding and regeneration of the skin (Takeo, Lee and Ito, 2015). Through this investigation, the biocompatibility studies remain expedient and provide insightful potential applications for the C-CAP material with no recorded skin irritation or cytotoxicity. Although, this should be treated as a dubious outcome, where if it were used in a device applied for longer periods of time, it may incite a sensitive response.

7.3.4 Carbon-Polystyrene Microneedles with Palladium Nanoclusters

The use of palladium as a catalyst for the HER process was considered in the initial investigation and was sputtered onto the microneedles as a facile means of modifying the electrode surface. The use of solid Pd particles as a means of producing composite MN arrays has already been documented by McConville and Davis (2016) but the manufacturing process led to a rather granular texture. Further refinement using this fabrication methodology was largely prevented by the lack of availability of sub-micron particles in contrast to the nm dimension of the carbon used previously for the CAP MNs. An alternative approach to the surface modification of the MN surface with Pd was investigated through the passive accumulation of Pd(II) ions from solution through chelation with carboxyl moieties at the carbon interface as indicated in **Figure 7.3.9**. It was envisaged that subsequent electro-reduction of the captured Pd(II) would then lead to discrete Pd nanoclusters dispersed on the MN surface, which could exhibit catalytic properties, whilst also retaining the wide potential window of the underlying carbon electrode.

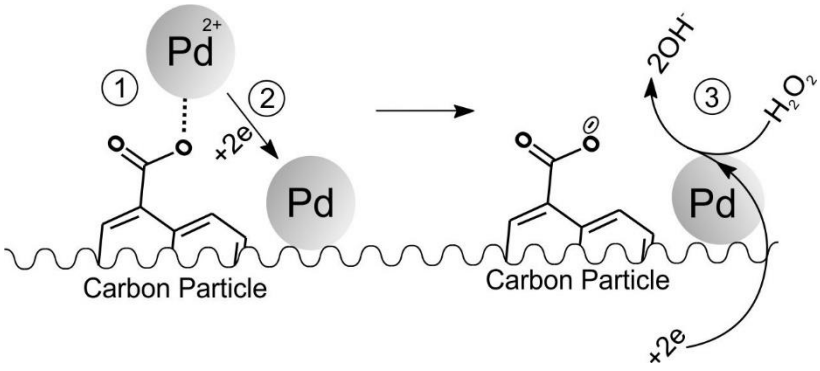

Figure 7.3.9 Mechanism of palladium catalysing peroxide reduction at the anodised carbon microneedle interface. Passive chelation of Pd^{2+} ions (1). Electrochemical reduction of Pd^{2+} to Pd metal (2). Electroreduction of peroxide catalysed by Pd clusters immobilised on MN surface (3).

Oxygen functionalities on carbon can be influential in terms of improving the electrode response (Chapter 4 and 5) and providing intrinsic mechanisms for the measurement of pH (Chapter 6). Here, it was envisaged that the exploitation of carboxyl functionalities could significantly broaden the applicability of the core MN structure for either drug release or for further biosensing systems. Within this secondary investigation, electrochemical exfoliation of the interfacial carbon nanoparticles was again proposed as a means of nano-structuring the carbon surface which constitutes the conductive element of the MN array (Hegarty, McConville, *et al.*, 2019). It was anticipated that this approach would effectively increase the population of oxo-groups, principally carboxylate groups, which could then be expected to improve the passive chelation of palladium (II) ions and the subsequent population of palladium nanoclusters (**Figure 7.3.9**).

One issue to this approach became apparent at an early stage which relates to the instability of CAP in the NaOH electrolyte normally used to anodise the carbon surfaces. As such, the MN would rapidly dissolve before any meaningful modification of the surface could take place. Nevertheless, an initial investigation of the suitability of the Pd nanocluster approach to the simpler carbon-polystyrene MN was conducted to determine proof of principle. It was expected that, if successful, then it could still remain a viable approach to the preparation of biosensing systems (if not drug release). In order to assess the effectiveness of the strategy, hydrogen peroxide was chosen as the model analyte.

Hydrogen peroxide is a very common oxidising agent, known as a by-product of numerous oxidase enzymes and a critical mediator used in medical, industrial, food and environmental analysis. In recent years, a surge of interest has surrounded research of new electrocatalysts for reagentless electrochemical H_2O_2 sensors (Lin *et al.*, 2009; Luo *et al.*, 2012). Noble metal nanoparticles in particular have been demonstrated to exhibit high electrocatalytic activities towards H_2O_2 reduction (Chen *et al.*, 2013). Silver, gold and platinum are among the group of materials which have been endorsed as complementary metals in the detection of H_2O_2 (Barrett *et al.*, 2015; Chinnadayyala, I. Park and Cho, 2018; Kim *et al.*, 2019). Nonetheless, the low-cost, robustness and superior electron transfer properties of palladium has subsequently seen this choice of metal emerge as the higher calibre material for sensing hydrogen peroxide (Ping *et al.*, 2011; Chen *et al.*, 2013; Hamidi and Haghighi, 2016; Xue *et al.*, 2018). Thus, the incorporation of palladium into electrode design, tailored for H_2O_2 sensing is ever growing, although, it should be noted that the geometry and crystalline structure of noble metallic nanoparticles determines their electrocatalytic capability (Tang and Cheng, 2013; McConville, Mathur and Davis, 2019). Therefore, an amplified sensitivity during electroanalysis was anticipated due to the large surface area to volume ratio of palladium nanoparticles at the electrode surface, which was then compared with already existing peroxide sensing systems (Baccar *et al.*, 2013).

The effect of anodisation on the carbon-based MN system was analysed by XPS, as shown in the high resolution C1s spectra in **Figure 7.3.10**, detailing the presence of oxo-groups at the electrode surface pre- and post-anodisation. The unmodified carbon-polystyrene MN surface is dominated by a large sp^2/sp^3 spectral peak, which can be attributed to the graphitic nature of the material composition of the carbon nanoparticles and polystyrene. However, once anodised, a greater population of carbon-oxygen functionality groups are generated at the surface and so too, increase the relatively insignificant concentration of endogenous carboxyl groups to almost 3%. The spectra obtained from the composite systems are similar to other studies of carbon fibres documenting the reorganisation of sp^2 components becoming oxidised and forming a surplus of C-O groups after electrochemical treatment (Casimero *et al.*, 2020). Here, the reformation of the sp^2 peak is less pronounced primarily due to the influence of the phenyl ring in the polystyrene binder which remains unaffected by anodisation. Moreover, the electrochemical anodisation is successful in escalating the formation of carboxyl functionalities, which is fundamentally vital to the electrode modification design.

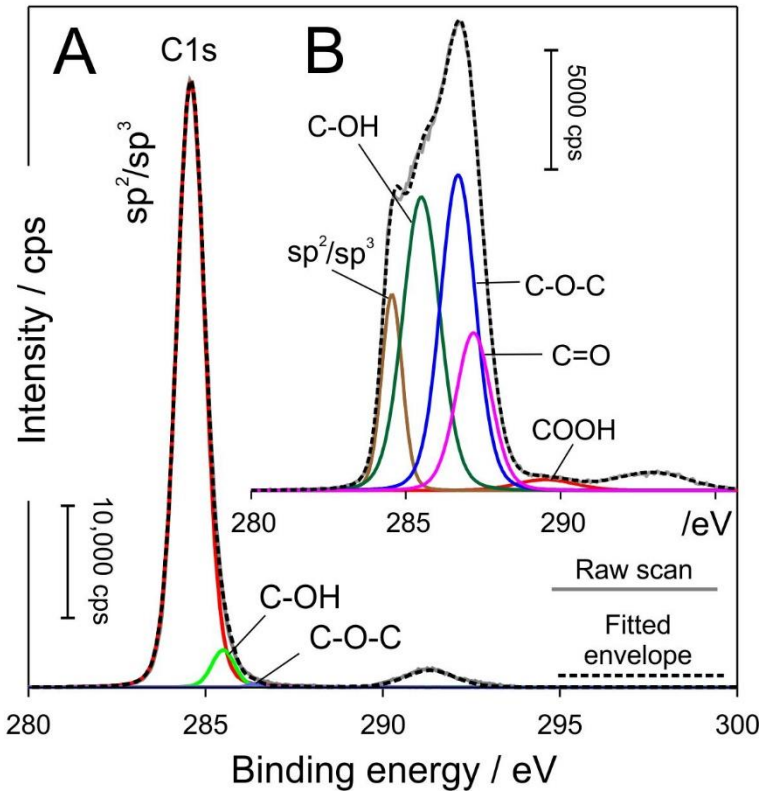

Figure 7.3.10 XPS spectra of the carbon-polystyrene microneedle before (**A**) and after (inset: **B**) electrochemical anodisation highlighting the increased presence of oxygen functionalities at the MN surface.

Exploiting chelating groups conjugated at electrode surfaces is a defined method of facilitating the passive capture of metallic ions. Through the addition of an appropriate reducing agent (typically $NaBH_4$ or hydrazine), the entrapment of these metal ions can then be converted to nanoparticulate clusters (Chen *et al.*, 2013; Bozkurt *et al.*, 2017; Gupta *et al.*, 2018; Baghayeri, Amiri and Razghandi, 2019). Within this investigation, by immersing the anodised MN in a solution of sodium tetrachloropalladate (II) (1 mM) for 10 minutes, palladium ions were chelated by the endogenous carboxylate groups at the MN interface. The microneedle electrode (with captured Pd(II)) was then subjected to a reducing potential (-1 V), thereby converting the Pd^{2+} to Pd and then rinsed with copious amounts of deionised water. The presence of palladium at the MN surface was confirmed by XPS analysis as depicted in **Figure 7.3.11**, showing pre- and postexposure to Pd^{2+} (after electroreduction). The definitive double peak attributed to Pd 3d2/2 and Pd 3d5/2 components with the respective binding energies of 334.96 and 340.36 eV are consistent with anticipated values

for Pd^{o} (Rastogi, Ganesan and Krishnamoorthi, 2014b, 2014a). The atomic% concentration of Pd at the electrode surface was found to be 0.85% (n = 3), which is expected considering it is a distribution of Pd nanoclusters rather than a layer of Pd deposited on the surface.

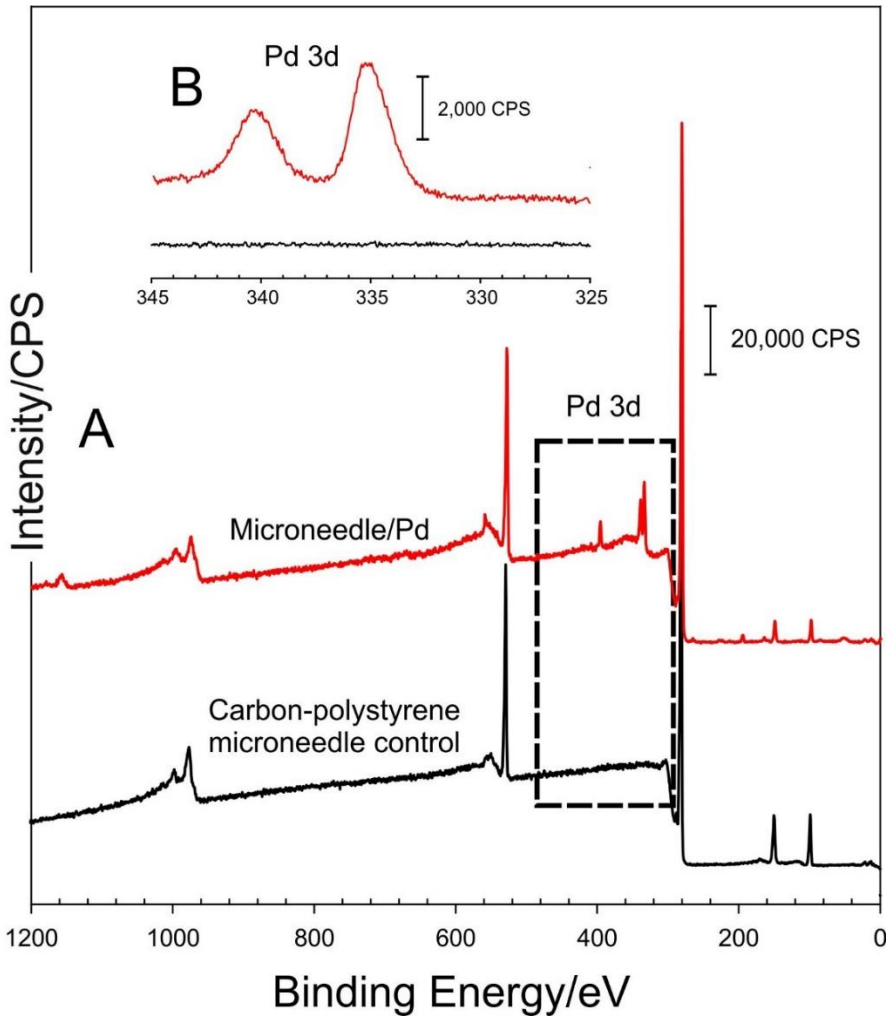

Figure 7.3.11 XPS spectra highlighting the capture and electroreduction of Pd^{2+} to Pd^{o} at the microneedle surface.

7.3.5 Detection of Hydrogen Peroxide

Cyclic voltammetry was used to analyse the sensitivity of the system towards hydrogen peroxide utilising increasing concentrations of H_2O_2 in pH 7 Britton Robinson buffer (+0.8 V to -0.8 V, 50 mV/s). **Figure 7.3.12** represents cyclic voltammograms detailing the response of the Pd modified and unmodified carbon-polystyrene MN system towards peroxide. The

palladium modified MN response to the absence of peroxide in blank buffer solution demonstrates a reduction (-0.034 V) and oxidative (-0.371 V) peak, which is coherent with previous reports of Pd clusters on the surface of modified electrodes (Chen *et al.*, 2013; Bozkurt *et al.*, 2017; Gupta *et al.*, 2018). Upon the addition of peroxide to the testing solution, the Pd modified MN system displays a contrasting response with an increasing magnitude in reduction peak process. This definitive change in reduction response is markedly different to the unmodified MN electrode as shown in **Figure 7.3.12**. An observed change in oxidative peak process is also evident, however, it is substantially smaller in sensitivity compared to that of the reduction response.

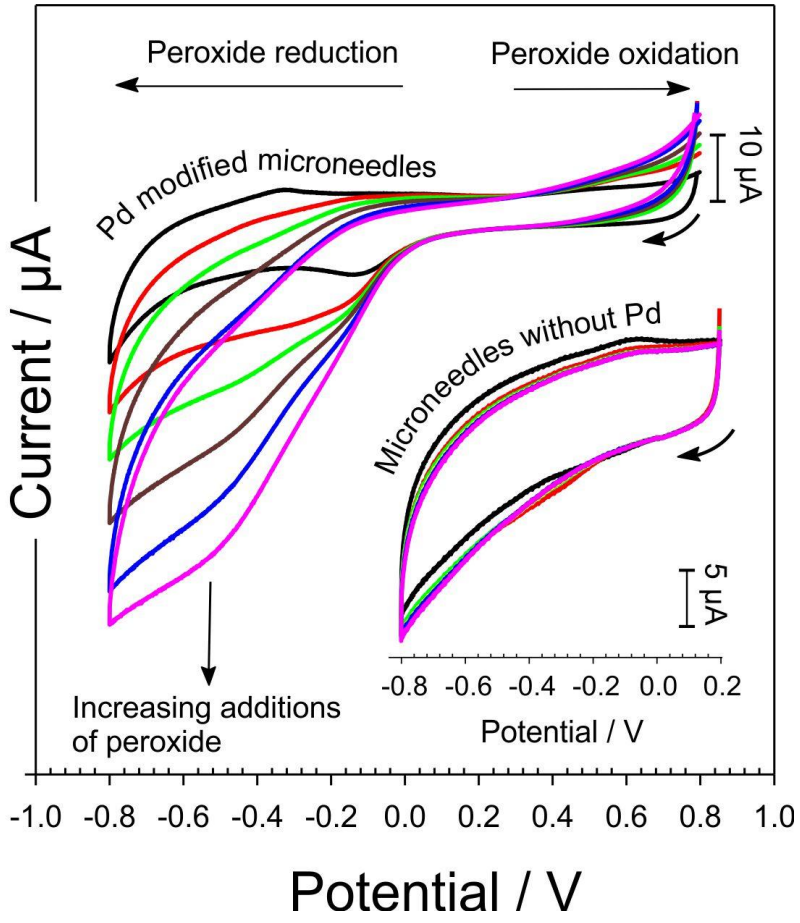

Figure 7.3.12 Cyclic voltammograms detailing response of a Pd modified carbon-polystyrene microneedle towards increasing concentrations of peroxide (0 to 500 µM) in pH 7 Britton Robinson buffer at a scan rate of 50 mV/s. Inset: CV response of unmodified carbon-polystyrene microneedle array towards same conditions.

Electrodes modified with nanoparticles exhibiting sensitive and selective responses towards the detection of peroxide has been extensively researched, some of which are outlined in **Table 7.3.1**, alongside the Pd modified MN system used in this investigation (–0.3 V: 49.7 ± 2.8 $\mu A \cdot mM^{-1} \cdot cm^{-2}$; –0.5 V: 102.1 ± 2.32 $\mu A \cdot mM^{-1} \cdot cm^{-2}$; N = 3). When compared to the existing technologies in **Table 7.3.1**, the Pd modified MN array is presented as a competitive electrode system with the added benefit of a low-cost, facile means of fabrication.

Table 7.3.1 Comparison of electrode sensitivities towards peroxide.

Electrode type	**Detection potential / V**	**Sensitivity ($\mu A\ mM^{-1}\ cm^{-2}$)**
Nafion Pd C-F (McConville and Davis, 2016)	+0.8	27.71
PdNPs-MWCNTs/GCE (Hamidi and Haghighi, 2016)	+0.35	0.17
ZnO/Co_3O_4/$NiCo_2O_4$/Ni (Xue *et al.*, 2018)	+0.55	388
Co3O4 NPs (Ni *et al.*, 2017)	+0.2	72.75
Pd C-F (McConville and Davis, 2016)	-0.2	148.89
ER-GNO/IL-SPE (Ping *et al.*, 2011)	-0.2	78.13
rGO/ZnO/GCE (Palanisamy, Chen and Sarawathi, 2012)	-0.38	0.01
Nafion/CAT/rGO/GCE (Ting *et al.*, 2011)	-0.45	7.76
Au-Pd/MoS_2/GCE (Li and Du, 2017)	-0.1	184.90
Pd/C Microneedle (TW)	**-0.3**	**49.7**
Pd/C Microneedle (TW)	**-0.5**	**102.1**

TW = This work; ER-GNO = Electrochemically reduced graphene oxide; rGO = Reduced graphene oxide; IL = Ionic Liquid; SPE = Screen printed electrode; GCE = Glassy carbon electrode; MWCNT = Multiwall carbon nanotube; C-F = Carbon fiber; CAT = Catalase.

From **Figure 7.3.12**, the modified system exhibits a clear advantage over the bare, unmodified MN array, ultimately outlining that the sensitivity is reliant on the electrode surface being occupied with Pd nanoclusters. Hence theoretically, increasing the population of carboxyl groups at the electrode interface during the anodisation process, beyond the 3% exhibited here, could be expected to increase Pd loading and subsequently, further enhance peroxide response. Although, when anodisation time was lengthened (even up to 1 hour), the change of interfacial carboxyl group concentration beyond the 3% was negligible. This can be ascribed to the competing processes of chemical reformation at the electrode surface

and the morphological exfoliation of the interfacial lattice components from the embedded graphitic particulate (Casimero *et al.*, 2020). Other chemical means of generating carboxyl moieties at the carbon-based surface are available offering a resolution to this limitation which potentially could be used as a solitary method or in conjunction with the technique described here.

7.4 Conclusions

The use of silicone templates has been proven to a be a highly flexible alternative to conventional micromachining techniques where different formulations (such as CAP) can be rapidly prototyped. The reducing potentials applied to manipulate swelling and dissolution of the C-CAP composite MNs in this work were chosen to easily promote drastic change and be readily observed for proof of principle. Utilising less negative potentials would curtail the degree of change in local pH, which would impede the former rapid release and could provide more control over the drug release without the eradication of the needle framework. This would significantly reduce the associated effects of carbon/palladium fragmentation in the skin. The electrochemically controlled release mechanism highlighted here offers a new direction in which microneedles may be controlled in situ.

With relation to the carbon-polystyrene MNs, modifying the electrode by electrochemical anodisation was successful in facilitating the chelation of Pd(II) ions and their subsequent conversion to nanoclusters to the surface. The latter has been shown to capable of serving as a highly sensitive and effective peroxide detection system, evidently competitive with existing technologies. The facile means of MN sensor fabrication and reduced complexity of administering a metallic catalyst for peroxide detection, instigates the exploration of immobilising other catalytic enzymes (such as glucose oxidase) sensitive to H_2O_2 to the electrode surface. Additionally, the benefit of using the reduction peak process to analyse peroxide concentration avoids interference with other easily oxidised electroactive species found within biofluids (such as ascorbate, tyrosine and urate). Otherwise, interference with such species would lead to superposition of the magnitude of current signal response and subsequent over estimation of peroxide concentration.

CHAPTER 8

Preliminary Evaluation of a Composite Microneedle Array as a Transdermal Potentiometric Sodium Sensor

Abstract

Serum sodium level provides critical detail for a person presenting with hyponatraemia. Currently there is no widely accepted point of care diagnostic method to alleviate the struggles of conventional laboratory analysis. Hence, within this investigation, a microneedle system modified with sodium selective ionophores was proposed as a potentiometric sensor. A preliminary investigation of three ionophores (4'-Aminobenzo-15-crown 5-ether, $Na_4TiO(PO_4)_3$ and $NaTi_2(PO_4)_3$) was conducted, by directly integrating sodium selective membrane components into the microneedle casting formulation. The microneedle arrays were responsive to sodium ions, however, the response was sub Nernstian with poor inter electrode reproducibility. Despite this, the direct application of sodium ionophore within the microneedle structure (without disruption of the needle structure) is promising and could offer a new avenue for future investigations.

8.1 Introduction

Hyponatraemia is an established key risk factor concerning cardiovascular disease and more specifically stroke (Rodrigues *et al.*, 2014). Hyponatraemia is characterised as low serum sodium levels ($Na^+ \leq 135$ mmol/L) and is known to be the most common electrolyte disorder among patients in care (Goldberg *et al.*, 2006). Sodium levels in the blood are directly related to blood pressure and, in turn, hyponatraemia can promote detrimental effects for patients that suffer from stroke (Yousuf *et al.*, 2014). The most perturbing case of hyponatraemia is the rapid decrease in sodium level (acute hyponatraemia), which progresses the risk of cerebral oedema and hyponatraemic encephalopathy (Goh, 2004). The body's response to counteracting rapid onset hyponatraemia leaves the patient at risk of cerebral demyelination, causing persistent altered sensorium and ultimately, this can lead to permanent neurological deterioration (Yousuf *et al.*, 2014). Distinguishing between the inappropriate secretion of antidiuretic hormone (SIADH) and cerebral salt wasting (CSW) as the root cause of hyponatraemia becomes essential in treating the patient.

A hyponatraemic state caused by cerebral salt wasting occurs after cerebral injury, leading to sodium and water dysregulation by the kidneys and ultimately excessive sodium excretion through urine, otherwise known as natriuresis (Yee, Burns and Wijdicks, 2010). Contrastingly, SIADH involves the sustained secretion of the antidiuretic hormone, arginine vasopressin, resulting in the unrelenting escalation of solute-free water renal absorption, thereby constructing a hyponatraemic state (Betjes, 2002). Since a patient with CSW is treated with hypertonic fluid, if this treatment was prescribed to a SIADH patient, this could result in osmotic demyelination. Furthermore, SIADH is treated by fluid restriction, which if prescribed to a CSW patient, will only worsen their hyponatraemic state. Differentiating between CSW and SIADH has proven difficult since they both share many of the same biomarkers. Although, uric acid, as a sensitive characteristic of effective arterial blood volume, has recently been demonstrated as a key differentiating factor between CSW and SIADH (Palmer, 2000; Momi, 2010). Additionally, misdiagnosis due to hyponatraemia mimicking acute stroke has been estimated to occur in 19% of all patients diagnosed with acute ischemic stroke (Yahia and Bashir, 2018). Severe cases of hyponatraemia are often similar to stroke symptoms: altered levels of consciousness, seizures, hemiparesis, ataxia and comas. Tissue plasminogen activator (t-PA) is the known prescription for ischemic stroke.

However, if administered to sub-optimal patients, mortality is significantly increased. Thus, it is critical to eliminate stroke mimicry via hyponatraemia by the monitoring of serum sodium level prior to t-PA administration (Berry, Al-Zubidi and Seifi, 2015).

Historically, blood samples were analysed by flame photometry, where the intensity of light emitted at a specified wavelength was used to determine the concentration of the element of interest in the sample (Levy, 1981). Nowadays, patient's samples are typically analysed by potentiometry using ion-selective electrodes (ISE); either by direct ISE blood gas analysers (BGA) or indirect ISE automated biochemical laboratory analysers (BLA). The concentration of the specified electrolyte is measured by assessing the potential derived between 2 electrodes caused by the electrochemical activity of the substance in the sample. However direct and indirect potentiometry methods are procedurally different which is demonstrated in **Table 8.1.1** (Nguyen *et al.*, 2007; Solak, 2016). Blood gas analysers are typically used in the emergency department, intensive care unit (ICU) and surgery settings where more immediate results are a necessity. BGA equipment such as Stat Profile Critical Care or iSTAT© analysers are available for point of care (POC) testing of electrolytes, but the operational running cost of such equipment is a major limitation to their utilisation in the development of health care. An iSTAT© device can cost approximately 7000 – 10,000 US$ with additional consumable costs of 5/6US$ per sample run (Geoghegan *et al.*, 2015). Additionally, there has been much discrepancy with the agreement of BGA and BLA sodium specific analyses of blood samples. Studies have shown that sodium level results obtained via BGA are not completely reliable when making clinical decisions and therefore, if time permits, BLA are the preferred choice of analysis to avoid pseudohyponatraemia, pseudonormonatraemia or pseudohypernatraemia diagnosis (Jain, Subhan and Joshi, 2009; Zelmat, 2015). However, in the absence of an alternative reliably sensitive POC diagnostic test, BGA are the only aid in monitoring electrolyte disorders in the acute care setting to help guide appropriate therapeutic interventions (Bingham, Kendall and Clancy, 1999).

Table 8.1.1 Blood gas analyser and biochemical laboratory analyser differences.

Blood gas analysers	Biochemical laboratory analysers
Processing time is short	Processing time is long
Direct ion-selective electrode	Indirect ion-selective electrode
Analyses whole blood	Analyses serum
No effect of protein levels in blood	Affected by protein levels in the blood
Uses heparin-diluted sample	Serum sample diluted with fixed volume
Arterial sample used conventionally	diluent
	Venous sample used conventionally

In an attempt to improve the selectivity of sodium sensors for clinical diagnosis, there are a variety of developments underway. Optical-based sensors are a promising technology that is aiming to simplify the fabrication of in vivo diagnostics in extracellular media. One of the most successful and highly sensitive optical detection methods available is intramolecular photo-induced electron transfer (PET) (de Silva *et al.*, 1997). There is ongoing research into chromoionophores and their incorporation into optodes and ion-selective electrodes using polymer membranes for use in clinical settings, although, much work is still required to optimise these complex fabrications. A sodium selective ionophore of particular interest is calix[4]arene ionophore, represented in **Figure 8.1.1**, which has been established as highly selective for sodium ions over potassium. Previously, it has been demonstrated that the binding of sodium ions to the calix[4]arene along with chromophore proton release influences fluorescence emission. Despite considerable progress into simplifying the fabrication of such processes, optimising the sensor system for clinical use is still proving difficult. For example, a sodium specific chromoionophore consisting of acridine and calix[4]arene ionophore incorporated into an acrylate polymer showed promising fluorescent results within the specified sodium concentration range (0-1 M). However, the chosen chromophore is pH sensitive therefore making it unsuitable for diagnosis in a clinical setting (Adrian Waldner *et al.*, 2003). In an attempt to overcome pH sensitivity, other chromoionophores such as amide bonded rhodamine B to calix[4]arene have also been investigated and show optimistic results. Using the rhodamine B chromophore eliminates the need to correct for pH in physiological conditions since it is insensitive to pH. However, further research is required in this area to reduce response times, improve long-term

stability and to optimise the polymer membrane mixture thereby increasing selectivity (Benco, Nienaber and McGimpsey, 2002).

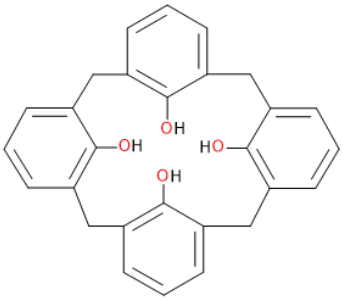

Figure 8.1.1 Structure of calix[4]arene sodium ionophore.

Alternatively, there are multiple advances in electrochemical ion-selective sensors with the aim of establishing reproducible selective sensors within the required detection limit. Electrochemical ion sensors typically in the form of thin films or membrane sensors have shown favourable results in terms of sodium selectivity. Again, the use of a calix[4]arene based ionophore incorporated in a polymeric matrix is the basis of the sensors, along with sodium super ionic conductor (NASICON) type materials or tungsten/molybdenum bronzes (Sauvage, Baudrin and Tarascon, 2007). A typical NASICON crystal structure is highlighted in **Figure 8.1.2** (Wu *et al.*, 2019).

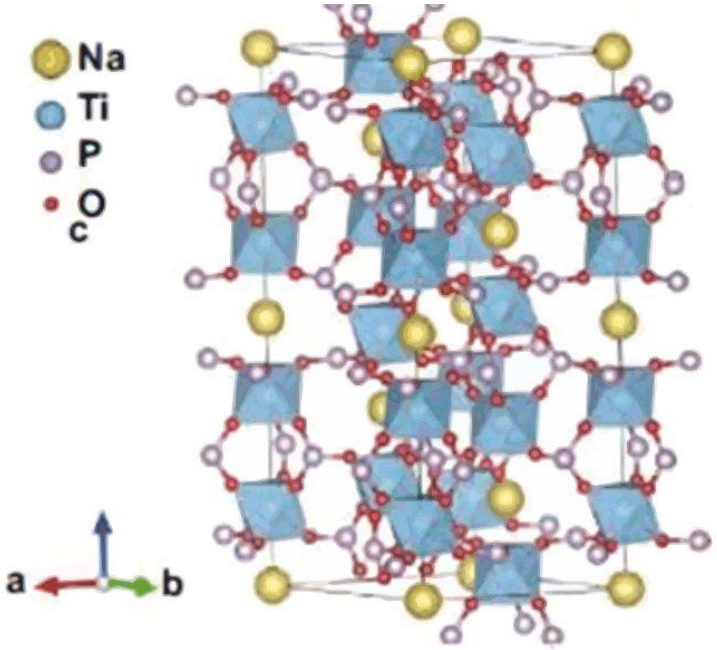

Figure 8.1.2 Crystal structure of NASICON insertion material $NaTi_2(PO_4)$.

One particularly successful NASICON ($Na_3Zr_2Si_2PO_{12}$) based microsensor for the detection of sodium in gingival fluid investigated the use of various thin film based solid state internal references. The NASICON ceramic proved very sensitive for in vivo measurements and the polyethylene oxide (PEO)-based salt reference system presented as the most stable with low impedance. However, further work is required to miniaturise the fabrication of the sensor into a microelectrode and to improve the long term stability of the sensor (Caravel *et al.*, 2001). A solid state sensing device would have considerable advantages over the predominantly used sodium glass electrodes due to narrow temperature ranges, fouling of the glass and pH application limitations. Therefore, there is great interest surrounding alkali metal bronzes in the formation of solid-state sensors. Molybdenum bronze single crystals integrated into sodium selective solid-state contact electrodes have been demonstrated as a competitive alternative to the traditional glass electrodes for industrial applications (Kakali, Ramanujachary and Greenblatt, 2001). Although, the sensing specifications of the electrodes were not refined for clinical use, since the interfering ions of hydrogen or potassium should ideally be of at least one magnitude smaller than the sodium ions to ensure selectivity. Further research would be required to characterise the metal oxide bronzes for sodium sensing in physiological conditions (Shuk, Greenblatt and Ramanujachary, 1996). **Table 8.1.2** shows a comparison of sodium selective electrodes which have emerged through research

surrounding this topical area. However, the commercially available sodium glass electrode is still preferred over these technologies as they remain difficult to optimise.

Table 8.1.2 Comparison of sodium selective electrodes.

Sensing mechanism	Sodium selectivity method	Testing sample	Range	LoD
FO - (Hideaki Hisamoto *et al.*, 1995)	15-Methyl15 - stearyl- oxymethyl - 1,4, 7, 10, 13 - pentaoxacyclohexa - decane (ODM16C5) in PVC membrane	Human serum	135 - 150 mM	
Pot - (Heng and Hall, 2001)	n bis[(12-crown-4)methyl]dodecylmethylmalonate in photocured poly(n-butyl acrylate) membrane	Human serum	10^{-7} - 10^{-1} M	$10^{-5.6}$ M
Pot - (Moody, Saad and Thomas, 1989)	bis[(12-crown-4)-2-ylmethyl]-2-dodecyl-2-methy in PVC membrane	Human serum	135 - 145 mM	$1.8x10^{-6}$ M
FO - (Chan *et al.*, 2002)	Calix[4]arene tetraester in a PVC membrane	Beverage and urine	$1x10^{-6}$ - 0.1 M	$4x10^{-7}$ M
Pot - (Caravel *et al.*, 2001)	$Na_3Zr_2Si_2PO_{12}$ (NASICON membrane)	Gingival fluid	10^{-2} – 1 M	10^{-4} M
FO - (Wang *et al.*, 1997)	bis[(12-crown-4)methyl] dodecylmethylmalonate in PVC membrane	Standard solutions	$5x10^{-6}$ - 0.5 M	$10^{-5.3}$ M
FO - (Yang, 2000)	4-tert-butylcalix[4]arene tetraacetic acid tetraethyl ester in PVC membrane	Standard solutions	$1x10^{-6}$ - 1 M	
FO - (Benco, Nienaber and McGimpsey, 2002)	4-tert-Butylcalix[4]arene-tetraaceticacid tetra- ethyl ester in custom polymer membrane	Standard solutions	0.01 – 0.2 M	
Pot - (Kakali, Ramanujachary and Greenblatt, 2001)	Single crystals of $Na_{0.9}Mo_6O_{17}$	Standard solutions	0.1 - 1 M	

FO = Fluorescent optode; Pot = Potentiometric; PVC = Polyvinyl Chloride; NASICON = Sodium superionic conductor

The necessity for sodium serum level monitoring within the blood is now well established, especially for patients at risk of or suffering from stroke (Rodrigues *et al.*, 2014). The existing method of assessing sodium in the blood is concerning as it is still not fully reliable to make a clinical diagnosis (Bingham, Kendall and Clancy, 1999). The lack of readily available POC diagnostic approaches for sodium monitoring is also worrying, as this could be the difference

in fatality for patients undergoing surgery, emergency, and intensive care patients. The limitations hindering recent technologies remain the sensitivity, lifetime and reference electrodes of the sensing devices (Sauvage, Baudrin and Tarascon, 2007). Not only this, but many of the technologies are not well adapted for microfabrication and still require blood withdrawal via hypodermic needles to obtain samples for analysis. Essentially, this makes the sample being analysed virtually out of date as soon as it is withdrawn from the body, especially since it is acute cases of hyponatraemia that are of paramount importance (Goh, 2004). This further emphasises the compelling need for a POC diagnostic tool that will continually monitor the levels of sodium in the blood (Strickland, Hill and Zaloga, 1989). As of yet, there are no sodium sensing microneedle (MN) patches available, therefore making this a topical area for research. Thus, in contrast to the development of voltammetric microneedle sensing systems detailed in chapters (5-7), a potentiometric approach for minimally invasive sodium sensing is proposed here by integration of a sodium selective formulation. The idealised concept is evaluated by preliminary electrochemical analysis and the applicability of the system is critically assessed.

8.2 Experimental Details

Carbon nanopowder (< 100 nm) and polystyrene pellets (MW 192000) were obtained from Sigma-Aldrich (Dorset, UK), along with all other chemicals used in the investigation, were of the highest attainable grade and were utilised without further purification strategies. Two NASICON variants to be investigated: $Na_4TiO(PO_4)_3$ and $NaTi_2(PO_4)_3$, were a kind gift provided by Prof Peter Slater (Chemistry, University of Birmingham). Silicone microneedle templates were procured from Micropoint® Technologies Pte Ltd (Singapore) and consisted of a 10 x 10 array of pyramidal shaped needles (200 µm base x 500 µm pitch x 700 µm height). Electrochemical measurements were recorded at 22°C $\pm$ 2°C, using a micro Autolab Type III potentiostat. A two-electrode setup was used with the carbon-polystyrene composite MN modified with the sodium selective formulation utilised as the working electrode and a silver modified composite MN serving as combined counter and pseudo-reference electrode as outlined in **Figure 8.2.1**.

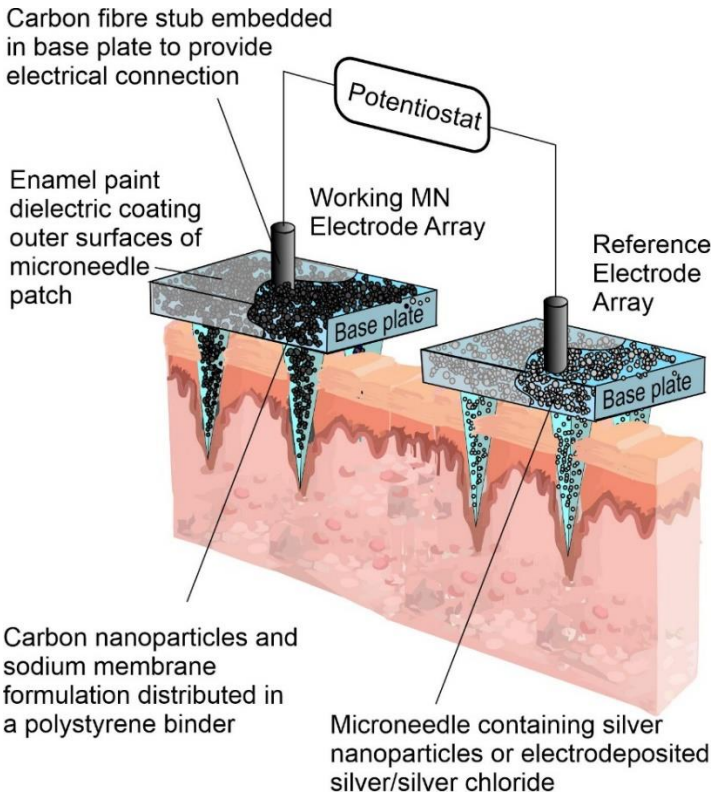

Figure 8.2.1 Proposed microneedle array electrode configuration.

It was envisaged that by documenting the response of the two-electrode system across a series of standard solutions with known Na+ ion concentration, a calibration graph of potential against Log(Na^+ concentration) could be determined. A calibration with a linear gradient of +59 mV per decade shift of Na^+ concentration would then indicate the system obeys Nernstian behaviour.

8.2.1 Sodium Membrane Fabrication

Over the years, ion-selective electrodes have capitalised on the use of crown ethers and their remarkable ability to complex ions based on their hole-size relationship (Jeng and Shih, 1984; Gokel, Leevy and Weber, 2004). Previously crown-based ionophores were utilised as receptors and then amplified by fluorophores (de Silva *et al.*, 1997; Zhao, Yang and Hong Chan, 2003). However, the approach detailed here relies on 4'-Aminobenzo-15-crown 5-ether, shown in **Figure 8.2.2**, and its selectivity for complexation of Na^+ ions due to optimal binding within the innate cavity of the crown ether.

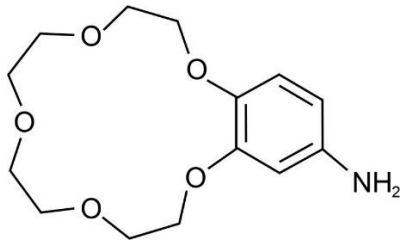

Figure 8.2.2 Structure of 4'-Aminobenzo-15-crown 5-ether sodium ionophore.

Thus, the formulation of the sodium membrane consisted of Polyvinyl Chloride (PVC) as the membrane matrix, Bis(2-ethylhexyl) phthalate (BEHP) as the plasticiser, potassium tetrakis (4-chlorophenyl) borate (K-TCPB) to maintain electrical charge balance and 4'-Aminobenzo-15-crown 5-ether as the sodium selective ionophore. The relative amounts of each membrane component was adapted from Zhao et al. (2003), which included: 50 mg of PVC, 101 µL of BEHP (496.1 g/mol), 4.8 mg of K-TCPB and 4.6 mg of the ionophore. The PVC, K-TCPB and ionophore were dissolved in 2 mL of cyclohexanone before adding the BEHP to the membrane mixture. The original intention was to directly cast the membrane onto the microneedle electrode surface however, the cyclohexanone was found to dissolve the polymeric binder within the composite microneedle causing the needles to collapse. Therefore, the sodium selective formulation was either cast onto a quartz glass slide to form a sodium selective membrane or directly included into the MN formulation prior to casting. For casting onto the quartz slide, 400 µL of the sodium selective mixture was pipetted onto the slide and left to air dry for a period of at least 6 hours allowing for solvent evaporation. After drying, the membrane could be detached from the quartz slide and stretched directly over the needle face of the MN array. It was identified that if the membrane was left for longer than 48 hours on the quartz slide, it lost elasticity and could not be peeled off the slide without crumbling. The same process was essentially repeated with the NASICON ionophores and were substituted for the crown ether on a similar weight for weight basis.

8.2.3 Microneedle Fabrication

Basic unmodified carbon-polystyrene microneedles, forming the basis of the working electrode used within this study, were prepared in accordance with the procedure outlined

in Chapter 5. The silver modified carbon-polystyrene microneedles were fabricated as outlined in Chapter 6. Microneedles modified with the sodium selective formulation included within the casting formulation were fabricated by pipetting 2 mL of the membrane mixture at the stage of dissolving the polystyrene in cyclohexanone. Once the polystyrene had visibly dissolved, the carbon nanoparticles were included, and the process outlined in Chapter 5 was continued. The MN arrays containing the sodium selective formulation were observed by scanning electron microscopy to examine the structural integrity of the needles. The images presented in **Figure 8.2.3** are representative of the NASICON formulations, with no morphological differences identified in the crown ether MN arrays. Much like the carbon-polystyrene MNs, the sodium selective MNs maintain the characteristic sharp needle tips with few topographical artifacts.

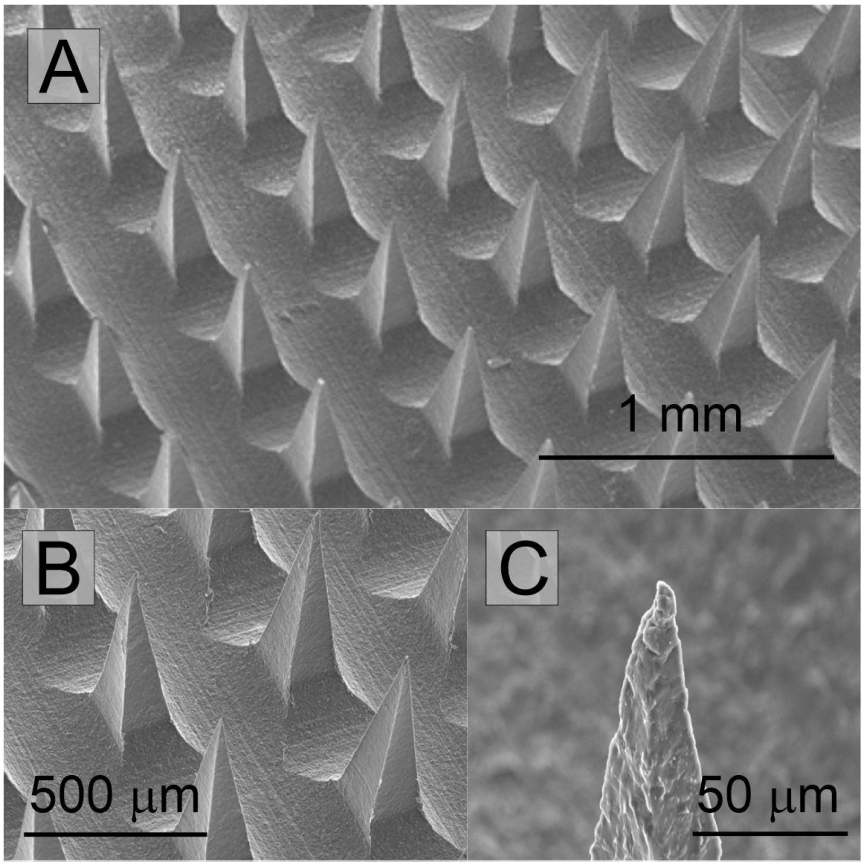

Figure 8.2.3 Scanning electron micrographs of carbon-polystyrene microneedles containing NASICON sodium selective formulation.

8.3 Results and Discussion

Prior to investigating the rather complex nature of the microneedle structures containing the sodium selective ionophores, the validity of the membranes being selective towards Na^+ was first analysed. To do so, the membranes were assessed on a 2D platform using conventional carbon fibre mesh (CFM) electrodes. The sodium selective formulations were directly cast onto the CFM electrodes, with the potentiometric response to increasing concentrations of NaCl recorded. **Figure 8.3.1** and **Figure 8.3.2** details the response and corresponding calibration curve of the $Na_4TiO(PO_4)_3$ NASICON system towards increasing sodium ion concentrations (in HEPES buffer pH 7) respectively.

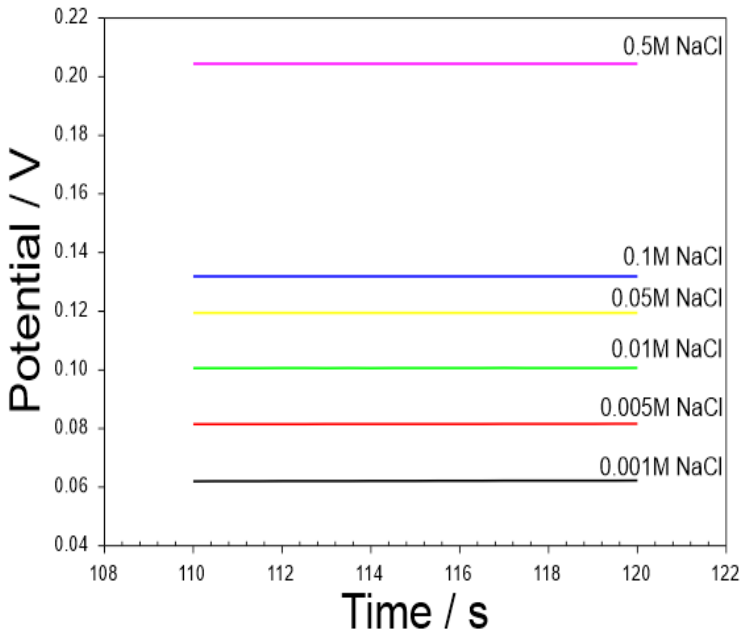

Figure 8.3.1 Potentiometric response of a carbon fibre mesh electrode with thin film coating of $Na_4TiO(PO_4)_3$ NASICON membrane towards increasing concentrations of Na^+ ions.

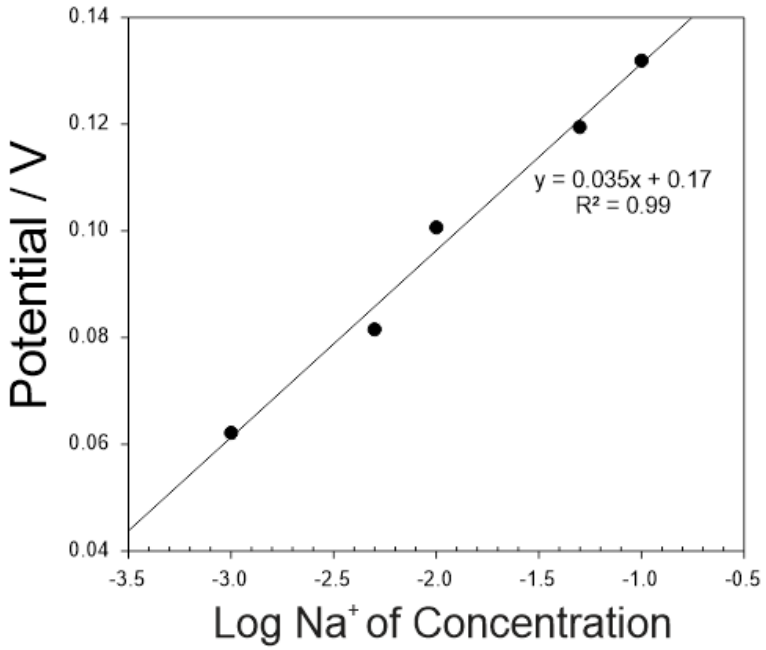

Figure 8.3.2 Calibration curve of carbon mesh electrode with thin film coating of $Na_4TiO(PO_4)_3$ NASICON membrane towards increasing concentrations of Na^+ ions.

Whilst the NASICON ($Na_4TiO(PO_4)_3$) membrane is responsive over the series of concentrations representative of a physiological range of Na+, the potentiometric response is sub Nernstian. This poses as a limitation for detecting samples of unknown sodium ion concentrations, where slight error or drift would have severe consequence on the calculated ion concentration. The second NASICON derivative ($NaTi_2(PO_4)_3$) and crown ether systems displayed similar responses as shown in **Table 8.3.1**.

Table 8.3.1 Potentiometric response of sodium selective membranes on carbon fibre mesh electrodes.

Type	Linear regression equation	R^2
NASICON: $Na_4TiO(PO_4)_3$	E = 0.035 Log[Na+] +0.17	0.99
NASICON: $NaTi_2(PO_4)_3$	E = 0.022 Log[Na+] +0.2	0.99
4'-Aminobenzo-15-crown 5-ether	E = 0.023 Log[Na+] +0.1	0.99

Moving forward, it was hoped that by encompassing the sodium selective formulation within the MN structure, a better analytical response could be achieved. All three ionophores were included within MN structures, this time by including the sodium selective formulation within the carbon-polystyrene casting mixture during fabrication stages. Since the $Na_4TiO(PO_4)_3$

NASICON membrane demonstrated a slightly better response than the $NaTi_2(PO_4)_3$ and crown ether ionophores, this became the primary focus continuing with the investigation. The potentiometric response of microneedle arrays containing $Na_4TiO(PO_4)_3$ NASICON towards varying concentrations of sodium ions were evaluated by immersing in HEPES buffer solutions, which maintained the solution at pH7. Initially, the MNs were assessed without anodisation with the respective response and calibration graph detailed in **Figure 8.3.3** and **Figure 8.3.4** respectively.

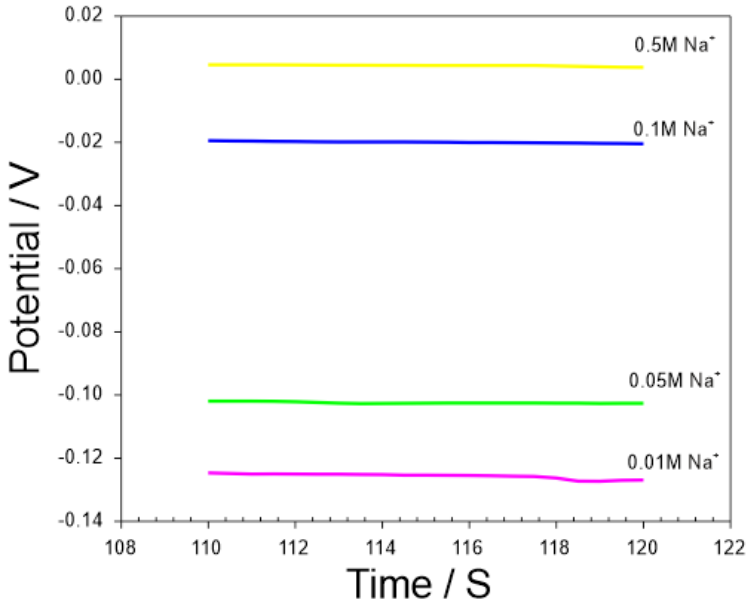

Figure 8.3.3 Response of $Na_4TiO(PO_4)_3$ unanodised microneedle towards Na^+ ion in HEPES buffer (pH 7).

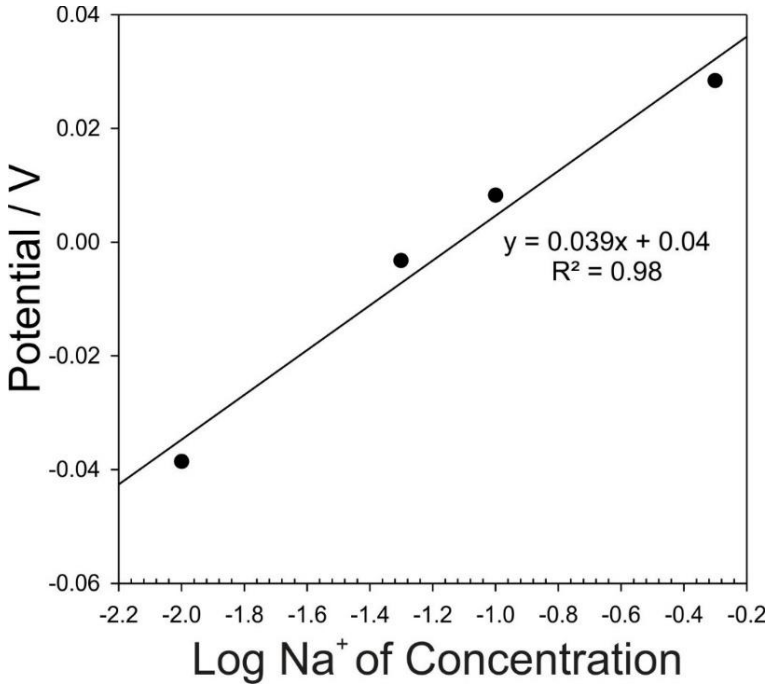

Figure 8.3.4 Calibration of $Na_4TiO(PO_4)_3$ unanodised microneedle towards Na^+ ion in HEPES buffer (pH 7).

Unfortunately, the response of the NASICON MN remained sub Nernstian and was similar to the response documented by the CFM electrode coated with a thin film of the sodium membrane. As recognised in previous chapters, anodisation of carbon based MNs has been shown to significantly improve electroanalytical performance. Thus, a preliminary study was carried out, investigating if anodisation would have a similar effect in this case. It was proposed that anodisation could improve the hydrophilicity of the electrode surface, thereby, exposing more of the ionophore at the electrode solution interface. This was approached with a degree of hesitance as it could be anticipated that the anodisation process could also sabotage or invoke leaching of the ionophore. Anodisation of the NASICON MNs was executed as per the procedures outlined in previous chapters (6-7), by immersing the electrode in 0.1 M NaOH solution and imposing an anodic potential (+2 V) for 3 minutes. **Figure 8.3.5** and **Figure 8.3.6** depict the response and corresponding calibration graph of the $Na_4TiO(PO_4)_3$ NASICON MN towards increasing concentrations of sodium ions in HEPES buffer (pH 7) after anodisation. The response dejectedly displays as sub Nernstian again, with no significant improvement from the unanodised MNs. However, this would also indicate that the anodisation process does not destabilise the ionophore, leaving room for future investigations.

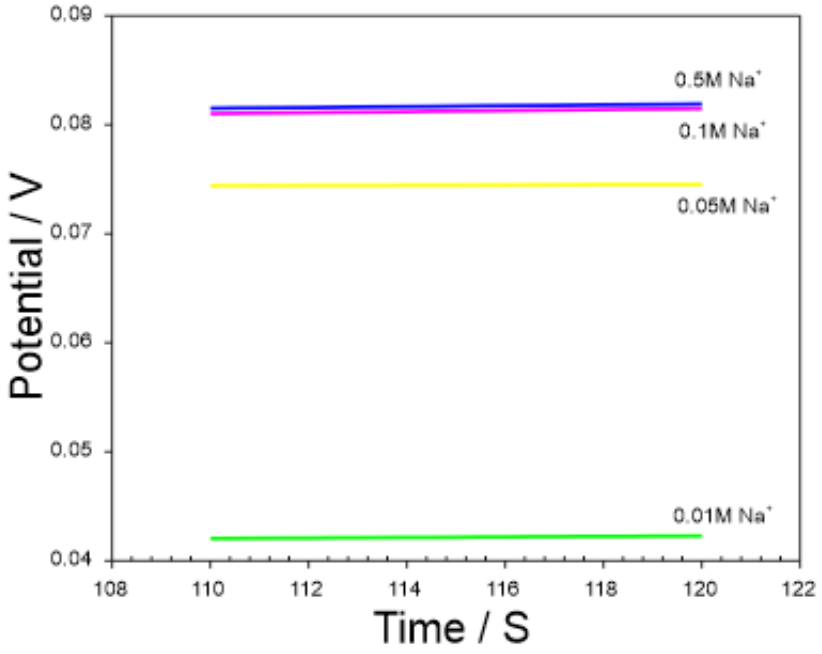

Figure 8.3.5 Response of $Na_4TiO(PO_4)_3$ microneedle after anodisation towards Na^+ ion in HEPES buffer (pH 7).

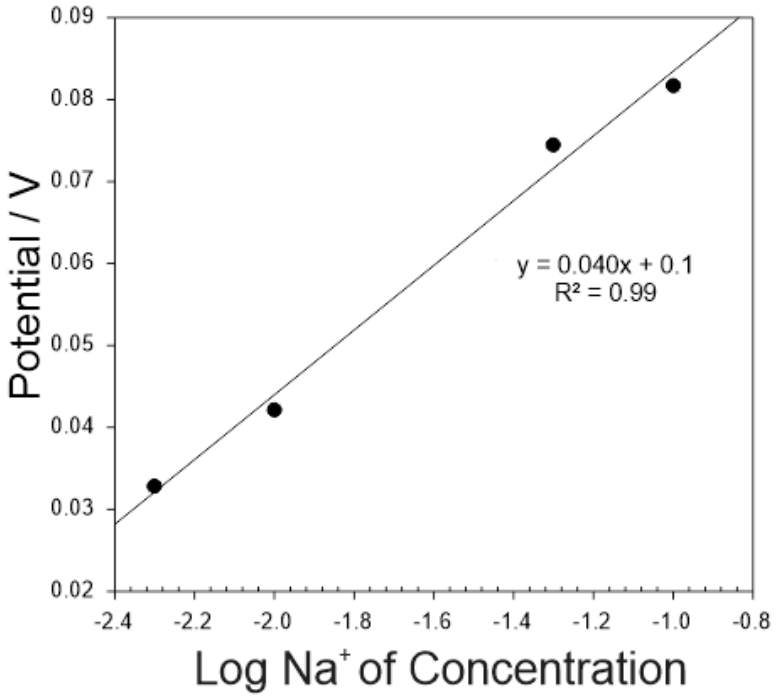

Figure 8.3.6 Calibration of $Na_4TiO(PO_4)_3$ microneedle after anodisation towards Na^+ ion in HEPES buffer (pH 7).

Despite the substandard performance of the NASICON MN response to Na^+ ion, the inter electrode reproducibility of the anodised and unanodised MN arrays were also assessed as shown in **Figure 8.3.7** and **Figure 8.3.8** respectively. Evidently, there was again no significant difference between the unanodised and anodised MNs, with both systems presenting with large error bars, which is indicative of poor inter electrode reproducibility. The latter could be expected given the nature of the manufacturing process and the inherent vagaries of bench production. To overcome this, each MN would require individual calibration prior to use which of course would be a huge limitation for transdermal application. Nevertheless, the $Na_4TiO(PO_4)_3$ NASICON microneedles are operatively comparative to Na^+ ion selective electrodes which depend on routine calibration.

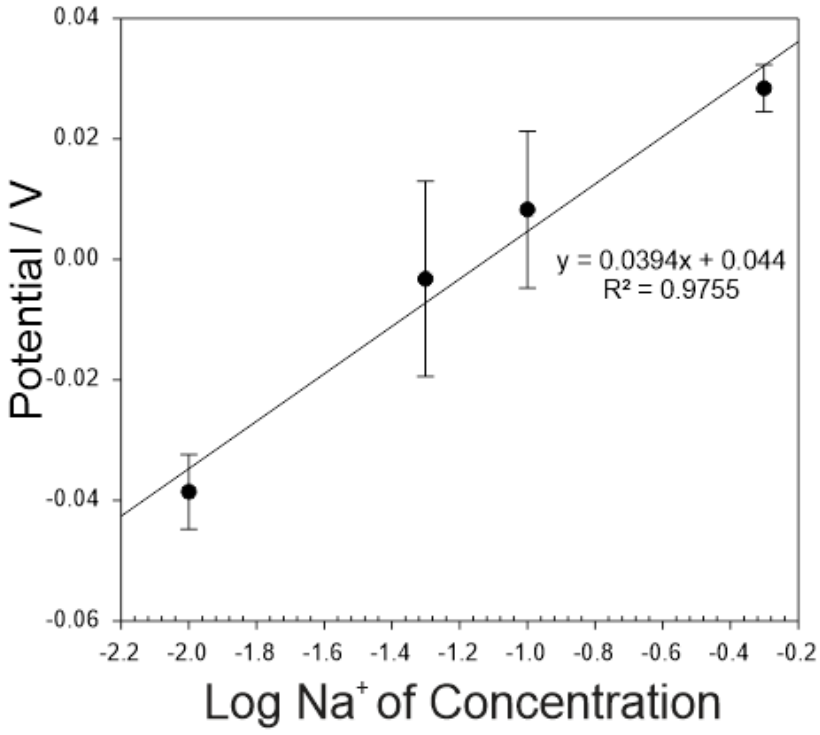

Figure 8.3.7 Calibration of three unanodised $Na_4TiO(PO_4)_3$ microneedle arrays in HEPES buffer (pH 7) (error bars based on stdev N=3).

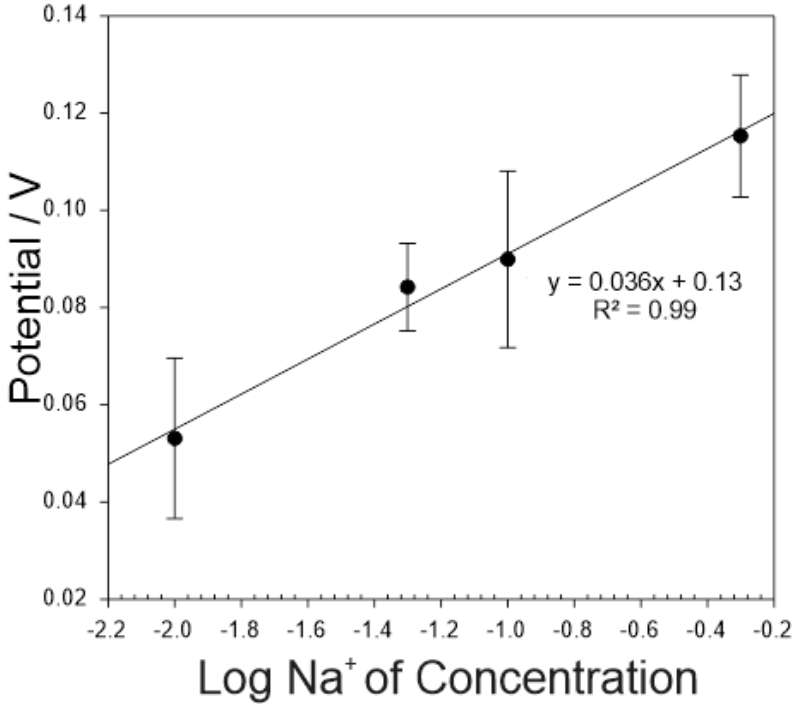

Figure 8.3.8 Calibration of three anodised $Na_4TiO(PO_4)_3$ microneedle arrays in HEPES buffer (pH 7) (error bars based on stdev N=3).

8.4 Conclusions

Within this investigation, the potential for a microneedle system as a potentiometric sodium sensing system was assessed. Evidently, the inclusion of sodium selective ionophores within the casting formulation provides a facile means of fabricating ion selective microneedles with no deterioration of the MN structure. Whilst the MNs were responsive towards sodium ions, the wide variation in electrode response would require independent calibration for each MN prior to use. Although, this is regarded as a customary procedure for ion selective electrodes used for environmental analysis, it would be deemed an unacceptable burden in point of care applications which insist on straightforward sampling/analysis strategies with as little intervention by the patient/healthcare professional as possible. Thus, it would be inadequate for the user (patient or healthcare professional) to compile a two-point calibration in preparation for MN application and analysis. Despite these limitations, the MN system illustrated a response towards sodium ions and, although it was sub Nernstian, it may become favourable if the fabrication process could be refined and standardised.

Nevertheless, the potentiometric MN approach described here, although very preliminary, highlights the potential for future investigations and further development towards minimally invasive sampling for in vivo analysis of biological markers.

CHAPTER 9

Conclusions and Further Work

9.1 Conclusions

Traditional blood withdrawal procedures present many issues associated with patient compliance, needle phobia, therapeutic turnaround times (TAT) and discrepancies between blood laboratory analysers or blood gas analysers. The need for an alternative approach which can address these issues has long been recognised. In addition to this, significant research has highlighted the prevalence of needle-stick injuries (NSI) surrounding the use of conventional hollow-bore needles or sharps and the consequent transmission of blood borne pathogens (BBP). With particular reference to the diabetic community, where patient compliance and the reuse of needles is problematic, there is an enduring necessity to replace the finger prick method of blood sampling. Of late, there have been a few innovative commercial attempts to conquer these limitations, including the FreeStyle Libre® glucose monitoring system. Although, despite its success, the controversy of painful application that needs to be replaced every 2 weeks still remains. Notably, a new wave of medical grade, wearable sensor technology has come with a pressing need to further miniaturise such devices with integrated sensors and actuators to help aid the leap towards community based care. Hence, the thesis outlined here promotes an alternative route from conventional methods of blood analysis, offering, in principle, a minimally invasive approach for point of care (POC) sensing by means of a microneedle (MN) system.

The concept of microneedles has been circulating since the 1970s and their design recognised as having significant medical potential, particularly for application as a transdermal drug delivery system. This has driven relentless interest in the research community however, no commercialisation of microneedle sensors or drug delivery systems (at the time of writing) have come to fruition beyond cosmetic treatments. Many of the MN sensors are currently manufactured by micromachining and etching techniques, which are known to be costly and require a level of specialist training to operate. The past decade in technology advancement has subsequently increased the production of micromoulded MNs, predominantly for drug delivery applications. Availability of micromoulding templates has provided a cheaper and more simplistic method for MN fabrication over micromachining or even 3D printing approaches, which often struggle to produce MNs at the required resolution. Imperative to this research, micromoulding of MNs provides an opportunity to manipulate the casting formulation to include not only a conductive particles, but additional

components that considerably alter the properties of the base structure. The ease with which this can be done could stimulate new avenue for microneedle sensor and actuator fabrication. This thesis has explored the translation of electrochemical sensing strategies from standard carbon based screen printed electrodes to composite microneedle technology.

Within Chapter 4, a bespoke flavin derivative (10-(4-hydroxyphenyl) benzo[g]pteridine-2,4(3H,10H)-dione) was shown to be successfully electropolymerised onto a carbon-based screen printed electrode (SPE) to serve as a voltammetric disposable pH sensor. By modifying the interfacial chemistries of the carbon tracks present on the SPE, more edge plane sites were exposed, increasing the presence of oxygen functionality groups which ultimately enhanced electrochemical performance. Oxidation of the phenolic substituent was shown to induce polymerisation of the flavin derivative, displayed by the material aggregation at the electrode surface and corresponding increase in flavin peak with each polymerisation scan. The distinct and characteristic flavin redox peaks were maintained after polymerisation and used to indirectly denote pH measurement. Notably, the redox signature displayed by the flavin derivative occurs within a region of the scanning window which is free from impeding electroactive species. Fluctuations in response with respect to variations in chloride ion concentrations was recognised as a limitation for a solid-state sensing system. Thus, ferrocyanide was integrated as a pH insensitive redox probe to act as an internal reference. The flavin modified SPE (with and without the internal ferrocyanide standard) was demonstrated as being robust (potential drift < 4 mV) and the accuracy of the system examined in complex biological media, which was corroborative with commercial pH sensors. Whilst using a disposable SPE approach has the added advantage of being a procedurally simple, low-cost fabrication method which is scalable for production, it is restricted to single-shot discrete measurements and would not be suitable for continuous monitoring.

Silicone moulds were exploited to fabricate conductive composite microneedles, rather than using traditional high precision machining methods in Chapter 5. The significant advantage of using a micro-moulding process allows the integration of various constituents within the casting formulation and the option to interchange the core components for respective purpose. Additionally, this low-cost, facile, and rapid prototyping approach is readily

available to conventional laboratories and bench based production, thereby expanding the potential research and development of MN application. Within the investigation, conductive carbon nanoparticles were dispersed in a polymeric binder to form MNs which were conductive from needle tip to base plate. Carbonaceous electrodes are established as having rich surface chemistries thus, by incorporating carbon nanoparticles within the needle framework, this further diversifies the possible sensing opportunities. The minimally invasive nature of the MN arrays makes them an attractive solution for painless transdermal sensing, potentially eradicating issues like patient compliance. Therefore, the scope for transdermal biosensing via conductive composite MN systems was explored within this Chapter.

Where the force required for successful skin penetration by microneedles has previously been estimated (< 0.03 N), the composite MNs were subject to mechanical force testing and proven to be capable of skin puncture. The possibility of NSIs within a conventional laboratory setting by microneedles was also considered. A preliminary posture-force study was implemented to assess the potential for accidental MN insertion due to carelessly discarded MN patches. This preliminary study was to assess possible risk associated with both their use in laboratory environments but, more importantly, their translation to domestic/community care scenarios. The typical forces exerted on a lab bench illustrated that each motion expended a force which would be more than sufficient for accidental MN skin penetration. Although, the possibility of BBP transmission was discarded as being minimal risk due to the relative surface area of the needles and the wearing of typical nitrile gloves acting as a safeguard.

The inclusion of carbon within the MN arrays provided a suitable platform to manipulate the generation of oxo-groups at the MN surface using the simplistic modification technique electrochemical anodisation. The increased population of oxygen functionalities were confirmed through X-ray photoelectron spectroscopy (XPS) analysis. Electroanalytical capability of the MN electrodes was drastically improved by anodisation as evidenced by the MN response towards uric acid. Exploration of using the MN arrays as an analytical sensor was also validated by detecting uric acid within biological media and compared against other electrode modification strategies used for the detection of urate. Whilst the detection limit of the proposed approach was not as competitive, many of the other modification strategies

would not be suitable for transdermal application. Hence, this further highlighted the potential for composite microneedles to be adopted for use in biomedical applications.

The validity of applying the carbon-based composite MN arrays as a transdermal biosensor was further explored in Chapter 6. The electrochemical performance of the carbon-polystyrene composite system was characterised in ferrocyanide and ruthenium hexamine, which further illustrated the benefit of the anodisation modification employed in previous chapters. It is through this modification that pH sensitive moieties, endogenous to the interfacial carbon, were exploited to indirectly monitor changes in pH. Furthermore, the wide potential range exhibited by the system highlighted the versatility of its composite nature, lending itself to a plethora of sensing applications. Within the investigation, the fabrication process was also shown to be adapted to construct a composite pseudo-reference microneedle array. A 2 electrode and 3 electrode transdermal sensing approach was demonstrated by successful penetration of the MNs into tomato mesocarp. Whilst maintaining the structural integrity of the needles, the ability of the system to detect pH was assessed, detailing responses which were comparative and consistent with commercial pH probes. Again, the significance of the investigation lies in the promotion of MN sensing capabilities within biomedical diagnostics.

Interchangeability of the core components of the composite MN approach was utilised within Chapter 7 for the purpose of composing a microneedle system with an integrated actuator for controlled drug release. Electrochemically controlled drug release was investigated through the proposition of including conductive carbon nanoparticles within a cellulose acetate phthalate (CAP) binder. In doing so, a reducing potential applied to the conductive MNs enabled control over the swelling and subsequent dissolution of the CAP polymer. By additional modification with layers of palladium at the MN surface, exploitation of the hydrogen evolution reaction (HER) process was utilised to induce CAP dissolution through changes in local pH. The electrochemical release mechanism was validated in a skin mimic composed of a parafilm layer covering a gelatin matrix. Incorporating toluidine blue (TBO) into the casting formulation facilitated visualisation of successfully controlled released of a model drug. Biocompatibility testing of the carbon-CAP MN arrays concluded no skin irritation or cytotoxicity which is a positive result for future use of the material. Although, this should be considered with caution due with respect to long term application.

In an ideal scenario, the Pd modified carbon-CAP system would enable sensing capabilities parallel to electrochemically controlled drug release. However, the necessary parameters to electrochemically anodise the interfacial carbon would compromise the CAP binder. Whilst consolidating palladium particles within the casting mixture was initially considered, the limitation lies in the accessibility of sub-micron particulate to prevent a granular morphology at the MN surface. The sputter technique used to layer Pd particulate was also acknowledged as a possible cause for concern due to the 3D nature of the needle surface. Thus, proof of principle was continued using carbon-polystyrene composite MNs, which were modified by chelation of palladium nanoclusters at the electrode surface. The Pd modified carbon-polystyrene strategy was demonstrated as a highly sensitive and effective peroxide sensor, which was competitive with existing technologies. Ultimately, the investigation demonstrated the merit in exploring additional capabilities of the composite MN system as well as instigating new methods for controlled drug release. The freedom provided by the composite approach and subsequent positive performance, holds promise for a fully autonomous MN system in the future.

The composite MN approach is multifaceted, with a broad horizon of opportunities both for transdermal biosensing and drug delivery. Thus far, the investigations had largely focused on voltametric/amperometric methodologies. In Chapter 8, however, a potentiometric MN sensing approach for detecting sodium ion was explored. Hyponatraemia has been long established as a clinical downfall, currently with no medically certified point of care diagnostic tool to flag intervention. Serum sodium has been pinpointed as a key biomarker to monitor the development and effects of hyponatraemia. Thus, a preliminary assessment of the capability of the composite MN system to monitor changes in sodium levels was examined. The key challenge here was to determine if the versatility of the formulation could be expanded to include multiple components necessary to drive the selective potentiometric recognition of the target analyte. The fabrication method was a suitable platform for manipulation, allowing direct inclusion of the sodium selective ionophores during manufacture. This allowed the investigation of three separate ionophores (4'-Aminobenzo-15-crown 5-ether, $Na_4TiO(PO_4)_3$ and $NaTi_2(PO_4)_3$) which could be interchanged in a Polyvinyl Chloride based membrane and dispersed within the needle framework. Although the potentiometric response of the MN systems modified with the sodium ionophores were

responsive towards sodium ions, the response was sub Nernstian and displayed poor inter electrode reproducibility. Much like existing ion selective electrodes, this would require each MN to be individually calibrated before application, which would be unsuitable for a POC diagnostic sensor. Nonetheless, the addition of ionophores during fabrication stages displayed no adverse effect to the MN structure, therefore presenting a new approach for future investigations of ion selective sensing.

9.2 Scope for Future Work

Beyond the thesis outlined here, there is clearly scope to continue development of the microneedle technology. In terms of electrochemical sensing, the limited investigations described in this thesis, exhibit the versatility of the microneedle sensing approach. In addition to these investigations, a preliminary market feasibility study was completed over a duration of 12 weeks, through the Innovation to commercialisation of university research (ICURe) programme (supported by funding from Innovate UK). This involved a customer discovery journey to establish a potential market for a smart wearable MN sodium sensing system, which would effectively lay the foundations for a commercialisation pathway. To validate if there was indeed a significant market available to commercialise a smart sensing microneedle system, a map of the key sectors with interest in wearables were targeted for customer outreach as shown in **Figure 9.1**. Throughout the 12 weeks, over 70 organisations were contacted in relation to a smart sensing MN concept, with their invaluable feedback and insight into pre-existing technologies recorded.

During the customer discovery phase, two things became increasingly clear. Firstly, the lengthy time and research that would be necessary to progress and develop a smart wearable device from proof of principle to commercialisation would be a huge disadvantage to a University spin out company. Alternatively, many of these organisations already have the expertise necessary and have refined these processes over many years. Thus, many of these organisations expressed their interest in integrating the MN technology within their existing wearables. The second factor that became clear, was that the need for a commercialised POC sodium diagnostic sensor was evidently consistent with the literature. Moreover, there was a huge demand for a vast number of other biomarkers that these

organisations wanted to monitor. Notably, it was recognised that the minimally invasive nature of the MN system would be a huge advantage in the field of wearable diagnostics and provide a significant competitive edge over existing technologies. From the customer discovery, the opportunities for discrete and unobtrusive sensing, covering a spectrum of applications was unambiguous. This introduces many more avenues for exploitation other than simply sodium. Some of the market segments which were identified as a result of the customer phase are highlighted in **Figure 9.1**. Ultimately, the market for a microneedle system capable of sensing sodium and a plethora of other viable biomarkers was justified, provided the microneedle technology could be incorporated within an already established smart wearable.

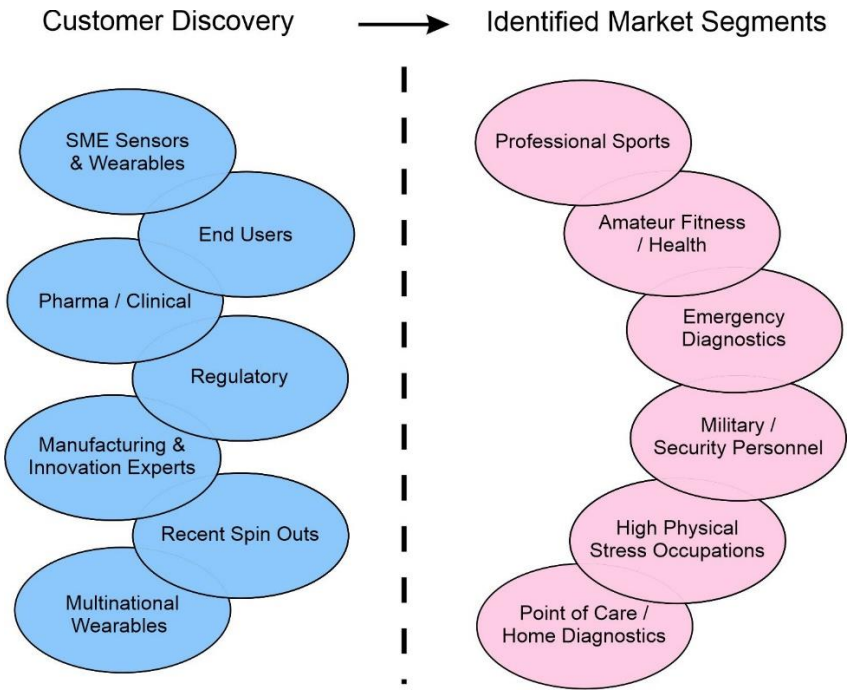

Figure 9.1 Key sectors targeted during customer discovery phase of market validation and the resulting market segments identified for potential commercialisation.

Moving forward, there is potential to expand the technology as a multifaceted system capable of detecting the commercially relevant biomarkers sanctioned through the market feasibility study. The fabrication technique utilised to manufacture conductive composite microneedles implements an ideal platform for further exploration of microneedle development. Within this thesis, tailoring the core components of the MN casting formulation has evidently broadened their potential biomedical application. By continuing

to experiment with conductive particles, polymers and even immobilisation of enzymes to the electrode interface, the prospective for minimally invasive diagnostics is immeasurable. Whilst this holds an enticing future, caution should be at the forefront of MN design, relating biocompatibility and structural integrity with material selection.

Looking towards smart wearable amalgamation, certain user and design requirements become imperative, such as product size, placement, adhesion and attachment. Miniaturisation of microelectronics, defining power requirements for wireless charging and Bluetooth communication will also play a vital role in remote telemetry of the system. Parallel to this, data acquisition and display outputs, including cosmetic aesthetics, become critical for commercial adoption. The capacity for a commercialised smart wearable microneedle sensing system has been demonstrated and the consideration of a next generation system to include autonomous controlled drug delivery is not beyond the potential reach of this technology.

References

Abel, G. (2015) 'Current status and future prospects of point-of-care testing around the globe', *Expert Review of Molecular Diagnostics*, 15(7), pp. 853–855.

Abellán-Llobregat, A. *et al.* (2018) 'Evaluation of herringbone carbon nanotubes-modified electrodes for the simultaneous determination of ascorbic acid and uric acid', *Electrochimica Acta*, 285, pp. 284–291.

Adamu, L. *et al.* (2012) 'Metabolic responses in endurance horses during racing in relation to uric acid profile, leucocytes, heart rate and plasma biochemical parameters', *Veterinární Medicína*, 57(No. 11), pp. 591–596.

Adrian Waldner, A. (CH); *et al.* (2003) 'Flouroionophores and their use in optical ion sensors', *United States Patent*. United States. Available at: https://patents.google.com/patent/US6576192.

Ali, M. *et al.* (2018) 'Quantitative detection of uric acid through ZnO quantum dots based highly sensitive electrochemical biosensor', *Sensors and Actuators A: Physical*, 283, pp. 282–290.

Ambrosi, A. *et al.* (2016) 'Graphene and its electrochemistry – an update', *Chemical Society Reviews*, 45(9), pp. 2458–2493.

Anastasova, S. *et al.* (2017) 'A wearable multisensing patch for continuous sweat monitoring', *Biosensors and Bioelectronics*, 93(June 2016), pp. 139–145.

Anderson, A. *et al.* (2014) 'Investigating the use of endogenous quinoid moieties on carbon fibre as means of developing micro pH sensors', *Materials Science and Engineering: C*, 43, pp. 533–537.

Anderson, A. *et al.* (2019) 'Electrochemically Controlled Dissolution of Nanocarbon-Cellulose Acetate Phthalate Microneedle Arrays', *ACS Applied Materials and Interfaces*, pp. 35540–35547.

Anderson, A., McConville, A. and Davis, J. (2015) 'Electrochemical bubble rip: A new approach to controlled drug release', *Electrochemistry Communications*, 60, pp. 88–91.

Antolini, E. (2009) 'Palladium in fuel cell catalysis', *Energy and Environmental Science*, 2(9), pp. 915–931.

Apollo, N. V. *et al.* (2015) 'Soft, Flexible Freestanding Neural Stimulation and Recording Electrodes Fabricated from Reduced Graphene Oxide', *Advanced Functional Materials*, 25(23), pp. 3551–3559.

Arduini, F. *et al.* (2016) 'Electrochemical biosensors based on nanomodified screen-printed electrodes: Recent applications in clinical analysis', *TrAC Trends in Analytical Chemistry*, 79, pp. 114–126.

Arya, J. and Prausnitz, M. R. (2016) 'Microneedle patches for vaccination in developing countries', *Journal of Controlled Release*, 240, pp. 135–141.

Azeredo, N. F. B. *et al.* (2020) 'Uric acid electrochemical sensing in biofluids based on Ni/Zn hydroxide nanocatalyst', *Microchimica Acta*, 187(7), p. 379.

Azzouz, A. *et al.* (2019) 'Nanomaterial-based electrochemical sensors for the detection of neurochemicals in biological matrices', *TrAC Trends in Analytical Chemistry*, 110, pp. 15–34.

Baccar, H. *et al.* (2013) 'Chronoamperometric-based detection of hydrogen peroxide using palladium nanoparticles', *International Journal of Nanotechnology*, 10(5–7), pp. 563–576.

Baek, S. *et al.* (2018) 'Monitoring of Water Transportation in Plant Stem With Microneedle Sap Flow Sensor', *Journal of Microelectromechanical Systems*, 27(3), pp. 440–447.

Baghayeri, M., Amiri, A. and Razghandi, H. (2019) 'Employment of Pd nanoparticles at the structure of poly aminohippuric acid as a nanocomposite for hydrogen peroxide detection', *Journal of Electroanalytical Chemistry*, 832(October 2018), pp. 142–151.

Baig, N., Rana, A. and Kawde, A. (2018) 'Modified Electrodes for Selective Voltammetric Detection of Biomolecules', *Electroanalysis*, 30(11), pp. 2551–2574.

Barrett, C. *et al.* (2015) 'Development of Low Cost Rapid Fabrication of Sharp Polymer Microneedles for In Vivo Glucose Biosensing Applications', *ECS Journal of Solid State Science and Technology*, 4(10), pp. S3053–S3058.

Bause, S. *et al.* (2018) 'Development of an iridium-based pH sensor for bioanalytical applications', *Journal of Solid State Electrochemistry*, 22(1), pp. 51–60.

Becton Dickinson (2006) *A Look at the Reuse of Insulin Needles The Early Days of Needle Reuse*. Available at: https://www.bd.com/documents/white-paper/DC_A-Look-at-the-Reuse-of-Insulin-Needles_WP_EN.pdf.

Bejugam, M. *et al.* (2007) 'Trisubstituted Isoalloxazines as a New Class of G-Quadruplex

Binding Ligands: Small Molecule Regulation of c-kit Oncogene Expression', *Journal of the American Chemical Society*, 129(43), pp. 12926–12927.

Belhadj Tahar, N. and Savall, A. (2009) 'Electropolymerization of phenol on a vitreous carbon electrode in alkaline aqueous solution at different temperatures', *Electrochimica Acta*, 55(2), pp. 465–469.

Benco, J. S., Nienaber, H. A. and McGimpsey, W. G. (2002) 'A sodium ion sensor based on a covalently-linked aminorhodamine B-calix[4]arene chromoionophore', *Sensors and Actuators, B: Chemical*, 85(1–2), pp. 126–130.

Berry, K. M., Al-Zubidi, N. and Seifi, A. (2015) 'Should serum sodium level be part of stroke protocol prior to t-PA administration?', *Journal of the Neurological Sciences*, 357(1–2), pp. 317–318.

Betjes, M. G. H. (2002) 'Hyponatremia in acute brain disease: The cerebral salt wasting syndrome', *European Journal of Internal Medicine*, 13(1), pp. 9–14.

Bhalla, N. *et al.* (2016) 'Introduction to biosensors', *Essays in Biochemistry*. Edited by P. Estrela, 60(1), pp. 1–8.

Bhowmik, T., Kundu, M. K. and Barman, S. (2016) 'Palladium Nanoparticle–Graphitic Carbon Nitride Porous Synergistic Catalyst for Hydrogen Evolution/Oxidation Reactions over a Broad Range of pH and Correlation of Its Catalytic Activity with Measured Hydrogen Binding Energy', *ACS Catalysis*, 6(3), pp. 1929–1941.

Bingham, D., Kendall, J. and Clancy, M. (1999) 'The portable laboratory: an evaluation of the accuracy and reproducibility of i-STAT.', *Annals of clinical biochemistry*, 36 (Pt 1), pp. 66–71.

Biswas, S. *et al.* (2018) 'Sol-gel synthesis of cubic titanium dioxide nanoparticle using poly(ethylene glycol) as a capping agent: voltammetric simultaneous determination of uric acid and guanine', *Microchimica Acta*, 185(11), p. 513.

Blenkharn, J. I. and Odd, C. (2008) 'Sharps Injuries in Healthcare Waste Handlers', *Ann. Occup. Hyg*, 52(4), pp. 281–286.

Bogavac-Stanojevic, N. and Jelic-Ivanovic, Z. (2017) 'The Cost-Effective Laboratory: Implementation of Economic Evaluation of Laboratory Testing', *Journal of Medical Biochemistry*, 36(3), pp. 238–242.

Bozkurt, S. *et al.* (2017) 'A hydrogen peroxide sensor based on TNM functionalized reduced graphene oxide grafted with highly monodisperse Pd nanoparticles', *Analytica Chimica Acta*, 989, pp. 88–94.

Brownlee, B. J. *et al.* (2018) 'Electrochemical Glucose Sensors Enhanced by Methyl Viologen and Vertically Aligned Carbon Nanotube Channels', *ACS Applied Materials & Interfaces*, 10(34), pp. 28351–28360.

Caffarel-Salvador, E. *et al.* (2015) 'Hydrogel-forming microneedle arrays allow detection of drugs and glucose in vivo: Potential for use in diagnosis and therapeutic drug monitoring', *PLoS ONE*, 10(12).

Caravel, G. *et al.* (2001) 'Microsensor based on NASICON for the analysis of Na+ in the gingival fluid', *Sensors and Actuators B: Chemical*, 76(1–3), pp. 506–511.

Casey, J. R., Grinstein, S. and Orlowski, J. (2010) 'Sensors and regulators of intracellular pH', *Nature Reviews Molecular Cell Biology*, 11(1), pp. 50–61.

Casimero, C. *et al.* (2020) 'Ultrasonic exfoliation of carbon fiber: electroanalytical perspectives', *Journal of Applied Electrochemistry*, 50(3), pp. 383–394.

CDC (2008) *Workbook for Designing, Implementing and Evaluating a Sharps Injury Prevention Program*. Atlanta. Available at: https://www.cdc.gov/sharpssafety/pdf/sharpsworkbook_2008.pdf (Accessed: 27 February 2020).

Celiešiūtė, R. *et al.* (2017) 'A Strategy to Employ Polymerised Riboflavin in the Development of Electrochemical Biosensors', *Electroanalysis*, 29(9), pp. 2071–2082.

Cha, K. J. *et al.* (2014) 'Simple and cost-effective fabrication of solid biodegradable polymer microneedle arrays with adjustable aspect ratio for transdermal drug delivery using acupuncture microneedles', *Journal of Micromechanics and Microengineering*, 24(11), pp. 115015–115023.

Chan, W. H. *et al.* (2002) 'A sodium ion selective optode based on fluorescein octadecyl ether octadecyl ester and application in beverage and urine assay', *Microchemical Journal*, 72(2), pp. 201–207.

Chang, H. *et al.* (2017) 'A Swellable Microneedle Patch to Rapidly Extract Skin Interstitial Fluid for Timely Metabolic Analysis', *Advanced Materials*, 29(37), p. 1702243.

Chege, M., McConville, A. and Davis, J. (2017) 'Microneedle drug delivery systems: Appraising opportunities for improving safety and assessing areas of concern', *Journal of Chemical Health and Safety*, 24(2), pp. 6–14.

Chen, N. *et al.* (2017) 'The effect of the pH on thermal aggregation and gelation of soy proteins', *Food Hydrocolloids*, 66, pp. 27–36.

Chen, Xiao-mei *et al.* (2013) 'Ultrafine palladium nanoparticles grown on graphene nanosheets for enhanced electrochemical sensing of hydrogen peroxide', *Electrochimica Acta*, 97, pp. 398–403.

Cheng, H. *et al.* (2019) 'Recent progress of micro-needle formulations: Fabrication strategies and delivery applications', *Journal of Drug Delivery Science and Technology*, 50(January), pp. 18–26.

Cheung, K. and Das, D. B. (2014) 'Microneedles for drug delivery: trends and progress', *Drug Delivery*, 23(7), pp. 1–17.

Chiaranairungroj, M., Pimpin, A. and Srituravanich, W. (2018) 'Fabrication of high-density microneedle masters towards the commercialisation of dissolving microneedles', *Micro & Nano Letters*, 13(3), pp. 284–288.

Chinnadayyala, S. R., Park, I. and Cho, S. (2018) 'Nonenzymatic determination of glucose at near neutral pH values based on the use of nafion and platinum black coated microneedle electrode array', *Microchimica Acta*, 185(5), p. 250.

Chinnadayyala, S. R., Park, K. D. and Cho, S. (2018) 'Review—In Vivo and In Vitro Microneedle Based Enzymatic and Non-Enzymatic Continuous Glucose Monitoring Biosensors', *ECS Journal of Solid State Science and Technology*, 7(7), pp. Q3159–Q3171.

Christodouleas, D. C., Kaur, B. and Chorti, P. (2018) 'From Point-of-Care Testing to eHealth Diagnostic Devices (eDiagnostics)', *ACS Central Science*, 4(12), pp. 1600–1616.

Christopher Love, J. *et al.* (2003) 'Formation and structure of self-assembled monolayers of alkanethiolates on palladium', *Journal of the American Chemical Society*, 125(9), pp. 2597–2609.

Cinti, S., Moscone, D. and Arduini, F. (2017) 'Screen-printed electrodes as versatile electrochemical sensors and biosensors', in *2017 IEEE East-West Design & Test Symposium (EWDTS)*. IEEE, pp. 1–4.

Ciui, B. *et al.* (2018) 'Wearable Wireless Tyrosinase Bandage and Microneedle Sensors: Toward Melanoma Screening', *Advanced Healthcare Materials*, 7(7), p. 1701264.

Cline, K. K., McDermott, M. T. and McCreery, R. L. (1994) 'Anomalously slow electron transfer at ordered graphite electrodes: Influence of electronic factors and reactive sites', *Journal of Physical Chemistry*, 98(20), pp. 5314–5319.

Coker, A. *et al.* (2009) 'Medical waste management in Ibadan, Nigeria: Obstacles and prospects', *Waste Management*, 29(2), pp. 804–811.

Costello, J. and Parikh, A. (2013) 'The Sticking Point: Diabetic Sharps Disposal Practices in the Community', *Journal of General Internal Medicine*, 28(7), pp. 868–869.

Cowden, W. B. *et al.* (1991) 'Flavins as potential antimalarials. 2. 3-Methyl-10-(substituted-phenyl)flavins', *Journal of Medicinal Chemistry*, 34(6), pp. 1818–1822.

Dashper, S. G. *et al.* (2012) 'Acidogenic potential of soy and bovine milk beverages', *Journal of Dentistry*, 40(9), pp. 736–741.

Davis, S. P. *et al.* (2004) 'Insertion of microneedles into skin: measurement and prediction of insertion force and needle fracture force', *Journal of Biomechanics*, 37(8), pp. 1155–1163.

Desai, D. *et al.* (2018) 'Ultrasensitive sensor for detection of early stage chronic kidney disease in human', *Biosensors and Bioelectronics*, 105, pp. 90–94.

Dharadhar, S. *et al.* (2019) 'Microneedles for transdermal drug delivery: a systematic review', *Drug Development and Industrial Pharmacy*, 45(2), pp. 188–201.

Dhawan, A. P. (2018) 'Editorial Trends and Challenges in Translation of Point-of-Care Technologies in Healthcare', *IEEE Journal of Translational Engineering in Health and Medicine*, 6, pp. 1–8.

Donnelly, R. F. and Larrañeta, E. (2018) 'Microarray patches: potentially useful delivery systems for long-acting nanosuspensions', *Drug Discovery Today*, 23(5), pp. 1026–1033.

Duarah, S., Sharma, M. and Wen, J. (2019) 'Recent advances in microneedle-based drug delivery: Special emphasis on its use in paediatric population', *European Journal of Pharmaceutics and Biopharmaceutics*, 136, pp. 48–69.

Dubouis, N. and Grimaud, A. (2019) 'The hydrogen evolution reaction: from material to interfacial descriptors', *Chemical Science*, 10(40), pp. 9165–9181.

Dutt, J. S. N. *et al.* (2005) 'Diagnostic Implications of Uric Acid in Electroanalytical Measurements', *Electroanalysis*, 17(14), pp. 1233–1243.

Economou, A. (2018) 'Screen-printed electrodes modified with "green" metals for electrochemical stripping analysis of toxic elements', *Sensors (Switzerland)*, 18(4), pp. 1–23.

Eliana and Bojorge, N. (2011) 'Graphite-Composites Alternatives for Electrochemical Biosensor', in *Metal, Ceramic and Polymeric Composites for Various Uses*. InTech, pp. 598–620.

Elseviers, M. M. *et al.* (2014) 'Sharps injuries amongst healthcare workers: review of incidence, transmissions and costs.', *Journal of Renal Care*, 40(3), pp. 150–156.

Extrand, C. W. and Kumagai, Y. (1997) 'An Experimental Study of Contact Angle Hysteresis', *Journal of Colloid and Interface Science*, 191(2), pp. 378–383.

Feliciano-Ramos, I. *et al.* (2010) 'Self-assembled monolayers of l-cysteine on palladium electrodes', *Journal of Electroanalytical Chemistry*, 650(1), pp. 98–104.

Foroughi, F., Rahsepar, M. and Kim, H. (2018) 'A highly sensitive and selective biosensor based on nitrogen-doped graphene for non-enzymatic detection of uric acid and dopamine at biological pH value', *Journal of Electroanalytical Chemistry*, 827, pp. 34–41.

Geoghegan, P. *et al.* (2015) 'Agreement between whole blood and plasma sodium measurements in profound hyponatremia', *Clinical Biochemistry*, 48(7–8), pp. 525–528.

Gerstel, M. S. and Place, V. A. (1976) 'United States Paten Gerstel et al. (19) (54) 75 Drug Delivery Device'. United States. Available at: https://patents.google.com/patent/US3964482A/ (Accessed: 31 January 2020).

Ghasemi, S. *et al.* (2015) 'Palladium nanoparticles supported on graphene as an efficient electrocatalyst for hydrogen evolution reaction', *International Journal of Hydrogen Energy*, 40(46), pp. 16184–16191.

Goel, V. *et al.* (2017) 'Occurrence of Needlestick and Injuries among Health-care Workers of a Tertiary Care Teaching Hospital in North India', *Journal of Laboratory Physicians*, 9(01), pp. 020–025.

Goh, K. P. (2004) 'Management of hyponatremia', *American Family Physician*, 69(10), pp. 2387–2394.

Gokel, G. W., Leevy, W. M. and Weber, M. E. (2004) 'Crown Ethers: Sensors for Ions and

Molecular Scaffolds for Materials and Biological Models', *Chemical Reviews*, 104(5), pp. 2723–2750.

Goldberg, A. *et al.* (2006) 'Hyponatremia and Long-term Mortality in Survivors of Acute ST-Elevation Myocardial Infarction', *Archives of Internal Medicine*, 166(7), p. 781.

Gopal Rao, G. (2003) 'Pathology tests: is the time for demand management ripe at last?', *Journal of Clinical Pathology*, 56(4), pp. 243–248.

Goud, K. Y. *et al.* (2019) 'Wearable Electrochemical Microneedle Sensor for Continuous Monitoring of Levodopa: Toward Parkinson Management', *ACS Sensors*, 4(8), pp. 2196–2204.

Gouvea, C. (2011) 'Biosensors for health applications', in *Biosensors for Health, Environment and Biosecurity*. InTech, pp. 71–86.

Grimmond, T. and Good, L. (2017) 'Exposure Survey of Trends in Occupational Practice (EXPO-S.T.O.P.) 2015: A national survey of sharps injuries and mucocutaneous blood exposures among health care workers in US hospitals', *American Journal of Infection Control*, 45(11), pp. 1218–1223.

Gupta, R. *et al.* (2018) 'Palladium nanoparticles supported on mesoporous silica microspheres for enzyme-free amperometric detection of H2O2 released from living cells', *Sensors and Actuators B: Chemical*, 276(August), pp. 517–525.

Hamidi, H. and Haghighi, B. (2016) 'Fabrication of a sensitive amperometric sensor for NADH and H2O2 using palladium nanoparticles-multiwalled carbon nanotube nanohybrid', *Materials Science and Engineering: C*, 62, pp. 423–428.

Hanssen, B. L., Siraj, S. and Wong, D. K. Y. (2016) 'Recent strategies to minimise fouling in electrochemical detection systems', *Reviews in Analytical Chemistry*, 35(1), pp. 1–28.

Harper, A. and Anderson, M. R. (2010) 'Electrochemical Glucose Sensors—Developments Using Electrostatic Assembly and Carbon Nanotubes for Biosensor Construction', *Sensors*, 10(9), pp. 8248–8274.

Al Hayek, A. A., Robert, A. A. and Al Dawish, M. A. (2020) 'Acceptability of the FreeStyle Libre Flash Glucose Monitoring System: The Experience of Young Patients With Type 1 Diabetes', *Clinical Medicine Insights: Endocrinology and Diabetes*, 13.

He, S. *et al.* (2018) 'Poly(glycine)/graphene oxide modified glassy carbon electrode:

Preparation, characterization and simultaneous electrochemical determination of dopamine, uric acid, guanine and adenine', *Analytica Chimica Acta*, 1031, pp. 75–82.

Hegarty, C. *et al.* (2018) 'Disposable solid state pH sensor based on flavin polymer-ferrocyanide redox couples', *Microchemical Journal*, 139, pp. 210–215.

Hegarty, C., McConville, A., *et al.* (2019) 'Design of composite microneedle sensor systems for the measurement of transdermal pH', *Materials Chemistry and Physics*, 227(August 2018), pp. 340–346.

Hegarty, C., McKillop, S., *et al.* (2019) 'Microneedle array sensors based on carbon nanoparticle composites: interfacial chemistry and electroanalytical properties', *Journal of Materials Science*, 54(15), pp. 10705–10714.

Heng, L. Y. and Hall, E. A. H. (2001) 'Assessing a photocured self-plasticised acrylic membrane recipe for Na+ and K+ ion selective electrodes', *Analytica Chimica Acta*, 443(1), pp. 25–40.

Henry, S. *et al.* (1998) 'Microfabricated microneedles: A novel appraoch to transdermal drug delivery', *Proceedings of the Controlled Release Society*, 87(8), pp. 922–925.

Hickman, J. J. *et al.* (1991) 'Molecular Self-Assembly of Two-Terminal, Voltammetric Microsensors with Internal References', *Science*, 252(5006), pp. 688–691.

Hideaki Hisamoto *et al.* (1995) 'Ion sensing film optodes: disposable ion sensing probes for the determination of Na+, K+, Ca2+ and Cl− concentrations in serum', *Sensors and Actuators B: Chemical*, 29(1–3), pp. 378–385.

Huang, H. and Dasgupta, P. K. (1997) 'Renewable liquid film-based electrochemical sensor for gaseous hydroperoxides', *Talanta*, 44(4), pp. 605–615.

Ialongo, C. and Bernardini, S. (2016) 'Phlebotomy, a bridge between laboratory and patient', *Biochemia Medica*, 26(1), pp. 17–33.

Ita, K. (2018a) 'Ceramic microneedles and hollow microneedles for transdermal drug delivery: Two decades of research', *Journal of Drug Delivery Science and Technology*, 44, pp. 314–322.

Ita, K. (2018b) 'Modulation of transdermal drug delivery with coated microneedles', *Journal of Drug Delivery Science and Technology*, 45, pp. 203–212.

Jagger, J. *et al.* (2008) 'The impact of U.S. policies to protect healthcare workers from

bloodborne pathogens: The critical role of safety-engineered devices', *Journal of Infection and Public Health*, 1(2), pp. 62–71.

Jain, A., Subhan, I. and Joshi, M. (2009) 'Comparison of the point-of-care blood gas analyzer versus the laboratory auto-analyzer for the measurement of electrolytes', *International Journal of Emergency Medicine*, 2(2), pp. 117–120.

Jeng, J. and Shih, J. S. (1984) 'Sodium ion-selective electrode based on crown ether-phosphotungstic acid precipitates', *The Analyst*, 109(5), p. 641.

Jeon, E. *et al.* (2017) 'Development of electrical conductivity measurement technology for key plant physiological information using microneedle sensor', *Journal of Micromechanics and Microengineering*, 27(8), p. 085009.

Jeong, H.-R. *et al.* (2017) 'Considerations in the use of microneedles: pain, convenience, anxiety and safety', *Journal of Drug Targeting*, 25(1), pp. 29–40.

Ji, D. *et al.* (2018) 'Smartphone-based integrated voltammetry system for simultaneous detection of ascorbic acid, dopamine, and uric acid with graphene and gold nanoparticles modified screen-printed electrodes', *Biosensors and Bioelectronics*, 119(August), pp. 55–62.

Ji, X., Zhang, Xin and Zhang, Xianwen (2015) 'Three-Dimensional Graphene-Based Nanomaterials as Electrocatalysts for Oxygen Reduction Reaction', *Journal of Nanomaterials*, 2015, pp. 1–9.

Jović, B. M. *et al.* (2017) 'Hydrogen evolution in acid solution at Pd electrodeposited onto Ti2AlC', *Electrochimica Acta*, 224, pp. 571–584.

Kakali, G., Ramanujachary, K. V. and Greenblatt, M. (2001) 'Application of alkali metal molybdenum bronzes as Na+-ion selective sensors up to 70°C', *Sensors and Actuators, B: Chemical*, 79(1), pp. 58–62.

Kei, A. *et al.* (2018) 'Uric acid and cardiovascular risk: What genes can say', *International Journal of Clinical Practice*, 72(1), p. e13048.

Kelley, K. E. *et al.* (2012) 'Identification of Phthalates in Medications and Dietary Supplement Formulations in the United States and Canada', *Environmental Health Perspectives*, 120(3), pp. 379–384.

Khanna, P. *et al.* (2008) 'Microneedle-based automated therapy for diabetes mellitus', *Journal of Diabetes Science and Technology*, 2(6), pp. 1122–1129.

Kibler, L. A. (2008) 'Dependence of electrocatalytic activity on film thickness for the hydrogen evolution reaction of Pd overlayers on Au(111)', *Electrochimica Acta*, 53(23), pp. 6824–6828.

Kim, K. B. *et al.* (2019) 'Continuous glucose monitoring using a microneedle array sensor coupled with a wireless signal transmitter', *Sensors and Actuators B: Chemical*, 281(April 2018), pp. 14–21.

Kiss, L. *et al.* (2020) 'Electrochemical polymerization of phenol on platinum and glassy carbon electrodes in mesityl oxide', *Chemical Physics Letters*, 754(137642), pp. 1–7.

Klosinski, D. D. (1997) 'Collecting specimens from the elderly patient', *Laboratory Medicine*, 28(8), pp. 518–522.

Koyun, A., Ahlatcolu, E. and Koca, Y. (2012) 'Biosensors and Their Principles', in *A Roadmap of Biomedical Engineers and Milestones*. InTech, pp. 115–142.

Krieger, K. J. *et al.* (2019) 'Simple and customizable method for fabrication of high-aspect ratio microneedle molds using low-cost 3D printing', *Microsystems & Nanoengineering*, 5(42).

Kumagai, T. *et al.* (2017) 'Time to target uric acid to retard CKD progression', *Clinical and Experimental Nephrology*, 21(2), pp. 182–192.

Kumar, A. A. *et al.* (2015) 'From the Bench to the Field in Low-Cost Diagnostics: Two Case Studies', *Angewandte Chemie International Edition*, 54(20), pp. 5836–5853.

Kumar, Y. *et al.* (2018) 'Efficient electrochemical detection of guanine, uric acid and their mixture by composite of nano-particles of lanthanides ortho-ferrite XFeO3 (X = La, Gd, Pr, Dy, Sm, Ce and Tb)', *Journal of Electroanalytical Chemistry*, 830–831(October), pp. 95–105.

Lafitte, V. G. H. *et al.* (2008) 'Anthraquinone–ferrocene film electrodes: Utility in pH and oxygen sensing', *Electrochemistry Communications*, 10(12), pp. 1831–1834.

Lan, T., Zhang, J. and Lu, Y. (2016) 'Transforming the blood glucose meter into a general healthcare meter for in vitro diagnostics in mobile health', *Biotechnology Advances*, 34(3), pp. 331–341.

Larrañeta, E. *et al.* (2016) 'Microneedle arrays as transdermal and intradermal drug delivery systems: Materials science, manufacture and commercial development', *Materials Science and Engineering: R: Reports*, 104, pp. 1–32.

Lau, D. T. *et al.* (2008) 'Older patients' perceptions of medication importance and worth: An exploratory pilot study', *Drugs and Aging*, 25(12), pp. 1061–1075.

Lawrence, N. S., Beckett, E. L., *et al.* (2002) 'Advances in the Voltammetric Analysis of Small Biologically Relevant Compounds', *Analytical Biochemistry*, 303(1), pp. 1–16.

Lawrence, N. S., Thompson, M., *et al.* (2002) 'Carbon–epoxy electrodes: unambiguous identification of authentic triple-phase (insulator/solution/electrode) processesElectronic supplementary information (ESI) available: AFM image of the carbon–epoxy electrode. See http://www.rsc.org/suppdata/cc/b2/b201', *Chemical Communications*, 2(10), pp. 1028–1029.

Lawrence, N. S. *et al.* (2007) 'Triple Component Carbon Epoxy pH Probe', *Electroanalysis*, 19(4), pp. 424–428.

Lee Hamm, L., Nakhoul, N. and Hering-Smith, K. S. (2015) 'Acid-base homeostasis', *Clinical Journal of the American Society of Nephrology*, 10(12), pp. 2232–2242.

Lee, J. M. *et al.* (2005) 'Needlestick Injuries in the United States: Epidemiologic, Economic, and Quality of Life Issues', *AAOHN Journal*, 53(3), pp. 117–133.

Lee, S.-M. *et al.* (2013) 'Soy milk suppresses cholesterol-induced inflammatory gene expression and improves the fatty acid profile in the skin of SD rats', *Biochemical and Biophysical Research Communications*, 430(1), pp. 202–207.

Lenicek Krleza, J. *et al.* (2015) 'Capillary blood sampling: National recommendations on behalf of the Croatian society of medical biochemistry and laboratory medicine', *Biochemia Medica*. Biochemia Medica, Editorial Office, pp. 335–358.

Levy, G. B. (1981) 'Determination of sodium with ion-selective electrodes', *Clinical Chemistry*, 27(8), pp. 1435–1438.

Li, M. *et al.* (2017) 'Applications of screen-printed electrodes in current environmental analysis', *Current Opinion in Electrochemistry*, 3(1), pp. 137–143.

Li, X. *et al.* (2014) 'Peeling mechanism of tomato under infrared heating: Peel loosening and cracking', *Journal of Food Engineering*, 128, pp. 79–87.

Li, X. and Du, X. (2017) 'Molybdenum disulfide nanosheets supported Au-Pd bimetallic nanoparticles for non-enzymatic electrochemical sensing of hydrogen peroxide and glucose', *Sensors and Actuators B: Chemical*, 239, pp. 536–543.

Lim, D. *et al.* (2018) 'Microneedles: A versatile strategy for transdermal delivery of biological molecules', *International Journal of Biological Macromolecules*, 110, pp. 30–38.

Lin, D. and Lasia, A. (2017) 'Electrochemical impedance study of the kinetics of hydrogen evolution at a rough palladium electrode in acidic solution', *Journal of Electroanalytical Chemistry*, 785, pp. 190–195.

Lin, W.-J. *et al.* (2009) 'Graphene modified basal and edge plane pyrolytic graphite electrodes for electrocatalytic oxidation of hydrogen peroxide and β-nicotinamide adenine dinucleotide', *Electrochemistry Communications*, 11(11), pp. 2153–2156.

Liu, F. *et al.* (2011) 'Evolution of a physiological pH6.8 bicarbonate buffer system: Application to the dissolution testing of enteric coated products', *European Journal of Pharmaceutics and Biopharmaceutics*, 78(1), pp. 151–157.

Liu, J. *et al.* (2010) 'A surface treatment technique of electrochemical oxidation to simultaneously improve the interfacial bonding strength and the tensile strength of PAN-based carbon fibers', *Materials Chemistry and Physics*, 122(2–3), pp. 548–555.

Lomonte, C. *et al.* (2016) 'The vascular access in the elderly: a position statement of the Vascular Access Working Group of the Italian Society of Nephrology', *Journal of Nephrology*, 29(2), pp. 175–184.

Lu, M. and Compton, R. G. (2014) 'Voltammetric pH sensing using carbon electrodes: glassy carbon behaves similarly to EPPG', *The Analyst*, 139(18), pp. 4599–4605.

Luo, L. *et al.* (2012) 'Non-enzymatic hydrogen peroxide sensor based on MnO2-ordered mesoporous carbon composite modified electrode', *Electrochimica Acta*, 77, pp. 179–183.

Lutton, R. E. M. *et al.* (2015) 'A novel scalable manufacturing process for the production of hydrogel-forming microneedle arrays', *International Journal of Pharmaceutics*, 494(1), pp. 417–429.

Madhuvilakku, R. *et al.* (2017) 'Green one-pot synthesis of flowers-like Fe3O4/rGO hybrid nanocomposites for effective electrochemical detection of riboflavin and low-cost supercapacitor applications', *Sensors and Actuators B: Chemical*, 253, pp. 879–892.

Magnusson, E. B. *et al.* (2013) 'Real-time optical pH measurement in a standard microfluidic cell culture system', *Biomedical Optics Express*, 4(9), pp. 1749–1758.

Makarona, E. *et al.* (2016) 'Point-of-Need bioanalytics based on planar optical

interferometry', *Biotechnology Advances*, 34(3), pp. 209–233.

Makower, J., Meer, A. and Denend, L. (2010) *FDA impact on US medical technology innovation: A survey of over 200 medical technology companies.*, *FDA impact on US medical technology innovation: A survey of over 200 medical technology companies.* Arlington (Virginia). Available at: https://www.advamed.org/sites/default/ files/resource/30_10_11_10_2010_Study_CAgenda_ makowerreportfinal.pd (Accessed: 20 February 2021).

Martin, A. *et al.* (2017) 'Microneedle Manufacture: Assessing Hazards and Control Measures', *Safety*, 3(4), p. 25.

Mascini, M. and Tombelli, S. (2008) 'Biosensors for biomarkers in medical diagnostics', *Biomarkers*, 13(7–8), pp. 637–657.

McConville, A. and Davis, J. (2016) 'Transdermal microneedle sensor arrays based on palladium: Polymer composites', *Electrochemistry Communications*, 72, pp. 162–165.

McConville, A., Hegarty, C. and Davis, J. (2018) 'Mini-Review: Assessing the Potential Impact of Microneedle Technologies on Home Healthcare Applications', *Medicines*, 5(2).

McConville, A., Mathur, A. and Davis, J. (2019) 'Palladium Nanoneedles on Carbon Fiber: Highly Sensitive Peroxide Detection for Biomedical and Wearable Sensor Applications', *IEEE Sensors Journal*, 19(1), pp. 34–38.

McMurtry, C. M. *et al.* (2015) 'Interventions for Individuals With High Levels of Needle Fear', *The Clinical Journal of Pain*, 31(10), pp. S109–S123.

Menegolo, M. *et al.* (2018) 'Elderly patient: which vascular access? Choice and management of vascular access in the elderly patient', *Nephrology @ Point of Care*, 4, pp. 1–5.

Metters, J. P., Kadara, R. O. and Banks, C. E. (2012) 'Electroanalytical sensing of chromium(iii) and (vi) utilising gold screen printed macro electrodes', *The Analyst*, 137(4), p. 896.

Mettler Toledo (2015) *Laboratory pH Sensor Datasheet*, *Laboratory pH Sensor Datasheet*. Available at: https://www.mt.com/int/en/home/library/datasheets/lab-analytical-instruments/InLab_Routine.html (Accessed: 17 March 2021).

Mikszta, J. A. *et al.* (2002) 'Improved genetic immunization via micromechanical disruption

of skin-barrier function and targeted epidermal delivery', *Nature Medicine*, 8(4), pp. 415–419.

Miller, P. R. *et al.* (2018) 'Extraction and biomolecular analysis of dermal interstitial fluid collected with hollow microneedles', *Communications Biology*, 1(173).

Miller, P. R., Narayan, R. J. and Polsky, R. (2016) 'Microneedle-based sensors for medical diagnosis', *J. Mater. Chem. B*, 4(8), pp. 1379–1383.

Moga, K. A. *et al.* (2013) 'Rapidly-Dissolvable Microneedle Patches Via a Highly Scalable and Reproducible Soft Lithography Approach', *Advanced Materials*, 25(36), pp. 5060–5066.

Momi, J. (2010) 'Hyponatremia—What Is Cerebral Salt Wasting?', *The Permanente Journal*, 14(2), pp. 62–65.

Moody, G. J., Saad, B. B. and Thomas, J. D. R. (1989) 'Studies on bis(crown ether)-based ion-selective electrodes for the potentiometric determination of sodium and potassium in serum', *The Analyst*, 114(1), p. 15.

Musa, A. E. *et al.* (2012) 'Thick-film voltammetric pH-sensors with internal indicator and reference species', *Talanta*, 99, pp. 737–743.

Nakatsuji, H. and Hada, M. (1985) 'Interaction of a hydrogen molecule with palladium', *Journal of the American Chemical Society*, 107(26), pp. 8264–8266.

Nambiar, S. and Yeow, J. T. W. (2011) 'Conductive polymer-based sensors for biomedical applications', *Biosensors and Bioelectronics*, 26(5), pp. 1825–1832.

Nayak, S. *et al.* (2017) 'Point-of-Care Diagnostics: Recent Developments in a Connected Age', *Analytical Chemistry*, 89(1), pp. 102–123.

Nguyen, M. K. *et al.* (2007) 'A new method for determining plasma water content: application in pseudohyponatremia', *AJP: Renal Physiology*, 292(5), pp. F1652–F1656.

Ni, Y. *et al.* (2017) 'In-situ growth of Co3O4 nanoparticles on mesoporous carbon nanofibers: a new nanocomposite for nonenzymatic amperometric sensing of H2O2', *Microchimica Acta*, 184(10), pp. 3689–3695.

Niamah, A. K., Sahi, A. A. and Al-Sharifi, A. S. N. (2017) 'Effect of Feeding Soy Milk Fermented by Probiotic Bacteria on Some Blood Criteria and Weight of Experimental Animals', *Probiotics and Antimicrobial Proteins*, 9(3), pp. 284–291.

Nicholas, D. *et al.* (2018) 'Rapid paper based colorimetric detection of glucose using a hollow microneedle device', *International Journal of Pharmaceutics*, 547(1–2), pp. 244–249.

NIST (2012) *NIST X-ray Photoelectron Spectroscopy Database, NIST Standard Reference Database 20*, *NIST X-ray Photoelectron Spectroscopy (XPS) Database, NIST Standard Reference Database 20*.

O. Domínguez, R. and Arcos Martínez, M. J. (2007) 'Anodic stripping voltammetry of antimony using gold nanoparticle-modified carbon screen-printed electrodes', *Analytica Chimica Acta*, 589(2), pp. 255–260.

Olatunji, O. *et al.* (2013) 'Influence of Array Interspacing on the Force Required for Successful Microneedle Skin Penetration: Theoretical and Practical Approaches', *Journal of Pharmaceutical Sciences*, 102(4), pp. 1209–1221.

Orenius, T. *et al.* (2018) 'Fear of Injections and Needle Phobia Among Children and Adolescents: An Overview of Psychological, Behavioral, and Contextual Factors', *SAGE Open Nursing*, 4, pp. 1–8.

Osredkar, J. (2017) 'Point-of-Care testing in laboratory medicine', in *Point-of-Care Diagnostics - New Progresses and Perspectives*. IAPC Publishing, pp. 1–28.

Palanisamy, S., Chen, S. M. and Sarawathi, R. (2012) 'A novel nonenzymatic hydrogen peroxide sensor based on reduced graphene oxide/ZnO composite modified electrode', *Sensors and Actuators, B: Chemical*, 166–167, pp. 372–377.

Palmer, B. F. (2000) 'Hyponatraemia in a neurosurgical patient: syndrome of inappropriate antidiuretic hormone secretion versus cerebral salt wasting', *Nephrology Dialysis Transplantation*, 15(2), pp. 262–268.

Pandey, P. *et al.* (2019) 'Current Advancements in Transdermal Biosensing and Targeted Drug Delivery', *Sensors*, 19(5).

Panlilio, A. L. *et al.* (2004) 'Estimate of the Annual Number of Percutaneous Injuries Among Hospital-Based Healthcare Workers in the United States, 1997–1998', *Infection Control & Hospital Epidemiology*, 25(7), pp. 556–562.

Peyrot, M. *et al.* (2012) 'Insulin adherence behaviours and barriers in the multinational Global Attitudes of Patients and Physicians in Insulin Therapy study', *Diabetic Medicine*, 29(5), pp. 682–689.

Phair, J. *et al.* (2011) 'A disposable sensor for point of care wound pH monitoring', *The Analyst*, 136(22), p. 4692.

Ping, J. *et al.* (2011) 'Direct electrochemical reduction of graphene oxide on ionic liquid doped screen-printed electrode and its electrochemical biosensing application', *Biosensors and Bioelectronics*, 28(1), pp. 204–209.

Pletcher, D. *et al.* (1982) 'Fundamental concepts', in *Industrial Electrochemistry*. New York: Chapman and Hall Ltd., pp. 1–59.

Prausnitz, M. R. (2004) 'Microneedles for transdermal drug delivery', *Advanced Drug Delivery Reviews*, 56(5), pp. 581–587.

Public Health England (2017) *Health Protection Report: Public Health England*. London, UK. Available at: https://www.gov.uk/government/publications/health-protection-report-volume-11-2017 (Accessed: 19 August 2020).

Qingwen, L. *et al.* (2001) 'Studies on Self-Assembly Monolayers of Cysteine on Gold by XPS, QCM, and Electrochemical Techniques', *Electroanalysis*, 13(16), pp. 1342–1346.

Qingwen, L., Yiming, W. and Guoan, L. (1999) 'pH-Response of nanosized MnO2 prepared with solid state reaction route at room temperature', *Sensors and Actuators B: Chemical*, 59(1), pp. 42–47.

Quinn, H. L., Hughes, C. M. and Donnelly, R. F. (2018) 'In vivo and qualitative studies investigating the translational potential of microneedles for use in the older population', *Drug Delivery and Translational Research*, 8(2), pp. 307–316.

Quinn, M. M. *et al.* (2009) 'Sharps Injuries and Other Blood and Body Fluid Exposures Among Home Health Care Nurses and Aides', *American Journal of Public Health*, 99(S3), pp. S710–S717.

Ramakrishna, S. U. B. *et al.* (2016) 'Nitrogen doped CNTs supported Palladium electrocatalyst for hydrogen evolution reaction in PEM water electrolyser', *International Journal of Hydrogen Energy*, 41(45), pp. 20447–20454.

Ramírez-García, S. *et al.* (2002) 'Carbon composite electrodes: surface and electrochemical properties', *The Analyst*, 127(11), pp. 1512–1519.

Räsänen, L. A. *et al.* (1996) 'Accumulation of uric acid in plasma after repeated bouts of exercise in the horse', *Comparative Biochemistry and Physiology Part B: Biochemistry and*

Molecular Biology, 114(2), pp. 139–144.

Rastogi, P. K., Ganesan, V. and Krishnamoorthi, S. (2014a) 'Palladium nanoparticles decorated gaur gum based hybrid material for electrocatalytic hydrazine determination', *Electrochimica Acta*, 125, pp. 593–600.

Rastogi, P. K., Ganesan, V. and Krishnamoorthi, S. (2014b) 'Palladium nanoparticles incorporated polymer-silica nanocomposite based electrochemical sensing platform for nitrobenzene detection', *Electrochimica Acta*, 147, pp. 442–450.

Rawson, T. M. *et al.* (2018) 'Delivering precision antimicrobial therapy through closed-loop control systems', *Journal of Antimicrobial Chemotherapy*, 73(4), pp. 835–843.

Rawson, T. M. *et al.* (2019) 'Microneedle biosensors for real-time, minimally invasive drug monitoring of phenoxymethylpenicillin: a first-in-human evaluation in healthy volunteers', *The Lancet Digital Health*, 1(7), pp. e335–e343.

Raymundo-Pereira, P. A. *et al.* (2018) 'Thin Films and Composites Based on Graphene for Electrochemical Detection of Biologically-relevant Molecules', *Electroanalysis*, 30(9), pp. 1888–1896.

Rejinold, N. S. *et al.* (2016) 'Biomedical applications of microneedles in therapeutics: recent advancements and implications in drug delivery', *Expert Opinion on Drug Delivery*, 13(1), pp. 109–131.

Rezaei Nejad, H. *et al.* (2018) 'Low-cost and cleanroom-free fabrication of microneedles', *Microsystems & Nanoengineering*, 4(17073).

Ribet, F., Stemme, G. and Roxhed, N. (2018) 'Real-time intradermal continuous glucose monitoring using a minimally invasive microneedle-based system', *Biomedical Microdevices*, 20(4), p. 101.

El Ridi, R. and Tallima, H. (2017) 'Physiological functions and pathogenic potential of uric acid: A review', *Journal of Advanced Research*, 8(5), pp. 487–493.

Riyanto, R. (2016) 'A Highly Sensitive Electrochemical Glucose Sensor By Nickel-Epoxy Electrode With Non-Enzymatic Sensor', *Jurnal Eksakta*, 16(1), pp. 1–8.

Rodrigues, B. *et al.* (2014) 'Hyponatremia in the prognosis of acute ischemic stroke', *Journal of Stroke and Cerebrovascular Diseases*, 23(5), pp. 850–854.

Rzhevskiy, A. S. *et al.* (2018) 'Microneedles as the technique of drug delivery enhancement

in diverse organs and tissues', *Journal of Controlled Release*, 270, pp. 184–202.

Saha, B. *et al.* (2018) 'Comparative Study of Toluidine Blue O and Methylene Blue Binding to Lysozyme and Their Inhibitory Effects on Protein Aggregation', *ACS Omega*, 3(3), pp. 2588–2601.

Samant, P. P. and Prausnitz, M. R. (2018) 'Mechanisms of sampling interstitial fluid from skin using a microneedle patch', *Proceedings of the National Academy of Sciences*, 115(18), pp. 4583–4588.

Santos, C. da C. *et al.* (2019) 'Electropolymerization of phenol and aniline derivatives: Synthesis, characterization and application as electrochemical transducers', *Journal of Electroanalytical Chemistry*, 846(113–163), pp. 1–12.

Sauvage, F., Baudrin, E. and Tarascon, J. M. (2007) 'Study of the potentiometric response towards sodium ions of Na0.44-xMnO2for the development of selective sodium ion sensors', *Sensors and Actuators, B: Chemical*, 120(2), pp. 638–644.

Schneider, L. A. *et al.* (2007) 'Influence of pH on wound-healing: a new perspective for wound-therapy?', *Archives of Dermatological Research*, 298(9), pp. 413–420.

Sha, R., Vishnu, N. and Badhulika, S. (2019) 'MoS2 based ultra-low-cost, flexible, non-enzymatic and non-invasive electrochemical sensor for highly selective detection of Uric acid in human urine samples', *Sensors and Actuators B: Chemical*, 279(March 2018), pp. 53–60.

Sharma, S. *et al.* (2016) 'Evaluation of a minimally invasive glucose biosensor for continuous tissue monitoring', *Analytical and Bioanalytical Chemistry*, 408(29), pp. 8427–8435.

Sharma, S. *et al.* (2017) 'Rapid, low cost prototyping of transdermal devices for personal healthcare monitoring', *Sensing and Bio-Sensing Research*, 13, pp. 104–108.

Shuk, P., Greenblatt, M. and Ramanujachary, K. V. (1996) 'Sodium ion sensitive electrode based on a molybdenum oxide bronze', *Solid State Ionics*, 91(3–4), pp. 233–238.

de Silva, A. P. *et al.* (1997) 'Signaling Recognition Events with Fluorescent Sensors and Switches.', *Chemical reviews*, 97(5), pp. 1515–1566.

Singh, P. *et al.* (2019) 'Polymeric microneedles for controlled transdermal drug delivery', *Journal of Controlled Release*, 315(August), pp. 97–113.

Solak, Y. (2016) 'Comparison of serum sodium levels measured by blood gas analyzer and

biochemistry autoanalyzer in patients with hyponatremia, eunatremia, and hypernatremia', *American Journal of Emergency Medicine*, 34(8), pp. 1473–1479.

Spain, C. V. *et al.* (2016) 'Self-reported Barriers to Adherence and Persistence to Treatment With Injectable Medications for Type 2 Diabetes', *Clinical Therapeutics*, 38(7), pp. 1653–1664.

Spender, A. *et al.* (2019) 'Wearables and the internet of things: considerations for the life and health insurance industry', *British Actuarial Journal*, 24(e22), pp. 1–31.

Sriram, S. (2019) 'Study of needle stick injuries among healthcare providers: Evidence from a teaching hospital in India', *Journal of Family Medicine and Primary Care*, 8(2), p. 599.

Statista (2019) *Wearable technology - Statistics & Facts | Statista*, *Wearable technology - Statistics & Facts | Statista*. Available at: https://www.statista.com/topics/1556/wearable-technology/ (Accessed: 20 March 2020).

Stred'anský, M. *et al.* (2000) 'Amperometric pH-sensing biosensors for urea, penicillin, and oxalacetate', *Analytica Chimica Acta*, 415(1–2), pp. 151–157.

Strickland, R. A., Hill, T. R. and Zaloga, G. P. (1989) 'Bedside analysis of arterial blood gases and electrolytes during and after cardiac surgery', *Journal of Clinical Anesthesia*, 1(4), pp. 248–252.

Strimbu, K. and Tavel, J. A. (2010) 'What are biomarkers?', *Current Opinion in HIV and AIDS*, 5(6), pp. 463–466.

Takeo, M., Lee, W. and Ito, M. (2015) 'Wound Healing and Skin Regeneration', *Cold Spring Harbor Perspectives in Medicine*, 5(1), p. a023267.

Takeuchi, K. and Kim, B. (2018) 'Functionalized microneedles for continuous glucose monitoring', 5, p. 28.

Taleat, Z., Khoshroo, A. and Mazloum-Ardakani, M. (2014) 'Screen-printed electrodes for biosensing: A review (2008-2013)', *Microchimica Acta*, 181(9–10), pp. 865–891.

Tang, Y. and Cheng, W. (2013) 'Nanoparticle-modified electrode with size- and shape-dependent electrocatalytic activities', *Langmuir*, 29(9), pp. 3125–3132.

Tarantola, A., Abiteboul, D. and Rachline, A. (2006) 'Infection risks following accidental exposure to blood or body fluids in health care workers: A review of pathogens transmitted in published cases', *American Journal of Infection Control*, 34(6), pp. 367–375.

Tarbox, T. N. *et al.* (2018) 'An update on coating/manufacturing techniques of microneedles', *Drug Delivery and Translational Research*, 8(6), pp. 1828–1843.

Tatelbaum, M. F. (2001) 'Needlestick safety and prevention act.', *Pain physician*, 4(2), pp. 193–5.

Thomas, S. P. *et al.* (2008) 'Polystyrene/calcium phosphate nanocomposites: Contact angle studies based on water and methylene iodide', *Express Polymer Letters*, 2(7), pp. 528–538.

Ting, S. W. *et al.* (2011) 'Direct electrochemistry of catalase immobilized at electrochemically reduced graphene oxide modified electrode for amperometric H2O2 biosensor', *International Journal of Electrochemical Science*, 6(10), pp. 4438–4453.

Tomčík, P. (2013) 'Microelectrode Arrays with Overlapped Diffusion Layers as Electroanalytical Detectors: Theory and Basic Applications', *Sensors*, 13(10), pp. 13659–13684.

Trojanowicz, M. (2016) 'Impact of nanotechnology on design of advanced screen-printed electrodes for different analytical applications', *TrAC Trends in Analytical Chemistry*, 84, pp. 22–47.

Valdés-Ramírez, G. *et al.* (2014) 'Microneedle-based self-powered glucose sensor', *Electrochemistry Communications*, 47, pp. 58–62.

Valipour, A. and Roushani, M. (2017) 'Using silver nanoparticle and thiol graphene quantum dots nanocomposite as a substratum to load antibody for detection of hepatitis C virus core antigen: Electrochemical oxidation of riboflavin was used as redox probe', *Biosensors and Bioelectronics*, 89, pp. 946–951.

Vashist, S. (2017) 'Point-of-Care Diagnostics: Recent Advances and Trends', *Biosensors*, 7(4), p. 62.

Vestergaard, M. C. *et al.* (2015) *Nanobiosensors and nanobioanalyses*, *Nanobiosensors and Nanobioanalyses*. Springer Japan.

Vranić, E. *et al.* (2020) 'Microneedle-based sensor systems for real-time continuous transdermal monitoring of analytes in body fluids', in *IFMBE Proceedings*. Springer Verlag, pp. 167–172.

Waghule, T. *et al.* (2019) 'Microneedles: A smart approach and increasing potential for transdermal drug delivery system', *Biomedicine & Pharmacotherapy*, 109(July 2018), pp.

1249–1258.

Wang, E. *et al.* (1997) 'Optical sensors for sodium, potassium and ammonium ions based on lipophilic fluorescein anionic dye and neutral carriers', *Analytica Chimica Acta*, 357(1–2), pp. 85–90.

Wang, J. *et al.* (1996) 'Electrochemical activation of screen-printed carbon strips', *The Analyst*, 121(3), p. 345.

Wang, J. *et al.* (1998) 'Performance of screen-printed carbon electrodes fabricated from different carbon inks', *Electrochimica Acta*, 43(23), pp. 3459–3465.

Wang, J. and Chen, Q. (1994) 'Enzyme Microelectrode Array Strips for Glucose and Lactate', *Analytical Chemistry*, 66(7), pp. 1007–1011.

Wang, J. and Tian, B. (1993) 'Mercury-free disposable lead sensors based on potentiometric stripping analysis of gold-coated screen-printed electrodes', *Analytical Chemistry*, 65(11), pp. 1529–1532.

Wang, P. M., Cornwell, M. and Prausnitz, M. R. (2005) 'Minimally invasive extraction of dermal interstitial fluid for glucose monitoring using microneedles', *Diabetes Technology and Therapeutics*, 7(1), pp. 131–141.

Weschler, C. J. *et al.* (2011) 'Squalene and Cholesterol in Dust from Danish Homes and Daycare Centers', *Environmental Science & Technology*, 45(9), pp. 3872–3879.

Windmiller, J. R. *et al.* (2011) 'Microneedle array-based carbon paste amperometric sensors and biosensors', *Analyst*, 136(9), pp. 1846–1851.

WitkowskaNery, E., Santhiago, M. and Kubota, L. T. (2016) 'Flow in a Paper-based Bioactive Channel - Study on Electrochemical Detection of Glucose and Uric Acid', *Electroanalysis*, 28(9), pp. 2245–2252.

Wong, C. Y. *et al.* (2017) 'In-vitro evaluation of enteric coated insulin tablets containing absorption enhancer and enzyme inhibitor', *Journal of Pharmacy and Pharmacology*, 69(3), pp. 285–294.

World Health Organization (2010) 'Paediatric and neonatal blood sampling', in *WHO Guidelines on Drawing Blood: Best Practices in Phlebotomy.* Geneva: World Health Organization, pp. 35–37. Available at: https://www.ncbi.nlm.nih.gov/books/NBK138647/ (Accessed: 26 February 2020).

Wu, M. *et al.* (2019) 'NASICON-Structured NaTi2(PO4)3 for Sustainable Energy Storage', *Nano-Micro Letters*, 11(1), p. 44.

Wu, S. *et al.* (2016) 'Riboflavin-mediated extracellular electron transfer process involving Pachysolen tannophilus', *Electrochimica Acta*, 210, pp. 117–121.

Xiang, Y. and Lu, Y. (2011) 'Using personal glucose meters and functional DNA sensors to quantify a variety of analytical targets', *Nat Chem*, 3(9), pp. 697–703.

Xiong, L., Batchelor-McAuley, C. and Compton, Richard G (2011) 'Calibrationless pH sensors based on nitrosophenyl and ferrocenyl co-modified screen printed electrodes', *Sensors and Actuators B: Chemical*, 159(1), pp. 251–255.

Xiong, L., Batchelor-McAuley, C. and Compton, Richard G. (2011) 'Calibrationless pH sensors based on nitrosophenyl and ferrocenyl co-modified screen printed electrodes', *Sensors and Actuators B: Chemical*, 159(1), pp. 251–255.

Xue, B. *et al.* (2018) 'Ni foam-supported ZnO nanowires and Co3O4/NiCo2O4 double-shelled nanocages for efficient hydrogen peroxide detection', *Sensors and Actuators B: Chemical*, 262, pp. 828–836.

Yahia, M. M. and Bashir, S. (2018) 'Clinical Characteristics of Stroke Mimics Presenting to a Stroke Center within the Therapeutic Window of Thrombolysis', *Brain & Neurorehabilitation*, 11(1).

Yamanaka, K., Vestergaard, M. C. and Tamiya, E. (2016) 'Printable electrochemical biosensors: A focus on screen-printed electrodes and their application', *Sensors (Switzerland)*, 16(10).

Yang, H. *et al.* (2019) 'Hierarchical bi-continuous Pt decorated nanoporous Au-Sn alloy on carbon fiber paper for ascorbic acid, dopamine and uric acid simultaneous sensing', *Biosensors and Bioelectronics*, 124–125(October 2018), pp. 191–198.

Yang, J. *et al.* (2019) 'Recent advances of microneedles for biomedical applications: drug delivery and beyond', *Acta Pharmaceutica Sinica B*. Chinese Academy of Medical Sciences, pp. 469–483.

Yang, X. (2000) 'Development of a fluorescent optode membrane for sodium ion based on the calix[4]arene and tetraphenylporphine', *Talanta*, 52(6), pp. 1033–1039.

Yee, A. H., Burns, J. D. and Wijdicks, E. F. M. (2010) 'Cerebral Salt Wasting: Pathophysiology,

Diagnosis, and Treatment', *Neurosurgery Clinics of North America*, 21(2), pp. 339–352.

Yousuf, I. *et al.* (2014) 'Hyponatremia in stroke', *Annals of Indian Academy of Neurology*, 17(1), p. 55.

Yu, Y.-Y. *et al.* (2017) 'Sensitive amperometric detection of riboflavin with a whole-cell electrochemical sensor', *Analytica Chimica Acta*, 985, pp. 148–154.

Yun Yang, S. *et al.* (2013) 'A bio-inspired swellable microneedle adhesive for mechanical interlocking with tissue', *Nature Communications*, 4(1702).

Zelmat, M. S. (2015) 'Direct and Indirect Potentiometry: Differences Specified Through a Case of Waldenstrom Disease', *Annales de Biologie Clinique*, 73(3), pp. 345–352.

Zhang, L. *et al.* (2016) 'Recent advances in palladium-based electrocatalysts for fuel cell reactions and hydrogen evolution reaction', *Nano Energy*, 29, pp. 198–219.

Zhang, W. *et al.* (2018) 'Electrochemical sensing platform based on the biomass-derived microporous carbons for simultaneous determination of ascorbic acid, dopamine, and uric acid', *Biosensors and Bioelectronics*, 121(August), pp. 96–103.

Zhao, X., Yang, X. and Hong Chan, W. (2003) 'A Surface Fluorescent Sensing Membrane for Rapid Detection of Sodium', *Journal of Dispersion Science and Technology*, 24(3–4), pp. 547–555.

Zhao, Y. *et al.* (2019) 'In-situ growth of gold nanoparticles on a 3D-network consisting of a MoS2/rGO nanocomposite for simultaneous voltammetric determination of ascorbic acid, dopamine and uric acid', *Microchimica Acta*, 186(2), p. 92.

Zheng, L. *et al.* (2019) 'Palladium/Bismuth/Copper Hierarchical Nano-Architectures for Efficient Hydrogen Evolution and Stable Hydrogen Detection', *ACS Applied Materials & Interfaces*, 11(6), pp. 6248–6256.

Zhong, C. *et al.* (2017) 'Sex-Specific Relationship Between Serum Uric Acid and Risk of Stroke: A Dose-Response Meta-Analysis of Prospective Studies', *Journal of the American Heart Association*, 6(4), p. e005042.

Zhou, J.-X. *et al.* (2017) 'MoS 2 /Pt nanocomposite-functionalized microneedle for real-time monitoring of hydrogen peroxide release from living cells', *The Analyst*, 142(22), pp. 4322–4329.

Zhu, M. W. *et al.* (2009) 'Silica needle template fabrication of metal hollow microneedle

arrays', *Journal of Micromechanics and Microengineering*, 19(11), p. 115010.

Publications Resulting from this Research Work

Anderson, A., **Hegarty, C.**, Casimero, C. and Davis, J. (2019) 'Electrochemically Controlled Dissolution of Nanocarbon-Cellulose Acetate Phthalate Microneedle Arrays', *ACS Applied Materials and Interfaces*, pp. 35540–35547.

Cameron, S., Barber, R., Scott, C., Casimero, C., **Hegarty, C.**, O'Loughlin, L., Pourshahidi, K., *et al.* (2020) 'Laser Scribed Polyimide as a Platform for Monitoring pH within Smart Bandages', in *2020 7th International Conference on Signal Processing and Integrated Networks (SPIN)*. IEEE, pp. 654–658.

Casimero, C., Ruddock, T., **Hegarty, C.**, Barber, R., Devine, A. and Davis, J. (2020) 'Minimising Blood Stream Infection: Developing New Materials for Intravascular Catheters', *Medicines*, 7(9), p. 49.

Casimero, C., **Hegarty, C.**, McGlynn, R. J. and Davis, J. (2020) 'Ultrasonic exfoliation of carbon fiber: electroanalytical perspectives', *Journal of Applied Electrochemistry*, 50(3), pp. 383–394.

Devine, A., **Hegarty, C.**, Casimero, C., Molyneaux, R. L., Smith, R. B., Cardosi, M. F. and Davis, J. (2020) 'Electrochemically initiated release: exploring new modalities for controlled drug release', *Journal of Electroanalytical Chemistry*, p. 113926.

Hegarty, C., Kirkwood, S., Cardosi, M. F., Lawrence, C. L., Taylor, C. M., Smith, R. B. and Davis, J. (2018) 'Disposable solid state pH sensor based on flavin polymer-ferrocyanide redox couples', *Microchemical Journal*, 139, pp. 210–215.

Hegarty, C., McKillop, S., Dooher, T., Dixon, D. and Davis, J. (2019) 'Composite Microneedle Arrays Modified With Palladium Nanoclusters for Electrocatalytic Detection of Peroxide', *IEEE Sensors Letters*, 3(9), pp. 1–4.

Hegarty, C., McConville, A., McGlynn, R. J., Mariotti, D. and Davis, J. (2019) 'Design of composite microneedle sensor systems for the measurement of transdermal pH', *Materials Chemistry and Physics*, 227(August 2018), pp. 340–346.

Hegarty, C., McKillop, S., McGlynn, R. J., Smith, R. B., Mathur, A. and Davis, J. (2019) 'Microneedle array sensors based on carbon nanoparticle composites: interfacial chemistry and electroanalytical properties', *Journal of Materials Science*, 54(15), pp. 10705–10714.

McConville, A., **Hegarty, C.** and Davis, J. (2018) 'Mini-Review: Assessing the Potential Impact of Microneedle Technologies on Home Healthcare Applications', *Medicines*, 5(2).